Table Handling Task in Collaboration with a Human and a Humanoid Robot

Isabelle Maroger

Université Fédérale

Toulouse Midi-Pyrénées

THÈSE

En vue de l'obtention du

DOCTORAT DE L'UNIVERSITÉ DE TOULOUSE

Délivré par :

l'Institut National des Sciences Appliquées de Toulouse (INSA de Toulouse)

Présentée et soutenue le *30/09/2022* **par :**

Isabelle Maroger

Table Handling Task in Collaboration with a Human and a Humanoid Robot

---

JURY

Katja Mombaur	Professor	Rapporteur
Marilena Vendittelli	Associate Professor	Rapporteur
Pauline Maurice	Chargé de Recherche	Examinateur
Pierre-Brice Wieber	Chargé de Recherche	Examinateur
Eiichi Yoshida	Professor	Examinateur
Bruno Watier	Professeur des Universités	Directeur de thèse
Olivier Stasse	Directeur de Recherche	Co-directeur de thèse

École doctorale et spécialité :
EDSYS : Robotique 4200046

Unité de Recherche :
LAAS - Laboratoire d'Analyse et d'Architecture des Systèmes (UPR 8001)

Directeurs de Thèse :
Bruno Watier et *Olivier Stasse*

Rapporteurs :
Katja Mombaur et *Marilena Vendittelli*

Contents

List of Figures

List of Tables

Introduction

Contents

Context

With more than 200 Degrees of Freedom (DoFs), humans are flexible beings optimized through a long evolution process over multiple eras. Using their muscles and their complex joints, they can perform a wide range of motions in various environments. They can also deal with unexpected situations and even learn from them. On the opposite, robots commonly have rigid bodies with motors and rotational joints which limit their movement capacity. Moreover, robots, and especially humanoid robots, need to be robustly controlled in order to deal with unplanned perturbations and to efficiently and safely achieve given tasks. Even humanoid robots, which usually count more than 30 DoFs, are far from competing with the human to perform complex, or even very easy, tasks. Even when they are stronger than human beings, like the TALOS humanoid robot [10] built by *PAL Robotics*, they usually remain quite slow or dangerous to collaborate with. For example, on the one hand, the Atlas robot [11] built by *Boston Dynamics* is able to run at a $2.5\,\mathrm{m.s^{-1}}$ speed and to demonstrate a human-level agility but it is dangerous due to its very powerful actuation system made up of 28 hydraulic joints (burst pressure of $210\,\mathrm{kg.cm^{-2}}$ in the hoses). On the other hand, a robot like the Digit robot [12] built by *Agility Robotics* is far less dangerous regarding its hardware but less capable of performing highly diverse and agile locomotion.

Despite these limitations, humanoid robots arise as the most versatile solution to assist humans in various environments. Indeed, environments such as factories, hospitals or homes, were originally designed for human beings. Thus, they have stairs, doors, narrow corridors, heavy and tall furniture, etc. Nowadays, thanks to their anthropomorphic bodies, humanoid robots are the only robots designed to deal with all those obstacles. Thus, they are theoretically able to mimic human motions. However, few humanoid robots' motion planners are programmed to actually perform human-like motions. Moreover, as already mentioned, humanoid robots are hard to control due to their numerous DoFs and their natural instability. Hence, today, one of the major challenges in humanoid robotics is to develop human-aware planners and robust controllers in order to allow anthropomorphic systems to safely interact with humans.

Furthermore, safety is not the only black spot that prevents useful Human-Robot Interactions (HRIs). Assuming that a robot can safely interact with a human to assist him, it can still be a burden for its human partner. Indeed, if the robot passively follows the human motions, the human may have to compensate for the lack of reactivity and maneuverability of the robot. To avoid this problem, the robot should be proactive and should anticipate its partner's intentions in real-time, like a human partner would do. Thus, a better understanding of the mechanical parameters that underlie motor control in humans is a key to better HRIs. This is the field of study of biomechanics researchers working on the study, the modeling and the prediction of human motions. Over the past decades, more and more collaborations between those researchers and the roboticists have emerged around these issues. The roboticists brought powerful tools to compute kinematic and dynamic equations of treelike poly-articulated systems, while the researchers in human movement brought key elements to understand how humans move and how it would be beneficial for robot control to mimic them.

It is in this context of growing relationships between robotics and biomechanics that the CollaBorative roBot (CoBot) project has emerged. Funded by the French Agence Nationale de la Recherche (ANR), this project (ANR-CoBot [18CE10-0003]) targets a human-humanoid robot collaboration in the context of a load-carriage task. During this collaboration, the robot is aimed to safely and proactively assist its human partner to handle a load. To achieve this

goal, human-human load-carriage tasks should be carried out in order to identify the synergies and strategies implemented in such collaborations. Indeed, the idea of the ANR-CoBot project is, first, to understand the mechanisms at stake during a human-human collaboration and, then, to model and simulate them to finally implement them on a humanoid robot to perform the same task with a human partner. In order to have all the knowledge needed to successfully carry out the project, three laboratories have been involved. Thus, they all bring skills from different fields of study:

- Centre de Recherches sur la Cognition Animale (CRCA): biomechanics, motor control, collective behaviour, movement simulation.
- Laboratoire Ingénierie, Recherche, Intervention, Sport, Santé, Environnement (IRISSE): neuroscience, motor control, collective behaviour.
- Laboratoire d'Analyse et d'Architecture des Systèmes (LAAS-CNRS): biomechanics, motor control, collective behaviour, movement simulation, robotics.

As part of this project, 2 PhD theses and 3 Master internships were conducted. The thesis presented in this manuscript deals with **the transition from the modeling of human behaviour to the integration of this model into a humanoid robot**. The final goal of this thesis is to perform a **proactive HRI to carry a load**. In this thesis, the chosen load is a $\sim 20\,\text{kg}$ table and the chosen humanoid robot is the first TALOS robot [10] built by *PAL Robotics*. This robot was designed according to requirements provided by the Gepetto team from LAAS-CNRS. It is 1.75 m tall and weighs around 100 kg. It is represented in Fig.1. This robot was chosen for the project as it is powerful enough to lift and carry the table with a human partner, as Fig.2 demonstrates. Moreover, it can be both position and torque-controlled. Torque control is a promising solution to safely deal with unexpected contact with the environment or with humans [13, 14].

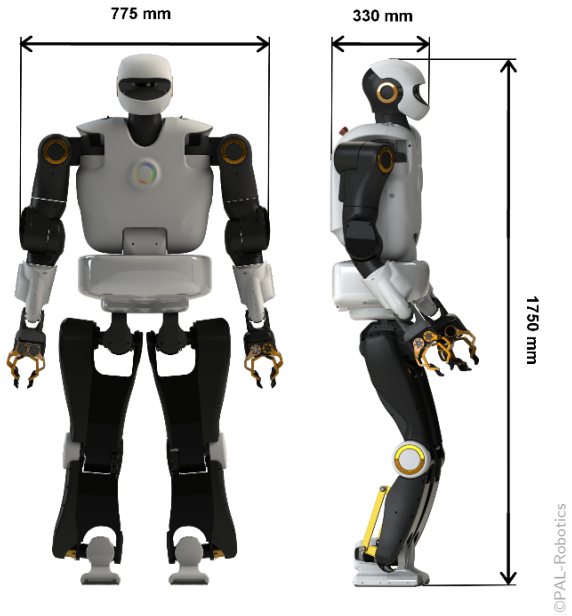

Figure 1: TALOS robot by *PAL Robotics*.

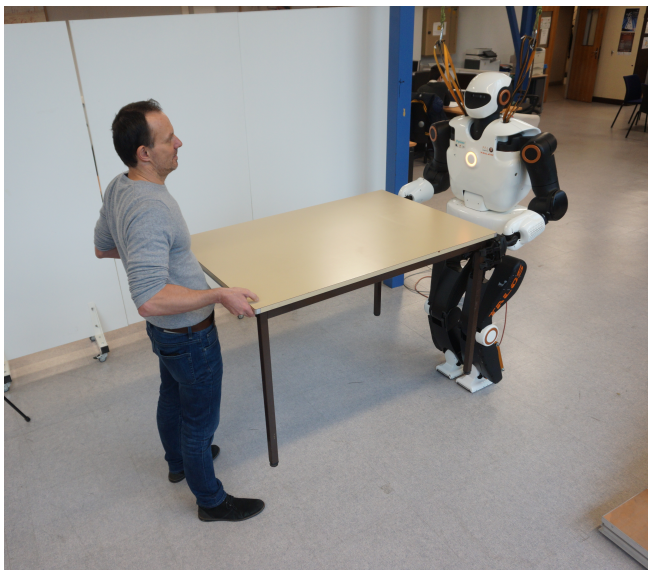

Figure 2: Human-robot collaborative load-carriage task.

Approach

To achieve the final goal of this thesis, five matters need to be handled:

- Localization: the robot needs to locate the table and its human partner in order to interact with them.
- Gait generation: the robot needs to walk toward the table at the beginning of the experiment and also needs to walk with the table towards an unknown location chosen by its human partner.
- Whole-body control: the robot needs to lift the table and handle it while walking.
- Balance: the robot should not fall during the experiment.
- Safety: the robot should not harm its human partner.

Among those matters, this thesis mainly focuses on the **gait generation**. The localization, the whole-body control and the balance are the research topics of other members in the Gepetto team at LAAS-CNRS.

Furthermore, as already stated, this thesis aims at a proactive collaboration between a human and a TALOS humanoid robot to carry a table. To achieve this pro-activity, the choice was made to, first, study and model human behaviour in order to, then, embed this model into the robot controller. This is expected to improve the HRI [15]. Indeed, it may allow the robot to be more reactive by anticipating its partner's motions and it may make the interaction less disturbing and more natural for the human, as the robot may act in a human-like manner. These both reasons may result in an efficient and useful collaboration.

As a first step, we chose to consider a reduced problem. Instead of working directly on making the robot walk while handling a table in a human-like way, we worked, first, on making the robot walk to the table in a human-like way. Thus, instead of modeling two subjects carrying a table, we focused only on modeling single walking subjects. In doing so, we wanted to quickly develop an efficient approach to model, and even predict, human trajectories in a basic situation without perturbations or interactions. Then, once the reduced problem was solved, we used the same approach to model pairs of subjects walking with a table.

The scientific approach implemented to solve both the reduced and the final problem in this thesis was the following:

1. Define the scientific problem and investigate the related works.
2. Design an experimental protocol to measure the human behaviour that we want to mimic with the humanoid robot.
3. Measure multiple subjects' behaviour using a Motion Capture system (MoCap).
4. Extract the data of interest from the measurements.
5. Analyze the measured data to identify the mechanical parameters at stake in the measured human behaviour.
6. Design and assess an optimization problem able to model and predict the measured human behaviour.
7. Embed the human prediction model in the TALOS robot Walking Pattern Generator (WPG) which is integrated into a whole-body controller designed by Noëlie Ramuzat, another PhD student in the Gepetto team at LAAS-CNRS.

8. Simulate on Gazebo to assess the integration.

9. Perform at least 5 successful experiments with the real TALOS robot to validate the whole framework.

This scientific approach is schematically represented in Fig.3 for both the reduced (Fig.3a) and the final (Fig.3b) problem.

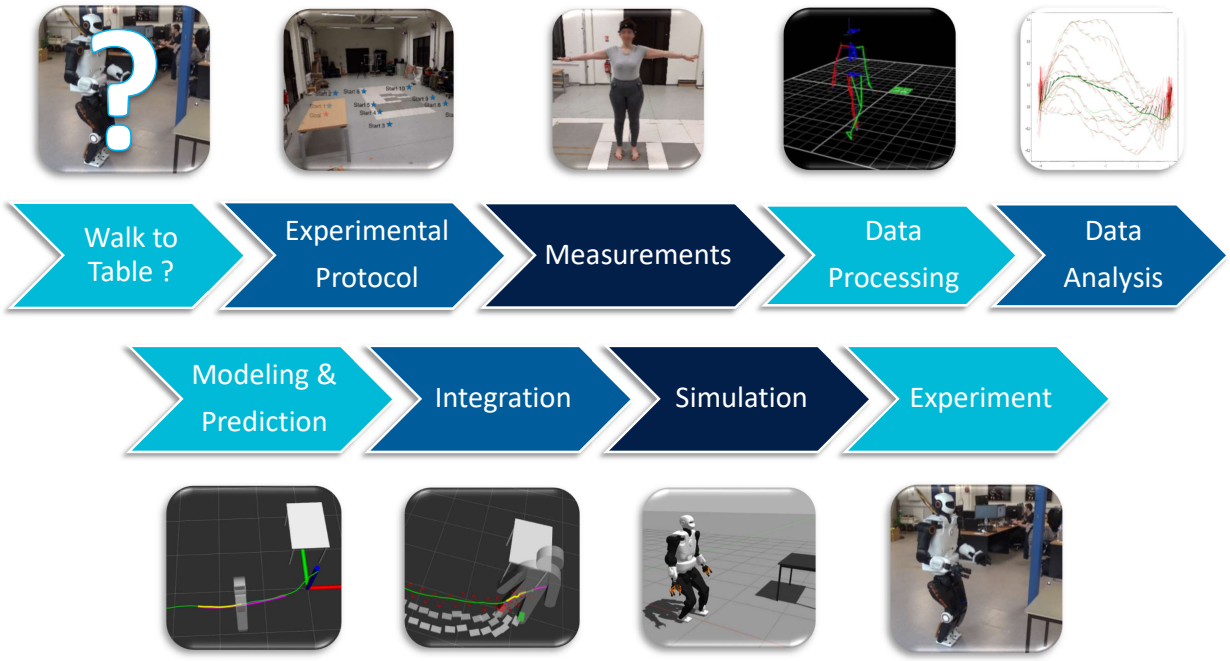

(a) Reduced problem: Make a robot walk to the table in a human-like manner.

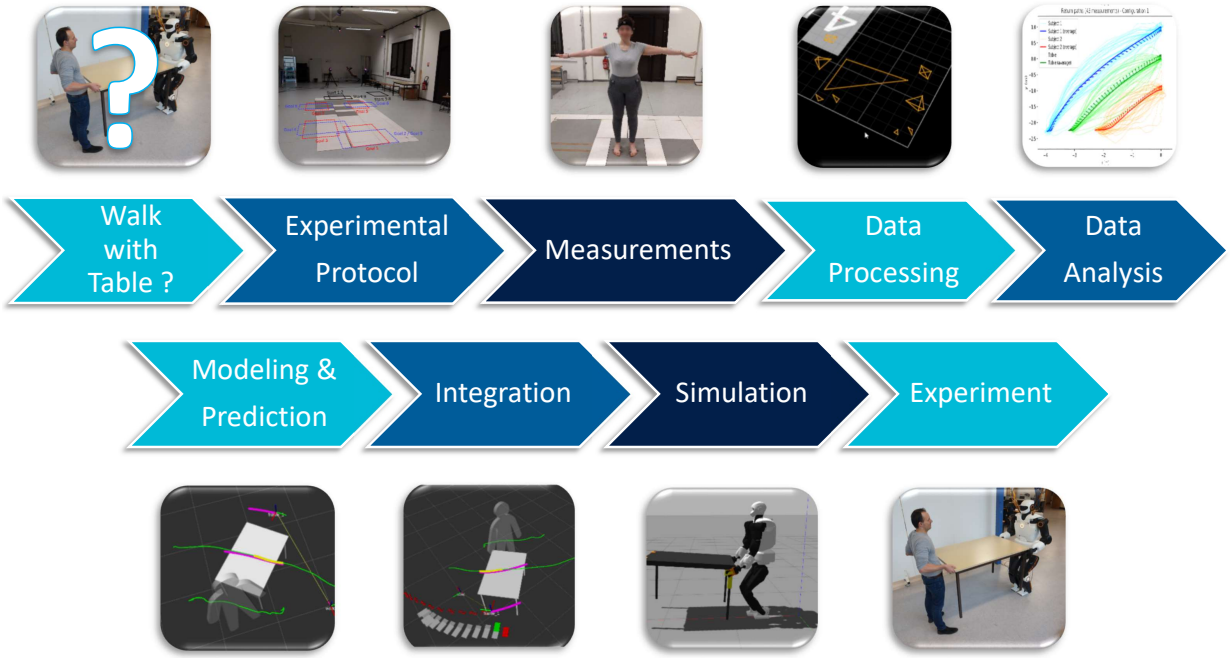

(b) Final problem: Make a robot proactively collaborate with a human partner to handle a table.

Figure 3: Graphical representation of the scientific approach of the problems tackled in this thesis.

Organization of the manuscript

This manuscript has one introductory part, 5 main chapters (from Chapter 1 to Chapter 5) and one conclusive part.

The first three chapters are gathered in Part I which focuses on the reduced problem and the development of a method to embed a given human behaviour in a humanoid robot. First of all, Chapter 1 focuses on the study of single walking human trajectories. After the implementation of some existing human locomotion models, a new and accurate model is introduced and assessed in this chapter. Once the human-likeness of the trajectories generated with this model was demonstrated, a prediction process based on this model is presented in Chapter 2. Then, Chapter 3 deals with the embedding of human behaviour modeled in the previous chapters in the TALOS robot gait generation.

Then, the last two chapters are gathered in Part II which focuses on the final problem using the approach developed in the previous part. The same method is, thus, used in Chapter 4 to study and model the locomotion paths of a pair of humans carrying a table. Finally, Chapter 5 focuses on the final goal of this thesis: the human-robot collaboration to carry a table. The problem of the localization of the robot with respect to the table and to its human partner is addressed in this chapter along with the simulation of a proactive table handling task based on the prediction of the table's trajectory. The remaining steps to go toward real experiments on the robot are also tackled in this chapter.

Contributions

This multidisciplinary thesis contributed to both biomechanics and robotics fields.

From a biomechanical point of view, the scientific contributions of this thesis are:

Chapter 1
- **The modeling of human trajectories during locomotion.**
  - ↪ The development of an original and rigorous experimental protocol to measure the CoM trajectories of single walking humans using a MoCap.
  - ↪ The creation of a dataset of 400 CoM trajectories. Those trajectories were measured following the afore-mentioned protocol.
  - ↪ The open-source implementation of two existing human trajectory models: a clothoid-based model and an optimal control one.
  - ↪ The introduction of an original metric to compare the measured trajectories and the trajectories generated using both models.
  - ↪ The optimization and the assessment of a slightly modified optimal control model using a bi-level inverse optimal control to generate trajectories that accurately fit the measurements.

Chapter 2
- **The real-time prediction of human trajectories during locomotion.**
  - ↪ The design of an accurate human trajectory prediction model using optimal control.
  - ↪ The assessment of this model with an original metric.

Chapter 4

The study of the human trajectories during collaborative carriage.

- ↪ The development of an original and rigorous experimental protocol to measure the CoM trajectories of pairs of subjects during collaborative carriages using a MoCap.
- ↪ The creation of a dataset of 3240 CoM trajectories. Those trajectories were measured following the afore-mentioned protocol.
- ↪ The extensive analysis of the trajectories performed by the pairs in order to determine if a shared strategy emerged from the measured data.
- ↪ The reconstruction of the trajectories of the subjects based on the trajectories of the table.
- ↪ The proposal of an optimal control model to simultaneously simulate the trajectories of both subjects during table handling tasks.

Chapter 5

The modeling and the real-time prediction of the table trajectories during collaborative carriage.

- ↪ The short analysis of the table trajectories during table handling tasks.
- ↪ The demonstration that the same approach can be used to model and predict table trajectories during a collaborative carriage than single walking human trajectories.

From a robotics point of view, they are:

Chapter 3

The embedding of a human locomotion model in the robot WPG.

- ↪ The experiments on the real TALOS robot to test the embedding of a human trajectory model on the robot using the walking pattern generator designed by *PAL Robotics*.
- ↪ The design of a new pattern generator which allows trajectory tracking.
- ↪ The embedding of the human trajectory prediction model designed in Chapter 2 in this new pattern generator.
- ↪ The simulation on Gazebo of a TALOS robot walking with this new pattern generator using the whole-body controller implemented by Noëlie Ramuzat, another PhD student in the Gepetto team at LAAS-CNRS.

Chapter 5

The resolutions of the localization problem and of the gait generation problem in the context of a human-robot table handling task.

- ↪ The experiments on the real TALOS robot to assess a LiDAR-based localization system implemented by Thibaud Lasguignes, another PhD student in the Gepetto team at LAAS-CNRS.
- ↪ The assessment of this localization system with respect to a MoCap.
- ↪ The simulation on Gazebo of a TALOS robot walking while actively assisting a simulated human partner to move a table to an unknown position.

Publications

This thesis resulted in the following publications:

Journals

- **I. Maroger**, M. Silva, H. Pillet, N. Turpin, O. Stasse, and B. Watier. "Walking Paths during Collaborative Carriages do not Follow the Simple Rules Observed in the Locomotion of Single Walking Subjects". In: *Scientific Reports*. Vol. 12. 15585. 2022
- **I. Maroger**, N. Ramuzat, O. Stasse, and B. Watier. "Human Trajectory Prediction Model and Its Coupling With a Walking Pattern Generator of a Humanoid Robot". In: *IEEE/RAS Robotics and Automation Letters (RA-L)*. vol. 6. 4. IEEE. 2021, pp. 6361–6369
  Also accepted on the 2021 *IEEE/RSJ Int. Conf. on Intelligent Robots and Systems (IROS)*.
- **I. Maroger**, O. Stasse, and B. Watier. "Inverse Optimal Control to Model Human Trajectories during Locomotion". In: *Computer Methods in Biomechanics and Biomedical Engineering*. Taylor & Francis, 2021, pp. 1–13

Conferences with proceedings

- **I. Maroger**, O. Stasse, and B. Watier. "From the Study of Table Trajectories during Collaborative Carriages toward Proactive Human-Robot Table Handling Tasks". In: *IEEE/RAS Int. Conf. on Humanoid Robotics (Humanoids)*. 2022
- **I. Maroger**, M. Silva, O. Stasse, and B. Watier. "Can the trajectories performed by the subjects be inferred from the trajectory of the load they carry?" In: *47ème congrès de la Société de Biomécanique*. 2022
- **I. Maroger**, O. Stasse, and B. Watier. "Description and Assessment of a Human Trajectory Prediction Model during Gait". In: *46ème congrès de la Société de Biomécanique*. 2021
- T. Lasguignes, **I. Maroger**, M. Fallon, M. Ramezani, L. Marchionni, O. Stasse, et al. "ICP Localization and Walking Experiments on a TALOS Humanoid Robot". In: *Int. Conf. on Advanced Robotics (ICAR)*. IEEE. 2021, pp. 800–805
- **I. Maroger**, O. Stasse, and B. Watier. "Walking Human Trajectory Models and Their Application to Humanoid Robot Locomotion". In: *IEEE/RSJ Int. Conf. on Intelligent Robots and Systems (IROS)*. IEEE. 2020, pp. 3465–3472
- **I. Maroger**, O. Stasse, and B. Watier. "Comparison of Human Experimental Trajectories and Simulations during Gait". In: *45ème congrès de la Société de Biomécanique*. 2020

Part I

Reduced Problem

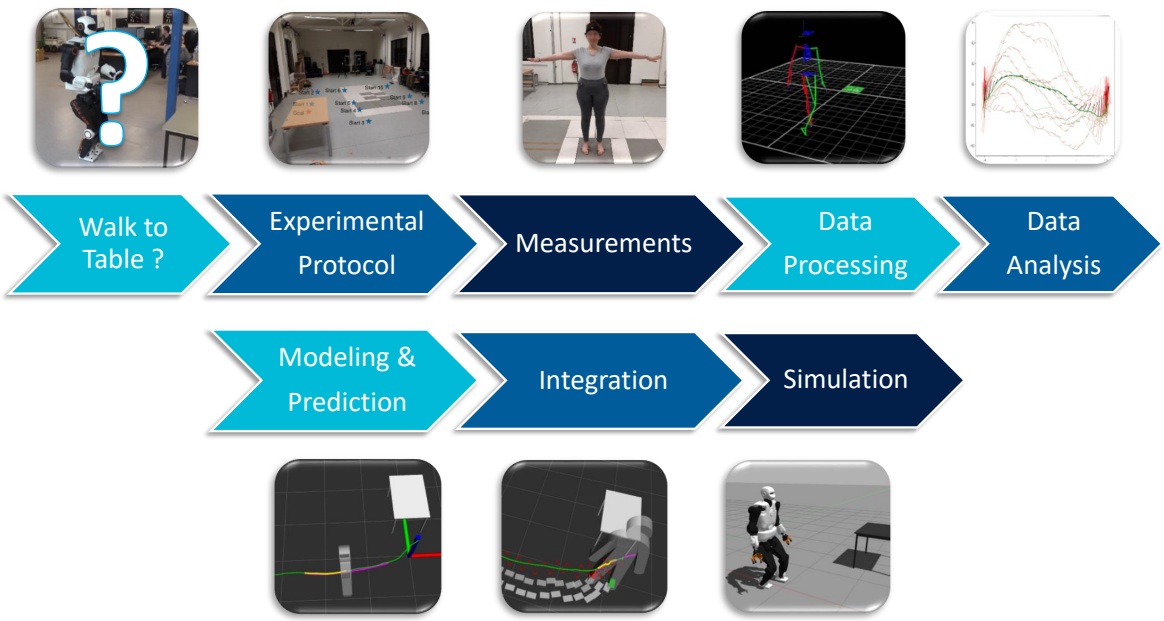

The first part of this thesis focuses on the reduced problem, namely the study of single walking humans' trajectories. This work aims to develop a method to embed a human locomotion model in a humanoid robot walking pattern generator. Such embedding is expected to make the robot more reactive in the context of a human-robot interaction.

This part is divided into three chapters. In Chapter 1, an accurate model of human trajectories during locomotion is developed using an optimal control problem. Then, in Chapter 2, this model is adapted to predict the future trajectory of single walking humans in real-time. Finally, in Chapter 3, this prediction model is coupled with the robot's footsteps planner to achieve in simulation a proactive co-navigation task.

Chapter 1

Single Human Locomotion

Contents

1.1 Introduction

1.1.1 Motivations

Making a robot actively cooperate with a human requires a good knowledge of human behaviour. Thus, as part of the ANR-CoBot project, models of human walking trajectories and forces applied by the human on the table are needed to allow the robot to assist its human partner in real-time. This chapter focuses on the first step of this co-manipulation task, namely reaching the table. This work aims to study, model and generate human trajectories during locomotion. The way humans walk with a table or interact to carry a table will be handled in Part II.

Being able to generate human-like trajectories has three main benefits in the context of the ANR-CoBot project. First, evidences of better HRIs under various forms of human control were already demonstrated by Sheridan [15]. Thus, we hypothesize that an accurate understanding and model of human locomotion will help the human partner to understand where the robot's endpoint is. Then, an accurate model of human walking trajectories could be useful to predict human behaviour. Such a prediction could help the robot to anticipate its partner's motions. Finally, single human locomotion is a more widely studied topic than pair locomotion, which means that numerous models and methods already exist to simulate a single human gait. Thus, the goal of this study is to develop a model which accurately fits human walking trajectories and reproduce the same method, later, to generate the trajectories of two humans carrying a table.

1.1.2 Related Works

1.1.2.1 Human locomotion

In biomechanics, numerous authors studied healthy human gait [16, 17]. Some authors were interested in human walking trajectories, especially during collision or obstacle avoidance [18, 19] while others studied and modeled the human joint trajectories during gait [20, 21]. Some more recent studies focused on the trajectories of human walking in crowded environment [22, 23, 24, 25]. Moreover, single walking human trajectories were recorded in various environments, with or without obstacles, to investigate the effect of the goal distance [26], the foot placements [27] or the relationship between the head and the trunk movements [28] for example.

Furthermore, numerous works focused on the modeling and the simulation of single walking humans. Those studies went from the simulation of a 3D whole-body skeletal model with 42 DoFs [29] or more basic 2D or 3D models [30] to the mere simulation of the CoM trajectory [31, 32, 33]. In this work, we choose to stick to a simple CoM trajectory model for two reasons. First, the more complex the models are, the higher the computational costs are. Then, to achieve our final goal, we only need the robot to know where its human partner is going in real-time. In our case, choosing an elaborate model would bring non-required information such as the human arm motions during gait and might prevent a real-time application due to a too high computation time. Thus, in what follows, the focus is on the existing trajectory models.

The generation of a path between a starting and a goal position was also a commonly tackled problem in robotics. For mobile wheeled robots, numerous ways have been introduced to generate paths. The easiest one was following a straight line, while more complicated

ones included B-splines [34] or curves generated with an Optimal Control (OC) model called the unicycle model [35, 36]. For humanoid robots, some solutions used parametric curves called clothoids [37] or curves generated with an OC model based on Inverse Optimal Control (IOC) [38]. As they were commonly used to generate human-like trajectories in the literature, the unicycle model, the clothoid-based model and the OC model will be detailed in Sec.1.3.

1.1.2.2 Inverse optimal control

An OC problem computes the optimal behaviour of autonomous systems with a given dynamics. However, nothing ensures the optimality of the parameters of the OC problem [39]. Those parameters could be of different nature according to the targeted problem. For example, to optimize a robot design, those parameters could be physical features of the studied system, like its mass or its size [40]. While, to model a human behaviour, they could be the weights of the jerk, the acceleration, the torque or the energy of the system in the objective function [41]. To guarantee that the computed optimal behaviour is the expected behaviour, these parameters need to be optimized beforehand. The optimization of the parameters of an OC problem is called IOC. For example, if one wants to model a human behaviour, IOC can allow to compute the OC parameters which best reproduce the measurements of this particular behaviour. In the literature, multiple methods have been proposed to solve this kind of problem. Here is a quick review of some of those methods.

First of all, each IOC algorithm can fall into one of these two formulations [42]:

- Classic IOC:

$$\phi = IOC(X, U)$$

  with X the state, U the control and ϕ the cost function an OC problem of the following form:

$$\min_{X,U} \int_0^T \phi(X(t), U(t))\mathrm{d}t$$

- Modern IOC also called Inverse Reinforcement Learning (IRL):

$$R = IOC(S, A)$$

  with S the state, A the action and R the reward function of a Markov Decision Process (MDP) of the following form:

$$\max_{\pi} E(\sum_t \gamma^t R(S_t, A_t)|\pi)$$

  with π the optimal policy.

Classic inverse optimal control

Classic IOC were used to model a wide range of behaviours: human arm motions during screwing task [41, 43], reaching tasks [44], yoyo playing [45], human walk [46, 47], etc. Moreover, numerous approaches exist to solve these kinds of IOC problems.

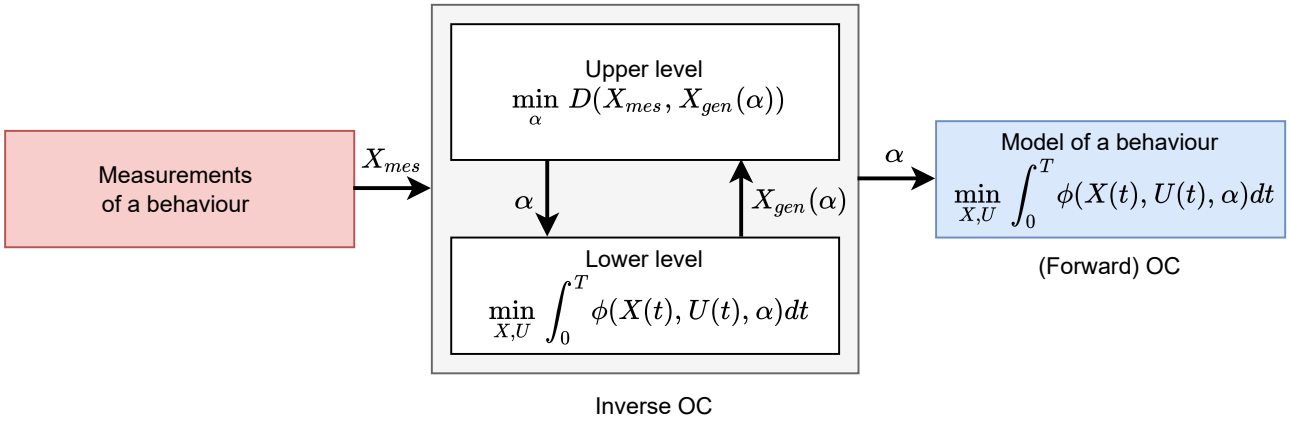

Figure 1.1: Bi-level optimization problem. In this graph, α is the parameter of the OC problem to be optimized and D is the IOC cost function.

Bi-level optimization. IOC problems can be treated as bi-level problems. The optimization of the OC parameters is done in the upper level. The goal of this optimization level is to compute the optimal parameters to improve the likeness of the generated behaviour with respect to the expected behaviour which was measured beforehand [46]. Commonly, the cost function of the upper level problem is a Root Mean Square Error (RMSE) between the generated and the measured data. Derivative-free methods [45, 46, 48] or genetic algorithms [40, 41, 49] can be used to solve the upper level problem. The lower level deals with generating new data with the optimized parameters given by the upper level. This bi-level formulation is represented in Fig.1.1. In the literature, the upper and lower levels can also respectively be called outer and inner optimizations.

In this work, we choose to solve our IOC problem with a bi-level approach as it is easy to understand and to implement thanks to multiple libraries which already implemented derivative-free methods or genetic algorithms. However, we could have also used other methods, such as the ones shortly described below.

Karush-Kuhn-Tucker (KKT) conditions. IOC problems can also be formulated as one-level problems by turning the lower level problem into a KKT system. In this approach, the parameters of the OC problem can be recovered by minimizing the residual functions based on the KKT conditions [50]. This approach was implemented in multiple works [43, 51, 52]. This method was also proposed to solve problems with time-varying objectives [53]. This is relevant for the modeling of complex motions where the control may change during the motion, like jumping motions.

Other methods of classic IOC can be cited, like the Pontryagin's minimum principle [54] and the Hamilton-Jacobi-Bellman equations [55, 56].

Inverse reinforcement learning

IRL is another formulation of IOC based on probabilistic models. IRL approaches aim to learn an unknown reward function of a MDP from expert's demonstrations [57]. This kind of approaches uses a probabilistic model of the expert's behaviour, like the maximum

entropy IRL model [58] for example. A quantity named the log likelihood is, then, computed. Maximizing this quantity amounts finding the reward function which leads to the most likely actions in a given state. Complex behaviours like human locomotion [59] or human reaching motions in shared workspace [60] or highway driving behaviours [61] can, thus, be learned.

1.1.3 Contributions

In the context of the ANR-CoBot, which aims at carrying a table, we want the robot to, first, walk toward the table in a human-like way and to stop at a comfortable distance to handle it. A comfortable distance refers to a distance short enough for the robot to grab the table but large enough not to risk any collision with the table. In our case, it is around 0.8 m. Thus, we need an accurate and generic model of human locomotion. The goal of this chapter is to improve the simulation of human trajectories during locomotion compared to the previous papers published on this topic with more modalities of distance and orientation.

First of all, the experiments carried out to measure human trajectories are introduced in Sec.1.2. The CoM trajectories of 10 different subjects were recorded using a MoCap. In the wake of those experiments, a database of 400 CoM trajectories of single walking humans was created.

Then, in Sec.1.3, two existing models were chosen to be implemented because they are both recognized as good approximations of human CoM path during locomotion. Their results were compared to the measured trajectories. As part of this study, a metric was defined to provide a numerical assessment.

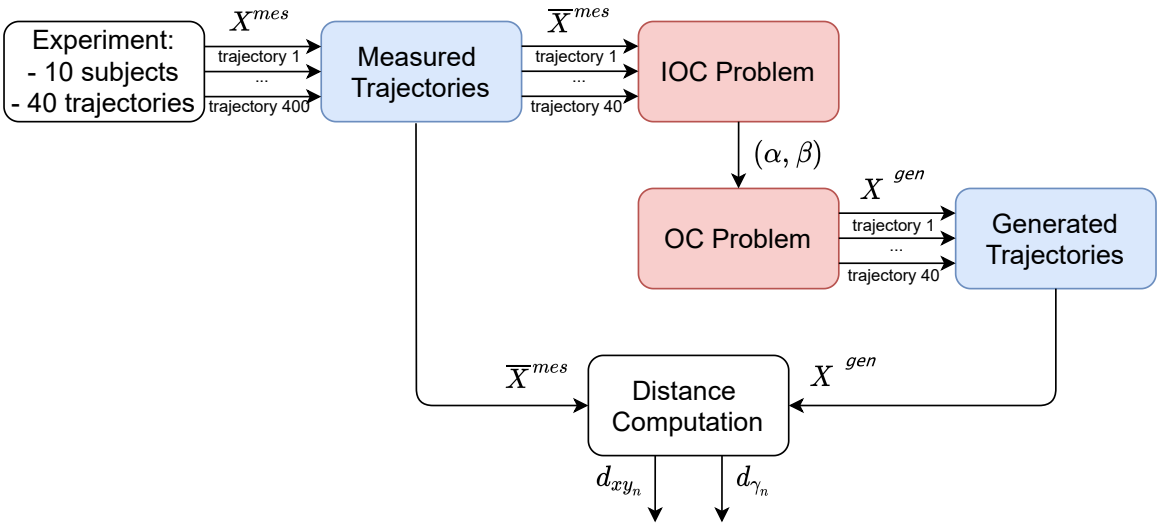

Figure 1.2: Description of the whole framework presented in Sec.1.4.The notations introduced in this chart are defined throughout the chapter.

Finally, in Sec.1.4, a novel IOC scheme was used to find a suited cost function which allows an OC model, first introduced in Mombaur et al. [38], to generate trajectories which accurately fit the 400 experimental trajectories. The developed model aims to compute both the position and the orientation of a human-like system between any starting position and a goal position. In order to assess this new OC model, the previously defined metric was used to measure

the distance between the experimental and the generated trajectories. The whole framework developed in this last section is shown in Fig.1.2. We hypothesize that this new model will be more efficient and accurate than the previous ones according to the defined metric. We believe this model will allow to better predict human behaviour and improve humanoid robot-human cooperation.

This work was published in **Maroger** et al. [1, 2, 3]. Moreover, the implementation of all the presented models uses open-source softwares with the aim to ease reproducibility. The data base of human CoM trajectories and the code of the models are available on: `https://github.com/imaroger/walking_human_trajectory_models`.

1.2 Experiments

In this section, we present the experiments performed in order to create a database of human walking trajectories. During these experiments, CoM trajectories of single humans walking without constraints were recorded. The goal of this study is to measure multiple typical trajectories in order to build an accurate and universal model of human walking trajectories.

1.2.1 Participants

Ten subjects (8 males and 2 females) volunteered for this study with a mean ($\pm$ standard deviation) age of 23.30 $\pm$ 2.32 years, height of 1.77 $\pm$ 0.06 m and mass of 73.90 $\pm$ 12.59 kg. They all have no pathological disorders or medical conditions likely to alter their gait. Every participant was informed of the experimental procedure and gave its written consent before the experiment. However, they were not informed of the expected results in order to preserve their natural behaviour. These experiments were conducted at the Centre de Ressources d'Expertise et de Performance Sportive (CREPS) in Toulouse (France) in accordance with the declaration of Helsinki and with the approval of the University of Toulouse ethical committee.

1.2.2 Experimental protocol

The participants were instructed to walk from 10 starting positions with 4 different starting orientations ($\theta_0 = \{-\frac{\pi}{2}, 0, \frac{\pi}{2}, \pi\}$ rad) to one goal position placed in front of a table always with the same orientation ($\theta_f = \frac{\pi}{2}$ rad). These positions are represented on Fig.1.3a. The subjects were asked to freely walk at a self-selected normal speed. The starting positions were chosen to measure a set of typical locomotion path within a range of 0.6 to 5.5 m from the goal. The distance between the starting position and the goal position is denoted $d_{Start/Goal}$ and called *global distance* in what follows.

1.2.3 Data collection

In order to record the kinematics data of the subjects during locomotion, 14 passive markers were fixed on the participants: 4 on their pelvis, 3 on each of their foot and 4 on the head, as Fig.1.4 shows. The 3D positions of these markers were collected thanks to a MoCap (15

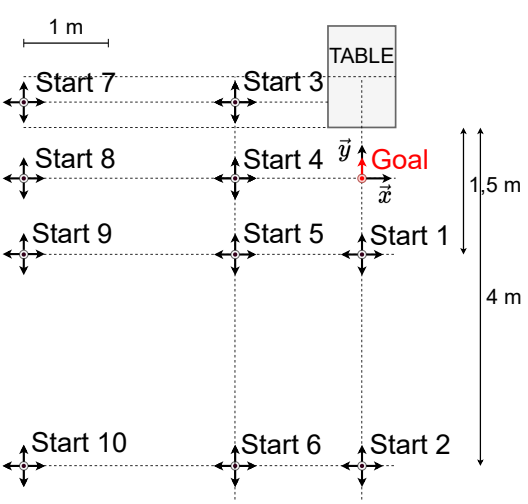

(a) Representation of the 10 starting positions and the goal position with their orientations

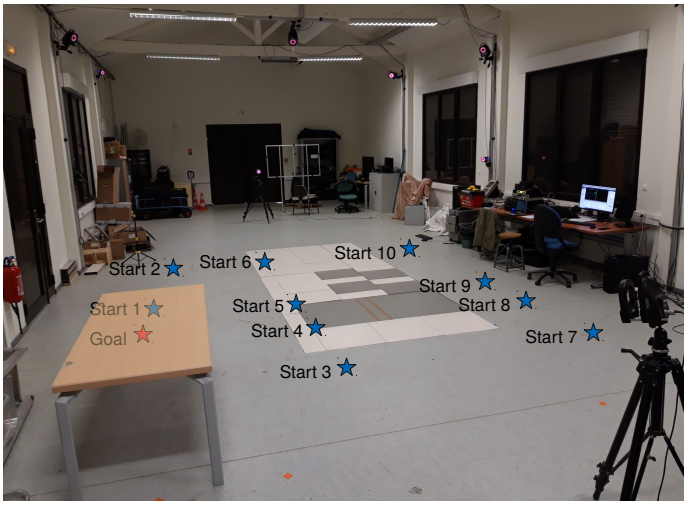

(b) Laboratory configuration

Figure 1.3: Experimental setup.

infrared VICON cameras sampling at 200 Hz). Then, the horizontal CoM position (x, y) was approximated by the barycentre of the trapeze shaped by the 4 markers placed on the pelvis, 2 on the antero-superior iliac spine (ASIS) and 2 on the postero-superior iliac spine (PSIS) [62]. The global orientation of the pelvis θ was computed as the angle between the global frame and the normal vector $\vec{n}$ to the segment between the two markers placed on the ASIS. The local orientation of the pelvis γ was computed as the angle between $\vec{n}$ and the velocity vector $\vec{V}$ which is tangent to the trajectory. Those vectors and angles are represented in Fig.1.5. The position of the other markers was recorded but was not analyzed afterwards. The laboratory configuration is represented in Fig.1.3b.

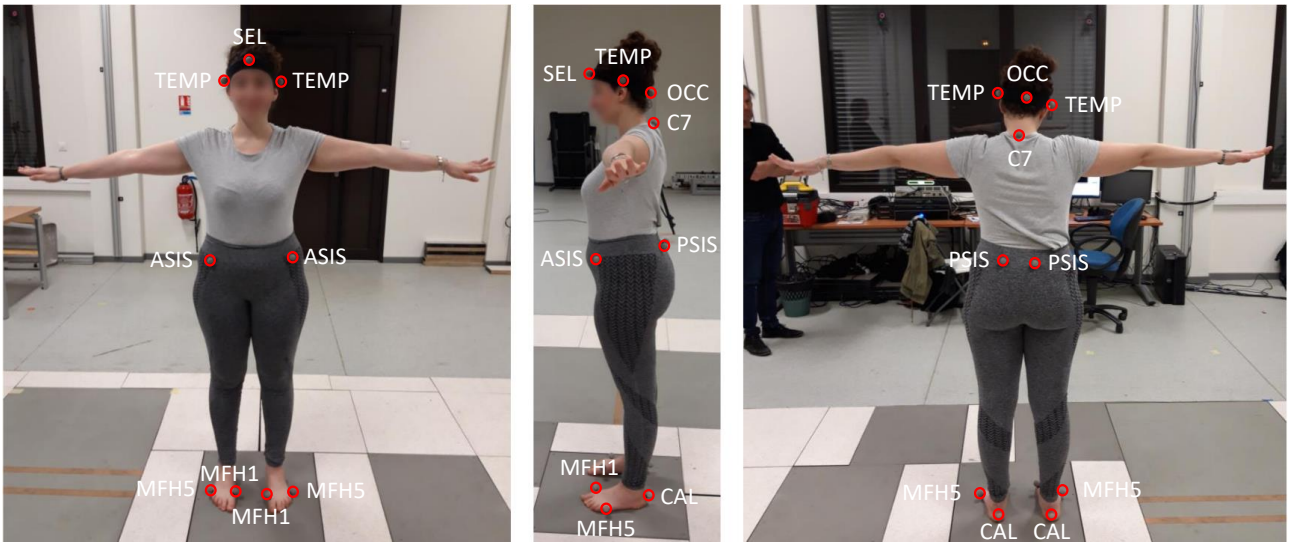

Figure 1.4: Passive markers fixed on the subjects. The markers' names match the names used for the whole body skeletal model described in Maldonado et al. [63] based on the recommendations of the International Society of Biomechanics (ISB).

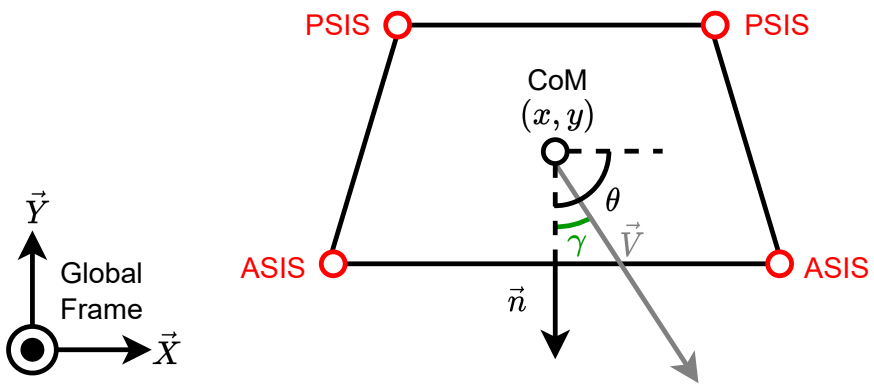

Figure 1.5: Representation of the trapeze shaped by the 4 markers placed on the subjects' pelvis.

1.2.4 Data processing

Kinematics data were filtered with a 4th order, zero phase-shift, low-pass butterworth with a 10 Hz cutoff frequency. Moreover, all the CoM trajectories were normalized from 1 to 100% with a step of 0.1. Then, for every of the 40 possible paths, from a starting position with one of the 4 orientations to the goal, a reference human trajectory was defined as the mean of the measured trajectories: $\bar{X}_i^{mes} = \frac{1}{10}\sum_{j=1}^{10} X_{i,j}^{mes}$ where $X_{i,j}^{mes} = (x_{i,j}^{mes}, y_{i,j}^{mes}, \gamma_{i,j}^{mes})$ with $j \in [1, 10]$ standing for the j^{th} subject and $i \in [1, N]$ with $N = 1000$ for the i^{th} point along the trajectory. This trajectory is called the *average human trajectory*. One example of such an average trajectory is represented in Fig.1.6

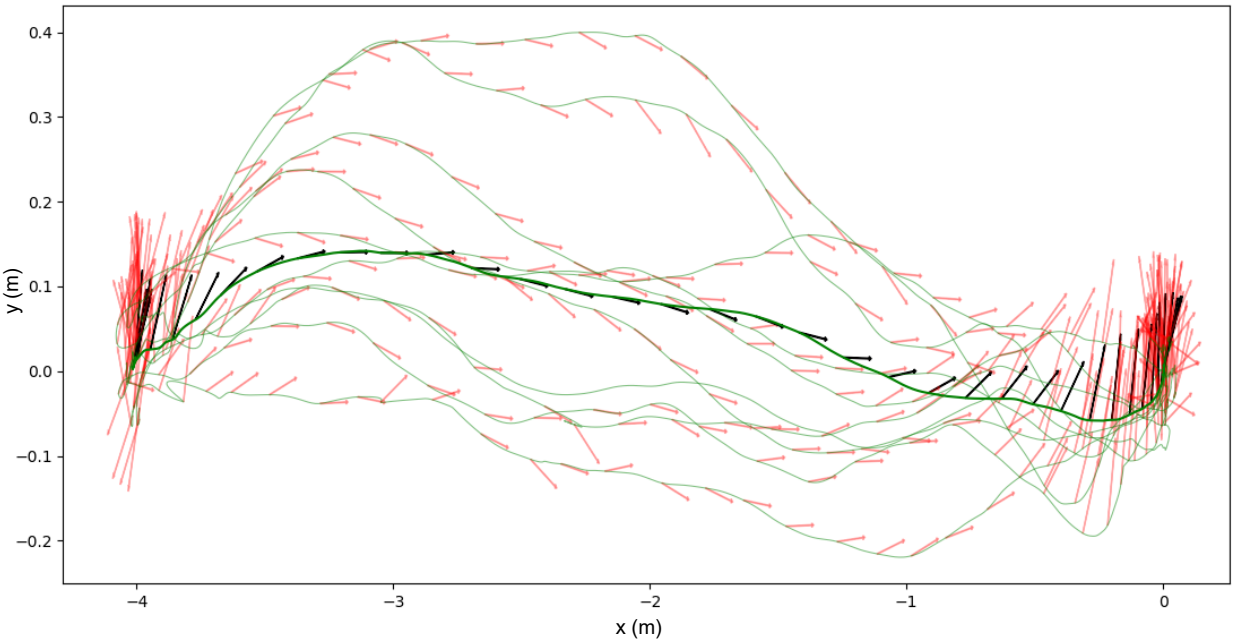

Figure 1.6: Average trajectory (*bold green*) computed from the measured trajectory performed by the subjects (*light green*) between Start 8 (see Fig.1.3a) with $\theta_0 = \frac{\pi}{2}$ rad. The arrows represent the global orientation of the pelvis during locomotion.

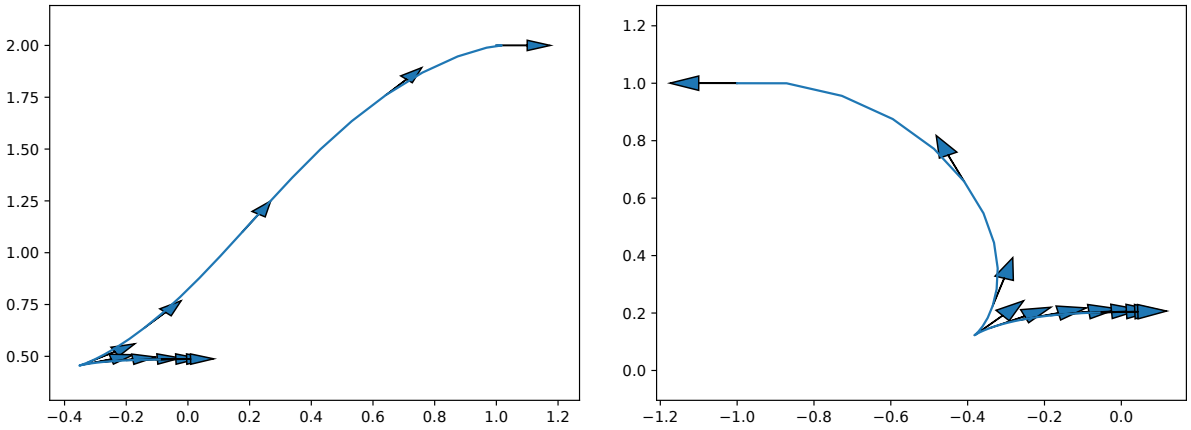

Figure 1.7: Non-holonomic trajectories with a cusp generated with the unicycle model.

1.3 Human-like locomotion models

Before introducing a new model of human CoM trajectory, it is essential to look for existing models in the literature. The goal of this section is to present the related works and to implement the most relevant ones. Then, we will compare the generated trajectories to the measurements in order to determine which model is the most human-like. This comparison was published in **Maroger** et al. [2, 3].

1.3.1 Unicycle model

First of all, it has been shown that humans can frequently be approximated by non-holonomic systems as they usually walk forward with the direction of their body (the vector $\vec{n}$ in Fig.1.5) tangent to their trajectory [31, 32]. Biologically, this can be explained by the anatomy of feet and legs. The non-holonomic locomotion problem, also known as the unicycle problem, is a well-known research topic in mobile wheeled robots [36]. However, the sideways motions are not taken into account by non-holonomic models. Moreover, the unicycle model can generate trajectories with cusps, as Fig. 1.7 shows, far from human-like behaviour.

1.3.2 Clothoid-based model

Then, clothoid curves (also known as Cornu spirals) are frequently used for path-smoothing in robotics [64, 65, 66] and to mimic human CoM path during locomotion. Indeed, clothoid curves are interesting to generate trajectories because it has been demonstrated that clothoid arcs give good approximations of human trajectories during gait [67]. A clothoid satisfies the following system of ordinary differential equations:

$$\begin{cases} \dot{x}(s) = \cos\theta(s) \\ \dot{y}(s) = \sin\theta(s) \\ \dot{\theta}(s) = \kappa_0 + \kappa_1 s \end{cases} \tag{1.1}$$

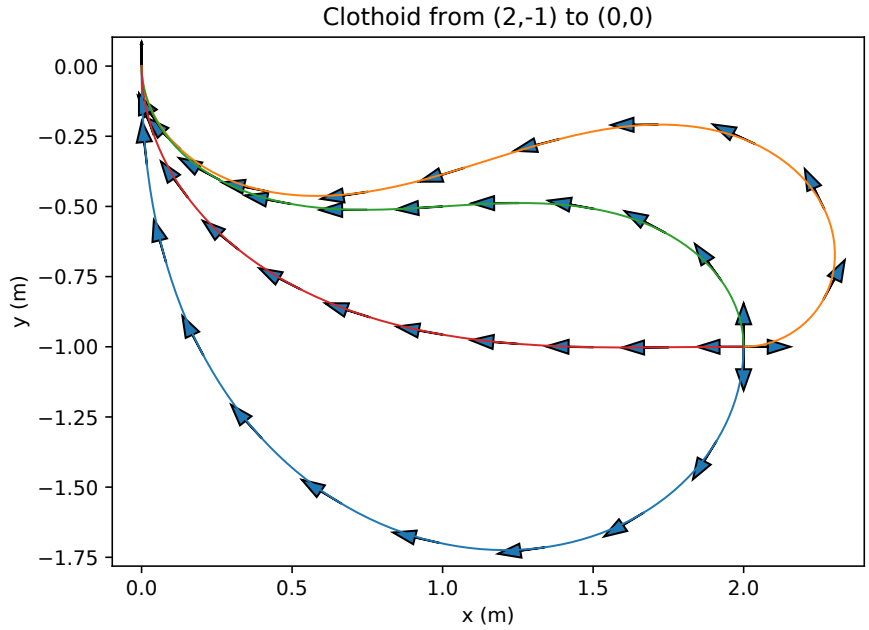

Figure 1.8: Clothoids from $(2, -1, -\frac{\pi}{2})$, $(2, -1, 0)$, $(2, -1, \frac{\pi}{2})$ and $(2, -1, \pi)$ to $(0, 0, \frac{\pi}{2})$ generated with a fitting algorithm *(respectively in blue, orange, green and red).*

with the following initial conditions: $x(0) = x_0$, $y(0) = y_0$ and $\theta(0) = \theta_0$. κ_0 is the initial curvature, κ_1 the sharpness of the curve and s the curvilinear abscissa. From this system, the parametric expressions of a clothoid coordinates can be define:

$$\begin{cases} x(s) = x_0 + \int_0^s \cos\left(\theta_0 + \kappa_0\xi + \frac{1}{2}\kappa_1\xi^2\right)d\xi \\ y(s) = y_0 + \int_0^s \sin\left(\theta_0 + \kappa_0\xi + \frac{1}{2}\kappa_1\xi^2\right)d\xi \end{cases} \tag{1.2}$$

Thus, one of the advantages of the clothoid curves is their linearly changing curvature, which allows an easy control of the trajectory curvature. However, due to their nature of transcendental curves, they cannot be solved analytically and the computational time remains important. In the robotics experiments with this model, we suppose that human behaviour follows Eq.1.1.

As the starting position and orientation of the robot and its goal position and orientation are known, a fitting method, described in Bertolazzi et al. [68], has been used to generate a clothoid arc between these two poses. This fitting method finds κ_0 and κ_1 so that the generated clothoid is computed between the desired starting and goal positions. Four examples are shown in Fig.1.8. In this figure, the arrows represent the current orientation of the system during the gait.

1.3.3 Optimal control model

The two previously described models are non-holonomic models. With those models, it is only possible to simulate locomotor systems which always move forward, never sideways. Nevertheless, as explained in Mombaur et al. [38], humans can also take oblique steps to avoid obstacles or go to close goals. Thus, holonomic locomotion models allow more degrees of freedom in the

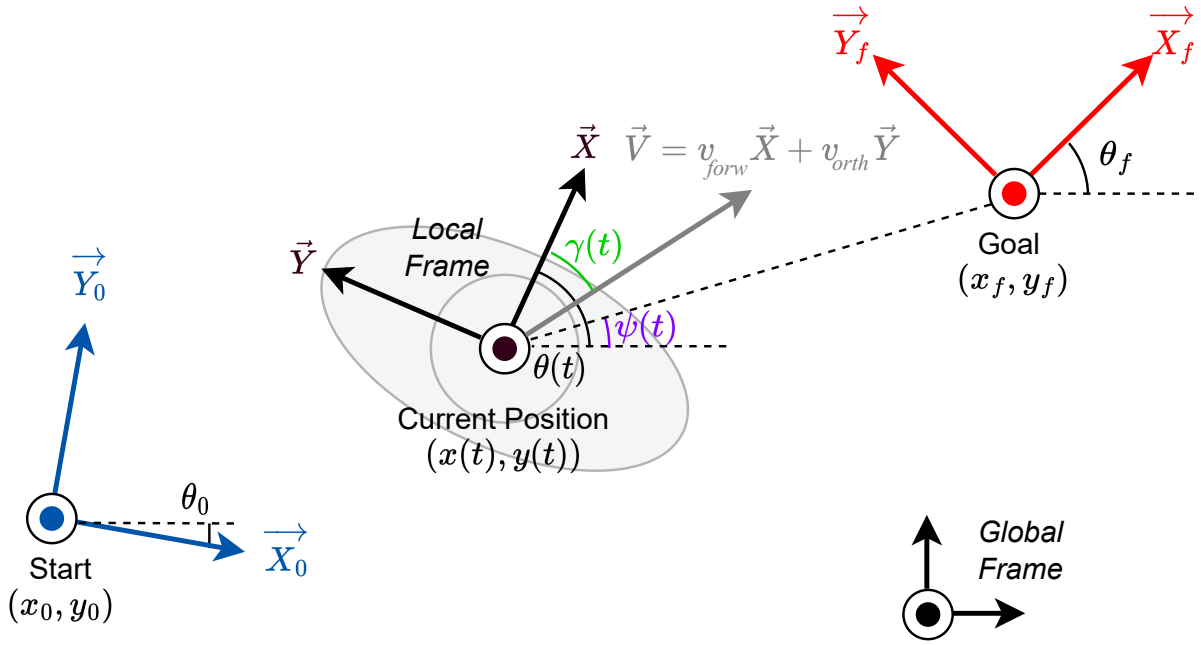

Figure 1.9: Representation of the coordinate systems and variables at stake in the OC problem to solve.

human gait, like the one described in Mombaur et al. [38], and should better describe human locomotion. In their work, a human subject is considered to be a full holonomic locomotor system with the following dynamics:

$$\begin{cases} \dot{x} = \cos\theta.v_{forw} - \sin\theta.v_{orth} \\ \dot{y} = \sin\theta.v_{forw} + \cos\theta.v_{orth} \\ \dot{\theta} = \omega \\ \dot{v}_{forw} = u_1 \\ \dot{v}_{orth} = u_2 \\ \dot{\omega} = u_3 \end{cases} \tag{1.3}$$

(x, y) is the position of the human CoM in the horizontal plane. θ is the postero-anterior orientation of his pelvis in a global frame. v_{forw} and v_{orth} are the forward and sideways velocities of the subject CoM in the local frame, in other words they are the tangent and orthogonal velocities with respect to the orientation of the pelvis. ω is his angular velocity. All the frames and variables involved here are represented in Fig.1.9. In what follows, u_1, u_2 and u_3 are respectively named the forward, the orthogonal and the angular accelerations. This dynamics does not take into account the medio-lateral oscillations due to the steps. It only allows us to generate smooth CoM trajectories.

In Mombaur et al. [38], the authors introduce an OC model of the following form:

$$\min_{X(.),U(.),T} \int_0^T \phi(X(t), U(t))\mathrm{d}t \tag{1.4}$$

under the following constraints:

$$\begin{cases} \dot{X}(t) = f(X(t), U(t)) & \text{Dynamical constraint (Eq.1.3)} \\ X(0) = X_0 & \text{Initial constraint} \\ X(T) = X_f & \text{Final constraint} \end{cases} \tag{1.5}$$

As part of the formulation of the OC model, $X = (x, y, \theta, v_{forw}, v_{orth}, \omega)^T$ is called the state and $U = (u_1, u_2, u_3)^T$ is called the control. The aim of the OC problem is to find the optimal state, from which can be deduced the position (x, y) and the orientation θ of the CoM, along a trajectory between a start $X_0 = (x_0, y_0, \theta_0, 0, 0, 0)$ and a goal positions $X_f = (x_f, y_f, \theta_f, 0, 0, 0)$.

Moreover, $\phi(X(t), U(t)) = \sum_{i=0}^{n-1} \alpha_i \phi_i(X(t), U(t))$ is an a priori unknown cost function with n the number of base functions needed to describe the cost function. Mombaur et al. [38] find out that the cost function that best fitted their measurements of human locomotion trajectories is:

$$\phi(X(t), U(t)) = \alpha_0 + \alpha_1 u_1^2(t) + \alpha_2 u_2^2(t) + \alpha_3 u_3^2(t) + \alpha_4 \psi(X(t), X_f)^2 \tag{1.6}$$

The function $\psi(X(t), X_f) = \arctan \frac{y_f - y(t)}{x_f - x(t)} - \theta(t)$ is the difference between the current orientation of the system and the angular difference between the orientation of the system and of its target. Thanks to this ψ function, there is no symmetry between back and forth trajectories. This is representative of human locomotion, as humans usually do not take the same path going from a start to a goal and from this goal to this start [38]. Then, the cost function weights were computed using IOC in Mombaur et al. [38], they are $(\alpha_0, \alpha_1, \alpha_2, \alpha_3, \alpha_4) = (1, 1.2, 0.7, 1.7, 5.2)$.

In this work, we adapt this OC problem in order to solve it with a Differential Dynamic Programming (DDP) solver [69] from the open-source Crocoddyl library [70]. For the interested reader, more details on the DDP algorithm are given in Tassa et al. [69]. The specifications of the implementation used here are given in Mastalli et al. [70]. This adaptation was a necessity as it seems that the Muscod software [71], which was used in Mombaur et al. [38], is discontinued.

As a DDP solver is an unconstrained OC solver, the cost function needs to be changed in order to satisfy the equality constraints in Eq.1.5. The dynamic of the system is given to the action model, the initial state is one of the parameters given to the shooting problem, so we just need to add a term to the cost function to take into account the final state. Eq.1.6 becomes:

$$\begin{aligned}\phi(X(t), U(t)) = \alpha_0 + \alpha_1 u_1^2(t) + \alpha_2 u_2^2(t) + \alpha_3 u_3^2(t) + \alpha_4 \psi(X(t), X_f)^2 \\ + \alpha_5((x_f - x(t))^2 + (y_f - y(t))^2) + \alpha_6(\theta_f - \theta(t))^2\end{aligned} \tag{1.7}$$

where the weights $\alpha_5 = 5$ and $\alpha_6 = 8$, have been heuristically found.

In this study, as the duration time T of the trajectory cannot be a free variable in the Crocoddyl solver, we solve a similar problem. Eq.1.4 becomes:

$$\min_{X(.), U(.)} \int_0^T \phi(X(t), U(t)) \mathrm{d}t \tag{1.8}$$

Physically, T represents the duration in which the locomotor system will perform the trajectory. As we want a realistic duration, we choose T close to $\Delta t = \frac{d}{v}$ with $d = \sqrt{(x_f - x_0)^2 + (y_f - y_0)^2}$ and v the nominal speed of the system. As the path is necessarily longer than the straight line, T is assumed to be between Δt and $\Delta t + 200$. Then, we take this range with a step of 5s the T for which the problem is solved and the cost function is minimal. Thus, smoothed CoM trajectories can be computed along time and the velocity profiles can be deduced. Four trajectory examples obtained with this model are shown in Fig.1.10.

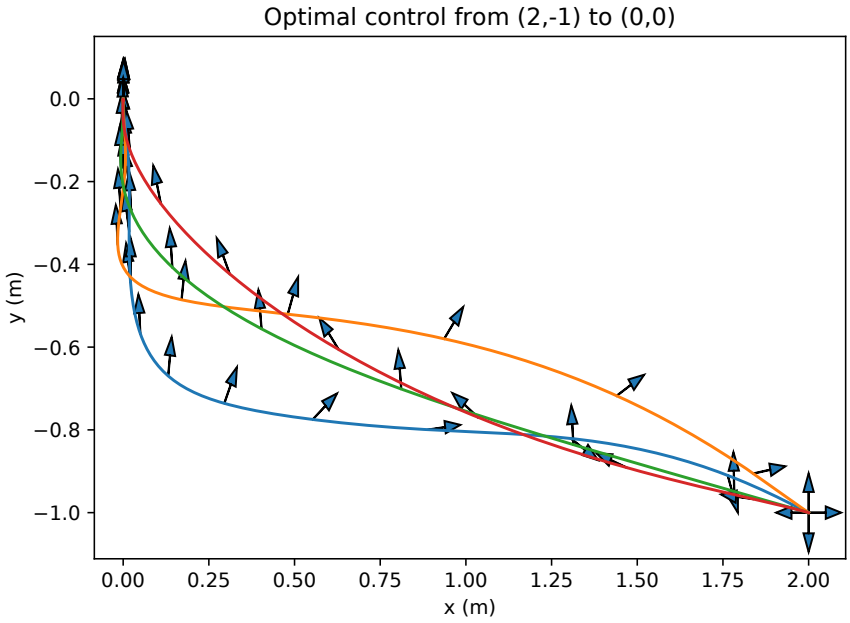

Figure 1.10: Trajectories from $(2, -1, -\frac{\pi}{2})$, $(2, -1, 0)$, $(2, -1, \frac{\pi}{2})$ and $(2, -1, \pi)$ to $(0, 0, \frac{\pi}{2})$ generated with an OC model adapted from Mombaur et al. [38] *(respectively in blue, orange, green and red)*. The arrows represent the current orientation of the system during the gait.

1.3.4 Comparison between the models and the measurements

1.3.4.1 Metric definition

In Section 1.2, we measured human CoM trajectories between 40 starting positions and one goal position. Now, that we have implemented the clothoid-based model and the OC model, we can generate paths between the same starting and goal positions as the average measured trajectories, as Fig.1.11a and Fig.1.11b show. Let us denote that, these plots are drawn so that the goal position is the origin of the frame. A few examples of comparison between the generated trajectories and the average measured trajectories are shown in Fig.1.12. Then, to compare those trajectories, we need to define a way to assess which model better fits the human data. So we need to measure the "closeness" between the experimental and the generated trajectories. Thus, we define a distance between measured and generated trajectories similar to the one proposed in Arechavaleta et al. [32]. The following distances can be computed:

$$\begin{cases} d_{xy} = \frac{1}{N} \sum_{i=1}^{N} \sqrt{(\bar{x}_i^{mes} - x_i^{gen})^2 + (\bar{y}_i^{mes} - y_i^{gen})^2} \\ d_\theta = \frac{1}{N} \sum_{i=1}^{N} |\bar{\theta}_i^{mes} - \theta_i^{gen}| \end{cases} \tag{1.9}$$

$(\bar{x}^{mes}, \bar{y}^{mes})$ is the average human trajectory over one path and (x^{gen}, y^{gen}) is the corresponding generated trajectory. $\bar{\theta}^{mes}$ is the average human orientation over one path in the global frame. θ^{gen} is the generated orientation along the trajectory.

In concrete terms, d_{xy} represents the mean distance between two trajectories and d_θ the mean angle between the experimental and the generated pelvis orientation. In the rest of the manuscript, d_{xy} and d_θ are, respectively, called *linear* and *angular distances*. Fig.1.13 shows the computation of the linear distance for one trajectory generated by both models.

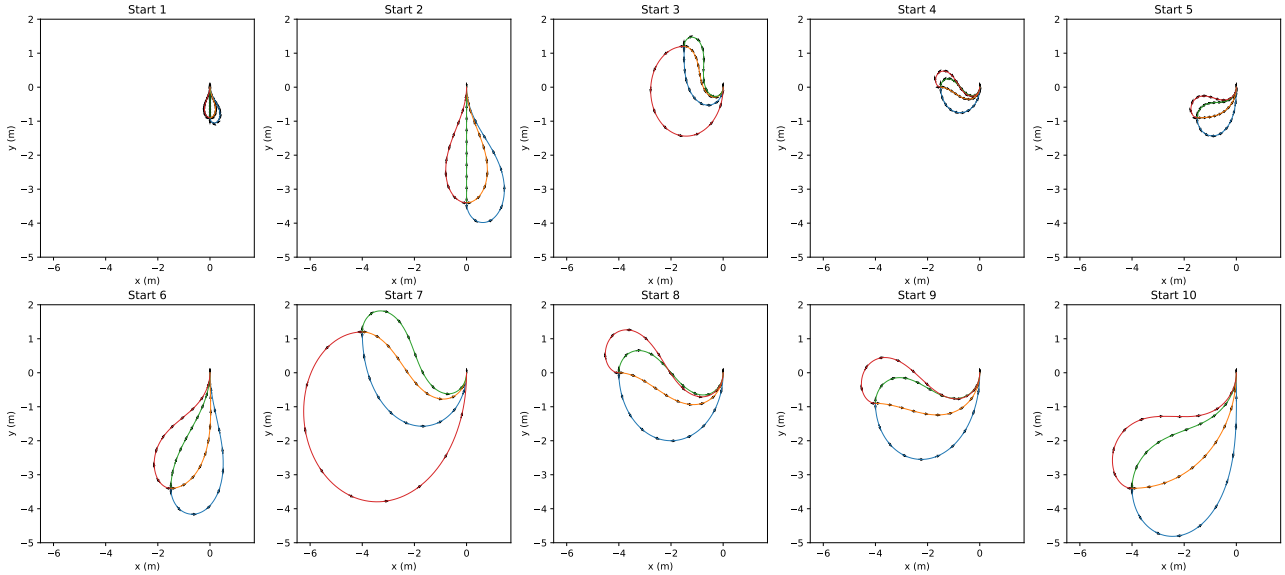

(a) Clothoid-based model

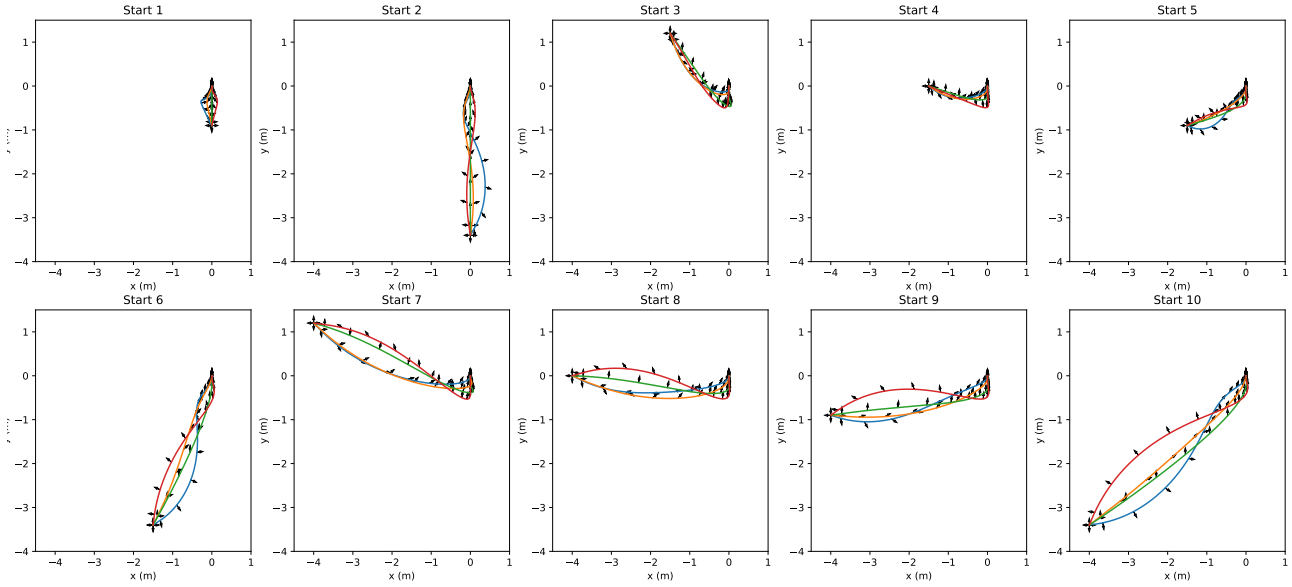

(b) OC-based model

Figure 1.11: Generation of all the trajectories with the same starting and goal positions than during the experiments. The goal position always is $(x_f, y_f) = (0, 0)$ with $\theta_f = \frac{\pi}{2}$ rad. On each plot, there is one trajectory per starting orientation ($\theta_0 = -\frac{\pi}{2}$ rad in *blue*, $\theta_0 = 0$ rad in *orange*, $\theta_0 = \frac{\pi}{2}$ rad in *green* and $\theta_0 = \pi$ rad in *red*).

To assess a trajectory generated with one model, we stated that the best generated trajectory minimizes the distances d_{xy} and d_θ. Furthermore, we hypothesized here that the best model is the one which lowers the mean distances over all the paths, namely $\bar{d}_{xy} = \frac{1}{N_{traj}} \sum_{n=1}^{N_{traj}} d_{xy_n}$ and $\bar{d}_\theta = \frac{1}{N_{traj}} \sum_{n=1}^{N_{traj}} d_{\theta_n}$ with $N_{traj} = 40$. Those mean distances are called *linear* and *angular errors*.

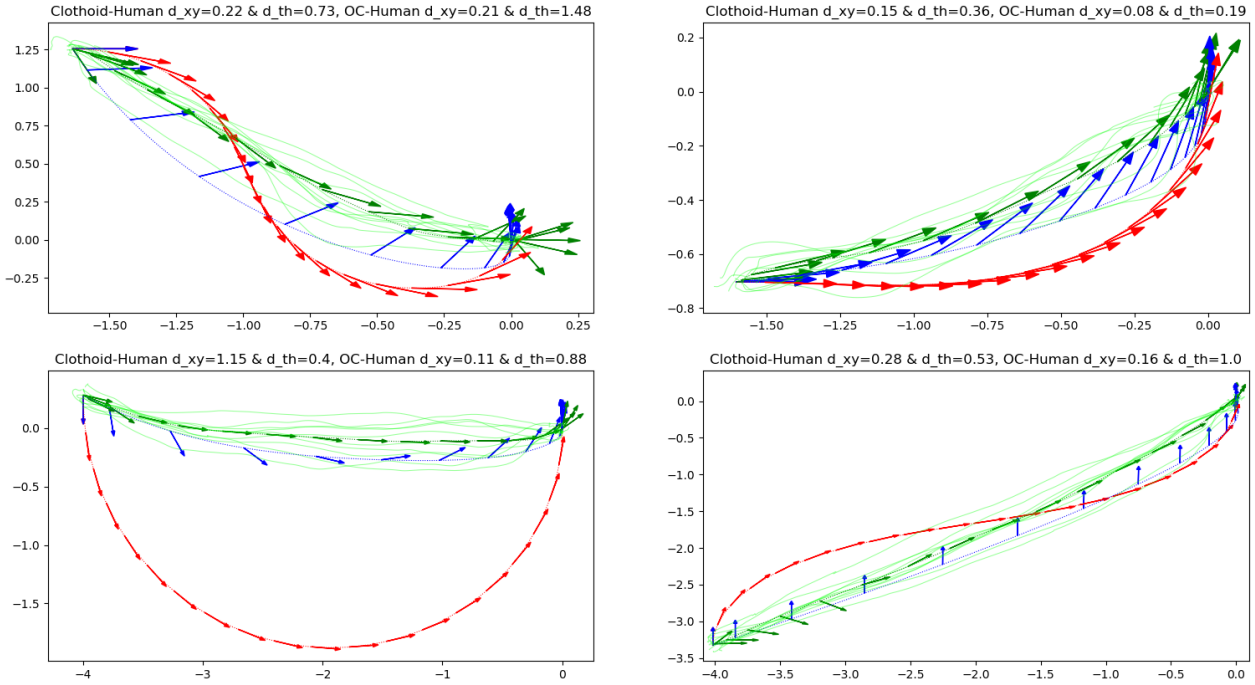

Figure 1.12: Examples of comparison between the 2 presented models (clothoid in *red* and OC in *blue*) and measurements on 10 subjects (average trajectory in *bold green* and measured trajectories in *light green*) for starts 7, 8, 9 and 10.

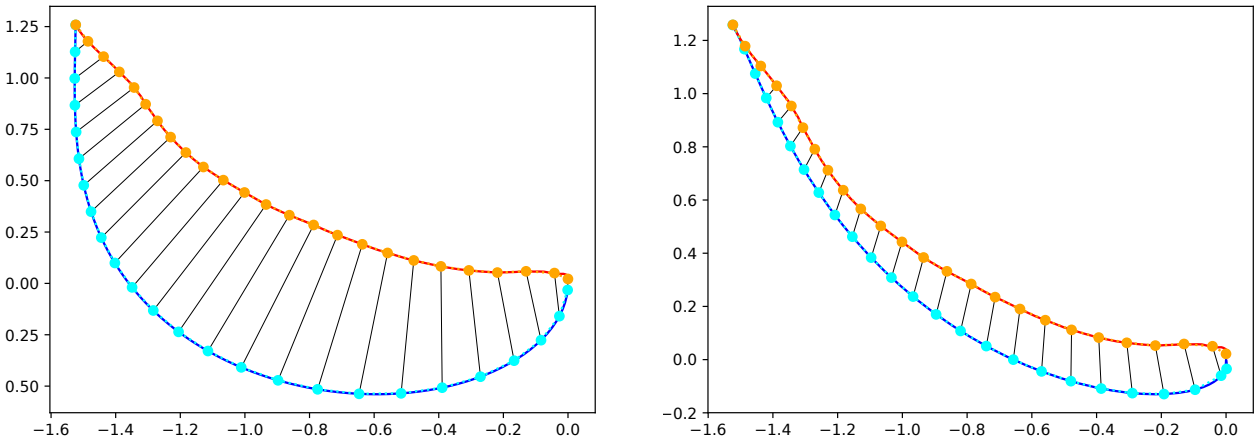

(a) Clothoid model ($d_{xy} = 0.456\,\mathrm{m}$)

(b) OC model ($d_{xy} = 0.124\,\mathrm{m}$)

Figure 1.13: Linear distance between a measured (*blue*) and a generated (*orange*) trajectory with $N = 25$.

1.3.4.2 Distance computation

The computed errors between both models and the average measurements are represented in Tab.1.1. These results demonstrate that the OC model better fits the geometric trajectory. However, the clothoid-based model describes better the evolution of the orientation of the pelvis during gait. Indeed, during most of the gait, the orientation of the pelvis is overall tangent to the trajectory, which is compatible with a non-holonomic model like the clothoid-based one. Nevertheless, as Fig.1.6 shows, this is only true during the middle stage of the gait but not at

	$\bar{d}_{xy}\pm$ std (m)	$\bar{d}_{\theta}\pm$ std (rad)
Clothoid	0.605 ± 0.628	0.521 ± 0.279
OC	0.188 ± 0.104	0.874 ± 0.530

Table 1.1: Average linear distance according to θ_0.

	$\theta_0 = -\frac{\pi}{2}$ rad	$\theta_0 = 0$ rad	$\theta_0 = \frac{\pi}{2}$ rad	$\theta_0 = \pi$ rad
$d_{xy_{Clothoid}}$ (m)	**0.812**	0.336	0.208	**1.063**
$d_{xy_{OC}}$ (m)	0.141	0.188	0.187	0.234

Table 1.2: Average linear distance according to θ_0.

the initial and final positions.

We also compute the linear distances not for all trajectories but for groups of trajectory according to the starting orientation and to the global distance. Those results can respectively be found in Tab.1.2 and Tab.1.3. Moreover, they are represented in Fig.1.14. They demonstrate that the results provided by the OC model do not seem to depend on the starting orientation, unlike those of the clothoid-based model. Moreover, we can note that the farther the starting position is from the goal the greater the distance between the models and the measurements will be, especially for the model based on clothoids.

1.3.4.3 Models weaknesses

The comparison between human trajectories and trajectories generated by one non-holonomic model (clothoids) and one holonomic model (OC) shows that the holonomic model better fits the measured trajectories as it demonstrates better results on the linear distance. However, it generates orientations which are mostly non-tangent to the trajectory which deteriorates the results on the angular distance. Nevertheless, it seems useful to keep the possibility to generate those non-tangent orientations as we observe that during the first and the last stage of the trajectory, the human takes sideways steps. Thus, in further studies, we choose to focus on this OC model adapted from Mombaur et al. [38]. Let us denote that, if we wanted to work with a clothoid-based model, the results on the linear distance might be improved by generating multiple clothoid arcs instead of only one clothoid curv between the starting and the goal positions.

From this preliminary work, 3 main issues were raised about the adapted OC model. First, the hard-coded optimization of the T is very computation-time consuming and flawed. Then, the fact that we put the final constraint in the cost function was not the best solution to implement this constraint. Indeed, the DDP solver allows us to implement a terminal cost function, which will be much more suitable. Furthermore, only half of the final constraint was

	$d_{Start/Goal} < 3$ m	$d_{Start/Goal} > 3$m
$d_{xy_{Clothoid}}$ (m)	0.320	**0.952**
$d_{xy_{OC}}$ (m)	0.175	0.234

Table 1.3: Average linear distance according to the distance between the starting and the goal position.

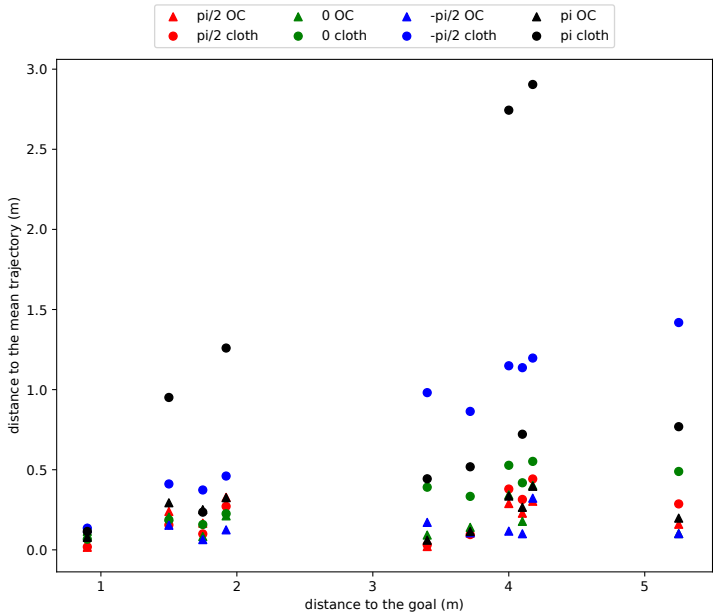

Figure 1.14: Distance between the generated paths (● for clothoid and ▲ for OC) and the mean human trajectory as function of the distance from each starting position to the goal. Colors are related to the starting orientation in the global frame represented in Fig.1.3a. For example to face the table the subject must have an orientation of $\theta_f = \frac{\pi}{2}$.

implemented, as there is no condition on the velocity. We should set the final velocity to zero. Finally, for the cost function, we use the same weights as those proposed in Mombaur et al. [38]. Our measurements of human trajectories can be used with an IOC scheme to determine the optimal weights. These weights might be different from those found by Mombaur et al. [38] as we adapted the model to solve it with a different solver. Moreover, the additional α_5 and α_6 weights have been heuristically determined. They could be optimized to provide more human-like results.

1.4 Improvement of the optimal control model

As previously mentioned, the adaptation of the OC model of Mombaur et al. [38] has some flaws that need to be fixed. Thus, this section presents the improvement made to the OC model introduced in Sec.1.3.3. This whole work was published in **Maroger** et al. [1].

1.4.1 Optimization of T

As T is a variable of the OC problem described in Eq.1.4, T has to be optimized. However, the DDP solver only optimizes the state and control. Thus, the OC problem must be solved with the DDP solver for different T in order to find the best T which minimizes the cost function. As T represents the duration of the path between the start and the goal, we assumed that $T \simeq \Delta t$. Thus, the optimization of T was done with the Nelder-Mead method of the Scipy library [72] using Δt as an initial guess.

1.4.2 Terminal cost

The formulation of the OC problem in DDP solver allows to add a terminal cost in the cost function. Thus, the OC problem can be written as follows:

$$\min_{X(.),U(.),T} \int_0^T \phi_r(X(t),U(t))\,\mathrm{d}t + \phi_t(X(T)) \tag{1.10}$$

with ϕ_r and ϕ_t the running and terminal cost function. This problem is solved under the following constraints:

$$\begin{cases} \dot{X}(t) = f(X(t),U(t)) & \text{Dynamical constraint (Eq.1.3)} \\ X(0) = X_0 & \text{Initial constraint} \end{cases} \tag{1.11}$$

This formulation allows to put the final constraint, introduced in Eq.1.5, not in the running cost as it was the case in Sec.1.3.3 but in a terminal cost which more accurate with respect to the system behaviour.

Then, ϕ_r and ϕ_t were chosen as follows:

$$\begin{cases} \phi_r(X(t),U(t)) = \alpha_0 + \alpha_1 u_1^2(t) + \alpha_2 u_2^2(t) + \alpha_3 u_3^2(t) + \alpha_4 \psi(X(t),X_f)^2 \\ \phi_t(X(T),U(T)) = \beta_0((x_f - x(T))^2 + (y_f - y(T))^2) + \beta_1(\theta_f - \theta(T))^2 \\ \qquad\qquad +\beta_2(v_{forw}(T)^2 + v_{orth}(T)^2) + \beta_3\omega(T)^2 \end{cases} \tag{1.12}$$

As a reminder, u_1, u_2 and u_3 are the control variables and they correspond to the forward, the orthogonal and the angular accelerations in the system dynamics (Eq.1.3). Moreover, the ψ function stands for the asymmetry between back and forth trajectories. The function ϕ_r is the same proposed to simulate CoM locomotion path in Mombaur et al. [38] (see Eq.1.6). Whereas, ϕ_t was added here to act as a final constraint which imposes the system to reach the goal position and orientation with a zero velocity. Moreover, $\alpha = (\alpha_0, \alpha_1, \alpha_2, \alpha_3, \alpha_4)$ are the weights of the running cost and $\beta = (\beta_0, \beta_1, \beta_2, \beta_3)$ the weights of the terminal cost. In order to make the model best fit the human behaviour, those weights need to be optimized using an IOC scheme.

1.4.3 Inverse optimal control

1.4.3.1 Application on our optimal control problem

As part of this work, we choose a bi-level approach to solve our IOC problem as it is easy to understand and quick to implement. Thus, we applied the same method, as presented by Mombaur et al. [46].

Our IOC problem aims to determine the weights of the cost functions defined in Eq.1.12, so that the solutions of the corresponding OC problem (X^{gen}, U^{gen}) best fit the measurements $(\bar{X}^{mes}, \bar{U}^{mes})$. Let us denote that the best fitting method minimizes the defined errors. Thus, the IOC problem can be defined as follows:

$$\min_{\alpha,\beta} \frac{1}{N_{traj}} \sum_{n=1}^{N_{traj}} D(\bar{X}_n^{mes}, X_n^{gen}(\alpha,\beta)) \tag{1.13}$$

with D the cost function associated with this problem such as:

$$D = d_{xy_n}(\bar{X}_n^{mes}, X_n^{gen}(\alpha, \beta)) + \frac{1}{2} d_{\gamma_n}(\bar{X}_n^{mes}, X_n^{gen}(\alpha, \beta)) \tag{1.14}$$

In this equation, d_{xy} is the linear distance defined in Eq.1.9and d_γ is a new angular distance named *local angular distance* and defined as:

$$d_\gamma = \frac{1}{N-1} \sum_{i=1}^{N-1} |\bar{\gamma}_i^{mes} - \gamma_i^{gen}| \tag{1.15}$$

with $\bar{\gamma}^{mes}$ the average human orientation in the local frame and γ^{gen} the angle between the vector tangent to the trajectory and the forward direction computed from the θ generated with the OC model as follows:

$$\gamma_{i+1} = \arctan \frac{y_{i+1} - y_i}{x_{i+1} - x_i} - \theta_i \tag{1.16}$$

In this study, we use the local angular distance instead of the angular distance defined in Eq.1.9. We made this choice because from a biomechanical point of view, looking at γ is much more meaningful than looking at θ as it is an indicator of tangency. Indeed, $\gamma = 0$ means that the pelvis orientation is tangent to the velocity vector.

Moreover, let us denote that in Eq.1.14 the sum is weighted in order to have d_{xy_n} and d_{γ_n} of the same magnitude.

This kind of problem can be solved with a derivative-free method [73] like the Powell method [74] of the Scipy library [72]. The IOC problem that we solved in this section is represented in Fig.1.15.

1.4.3.2 Results

The weights of the cost function presented in Eq.1.12 were optimized with the IOC problem described in Sec.1.4.3. Thus, the weights allowing the best fitting to human trajectories according to our metric and our model are the following:

$$\begin{cases} (\alpha_0, \alpha_1, \alpha_2, \alpha_3, \alpha_4) \approx (7.87, 4.00, 20.15, 1.00 \times 10^{-6}, 10.00) \\ (\beta_0, \beta_1, \beta_2, \beta_3) \approx (10.00, 10.00, 0.38, 3.36) \end{cases} \tag{1.17}$$

1.4.4 Comparison between the improved model and the measurements

1.4.4.1 Human data analysis

First of all, we focus on how representative of the individual trajectories the average trajectories are. This study is essential to assess the accuracy of the OC model.

The mean and standard deviation of the linear and local angular distances between the individual measurements and the average human trajectories are $0.1073 \pm 0.06519\,\text{m}$ and $0.4842 \pm 0.1788\,\text{rad}$. Moreover, the measurements present a great variability according to the subjects as one can see in Fig.1.16. Furthermore, a Kruskal test was performed to assess

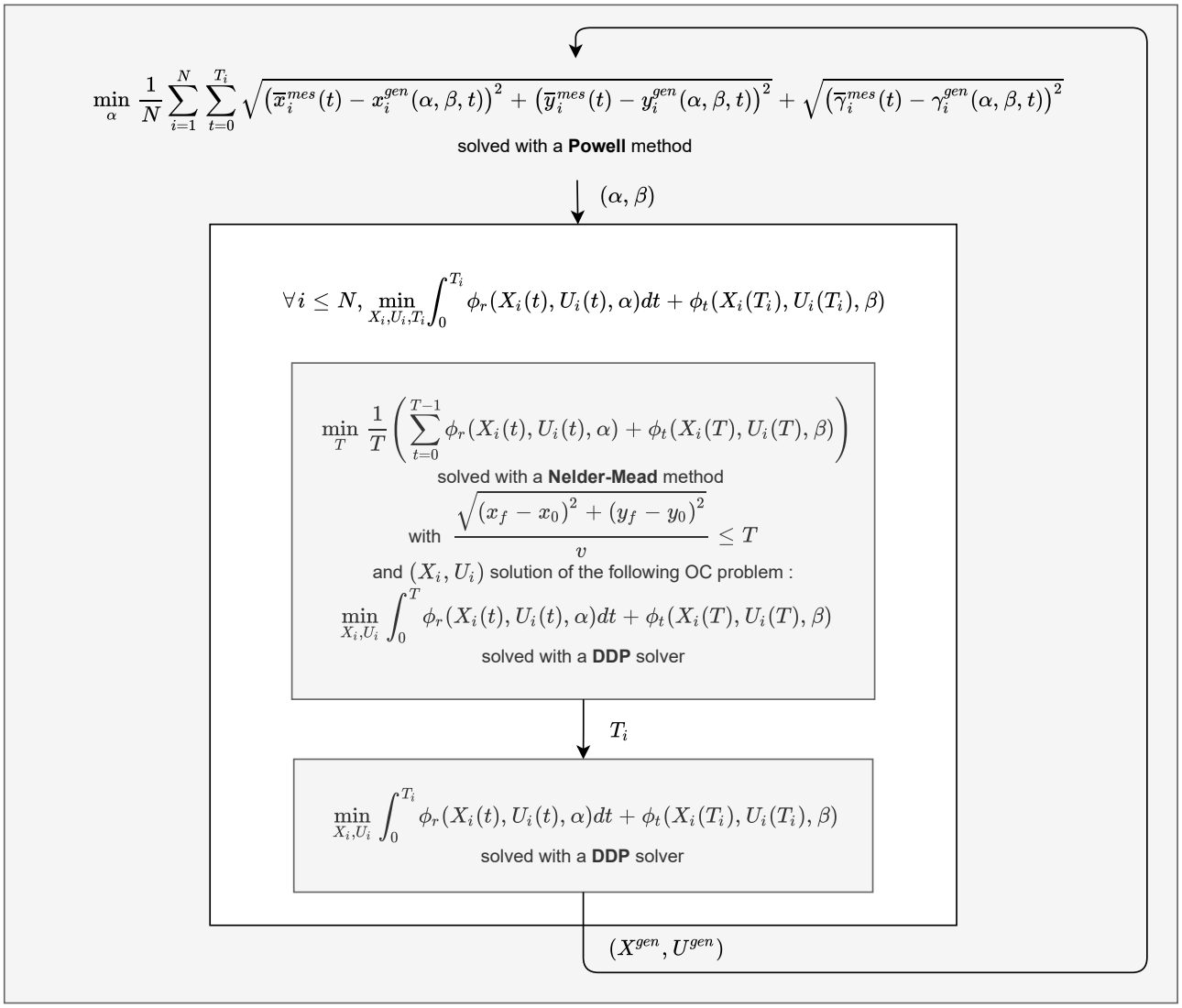

Figure 1.15: Algorithm to solve our IOC problem.

the variability of the chosen trajectory between the 10 subjects. It demonstrates significant differences between the subjects for the linear distance ($p < 10^{-5}$) and for the angular distance ($p < 10^{-5}$). However, some subjects are not statistically distinguishable. Indeed, when performing a Kruskal test on 6 of the 10 subjects, the obtained p-value is 0.31 for the linear distance and 0.34 for the angular distance. To conclude, some subjects have similar behaviour while others are totally distinguishable.

The box and whisker plots for linear and local angular distances between the measurements and the average human trajectories are represented in Fig.1.18a (on the right). These plots show the median, the lower and upper quartile values (Q_1 and Q_3) and extend from the maximum to the minimum within $[Q_1 - 1.5(Q_3 - Q_1), Q_3 + 1.5(Q_3 - Q_1)]$. The other values are considered as outliers.

1.4.4.2 Distance computation

With the optimal weights presented in Eq.1.17, 40 trajectories corresponding to the same starting and goal positions as the human trajectories were generated using the OC model in

order to evaluate this model. The average computational time of these generations scored 1.45 s. The generated curves, for each starting position and orientation, are shown in Fig.1.16.

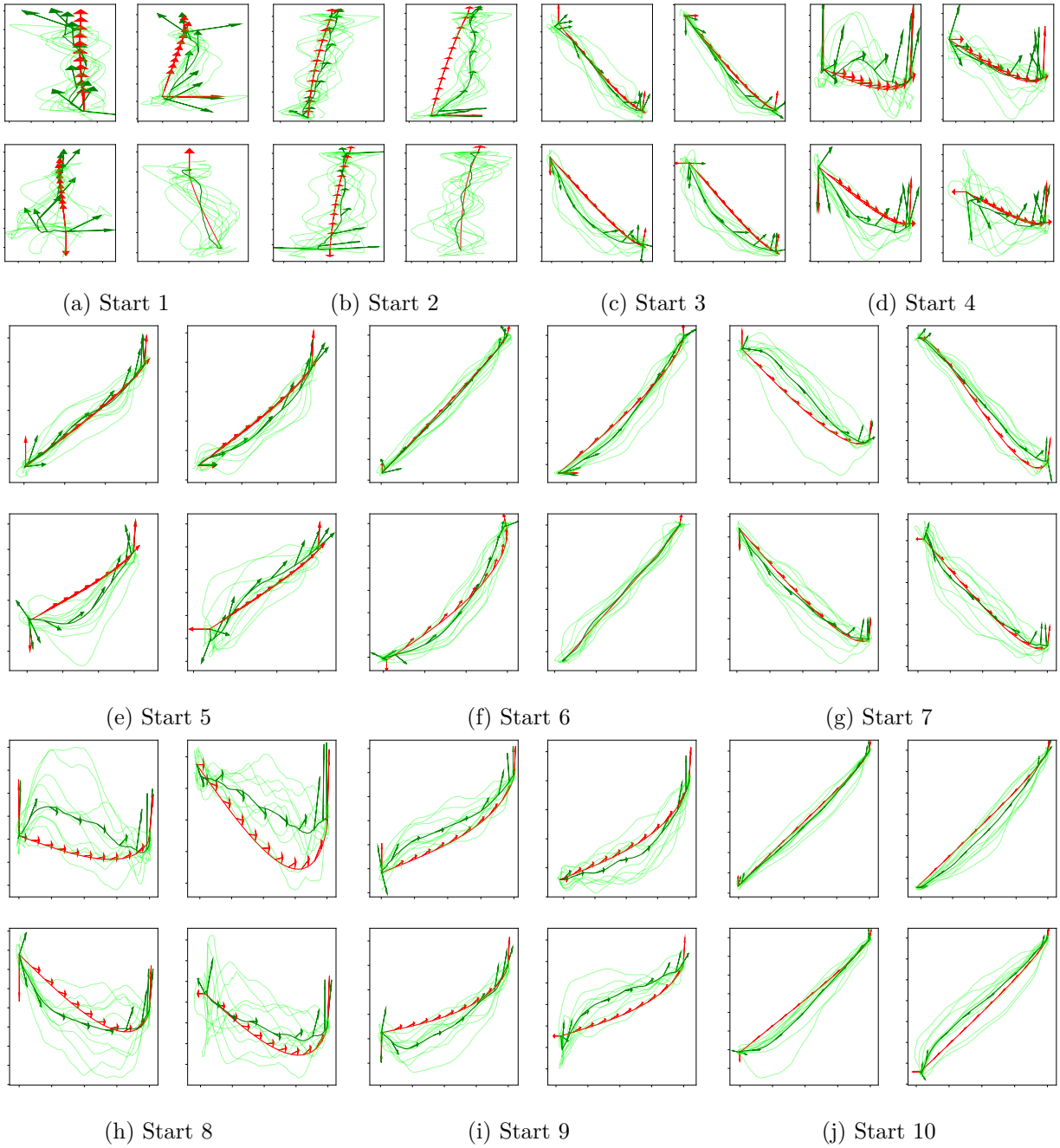

(a) Start 1 (b) Start 2 (c) Start 3 (d) Start 4

(e) Start 5 (f) Start 6 (g) Start 7

(h) Start 8 (i) Start 9 (j) Start 10

Figure 1.16: Comparison between human trajectories (average in *bold green* and measurements in *lime green*) and generated trajectories (in *red*). The arrows represent the orientation of the pelvis during locomotion.

The linear and local angular distances were computed for each 40 generated trajectories. The obtained results for each starting position and orientation are plotted in Fig.1.17. Let us denote a moderate positive correlation between the mean linear distance and the global distance (with a Pearson correlation coefficient equal to 0.63) whereas there is a strong negative correlation between the mean angular distance and the global distance (with a Pearson correlation coefficient equal to -0.81).

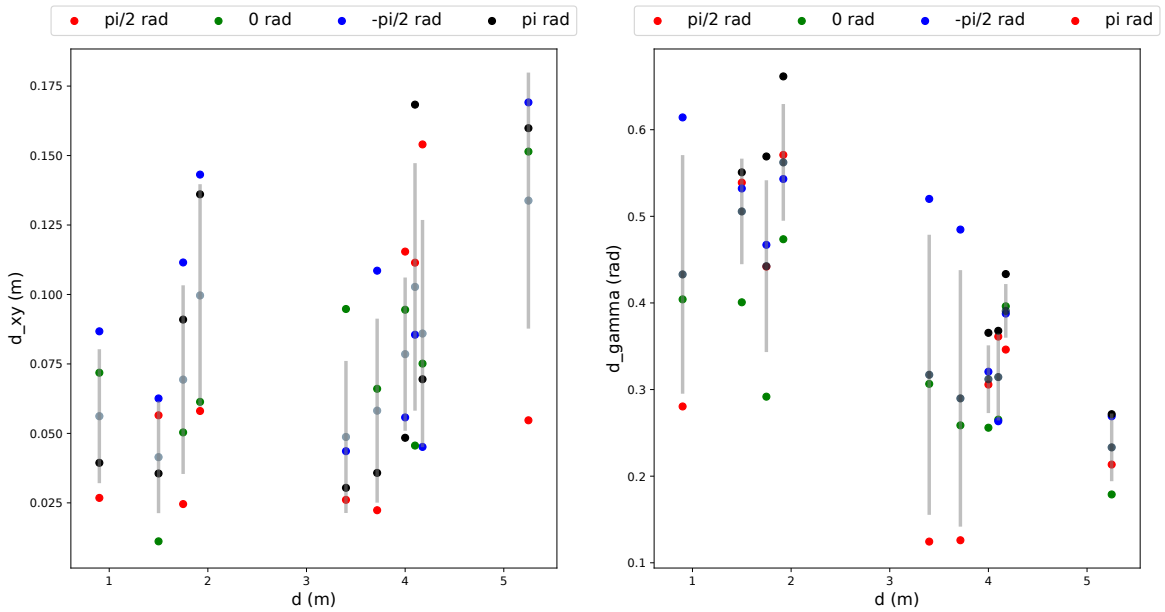

Figure 1.17: Linear distance (*on the left*) and local angular distance (*on the right*) between the average human trajectories and the generated trajectories according to the global distance for all orientations (in *grey* mean ± standard deviation).

Moreover, the computed errors (± standard deviation) are $\bar{d}_{xy} = 0.0767 \pm 0.0450\,\text{m}$ and $\bar{d}_{\gamma} = 0.3786 \pm 0.1336\,\text{rad}$. Thus, the results of the described OC model are close to the average human behaviour. Mann-Whitney tests were also conducted to find out if the distances between the generated trajectories and the average human trajectories and the distances between the measured trajectories for every subject and the average human trajectories are significantly different ($p < 0.05$). They demonstrate significant differences between the two data sets ($p < 10^{-3}$ for the linear error and $p < 10^{-3}$ for the angular error). On the opposite, when performing a kruskal test with the linear error and the distance between the measured trajectories of the 6 indistinguishable subjects and the average human trajectories, the p-value is superior to the threshold ($p = 0.07$). Thus, it can be asserted that the OC model precisely describes the average human behaviour. Nevertheless, it cannot fit every individual behaviour (6 over 10 in this study).

The box and whisker plots for linear and local angular distances are represented in Fig.1.18a (on the left). Similar plots are presented in Fig.1.18b where the linear distances are split into 4 groups one for each starting orientation and in Fig.1.18c where they are split into 2 groups according to the global distance superior or inferior to 3 m. As these diagrams present similar medians, they show no significant differences between those groups. However, statistical tests needed to be performed to confirm this assumption. Thus, ANalysis Of VAriance (ANOVA) tests were performed to detect the influence of those criteria on the errors defined above ($p < 0.05$). Those tests were performed after checking the normality of the data with a Kolmogorov-Smirnov test. The p-value was superior to the threshold when applying the test to the 4 orientation-discriminated groups ($p_{xy} > 0.6$), to the 2 global distance-discriminated groups ($p_{xy} > 0.2$) and to every groups ($p_{xy} > 0.7$). This demonstrates that the presented model provides homogeneous results for every global distance (within the chosen range) and every orientation (among the chosen ones).

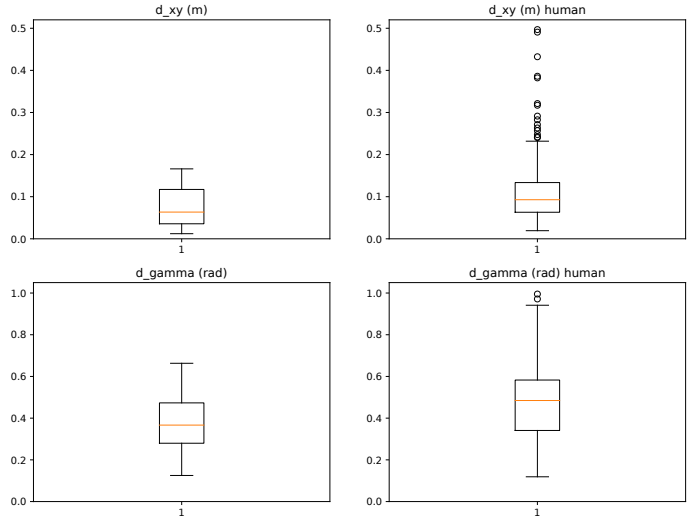

(a) Linear and angular distance distribution: OC model on the left and human measurements on the right

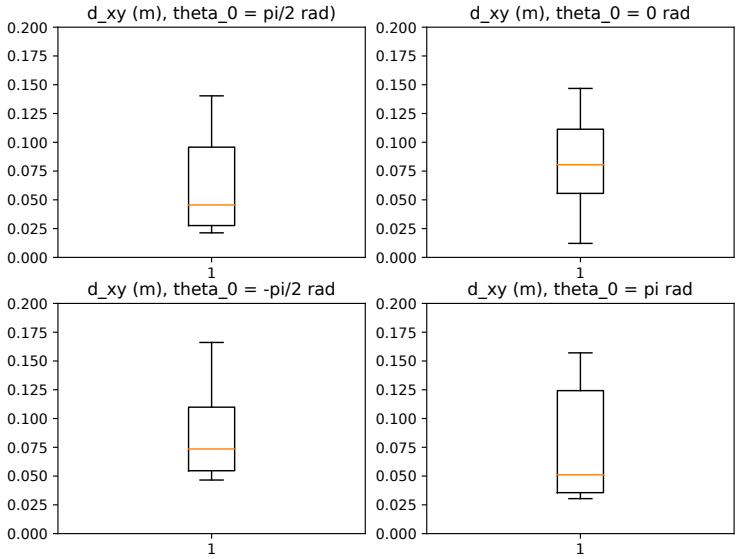

(b) Linear distance distribution of generated trajectories according to the starting orientation (θ_0)

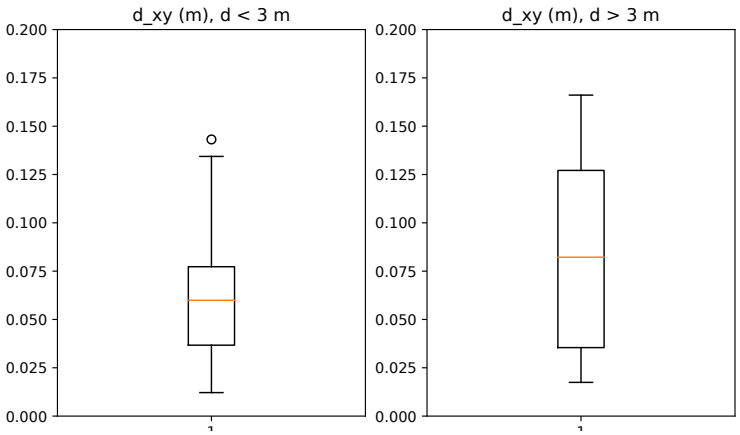

(c) Linear distance distribution of generated trajectories according to the global distance (d)

Figure 1.18: Distribution of the computed distance.

1.5 Discussion

In the work presented in the previous section, the weights of the cost function (Eq.1.12) were optimized. A quick analysis of this result shows that the weight factor corresponding to the angular acceleration is very low, close to zero. This means that either the orientation of the pelvis does not influence human walking trajectories, which does not seem reasonable, or, more certainly, this factor is redundant with the forward and orthogonal accelerations and the ψ function, which all depend on θ. On the opposite, the weight associated with the orthogonal acceleration is quite important in regard to the weight of the forward acceleration. This demonstrates the importance of the possibility for sideward motions, which is totally missing in non-holonomic models, like the unicycle model. This corroborates the starting hypothesis to consider a model with additional degrees of freedom rather than a non-holonomic model to best fit human locomotion. Thus, a holonomic system is an accurate approximation of a human subject. Those weights can be compared to the ones computed in Mombaur et al. [38]. They are not of the same magnitude, especially for the weight factor corresponding to the angular acceleration. The reason why those weights are so different remains unclear, but it may be due to the difference of solvers and to differences in the experimental protocol. For example, during their experiments, the performed distances did not exceed 3.5 m. Moreover, we cannot know if the instructions given to the participants prior to the trials were exactly the same as the ones we gave.

To the best of our knowledge, few authors compare a human-like locomotion path to measurements using a metric similar to the one presented in this work. Thus, it is difficult to assess the presented results with respect to other studies. Only in Arechavaleta et al. [32], a similar metric is used to compute the linear error and alike results are found with a model based on the unicycle model. However, not a lot of information is given about their results. So, a comparison with our model only leads to the conclusion that we have results of the same order of magnitude for the linear error. There is no evaluation of the angular error in the literature as far as we know. At least, the results of the improved OC model presented in Sec.1.4 can be compared with the results of the models in Sec.1.3. Comparison shows that the new OC model is much better than the ones tested before where the mean linear distance was around 0.2 m and the mean angular distance around 0.9 rad using the same metric.

Even if our study leads to a model which correctly approximates human behaviour, it has some limitations. First of all, the presented model has got only a weak optimality constraint on the final state. This can lead not to exactly reach the goal position. However, for the generated trajectories, the average final distances are 0.016 m and 0.19 rad which is largely acceptable for the robotic targeted application, namely a collaborative task between a humanoid robot and a human.

Furthermore, the orientation computation is flawed. Indeed, during the measurements some markers were obliterated and data was not collected. We were unable to compute the orientation of the subjects'pelvis for 125 of 400 analyzed trajectories due to the loss of some markers. This leads to 3 of 40 average human trajectories without average orientations. These trajectories were not taken into account in the IOC process and in the distance computation.

Moreover, the presented OC model greatly depends on the chosen dynamics (Eq.1.3) and

Trajectory Index	**Initial Guess**	**Initial Cost**	**Final Weights**	**Duration** (s)	**Final Cost**
20	[1,1,1,1.10^{-6}, 1,1, 1,1,1]	0.36 + 0.24	[2.38,0.8,1,1.10^{-6}, 1,1,1,1,1]	2140	0.063 + 0.2
20	α and β	0.05 + 0.2	[9.87,4,2.02,4.10^{-3}, 9.38,10,10,0.38,3.35]	1592	0.028 + 0.2
10	α and β	0.14 + 0.05	[6.12,5,21.3,1.3.10^{-7}, 1.13,10,10,0.38,3.35]	316	0.16 + 0.02
38	α and β	0.13 + 0.034	[8.23,41.4,20.3, 2.71.10^{-4},9.95, 10,10,0.29,3.32]	1875	0.09 + 0.06

Table 1.4: Test of IOC on one full trajectory only

the chosen cost function for the OC (Eq.1.12) and for the IOC (Eq.1.14). Indeed, other choices can be made for the OC cost function and maybe adding or removing terms can improve the model. For example, further studies may analyze the velocity profile in order to also make it fit to human dynamics and introduce a term which binds the velocity to the curvature of the trajectory to generate realistic velocity profiles. Thus, the velocity profile may respect the two-thirds power law [75]. Jerk [76] or kinetic energy [77] terms could also be added to the cost function. However, in Mombaur et al. [38], the authors show that adding velocity and jerk terms to the cost function does not improve their model. Moreover, terms can be added to the cost function for the IOC problem, like a distance evaluating the closeness between the linear and angular velocity profiles. Nevertheless, weights must be added as the different distances will not be on the same scale and a manual search of these weights may be a long process as each IOC run takes at least 36 hours.

This leads to another potential weakness of our method: the IOC scheme is very computation time consuming. Indeed, not only, with 40 trajectories and 10 subjects, each IOC run takes at least 36 hours, but also the IOC scheme is very computation-time consuming even to fit only one trajectory. Some results of IOC scheme on only one human trajectory are recorded in Tab.1.4. This prevents the customization of the model according to each subject, which could improve the generated trajectories. Indeed, we showed that the trajectories taken by the subjects present a great variability. This is why it may be relevant to individually recompute the OC cost function weights α and β for each subject. However, the huge computation time of the IOC scheme does not allow this re-computation for real-time applications like collaborative tasks. Nevertheless, using another method, like the ones presented in Sec.1.1.2.2, to solve the IOC problem might speed up the weights computation. The implementation of these methods is more complex but they may be more efficient and faster to solve an IOC problem.

A final point to discuss is the choice of the modeling approach.

First, it would also be interesting to investigate a model which takes into account the oscillations of the CoM due to the footsteps. Indeed, in this study, we choose to focus only on simulating smoothed CoM trajectories to simplify the problem. We made this choice to avoid adding footstep constraints to an already complex trajectory model. However, we could think of analyzing the recorded footsteps of the subjects and building a new model similar to the ones used to generate the CoM and support foot trajectories of the humanoid robots.

Nevertheless, this may not improve the results a lot, as the effect of these oscillations seems to be negligible. Indeed, these oscillations do not appear in those average trajectories and are only noticeable during short or straight measured trajectories. Moreover, these observed oscillations are relatively small (± 5 cm). For example, oscillations are noticeable for Start 1, 2 and 4 on Fig.1.16.

Then, it is important to underline that we chose to study human locomotion only by looking at the CoM trajectories. We could have focused on more complex models such as whole-body 3D models or models taking into account the reaction forces on the ground. However, it is important to recall that this work was the first step toward a model of human locomotion which should be embedded in a robot's motion planner. This entailed that the model should be simple enough to aim a real-time application: the measured data should be easy to retrieve with only a MoCap (small number of MoCap markers and no force sensors) and the model should be able to run at 2 kHz on the real robot. Moreover, the chosen approach needed to be versatile enough to be adapted to a real-time situation (see Chapter 2) and to another human behaviour (see Chapter 4). This is why focusing only on the modeling of the CoM trajectories using an OC problem occurred as the best solution to model human locomotion as part of this work. However, to perform a complete analysis of human locomotion, the measurement of other variables such the reaction forces would be essential.

1.6 Conclusion

To sum-up, in Sec.1.2, the CoM trajectories in the horizontal plane and postero-anterior orientations of the pelvis of 10 subjects walking freely from 40 different starting positions to one goal position were collected. The analysis of the measured trajectories, performed in Sec.1.4.4, showed a great variability between the subjects. Then, in Sec.1.3, we implemented some existing models of human trajectories during locomotion. The one that gave the most human-like model was the one adapted from Mombaur et al. [38] presented in 1.3.3. Finally, this model was improved in Sec.1.4 in order to better fit the measurements. Indeed, in Sec.1.4.3, this OC model was optimized using the measured trajectories through a bi-level IOC scheme. The assessment of this final model shows mean linear and angular errors around, respectively, 0.08 m and 0.38 rad. Those results are of the same order of magnitude as the mean distances between the average human trajectories and the measured trajectories. Thus, this model provides a close approximation of the average human CoM trajectory and pelvis orientation during locomotion.

Moreover, it is interesting to denote that this model is generic. Indeed, as long as we consider a subject whose behaviour is not too far from the average behaviour, the developed model is able to accurately generate its trajectory between whatever starting and goal positions. However, if the considered subject's behaviour is far from the average one, the errors between the performed and the generated trajectories may be greater than the average errors.

Now, let us consider whatever HRI where the robot would estimate where the human should be, using the developed OC model. In this case, two problems may arise. First, if the human partner's behaviour is far from the average one, the robot's estimation may be wrong and this could prevent the interaction or, even, endanger its partner. Then, if the human partner decides

to change his goal position during the interaction, the robot would not be able to estimate where its partner is anymore. Thus, in the context of HRIs, we need to develop a more adaptive model which can take into account the past behaviour of the human in real-time. In doing so, the robot would be more reactive and more able to efficiently assist its partner. The development of such a model is tackled in the following chapter.

Chapter 2

Human trajectory Prediction Model

Contents

2.1 Introduction

2.1.1 Motivations

During a human-robot collaboration, a real-time prediction model of human behaviour allows the robot to anticipate its partner's behaviour. In the context of the ANR-CoBot project, a good knowledge of human dynamics while walking with a table is needed to allow the robot to anticipate its partner's movements. As a reminder, in the first place, the problem of walking with a table has been put aside and the issue has been reduced to predicting the trajectory of a single walking human. Thus, this work focuses on the prediction of a walking human's trajectories, based on the human locomotion model developed in Chapter 1, in order to allow the robot to adapt its behaviours, in real-time, in the context of a potential HRI.

2.1.2 Related Works

The prediction of human behaviour is a commonly tackled issue in the field of HRIs. Indeed, during a HRI, humans interact with one robot or more to perform a task together [78]. The robot is expected to proactively and safely assist its human partners. To achieve efficient HRI, numerous studies focused on the recognition [79] and the prediction of humans' motions. For example, in Mainprice et al. [80], a prediction model of human workspace occupancy was developed in the context of co-manipulation tasks. In this work, the authors used Gaussians Mixture Model (GMM) to classify and early detect human intents. Other methods like Hidden Markov Model (HMM) [81] or dynamic/integral Bag-of-Words (BoW) [82] were also used to perform early prediction of humans' motions. Another way to anticipate humans' motions was to predict their near future actions. This problem was tackled in Koppula et al. [83]. Indeed, in this work, the authors introduced a framework to anticipate human activities in order to trigger reactive robotic responses. It computed future scenarios based on a graphical model, called Conditional Random Field (CRF), of past human activities and object affordances.

Moreover, human-aware navigation is a key to efficient HRIs when the robot has to assist a moving human during a given collaborative task. For example, human-aware navigation allows a service robot to provide timely assistance whenever and wherever the human needs it. In this context, being able to predict where the human is going is essential. In Bruckschen et al. [84], the authors developed a human-aware navigation system based on human's navigation goal prediction [85] in indoor environments. This system using a Bayesian inference approach was rated as comfortable by humans and provided better results than other approaches based on social forces [86], reinforcement learning [87] or non-predictive following [88].

However, only predicting where the human is going is not always sufficient. Sometimes, the whole future path of the human needs to be predicted. The prediction of human trajectory is a well studied topic not only for collaborative robots but also for self-driving vehicles and for surveillance of crowds [89]. For example, on the one hand, Kooij et al. [90, 91] introduced a Dynamic Bayesian Network (DBN) which predicts changes in pedestrian dynamics using computer vision in order to avoid collisions between intelligent vehicles and pedestrians. On the other hand, numerous works focused on the forecasting of people's motion dynamics in crowded environments. Most of those studies used Long Short-Term Memory (LSTM)

networks [92, 93, 94]. However, other approaches exist, like social forces [95, 96], learning using HMM [97] or Markov chain Monte Carlo (McMC) [98] and the latest transformer networks [99]. Moreover, Schöller et al. [100] demonstrated that a simple Constant Velocity Model (CVM) can out-perform state-of-the-art neural models like the LSTM networks. Thus, to the best of our knowledge, an OC model based on human dynamics has never been used to predict a single walking human trajectories.

Thus, among the previously cited references, two main groups emerged: those studying action prediction and those focusing on trajectory prediction. However, as Chen et al. [101] demonstrated, according to the situation, it may be relevant to simultaneously predict the human trajectory and its targeted action.

2.1.3 Contributions

A generic human trajectory prediction model is introduced in this chapter. This OC model is aimed to provide an accurate estimation of the human CoM future trajectory based on its recent past trajectory. Such a real-time prediction model is expected to improve the collaboration between any walking human and its robot partner. Indeed, if a robot is able to predict its partner's behaviour, it will be able to anticipate its partner's motions and proactively assist its partner during his/her task [102]. Moreover, an original metric is presented in order to assess the relevance of this model.

This work was published in **Maroger** et al. [4, 5]. All the results and simulations presented in this chapter are reproducible as all the libraries are open-source and the source code and the data are available on: `https://github.com/imaroger/human_walking_trajectory_prediction`.

2.2 Modeling

In the previous chapter, we introduced an OC model which generates human-like trajectories during locomotion. As a reminder, the OC problem is of the following form:

$$\min_{X(.),U(.),T} \int_0^T \phi_r(X(t),U(t))\,\mathrm{d}t + \phi_t(X(T))$$

with $X = (x, y, \theta, v_{forw}, v_{orth}, \omega)^T$ and $U = (u_1, u_2, u_3)^T$. As a reminder, the control variables u_1, u_2 and u_3 respectively are the forward, the orthogonal and the angular accelerations (see Eq.1.3). This problem is solved under the following strict equality constraints: the dynamical constraint $\dot{X} = f(X(t), U(t))$ (Eq.1.3) and the initial constraint $X(0) = X_0$.

In this section, a similar OC problem is addressed to predict human walking behaviour. This model was published in **Maroger** et al. [4].

2.2.1 Assumptions

First, we hypothesize that a human is walking and that the human's CoM position in the horizontal plane and the global orientation of the human's pelvis (see Fig.1.5), denoted $C = (c^x, c^y, c^\theta)^T$, are recorded at all time with a sampling period T_{OC}. Then, the following assumptions are made:

- C is piecewise constant on each interval $[kT_{OC}, (k+1)T_{OC}]$ with $k \in \mathbb{N}$. Thus, at time $t = kT_{OC}$, the human trajectory can be described by $\begin{pmatrix} C_0 & C_1 & ... & C_k \end{pmatrix}^T$.
- The prediction process starts when $k \geq N_0 - 1$ as N_0 is the amount of measurements needed before being able to correctly predict the human future trajectory.
- The prediction process stops when the human stops walking at an a priori unknown time $k = N_f$.
- The prediction process is done on a sliding window of size $N_{OC} > N_0$.
- At time $t = kT_{OC}$, the prediction windows goes from $n+1$ to $n+N_{OC}$ and the prediction process uses the measured trajectory from $n+1$ to $n+N_0$ with $n \in [\![-1, n_f - N_0 + 1]\!]$ defined as $n = k - N_0$.

Thus, at time $t = kT_{OC}$, the prediction process will compute $\tilde{X}_{n+1} = \begin{pmatrix} X_{n+1} & X_{n+2} & ... & X_k & ... & X_{n+N_{OC}} \end{pmatrix}^T$. The optimal solution will be denoted $\tilde{X}^*_{n+1}$. This process is represented on Fig.2.1.

$\begin{pmatrix} X^*_k & ... & X^*_{n+N_{OC}} \end{pmatrix}^T$ is the part of the solution that corresponds to the future as Fig.2.1 shows, it will be called the *predicted trajectory* at time t. Let us denote that, as $k = n + N_0$, the predicted trajectory only exists if N_{OC} is greater than N_0, hence the previous hypothesis $N_{OC} > N_0$. Moreover, in what follows, N_0 and N_{OC} will be named the *prediction parameters*.

2.2.2 Optimal control model

To solve this prediction problem, an OC model has been developed based on the one described in Eq.1.10. This model can be expressed as follows at time $t = kT_{OC}$ with $k = n + N_0$:

$$(\tilde{X}^*_{n+1}, \tilde{U}^*_{n+1}) = \underset{\tilde{X}_{n+1}, \tilde{U}_{n+1}}{\arg\min} \sum_{i=n+1}^{n+N_{OC}} \varphi_i(C_i, X_i, U_i) \tag{2.1}$$

Under the following strict equality constraints:

$$\begin{cases} \dot{X}(t) = f(X(t), U(t)) & \text{Dynamical constraint (Eq.1.3)} \\ X_{n+1} = C_{n+1} & \text{Initial constraints} \end{cases} \tag{2.2}$$

With the following cost functions:

$$\forall i \in [\![n+1,\ k]\!], \varphi_i(c_i, X_i, U_i) = \alpha_0 + \alpha_1 u^2_{1,i} + \alpha_2 u^2_{2,i} + \alpha_3 u^2_{3,i} + \gamma_0((c^x_i - x_i)^2 + (c^y_i - y_i)^2) + \gamma_1(c^\theta_i - \theta_i)^2 \tag{2.3a}$$

$$\forall i \in [\![k+1, n+N_{OC}]\!],\ \varphi_i(c_i, X_i, U_i) = \alpha_0 + \alpha_1 u^2_{1,i} + \alpha_2 u^2_{2,i} + \alpha_3 u^2_{3,i} \tag{2.3b}$$

with $(\gamma_0, \gamma_1) = (10, 10)$ heuristically chosen so that the beginning of the prediction fits as much as possible the measurements and $(\alpha_0, \alpha_1, \alpha_2, \alpha_3) = (7.9, 4.0, 20.1, 1.0 \times 10^{-6})$ optimized

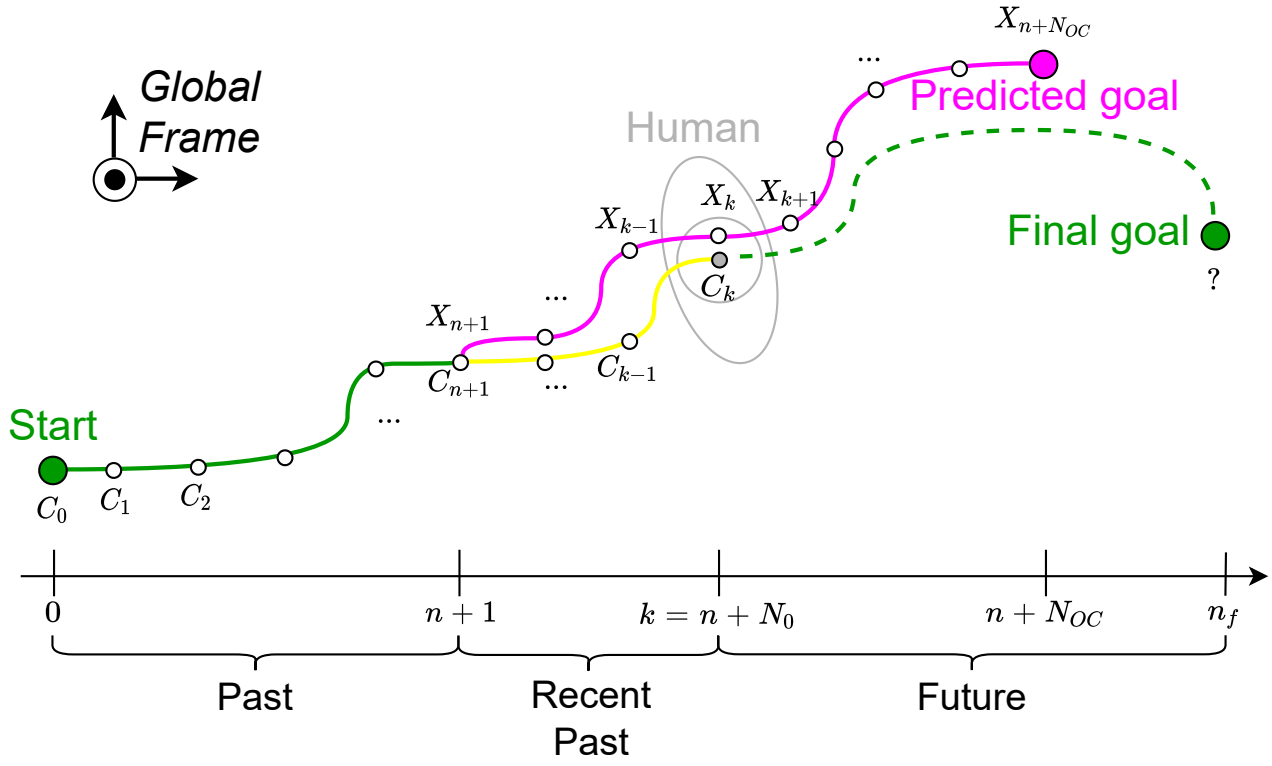

Figure 2.1: Prediction problem representation at time $t = kT_{OC}$ with $k = n + N_0$ (in *green* and *yellow* the whole past human trajectory, in *stippled green* the unknown future human trajectory and in *purple* the predicted trajectory).

in Sec.1.4.3.

Thus, at time $t = kT_{OC}$, $k = n + N_0$, this new OC model, also solved with a DDP solver from the Crocoddyl library [70], provides a predicted trajectory $\tilde{X}^*_{n+1}$.

2.2.3 Simulation

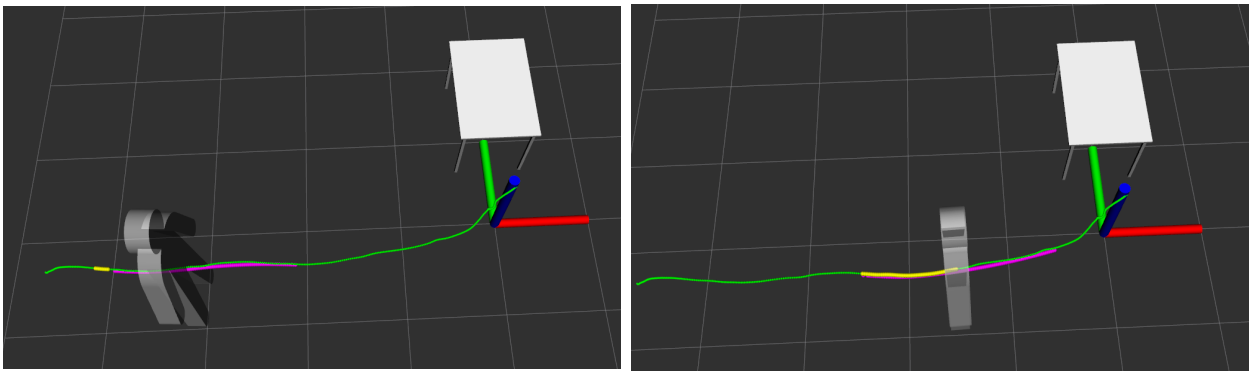

Figure 2.2: Example of the current predicted trajectory (in *purple*) of a human trajectory (in *green*) from his latest past trajectory (in *yellow*) with $N_0 = 50$ and $N_{OC} = 100$.

Thus, the described prediction process needs a human trajectory as an input. In this study, we used trajectories of 10 healthy subjects walking from 40 starting positions to one goal position in front of a table collected as part of a study of human walking trajectories (see Sec.1.2).

To simulate a human walking, the recorded trajectory was sent at a given rate, simulating the human velocity, to the prediction process thanks to a Robot Operating System (ROS) framework [103]. According to the chosen rate, the recorded trajectory could be sped up or slowed down. For example, if the trajectory counted 500 points and was traveled by the human in $\approx 8\,\mathrm{s}$, to simulate a prediction in real-time the rate should be $\approx 62.5\,\mathrm{Hz}$, if the rate was greater the trajectory would be sped up else it would be slowed down. As part of this work, we hypothesize that a measured human trajectory is independent of its travel velocity. Indeed, as our human trajectory model does not take into account the oscillations of the CoM due to footsteps, it may not depend on the travel velocity as much as a model which would be sensitive to these oscillations. One simulation on the RViz software is shown in Fig.2.2.

2.3 Model assessment

Once we designed a prediction model of human walking trajectories, we numerically assessed the predicted trajectories. This work was presented in **Maroger** et al. [5].

2.3.1 Metric definition

The previously described prediction process was tested over 40 trajectories, each one performed by 10 different subjects. Those trajectories were recorded as part of the study described in Sec.1.2. Fig.2.3 shows the predicted trajectories computed at all times for a given trajectory performed by one subject.

To assess the accuracy of those predicted trajectory, a metric needs to be developed. For each human trajectory, we will define and compute:

- The average *linear* and *angular errors* between the predictions for each $t = kT_{OC}$ and the human trajectory is defined as the average of the mean distance between the predicted trajectories at all times and the performed trajectory. Mathematically, it can be expressed as follows:
$$\begin{cases} \delta_{xy} = \frac{1}{N_{hum}} \sum_{k=N_0}^{N_f} \frac{1}{N_k} \sum_{i=k}^{N_k+k-1} \sqrt{(c_i^x - x_i^*)^2 + (c_i^y - y_i^*)^2} \\ \delta_{\theta} = \frac{1}{N_{hum}} \sum_{k=N_0}^{N_f} \frac{1}{N_k} \sum_{i=k}^{N_k+k-1} |(c_i^{\theta} - \theta_i^*)| \end{cases} \tag{2.4}$$
with $N_{hum} = N_f - N_0 + 1$ and $N_k = \min(k + N_{OC} - N_0, N_f) - k + 1$.
- The average *predicted distance* over one human trajectory:
$$d_{pred} = \frac{1}{N_{hum}} \sum_{k=N_0}^{N_f} \sqrt{(x_k^* - x_{k+N_{OC}-N_0}^*)^2 + (y_k^* - y_{k+N_{OC}-N_0}^*)^2} \tag{2.5}$$
The predicted distance at time t is the euclidean distance between the current position of the human at time t and the last point of the current predicted trajectory. It quantifies how far the prediction process is able to compute where the human is going. The greater this distance is, the more efficient the prediction will be to estimate the human position far from its current position. It is represented in Fig.2.4.

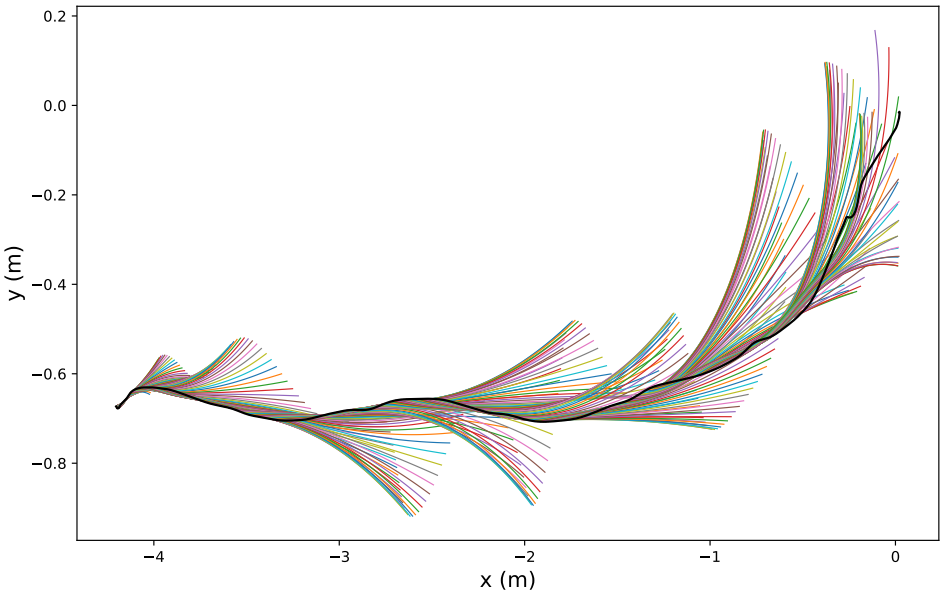

Figure 2.3: All the predictions for one given human trajectory in *black* with $N_0 = 50$ and $N_{OC} = 100$.

2.3.2 Results

The previously defined quantities were computed for the 400 measured trajectories composing the database created in Sec.1.2. As a reminder, the 40 trajectories performed by each subjects were chosen to be representative of common locomotion paths within a range of 0.6 to 5.5 m from the goal with four different starting orientations ($\theta_0 \in \{-\frac{\pi}{2}, 0, \frac{\pi}{2}, \pi\}$ rad).

The results were obtained with various sets of prediction parameters and are represented in Fig.2.5 according to the starting orientation and to the global distance. In those graphs, we observe that the linear error and the predicted distance are correlated to the distance between the starting and the goal position. This is confirmed by the computation of the Pearson correlation coefficients. For example, for $N_0 = 50$ and $N_{OC} = 100$, they are

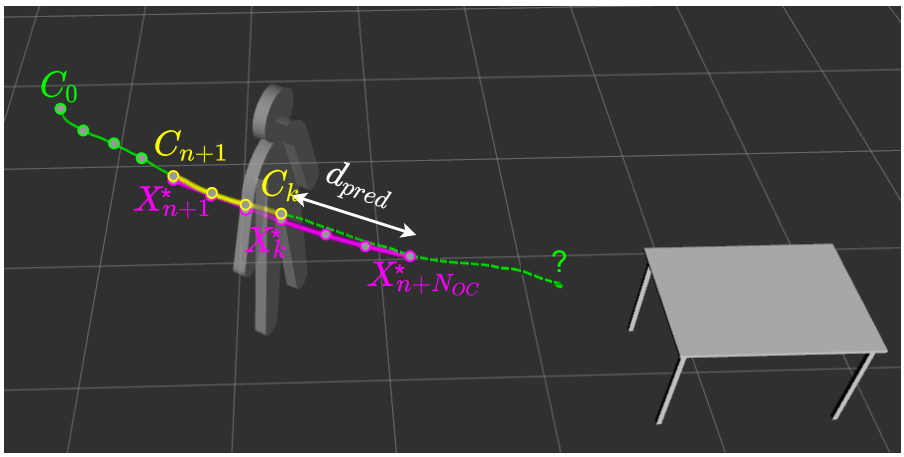

Figure 2.4: Predicted distance represented on a simulation with $N_0 = 50$ and $N_{OC} = 100$.

N_0	N_{OC}	δ_{xy} (m)	$\delta_\theta(rad)$	$d_{pred}(m)$
25	100	0.11 ± 0.04	0.42 ± 0.03	0.76 ± 0.29
50	100	0.08 ± 0.02	0.28 ± 0.01	0.48 ± 0.17
75	100	0.04 ± 0.01	0.14 ± 0.01	0.24 ± 0.08
50	200	0.18 ± 0.05	0.53 ± 0.07	1.40 ± 0.51

Table 2.1: Average errors and average predicted distance for different prediction parameters.

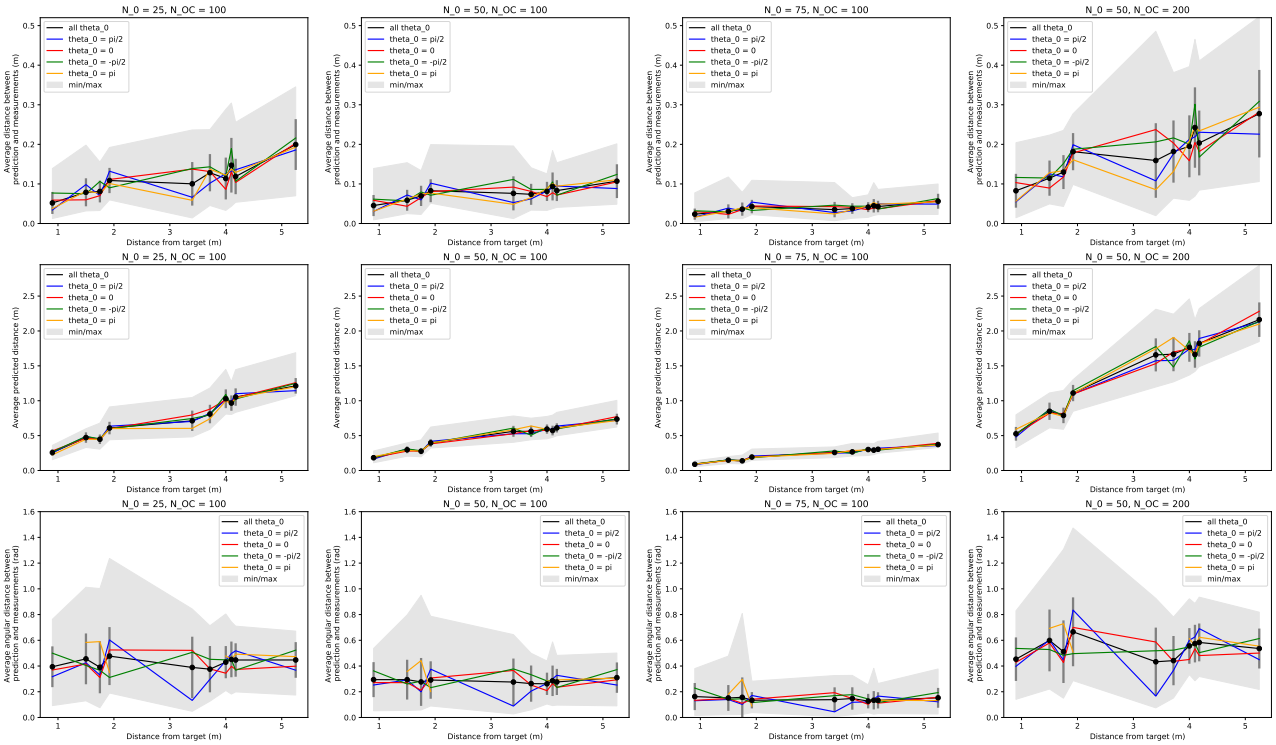

Figure 2.5: Average linear and angular errors and average predicted distance according to the distance between the starting position and the targeted position for every measured trajectory.

respectively equal to 0.87 and 0.98. Another observation that can be made from this figure is that there is a great variability according to the subjects, as the lower and upper grey curves, representing respectively the minimum and the maximum of computed quantities, show.

The averages of those quantities over all the trajectories with the same set of prediction parameters are presented in Tab.2.1. Thus, the closer N_0 is to N_{OC}, the smaller both errors and the predicted distance will be. Thus, the choice of the prediction parameters should be a compromise between predicting far away and predicting with accuracy. When the predicted trajectory counts as many terms as the given measured trajectory ($N_0 = 50$ and $N_{OC} = 100$), the model is able to predict an average 0.5 m future trajectory with a linear error of 0.08 m and an angular error of 0.3 rad.

2.4 Discussion

The prediction model assessment leads to the following conclusion: the prediction process efficiency depends a lot on the prediction parameters N_0 and N_{OC}. Indeed, when performing multiple tests, it seems that the greater N_0 is and the closer N_{OC} is from N_0 the more precise the prediction will be. An optimization problem could be proposed to find the optimal prediction parameters which maximize the predicted distance while minimizing the linear and angular errors. However, we can denote that, to give a satisfying result for the targeted application, the prediction process accepts a wide range of parameters. For example, when taking $(N_0, N_{OC}) = (25, 100)$ or $(N_0, N_{OC}) = (50, 200)$ the process is still able to predict human behaviour even if this prediction is less accurate than with $(N_0, N_{OC}) = (50, 100)$. Indeed, with those last parameters, the model is able to predict an average 0.5m future trajectory with a linear error (namely an average distance between the predicted and the measured trajectories) of 0.08m and an angular error of 0.3rad. This seems to be a good performance with respect to a CVM like the one described in Schöller et al. [100] which scores with a linear error of 0.28m. As a reminder, the CVM outperformed some state-of-the-art approaches like LSTM neural networks [100]. However, all those methods were assessed on benchmark datasets of crowded environments. It would be very interesting to test our prediction model on the same database to allow a relevant comparison. Nevertheless, our model may not be appropriate to generate future trajectories of people in a crowd as it was not designed to handle potential pedestrian interactions or to avoid collisions between individuals. Moreover, as far as we know, in the other state of the art approaches there is no similar assessed quantities which could allow a comparison between our model and theirs. Indeed, no assessment on the angular error or on the predicted distance was found in the literature.

2.5 Conclusion

To conclude, in this chapter, an OC model which predicts the future trajectories of single walking humans is developed. This model was tested and assessed over the 400 human trajectories performed as part of the experiments described in Sec.1.2. This assessment demonstrates that the set of prediction parameters $(N_0, N_{OC}) = (50, 100)$ looks like a good compromise for the targeted applications, namely a human-robot collaboration.

Moreover, it is interesting to denote that this model provides accurate results for all the subjects. This demonstrates the generic nature of the proposed prediction process. In the context of HRI, this is a key argument in favor of this model. Indeed, the fact that a robot can interact with any partner without tuning the model according to the partner is very convenient. However, work remains to be done to use this model in the HRI context. Indeed, even if this model works in real-time, it still needs to be embedded into the robot's motion planner. The following chapter deals with this issue.

Chapter 3

Embedding of a Human Locomotion Model into the Walking Pattern Generator of a Humanoid Robot

Contents

3.1 Introduction

3.1.1 Motivations

Interactions between humans and humanoid robots raise great challenges. Indeed, not only are the human behaviours not always well known, but also the humanoid robots are complex to control. Furthermore, the redundancy of the human musculoskeletal system allows multiple behaviours which make them hard to predict. These interactions go from avoiding humans to assisting them when doing complex tasks. In the context of collaborative tasks, humanoid robots classically follow passively the humans [104]. Nevertheless, those tasks could be performed more efficiently if the robot could predict and anticipate human motions. As part of the ANR-CoBot project, a proactive collaboration between a human and a TALOS humanoid robot to carry and move a table is aimed. For now, only the locomotion of single walking humans was studied in Chapter 1 and Chapter 2. Thus, in this chapter, the focus remains on the reduced problem where the issue of walking with a table has been put aside. The co-manipulation task targeted in the ANR-CoBot project is reduced to a co-navigation task where the humanoid robot has to proactively track a single walking human. Thus, this work focuses on embedding a human locomotion model into the robot WPG in order to improve its ability to assist a moving human partner. The main objective of this chapter is to couple the robot WPG with the real-time prediction model introduced in Chapter 2 in order to generate the footsteps of the robot along the predicted trajectory of a currently walking human.

3.1.2 Related Works

3.1.2.1 Walk generation for humanoid robots

As humanoid robots are very complex systems with numerous DoFs, making such robots walk is not a trivial issue. One of the major challenges in gait generation is guaranteeing the balance of the robot during locomotion. This problem can be solved by controlling a point called the Zero Moment Point (ZMP). Indeed, a robot will keep its balance if this point stays within its support polygon during the gait [105].

This idea was first introduced in Vukobratović et al. [106]. However, the first implementation of a ZMP controller to generate a humanoid robot walk was Kajita et al. [107]. In this work, the authors presented a ZMP preview control scheme which computed the CoM of the humanoid robot over a prediction horizon from imposed footsteps given to the controller. In Wieber [108], a new formulation of this ZMP preview control using a Model Predictive Control (MPC) scheme was proposed. MPC is a control scheme designed to compute a control by solving online, at each sampling instant, a sequence of OC problems over a finite horizon [109]. This kind of scheme can handle constrained problems such as the gait generation problem. Moreover, it is quite robust against perturbations. Thus, nowadays, this MPC approach is the most commonly adopted method to design a WPG for humanoid robots [110, 111, 112, 113]. Moreover, the original MPC has been improved to achieve automatic footstep placements by Herdt et al. [105]. This formulation divided the problem in two optimization problems, one tracking a reference translation speed and the other tracking a reference rotation speed. However, in order to avoid dealing with non-linear constraints introduced by the foot orientations, the rotations were computed before solving the MPC problem for the foot and CoM positions. The same approach was chosen in De Simone

et al. [114]. Thus, those formulations prevented the real-time computation of the foot rotations.

To address this problem, solutions have been proposed. First, non-linear reformulations of the MPC for gait generation were proposed [115, 116]. The Non-linear Model Predictive Control (NMPC) proposed by Naveau et al. [115] allowed to simultaneously compute the CoM and the footstep positions and orientations according to a reference velocity. Moreover, it was able to deal with quadratic, thus non-linear, constraints to avoid obstacles which might be useful in future works to avoid collisions while walking, for example. Another method to deal with non-linear constraints was introduced in Bohórquez et al. [117]. In this work, the authors used safe linear constraints which are always in the intersection at the non-linear constraints. However, unlike Naveau et al. [115], the footstep placements were not automatic, a sequence of step positions and orientations is given to the MPC scheme. Thus, as far as we know, the WPG dealing with footstep orientations either took as an input a velocity command or a sequence of predefined footsteps. None of them focused on automatically generating footsteps along a given trajectory.

3.1.2.2 Proactive human-robot interactions

To proactively collaborate with a human, a humanoid robot needs to predict, or at least guess, its partner's future actions [118]. As far as we know, the first experiment where a humanoid robot proactively interacts with a human was performed in Bussy et al. [102]. In this work, motion primitives like Stop, Side, Turn and Walk/Turn were used to generate the robot locomotion according to the human velocity. Since then, collaborative tasks are often aimed to be as proactive as possible in order to smooth the HRIs.

For example, in Otani et al. [119], a co-manipulation task was aimed. To achieve this goal, the authors designed a robot controller which can generate optimal motions in real-time equivalent to those generated by a human. As this controller took into account the whole-body dynamics of the human, it allowed more proactive interactions between the humanoid robot and the human. In this chapter, a similar method is enforced, only the goal differs. Indeed, here, we try to perform a co-navigation task instead of a co-manipulation task.

Furthermore, proactive co-navigation tasks have already been well studied. Indeed, in Teja et al. [120], the authors proposed a reactive trajectory planner for robots which takes into account the human predicted motions and goals to handle human-robot co-navigation. The estimation of human movements was based on its current velocity and three different navigation modes were presented to make the robot move forward without colliding with the human. Thus, even if our work also aims at a co-navigation task, the goal is not to smoothly avoid the human but to walk along with a human partner.

The co-navigation task we are trying to perform in this chapter is the first step toward a table handling task which can be compared to one aimed in Lanini et al. [121, 122]. Indeed, in those papers, the authors targeted a collaborative handling task while walking, where the humanoid robot identified its human partner's intentions. To guess human future motions, a training of a multiclass classifier of human intentions was performed using measurements collected from a human-human handling collaboration. The results of this training, namely the optimal features to discriminate a set of human motions, was then used to predict human

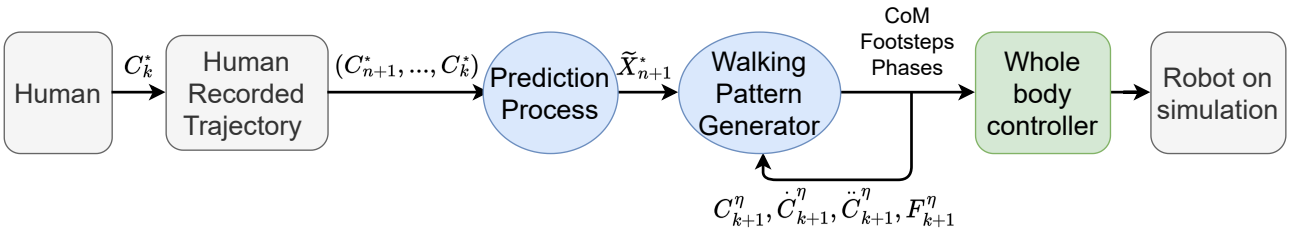

Figure 3.1: Description of the whole framework presented in this chapter. The notations introduced in this chart are defined throughout the chapter.

intentions. In this chapter, instead of using supervised learning to classify and guess human intentions, an OC scheme is built to predict the human future trajectory. To the best of our knowledge, machine learning [123, 124, 125] and probabilistic state machines [126] have already been studied to guess human intentions, but it's the first time that an OC model was proposed to solve such a real-time prediction problem. A real-time approach is more complex but gives more versatility for future works. Indeed, optimization problems allow to incrementally add obstacles or new constraints by adding new terms to the cost function.

3.1.3 Contributions

The work presented in this chapter is a step toward proactivity during HRIs. Indeed, this chapter deals with embedding human-like motions in a humanoid robot's behaviour. Making a robot move like a human improves the human-robot collaboration [15]. It has two main advantages. First, it makes the interaction smoother and swifter as the robot no longer is a passive follower but anticipates its partner's intentions. Then, as human-like motions are easily interpreted by a human being, it makes the interaction more natural for the human partner.

In Sec.3.2, a first way of embedding a human locomotion model in the robot WPG is tested. In the presented experiments, the TALOS robot walks using the WPG designed by *PAL Robotics*. The velocity command computed from the clothoid-based and the OC models presented in Sec.1.3 are sent to this WPG.

Then, in Sec.3.3, another method is introduced. A new WPG based on a NMPC scheme is developed. It allows us to generate CoM and the footstep trajectories along a given trajectory. This trajectory could be computed using the human locomotion model presented in Sec.1.4.

Finally, in Sec.3.4, this new WPG is coupled with the prediction model designed in Sec.2.2. Thus, the generated robot's CoM or footsteps can track or even outpace a walking human. Then, in Sec.3.5, the generated data is sent to a torque whole-body controller. The whole framework is assessed in simulation on Gazebo and is described in Fig.3.1. The final result is a successful simulation of a proactive co-navigation task.

This work was published in **Maroger** et al. [2, 4]. Videos of this work are available on: `https://www.youtube.com/watch?v=ZmAJzs6VDlw`, and on: `https://www.youtube.com/watch?v=hu-cuUYl-58&t=96s`. Moreover, the implementation of all the presented models uses open-source softwares with the aim to ease reproducibility. The Python implementation of the WPG is available on: `https://github.com/imaroger/nmpc_walkgen/tree/topic/python3/python3`.

3.2 Walking pattern generator of *PAL Robotics*

As a first step, we used the WPG provided by the TALOS robot manufacturer, *PAL Robotics*. To make the robot walk in a human-like way, we choose to send to the robot velocity command computed from the existing human-like locomotion models described in Sec.1.3. The implementation of the clothoid-based and the OC models on a TALOS robot implies respecting some velocity and computation time limits. This work was presented in **Maroger** et al. [2].

3.2.1 Experiments

The main goal of these experiments is to make a TALOS robot walk in a human-like way toward a table. To achieve that, a MoCap (20 infrared Qualisys Miqus M3 cameras sampling at 650 Hz with a 0.3 mm precision on the imaged area) is used to record in real-time the positions of the robot and the table. This allows to generate different trajectories using the clothoid-based and the OC model and play them on a TALOS robot.

Both models generate a CoM path between the initial pose (where the robot initially is) and the final pose (at 0.9 m from the closest edge of the table and oriented to face it). Then, a velocity command can be computed as follows:

$$\begin{cases} v_x(t) = (x_{sim}(t+1) - x_{real}(t)) \times f \\ v_y(t) = (y_{sim}(t+1) - y_{real}(t)) \times f \\ v_\theta(t) = (\theta_{sim}(t+1) - \theta_{real}(t)) \times f \end{cases} \tag{3.1}$$

with $(x_{sim}(t+1), y_{sim}(t+1), \theta_{sim}(t+1))$ the next pose in the computed trajectory, $(x_{real}(t), y_{real}(t), \theta_{real}(t))$ the current pose of the robot known thanks to the MoCap and f the sending rate. To be sent to the robot, this velocity command must be expressed in the local frame of the robot. Then, this command can be given to the *PAL Robotics* WPG. In order to be performed safely by the robot, it has to respect limits. No more than $0.1\,\mathrm{m.s^{-1}}$ for the linear velocity along the $\vec{x}$ and $\vec{y}$ axis in the local coordinate system and no more than $0.12\,\mathrm{rad}.s^{-1}$ for the angular velocity around the $\vec{z}$ axis.

To fulfill these requirements, a slowing parameter α has to be added to the clothoid description. Thus, Eq.1.1 becomes:

$$\begin{cases} \dot{x}_\alpha(s) = \alpha \cos\theta(s) \\ \dot{y}_\alpha(s) = \alpha \sin\theta(s) \\ \dot{\theta}(s) = \kappa_0 + \kappa_1 s \end{cases} \tag{3.2}$$

with $\alpha \leq 1$, to linearly slow the system. To respect the linear velocity limit, we take $\alpha = 0.1$. With a C++ algorithm that solves this system using the method presented in Sec.1.3.2, the computation duration is around 4.87×10^{-4} s with a Intel® Core™ i5-8400H CPU 2.50GHz processor. This allows us to swiftly recompute the trajectory if the table is moved or if the robot gets away from its nominal trajectory. However, let us point out that there is a risk of collision against the table if the table is moved toward the robot because the velocity associated with a clothoid curve is always positive, so the robot cannot walk backwards.

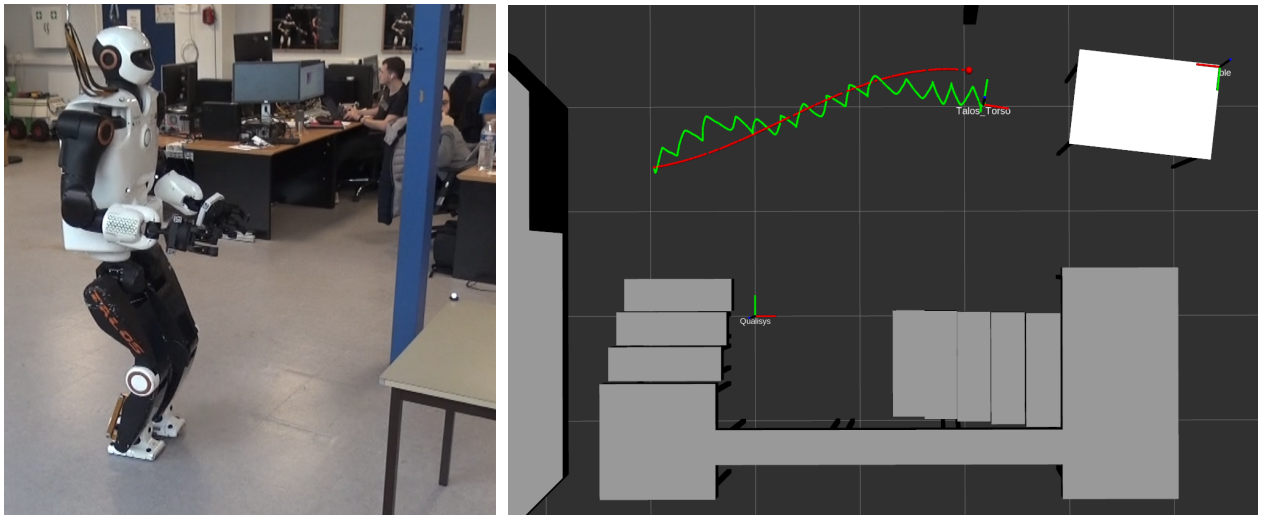

(a) TALOS robot walking toward a table

(b) Visualization of the trajectory of the CoM of the robot (in *green*) during one experiment aiming to follow a clothoid trajectory (in *red*), in the upper right corner is the table (in *white*)

Figure 3.2: Tracking of a clothoid curve by a TALOS humanoid robot using the *PAL Robotics*'s WPG.

The same idea is used to slow the trajectory generated by the OC model, Eq.1.3 becomes:

$$\begin{cases} \dot{x} = \alpha \times (\cos\theta.v_{forw} - \sin\theta.v_{orth}) \\ \dot{y} = \alpha \times (\sin\theta.v_{forw} + \cos\theta.v_{orth}) \\ \dot{\theta} = \omega \\ \dot{v}_{forw} = u_1 \\ \dot{v}_{orth} = u_2 \\ \dot{\omega} = u_3 \end{cases} \tag{3.3}$$

with $\alpha \leq 1$, the smaller α is the greater T will be. With a C++ algorithm using Crocoddyl library as presented in Sec.1.3.3, the computation duration depends on T and its optimization can be expensive. So, to be more precise with $\alpha = 0.1$, it is around 37.1 s on the same processor. This is far too much to allow an online implementation in the robot. So, to embed this trajectory model on the robot, the trajectory has to be previously generated and then played on the robot with no possibility to take into account the possible changes in the environment, a change in the table location, for example.

3.2.2 Results

Among 4 tests, the clothoid experiment produces the following results: the robot ends at about 0.065 m along the $\vec{x}$ axis and 0.205 m along the $\vec{y}$ axis from the goal position with an orientation of -0.028 rad from the goal orientation. Fig.3.2a and Fig.3.2b respectively show the robot walking toward the table and the visualization on RViz of one of the successful experiments. During one of the experiments, we moved the table and the robot successfully recomputed and followed a new clothoid in real-time.

Another conclusion which can be drawn from this experiment is that trying to make the robot follow a clothoid trajectory with the CoM velocity command imposed by the dynamics

of the model does not result in the expected behaviour. Indeed, as we see in Fig.3.2b, when the curvature increases, the robot does not succeed in following the desired trajectory. Moreover, the rate at which the commands are sent seems crucial for the robot to perform the expected behaviour.

We note that with no further control over the WPG parameters (like the stepping frequency, the duration of simple and double support), the robot cannot exactly follow a given dynamic. Therefore, if we can compute the footsteps and their timing along the trajectory, we could improve our results. This could be achieved using another WPG than the one currently provided by *PAL Robotics*. This leads to the conclusion that a more adaptable WPG should be developed.

To conclude, these experiments demonstrate that a simple velocity command based on a human-like locomotion model is not enough to make a humanoid robot walk in a human-like way. The development of a WPG embedding a human-like locomotion model is needed to achieve this goal.

3.3 Walking pattern generator for trajectory tracking

As we show in the previous section, we need to develop a WPG which can follow human dynamics. To achieve this goal, we choose to build a WPG able to generate CoM and footsteps trajectory along a given trajectory. If this trajectory is generated using the human-like locomotion model developed in Sec.1.4, the robot will then properly follow a human-like trajectory as expected.

Thus, in this section, we introduced a WPG for trajectory tracking. This new WPG published in **Maroger** et al. [4] is based on the WPG for velocity tracking presented in Naveau et al. [115].

3.3.1 Non-linear model predictive control for velocity tracking

In Naveau et al. [115], the authors present a WPG based on NMPC and its application on the HRP-2 humanoid robot. This WPG solves simultaneously the footstep position and orientation problems. Moreover, it is able to avoid and get around convex obstacles. This is the reason why we choose to base our work on this WPG. Indeed, in future works, we may need to implement constraints for obstacle avoidance later, to avoid collisions between the robot and the table legs, for example.

Let us denote that as there is no state feedback in the WPG described below. Thus the name NMPC should be replaced by OC model. However, for the sake of clarity, we keep the term NMPC to differentiate the humanoid robot walking generator section from the human locomotion prediction section.

This subsection presents the core equations of the NMPC introduced in Naveau et al. [115].

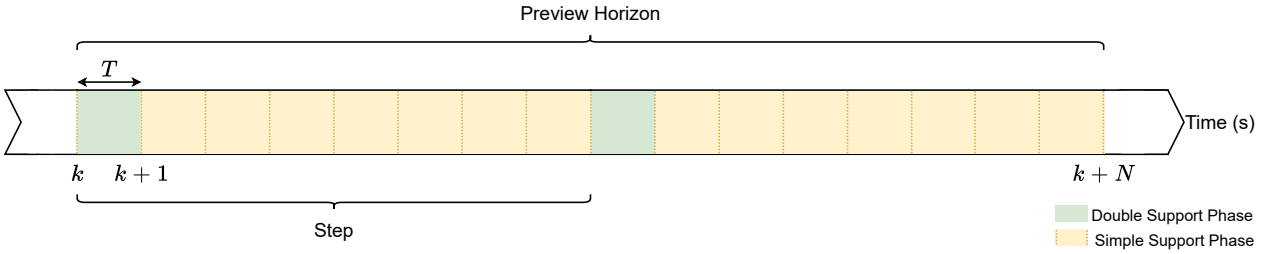

Figure 3.3: Model predictive control scheme.

3.3.1.1 Dynamics

Center of Mass

The jerk of the CoM is assumed to be piecewise constant on each sampling period of time T_{WPG} represented in Fig.3.3. Thus, the jerk is described as follows:

$$\forall t \in [kT_{WPG}, (k+1)T_{WPG}] \text{ with } k \in [\![1, N_{WPG}]\!],\ \dddot{c}^{\nu}_{k}(t) = \dddot{c}^{\nu}_{k}$$

with c the CoM position in the global frame and $\nu \in \{x, y\}$. Thus, using Taylor expansion, we get:

$$\begin{cases} c^{\nu}_{k+1} \approx c^{\nu}_{k} + \dot{c}^{\nu}_{k} T_{WPG} + \ddot{c}^{\nu}_{k} \frac{T^2_{WPG}}{2} + \dddot{c}^{\nu}_{k} \frac{T^3_{WPG}}{6} \\ \dot{c}^{\nu}_{k+1} \approx \dot{c}^{\nu}_{k} + \ddot{c}^{\nu}_{k} T_{WPG} + \dddot{c}^{\nu}_{k} \frac{T^2_{WPG}}{2} \\ \ddot{c}^{\nu}_{k+1} \approx \ddot{c}^{\nu}_{k} + \dddot{c}^{\nu}_{k} T_{WPG} \end{cases} \tag{3.4}$$

So we can write:

$$\hat{c}^{\nu}_{k+1} = A\hat{c}^{\nu}_{k} + B\dddot{c}^{\nu}_{k} \tag{3.5}$$

with $\hat{c}^{\nu}_{k} = \begin{pmatrix} c^{\nu}_{k} \\ \dot{c}^{\nu}_{k} \\ \ddot{c}^{\nu}_{k} \end{pmatrix}$, $A = \begin{pmatrix} 1 & T_{WPG} & \frac{T^2_{WPG}}{2} \\ 0 & 1 & T_{WPG} \\ 0 & 0 & 1 \end{pmatrix}$ and $B = \begin{pmatrix} \frac{T^3_{WPG}}{6} \\ \frac{T^2_{WPG}}{2} \\ T_{WPG} \end{pmatrix}$. This leads to:

$$\hat{c}^{\nu}_{k+N_{WPG}} = A^n \hat{c}^{\nu}_{k} + \sum_{i=0}^{n-1} A^i B \dddot{c}^{\nu}_{k+i} \tag{3.6}$$

The CoM over the preview horizon of length N_{WPG} and its derivatives are then defined as:

$$\begin{cases} C^{\nu}_{k+1} = \begin{pmatrix} c^{\nu}_{k+1} & \dots & c^{\nu}_{k+N_{WPG}} \end{pmatrix}^T = P_{ps} C^{\nu}_{k} + P_{pu} \dddot{C}^{\nu}_{k} \\ \dot{C}^{\nu}_{k+1} = \begin{pmatrix} \dot{c}^{\nu}_{k+1} & \dots & \dot{c}^{\nu}_{k+N_{WPG}} \end{pmatrix}^T = P_{vs} C^{\nu}_{k} + P_{vu} \dddot{C}^{\nu}_{k} \\ \ddot{C}^{\nu}_{k+1} = \begin{pmatrix} \ddot{c}^{\nu}_{k+1} & \dots & \ddot{c}^{\nu}_{k+N_{WPG}} \end{pmatrix}^T = P_{as} C^{\nu}_{k} + P_{au} \dddot{C}^{\nu}_{k} \\ \dddot{C}^{\nu}_{k+1} = \begin{pmatrix} \dddot{c}^{\nu}_{k+1} & \dots & \dddot{c}^{\nu}_{k+N_{WPG}} \end{pmatrix}^T \end{cases} \tag{3.7}$$

with P_{ps}, P_{vs}, $P_{as} \in \mathbb{R}^{N_{WPG} \times 3}$ and P_{pu}, P_{vu}, $P_{au} \in \mathbb{R}^{N_{WPG} \times N_{WPG}}$ obtained from a recursive application of the CoM dynamics (Eq.3.6). More details can be found in Herdt et al. [127].

Center of Pressure

According to the Linear Inverted Pendulum Model (LIPM) introduced in Kajita et al. [107], the

Center of Pressure (CoP), also called ZMP when it is in the support polygon, can be expressed as a linear function of the CoM pose as follows:

$$z_k^\nu = \begin{pmatrix} 1 & 0 & -\frac{h}{g} \end{pmatrix} \hat{c}_k^\nu \tag{3.8}$$

with h the height of the CoM with respect to the ground and g the gravity. We denote $\omega = \sqrt{\frac{h}{g}}$. Then, we define:

$$Z_{k+1}^\nu = \begin{pmatrix} z_{k+1}^\nu & \dots & z_{k+N_{WPG}}^\nu \end{pmatrix}^T = P_{zs} C_k^\nu + P_{zu} \dddot{C}_k^\nu \tag{3.9}$$

with $P_{zs} = P_{ps} - \omega^2 P_{as}$ and $P_{zu} = P_{pu} - \omega^2 P_{au}$.

Capture Point

The Capture Point (CP) or Divergent Component of Motion (DCM) was introduced by Hof et al. [128] and Pratt et al. [129]. It can be derived from the LIPM system equations and is defined as follows:

$$\xi_k^\nu = \begin{pmatrix} 1 & \frac{1}{\omega} & 0 \end{pmatrix} \hat{c}_k^\nu \tag{3.10}$$

Thus, the CP over the preview horizon can be defined as follows:

$$\Xi_{k+1}^\nu = \begin{pmatrix} \xi_{k+1}^\nu & \dots & \xi_{k+N_{WPG}}^\nu \end{pmatrix}^T = P_{\xi s} C_k^\nu + P_{\xi u} \dddot{C}_k^\nu \tag{3.11}$$

with $P_{\xi s} = P_{ps} + \frac{1}{\omega} P_{vs}$ and $P_{\xi u} = P_{pu} + \frac{1}{\omega} P_{vu}$.

Footsteps

The position and orientation of the support foot are described by:

$$F_{k+1}^\eta = \begin{pmatrix} f_{k+1}^\eta & \dots & f_{k+N_{WPG}}^\eta \end{pmatrix}^T = v_{k+1} f_k^\eta + V_{k+1} \tilde{F}_{k+1}^\eta \tag{3.12}$$

$f_k^\eta \in \mathbb{R}$ with $\eta \in \{x, y, \theta\}$ is the current position and orientation of the support foot. $F_{k+1}^\eta \in \mathbb{R}^{n_f}$ with n_f the maximum number of double support phase in the preview are the future positions and orientations of the support foot. The vector $v_{k+1} \in \mathbb{R}^N$ and the matrix $V_{k+1} \in \mathbb{R}^{N_{WPG} \times n_f}$ are called selection matrix, they indicate which foot is the support foot during the sampling interval. For example, with $N_{WPG} = 6$ and $nf = 2$, if the current footstep ends at $t = 2T_{WPG}$ and a footstep lasts $3T_{WPG}$, we will have: $F_{k+1}^\eta = \begin{pmatrix} f_{k+1}^\eta \\ \dots \\ f_{k+N_{WPG}}^\eta \end{pmatrix} = \begin{pmatrix} 1 \\ 1 \\ 0 \\ 0 \\ 0 \\ 0 \end{pmatrix} f_k^\eta + \begin{pmatrix} 0 & 0 \\ 0 & 0 \\ 1 & 0 \\ 1 & 0 \\ 1 & 0 \\ 0 & 1 \end{pmatrix} \tilde{F}_{k+1}^\eta$.

Let $f^{\theta,R}$ and $f^{\theta,L}$ respectively be the orientation of the right foot and the left foot, the orientation of the robot's base is then:

$$\begin{cases} C_{k+1}^\theta = \frac{1}{2}(f_{k+1}^{\theta,R} + f_{k+1}^{\theta,L}) \\ \dot{C}_{k+1}^\theta = \frac{1}{2}(\dot{f}_{k+1}^{\theta,R} + \dot{f}_{k+1}^{\theta,L}) \\ \ddot{C}_{k+1}^\theta = \frac{1}{2}(\ddot{f}_{k+1}^{\theta,R} + \ddot{f}_{k+1}^{\theta,L}) \end{cases} \tag{3.13}$$

Reference velocity

The controller is designed to track a reference velocity: $Vel_{k+1}^{ref} = \begin{pmatrix} Vel_{k+1}^{x,ref} & Vel_{k+1}^{y,ref} & Vel_{k+1}^{\theta,ref} \end{pmatrix}^T$

3.3.1.2 Optimization problem

Cost function

The cost function used in Naveau et al. [115] is the following:

$$J(U_k) = \frac{\alpha}{2}J_1(U_k) + \frac{\alpha}{2}J_2(U_k) + \frac{\beta}{2}J_3(U_k) + \frac{\gamma}{2}J_4(U_k) \tag{3.14}$$

with α, β and γ the weights of the cost function, U_k the free variables defined as $U_k = \begin{pmatrix} \dddot{C}_k^x & \tilde{F}_k^x & \dddot{C}_k^y & \tilde{F}_k^y & \tilde{F}_k^\theta \end{pmatrix}^T$ and:

$$\begin{cases} J_1(U_k) = ||\dot{C}_{k+1}^x - Vel_{k+1}^{x,ref}||_2^2 + ||\dot{C}_{k+1}^y - Vel_{k+1}^{y,ref}||_2^2 & \text{Linear velocity tracking} \\ J_2(U_k) = ||F_{k+1}^\theta - \int Vel_{k+1}^{\theta,ref} dt||_2^2 & \text{Angular velocity tracking} \\ J_3(U_k) = ||F_{k+1}^x - Z_{k+1}^x||_2^2 + ||F_{k+1}^y - Z_{k+1}^y||_2^2 & \text{CoP positioning} \\ J_4(U_k) = ||\ddot{C}_{k+1}^x||_2^2 + ||\ddot{C}_{k+1}^y||_2^2 & \text{Smoothing of the motion} \end{cases} \tag{3.15}$$

Let us denote that the choice to work with a piecewise constant jerk hypothesis aims to achieve a more stable behaviour for the humanoid robot. Indeed, working with a piecewise constant acceleration would lead to discontinuities between two accelerations which leads to discontinuities between two ZMP. These discontinuities could deteriorate the robot balance. Moreover, the minimisation of the jerk as proposed in Eq.3.15 is consistent with observations in human motor control [75].

Quadratic Problem

The optimization problem to solve is the following:

$$\min_{U_k} J(U_k) \tag{3.16}$$

In order to solve this problem with a Sequential Quadratic Problem (SQP) solver, we need to write it as:

$$\min_{U_k} \frac{1}{2}U_k^T Q_k U_k + p_k^T U_k \tag{3.17}$$

with $Q_k = \begin{pmatrix} Q_k^x & 0 & 0 \\ 0 & Q_k^y & 0 \\ 0 & 0 & Q_k^\theta \end{pmatrix}$ and $p_k = \begin{pmatrix} p_k^x \\ p_k^y \\ p_k^\theta \end{pmatrix}$. Let us notice that $Q_k^x = Q_k^y$ and can be write as $\begin{pmatrix} Q_k^{XX} & Q_k^{XF} \\ Q_k^{FX} & Q_k^{FF} \end{pmatrix}$. Moreover, we denote $p_k^\nu = \begin{pmatrix} p_k^{\nu X} \\ p_k^{\nu F} \end{pmatrix}$. We will detail the calculation of those coefficients below.

First we will express the cost function in a canonical form. To ease the readability some subscript and superscript have been removed:

- J_1 expansion:
  $||\dot{C} - Vel||^2 = (\dot{C} - Vel)^T(\dot{C} - Vel) = (C^T P_{vs}^T + \dddot{C}^T P_{vu}^T - Vel^T)(P_{vs}C + P_{vu}\dddot{C} - Vel)$
  $||\dot{C} - Vel||^2 = \dddot{C}^T \underbrace{P_{vu}^T P_{vu}}_{Q^{XX}} \dddot{C} + 2\underbrace{P_{vu}^T(P_{vs}C - Vel)}_{p^X}\dddot{C} + cste$
- J_3 expansion:
  $||F - Z||^2 = (F - Z)^T(F - Z) = (fv^T + \tilde{F}^T V^T - C^T P_{zs}^T - P_{zu}^T \dddot{C}^T)(vf + V\tilde{F} - P_{zs}C - P_{zu}\dddot{C})$

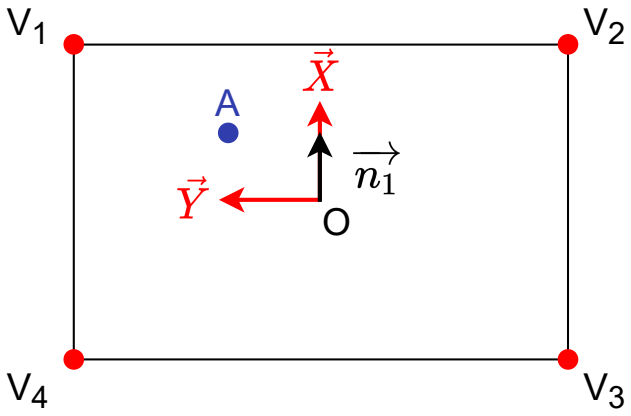

Figure 3.4: Robot support polygon representation.

$$||F-Z||^2 = \tilde{F}^T \underbrace{V^T V}_{Q^{FF}} \tilde{F} - F^T \underbrace{V^T P_{zu}}_{Q^{FX}} \dddot{C} - \dddot{C}^T \underbrace{P_{zu}^T V}_{Q^{XF}} F + \dddot{C}^T \underbrace{P_{zu}^T P_{zu}}_{Q^{XX}} \dddot{C} - 2\underbrace{V^T(P_{zs}C - vf)}_{p^F}$$
$$+ 2\underbrace{P_{zu}^T(P_{zs} - vf)}_{p^X} + cste$$

- J_4 expansion: $||\dddot{C}||^2 = \dddot{C}^T \,\mathrm{Id}\, \dddot{C}$

Now, we deduce:

$$\begin{cases} Q^{XX} = \alpha P_{vu}^T P_{vu} + \beta P_{zu}^T P_{zu} + \gamma \,\mathrm{Id} \\ Q^{XF} = -\beta P_{zu}^T V \\ Q^{FX} = -\beta V^T P_{zu} \\ Q^{FF} = \beta V^T V \\ p^X = \alpha P_{vu}^T (P_{vs}C - Vel) + \beta P_{zu}^T (P_{zs} - vf) \\ p^F = -\gamma V^T (P_{zs}C - vf) \end{cases} \tag{3.18}$$

Constraints

Three constraints are implemented in Naveau et al. [115]: the balance constraint, the foot feasibility constraint and the foot orientation constraint. In the present manuscript, only the first constraint will be fully explained. More details about the other constraints can be found in Naveau et al. [115].

Let us consider a point A represented on Fig.3.4. A is inside the support polygon if:

$$\forall i \in [\![1,4]\!],\ \langle \overrightarrow{OA}, \overrightarrow{n_i} \rangle < \langle \overrightarrow{OV_i}, \overrightarrow{n_i} \rangle \tag{3.19}$$

with $V_i = \begin{pmatrix} x_i \\ y_i \end{pmatrix}$ the vertices of the foot and $\overrightarrow{n_i} = \begin{pmatrix} dx_i \\ dy_i \end{pmatrix} = \begin{pmatrix} y_{i+1} - y_i \\ x_i - x_{i+1} \end{pmatrix}$ is a vector orthogonal to the edge $V_i V_{i+1}$. Then, for a given support polygon, we define the following matrices: $A_0 = \begin{pmatrix} A_0^x & A_0^y \end{pmatrix} = \begin{pmatrix} dx_1 & dy_1 \\ \dots & \dots \\ dx_{nb\_edge} & dy_{nb\_edge} \end{pmatrix}$ and $b_0 = \begin{pmatrix} dx_1 x_1 + dy_1 y_1 \\ \dots \\ dx_{nb\_edge} x_{nb\_edge} + dy_{nb\_edge} y_{nb\_edge} \end{pmatrix}$.

To ensure the robot balance while walking, the CoP must remain inside the support polygon [**wieber02**]. This constraint can be mathematically expressed as follows:

$$D_{k+1}^\nu Z_{k+1}^\nu < b_{k+1} + D_{k+1}^\nu v_{k+1} f_k^\nu \iff \underbrace{D_{k+1}^\nu P_{zu}}_{A_{CoP}} \dddot{C}_k^\nu < \underbrace{b_{k+1} - D_{k+1}^\nu P_{zc} C_k^\nu + D_{k+1}^\nu v_{k+1} f_k^\nu}_{ub_{CoP}} \tag{3.20}$$

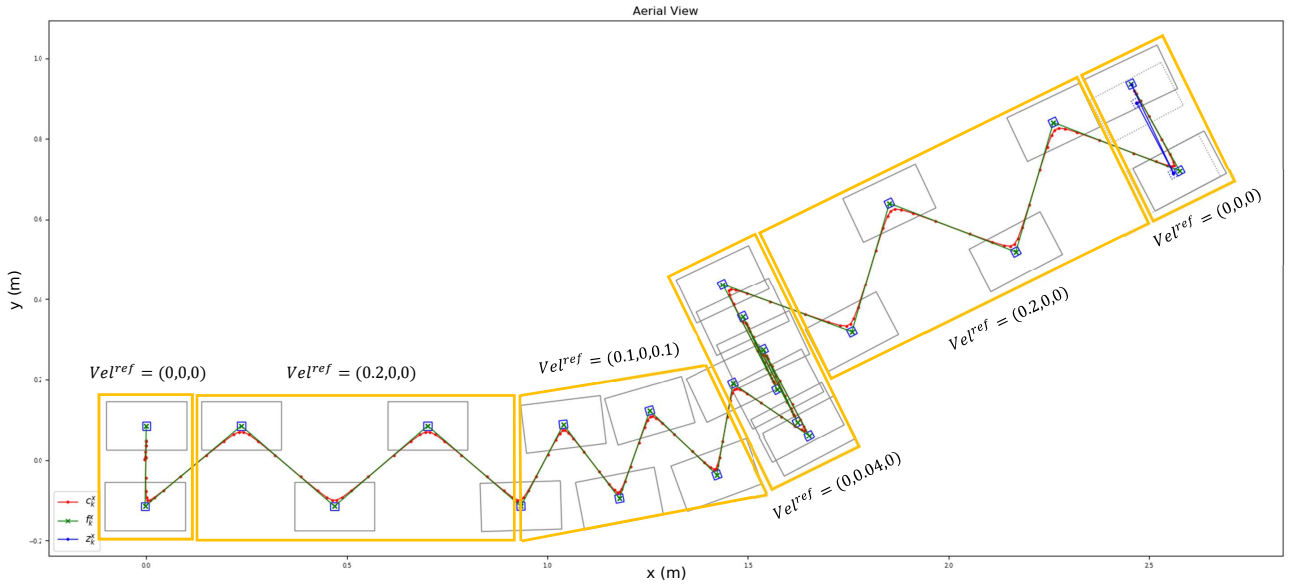

Figure 3.5: Generation of CoM and footsteps trajectories with the WPG with velocity tracking.

In this equation, $D_{k+1} = \begin{pmatrix} A_0^x R(f_{k+1}^\theta) & 0 & A_0^x R(f_{k+1}^\theta) & 0 \\ & \ddots & & \ddots \\ 0 & A_0^x R(f_{k+N_{WPG}}^\theta) & 0 & A_0^x R(f_{k+N_{WPG}}^\theta) \end{pmatrix}$ with $R(f_k^\theta) = \begin{pmatrix} \cos f_k^\theta & \sin f_k^\theta \\ -\sin f_k^\theta & \cos f_k^\theta \end{pmatrix}$ and $b_{k+1} = \begin{pmatrix} b_0 & \dots & b_0 \end{pmatrix}^T$. Thus, this constraint can be written as:

$$A_{CoP,k}(U_k^\theta) U_k^{x,y} < ub_{CoP,k} \tag{3.21}$$

This kind of canonical constraints can be dealt with a SQP solver.

Solver

In the end, the optimisation problem is of the following form:

$$\min_{U_k} \frac{1}{2} U_k^T Q_k U_k + p_k^T U_k \text{ s.t. } lb \leq AU_k \leq ub \tag{3.22}$$

This SQP can be solved with the qpOASES library [130]. More details about this solver can be found in Naveau et al. [115].

3.3.1.3 Results

This WPG allows to generate CoM and footsteps trajectory according to a given reference velocity. An example of those generated data is shown in Fig.3.5 with $N_{WPG} = 16$, $T_{WPG} = 0.2\,\text{s}$ and $n_f = 2$.

3.3.2 Adjustments for trajectory tracking

As a reminder, in the previous section, we developed the core equations of the NMPC described in Naveau et al. [115]. Here, we introduce a new WPG which has two main differences with

the one introduced in Naveau et al. [115]:

- The controller is designed to track a reference trajectory rather than a reference velocity, which implies a different cost function in comparison with Naveau et al. [115].
- A terminal constraint on the CP was added to avoid the internal instability issue in the problem formulation.

3.3.2.1 Cost function

The WPG described in Naveau et al. [115] tracks a constant reference linear and angular velocity over one preview horizon. In this new work, we choose to make it track a reference trajectory $\begin{pmatrix} X_1 & ... & X_N \end{pmatrix}^T$ with $X_i = (x_i, y_i, \theta_i) \forall i \in [\![1, N]\!]$ at a given velocity v. One asset of this modification is that, with a trajectory, the WPG can plan future curvature changes. With a constant reference velocity, the curvature cannot change over a preview. We believe that taking into account future curvature changes in the preview may improve the robot's gait.

The reference trajectory must be interpolated so that the distance between two points of the trajectory, denoted $d(X_i, X_{i+1}) = \sqrt{(x_{i+1} - x_i)^2 + (y_{i+1} - y_i)^2}$, can be travelled at the wished velocity v during T_{WPG}. Thus, the trajectory given to the WPG is $\begin{pmatrix} \tilde{X}_1, ..., \tilde{X}_M \end{pmatrix}^T$ with $M \in \mathbb{N}$ such as $\begin{cases} \tilde{X}_1 = X_1 \\ \tilde{X}_M = X_N \\ \forall i \in [\![0, M-1]\!],\ d(X_i, X_{i+1}) = vT_{WPG} \end{cases}$. Then, at each WPG loop, the reference trajectory will be:

$$C_{k+1}^{ref} = \begin{pmatrix} \tilde{X}_{k+1} & ... & \tilde{X}_{k+N_{WPG}} \end{pmatrix} \tag{3.23}$$

Now, we can define the new cost function for trajectory tracking as follows:

$$J'(U_k) = \frac{\alpha'}{2} J'_1(U_k) + \frac{\beta}{2} J_3(U_k) + \frac{\gamma}{2} J_4(U_k) \tag{3.24}$$

with $\alpha' = \alpha$, β and γ the weights of the cost function and:

$$\begin{cases} J'_1(U_k) = ||C^x_{k+1} - C^{x,ref}_{k+1}||_2^2 + ||C^y_{k+1} - C^{y,ref}_{k+1}||_2^2 + ||C^\theta_{k+1} - C^{\theta,ref}_{k+1}||_2^2 & \text{CoM tracking} \\ J_3(U_k) = ||F^x_{k+1} - Z^x_{k+1}||_2^2 + ||F^y_{k+1} - Z^y_{k+1}||_2^2 & \text{CoP positioning} \\ J_4(U_k) = ||\ddot{C}^x_{k+1}||_2^2 + ||\ddot{C}^y_{k+1}||_2^2 & \text{Control} \end{cases} \tag{3.25}$$

3.3.2.2 Stability problem

Through the described scheme, the balance stability is ensured by an inequality constraint which imposes that the ZMP remains within the support polygon at all times. However, this does not solve the inherent instability of the LIPM dynamics. Indeed, with the LIPM-based models, the CoM can diverge exponentially even if the CoP is maintained in the support polygon which generates an unfeasible walking pattern [131]. Two ways exist to solve this instability [132]:

- Use a long enough preview horizon
- Add a terminal constraint

The terminal constraint can be a capturability constraint which causes the robot to stop at the end of the planning horizon [133]. Scianca et al. [113] proposes an intrinsically stable MPC for gait generation based on this capturability criterion. However, a more trivial way to avoid the divergence of the LIPM model is described in Ciocca et al. [134] where the authors impose the following terminal constraint:

$$\begin{cases} \xi^{\nu}_{k+N_{WPG}} = Z^{\nu}_{k+N_{WPG}} \\ \dot{\xi}^{\nu}_{k+N_{WPG}} = 0 \end{cases} \tag{3.26}$$

This terminal constraint ensures that the robot can stop without making further steps [133]. This is called the 0-step capturability. Thus, a terminal inequality constraint which forces the CP to be in the support polygon at the end of the preview horizon was added in to the Quadratic Problem (QP). This constraint can be written as follows:

$$\begin{aligned} & D^{\nu}_{k+N_{WPG}} \Xi^{\nu}_{k+N_{WPG}} < b_{k+N_{WPG}} + D^{\nu}_{k+N_{WPG}} v_{k+N_{WPG}} f^{\nu}_{k} \\ \iff & \underbrace{D^{\nu}_{k+N_{WPG}} P_{\xi u}}_{A_{DCM}} \ddot{C}^{\nu}_{k} < \underbrace{b_{k+N_{WPG}} - D^{\nu}_{k+N_{WPG}} P_{\xi c} C^{\nu}_{k} + D^{\nu}_{k+N_{WPG}} v_{k+N_{WPG}} f^{\nu}_{k}}_{ub_{DCM}} \end{aligned} \tag{3.27}$$

3.3.2.3 Results

This WPG allows to generate CoM and footstep trajectory according to a given reference trajectory. Examples of the generated data are shown in Fig.3.6 with $N_{WPG} = 16$, $T_{WPG} = 0.2\,\mathrm{s}$, $n_f = 2$.

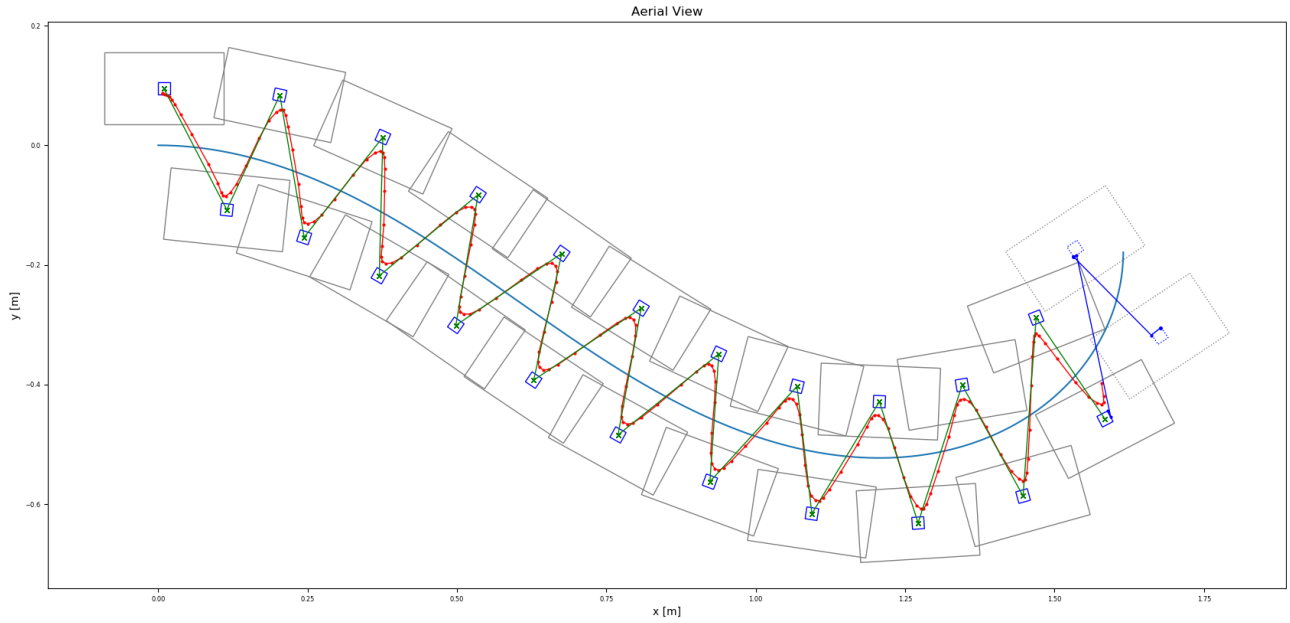

(a) $v = 0.1\,\mathrm{m.s^{-1}}$.

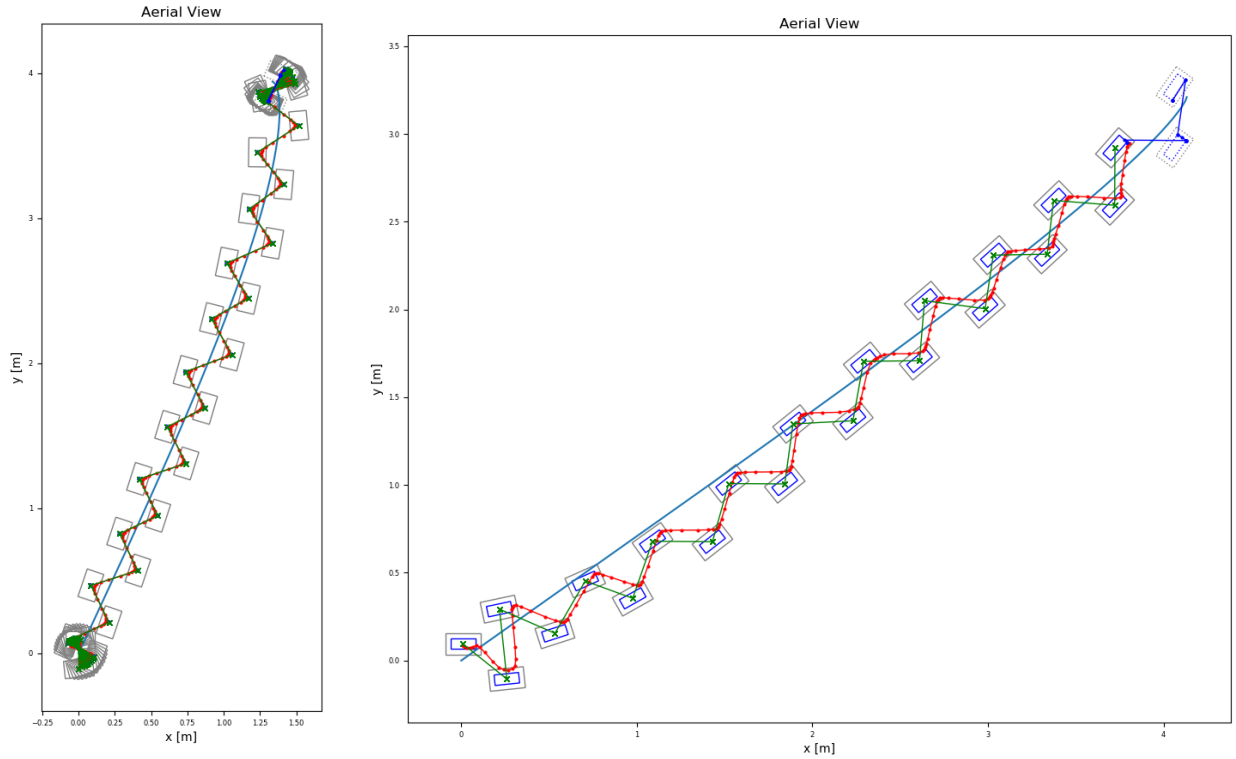

(b) $v = 0.25\,\mathrm{m.s^{-1}}$.

(c) $v = 0.29\,\mathrm{m.s^{-1}}$ with reduced security margins.

Figure 3.6: Generation of CoM and footsteps trajectories with the WPG with trajectory tracking.

3.4 Coupling with the prediction model

In the previous section, we designed a WPG which generates CoM and footsteps trajectories along a given trajectory. Now we would like to couple this WPG with the prediction model described in Chapter 2. This coupling aims to perform a co-navigation task where a humanoid robot proactively tracks a walking human. Thus, if the human accelerates, slows down or stops, the robot should act similarly while following the same trajectory as its partner. This work was published in **Maroger** et al. [4].

3.4.1 Reference Trajectory

We want the humanoid robot to follow the predicted trajectory defined in Sec.2.2. Moreover, as we want the robot to dynamically follow a human, the robot needs to follow the trajectory at the same velocity as the human's walking velocity.

As a reminder, at time $t = kT_{OC}$, $k = n + N_0$, the following data, defined in section 2.2, can be given to the WPG:

- The measured human trajectory until time t: $\begin{pmatrix} C_0^* & C_1^* & \dots & C_k^* \end{pmatrix}^T$. Let us denote that we add * to the notation introduce in Sec.2.2 in order not to mistake the human CoM for the robot CoM on the preview horizon defined in Eq.3.7.
- The solution given by the prediction process at time t: $\tilde{X}_{n+1}^* = \begin{pmatrix} X_{n+1}^* & \dots & X_k^* & \dots & X_{n+N_{OC}}^* \end{pmatrix}^T$. The predicted trajectory $\begin{pmatrix} X_k^* & \dots & X_{n+N_{OC}}^* \end{pmatrix}^T$ is in-

cluded in this solution.

From the measured human trajectory, an average current human walking velocity can be computed:

$$\bar{v}_{n+1} = \frac{\sqrt{(c_k^{*x} - c_{n+1}^{*x})^2 + (c_k^{*y} - c_{n+1}^{*y})^2}}{N_0 \times T_{OC}} \tag{3.28}$$

At this point, three scenarios should be considered:

1. The robot walks behind the human at a constant distance d_{behind}.
2. The robot and the human act synchronously so that no distance divides them. Experimentally, this scenario can be achieved by putting the robot and its human partner side by side to show that the robot is mimicking human motions without any delay.
3. The robot walks ahead of the human at a constant distance d_{ahead}.

Those scenarios are represented in Fig.3.7. In all those scenarios, the robot is always trying to follow the same trajectory as the human. However, according to its position with respect to its partner's position, the robot will be more or less active in the co-navigation task. Consequently, the robot will not have to follow the same part of the optimal trajectory given by the prediction process.

Thus, we have to take additional steps before giving the predicted trajectory to the WPG. On the one hand, the WPG predicts the footsteps over a preview horizon of length N_{WPG}. Then, this prediction lasts $N_{WPG} \times T_{WPG}$. On the other hand, the prediction process predicts the CoM trajectory $\tilde{X}_{n+1}^*$ over a preview horizon of length N_{OC} based on the recent past human trajectory of length N_0. Broadly speaking, $N_{WPG} \neq N_{OC}$ and $T_{WPG} \neq T_{OC}$ (for example, in our case $N_{WPG} = 16$ and $N_{OC} = 100$). This is why we have to manipulate the predicted trajectory before it is given to the WPG.

We will name the robot current CoM position X_m^*. According to the chosen scenario we have:

- Scenario 1: $0 \leq m < k$ such that $\sqrt{(c_k^{*x} - x_m^*)^2 + (c_k^{*y} - y_m^*)^2} \approx d_{behind}$.
- Scenario 2: $m = k$ such that the robot and the human are at the same place in the same time.In other words, at time $t = kT_{OC}$ the robot current CoM position is X_k^* and the human current CoM position is C_k^*.
- Scenario 3: $k < m \leq k + \lfloor \frac{N_{OC} - N_0}{2} \rfloor$ such that $\sqrt{(c_k^{*x} - x_m^*)^2 + (c_k^{*y} - y_m^*)^2} \approx d_{ahead}$.

If we want the robot and the human to be synchronized, we want the robot to travel the same distance as the human at the same time. This is why we look for the index l such as $\sum_{i=m}^{l} \sqrt{(x_i^* - x_{i-1}^*)^2 + (y_i^* - y_{i-1}^*)^2} \approx \bar{v}_{n+1} \times T_{WPG} \times N_{WPG}$. The part of the predicted trajectory which has to be given to the WPG is then $\begin{pmatrix} X_m^* & ... & X_l^* \end{pmatrix}^T$. However, broadly speaking, $m - l + 1 \neq N_{WPG}$. This is why we need to interpolate this trajectory to count N_{WPG} terms so that it can be used as a reference by the WPG. This interpolated trajectory, denoted $\begin{pmatrix} \tilde{X}_m^* & ... & \tilde{X}_l^* \end{pmatrix}^T$, is such as $\tilde{X}_m^* = X_m^*$, $\tilde{X}_l^* = X_l^*$ and its length is equal to N_{WPG}.Thus, the following vector can be sent to the WPG:

$$C_{k+1}^{ref} = \begin{pmatrix} \tilde{X}_m^* & ... & \tilde{X}_l^* \end{pmatrix}^T \tag{3.29}$$

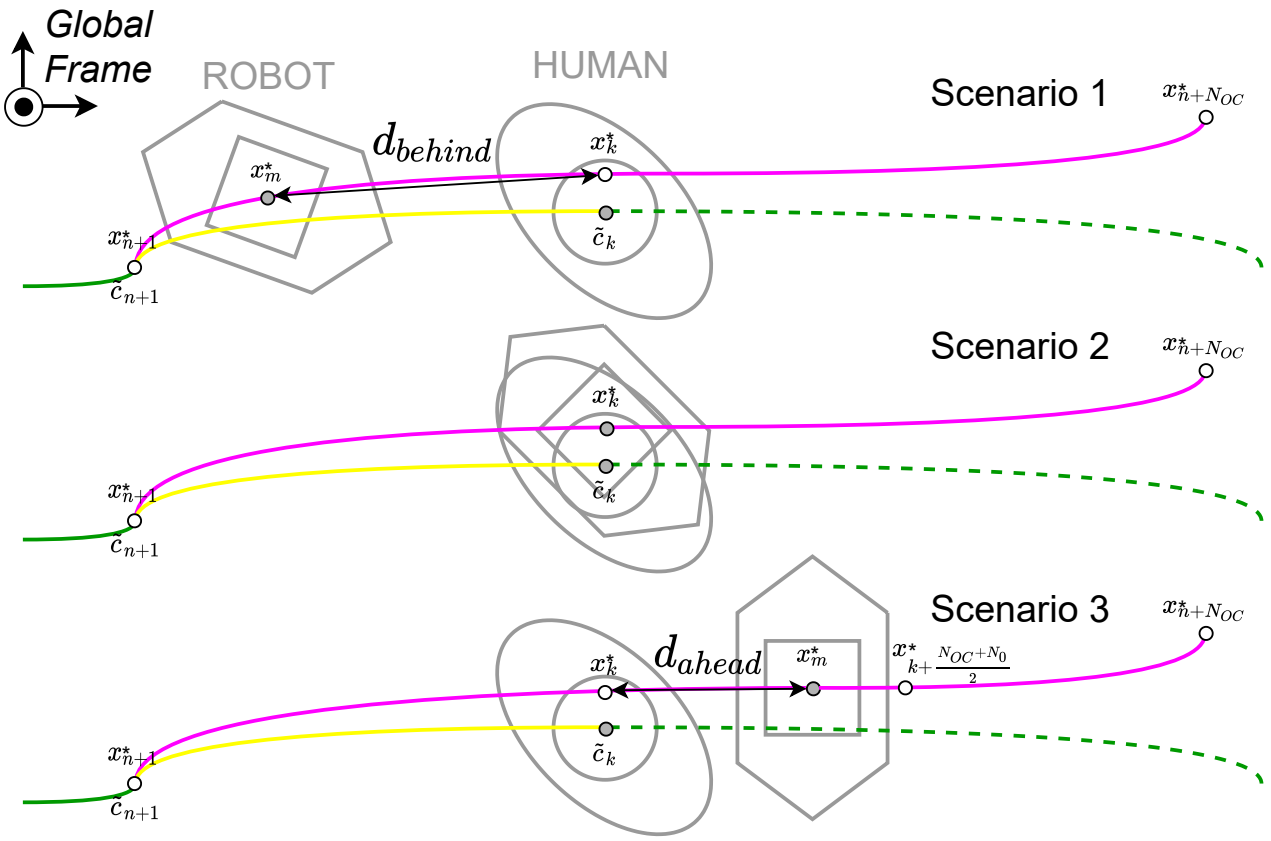

Figure 3.7: Representation of the 3 possible scenarios: at the top, the robot walks behind the human, on the middle they are synchronized, at the bottom the robot walks ahead of the human. In this figure, the solution computed by the prediction process is in *purple*, the past human trajectory is in *green*, its recent past trajectory in *yellow* and its a priori unknown future trajectory in *dashed green*.

Once the reference trajectory given, according to the chosen scenario, the optimization problem defined in Eq.3.24 can be solved. Thus, the CoM and the footstep trajectories of the robot are generated along the optimal trajectory given by the prediction model, resulting in a coupling of the prediction process and the WPG of the robot. In the case of the second and the third scenarios, they are generated along the predicted trajectory.

3.4.2 Simulation

In simulation, this coupling can be described as follows. First, a pre-recorded human trajectory is streamed and retrieved by the prediction process like in Sec2.2.3. Then, it sends the predicted trajectory to the WPG which computes the robot's CoM and feet positions and orientations over the preview horizon with respect to the human velocity computed with Eq.3.28. All those data are shared through a ROS [103] framework and displayed on the RViz software as shown in Fig.3.8 for a trajectory with $(x_0, y_0, \theta_0) = (-1.5, 4, 0)$ as a starting pose and $(x_f, y_f, \theta_f) = (0, 0, \frac{\pi}{2})$. In this figure, the chosen scenario is the second one in Fig.3.7, namely the synchronization of a robot and a human. This coupling matches with the blue boxes represented in Fig.1.2 which shows the whole framework. In the next section, the last steps of

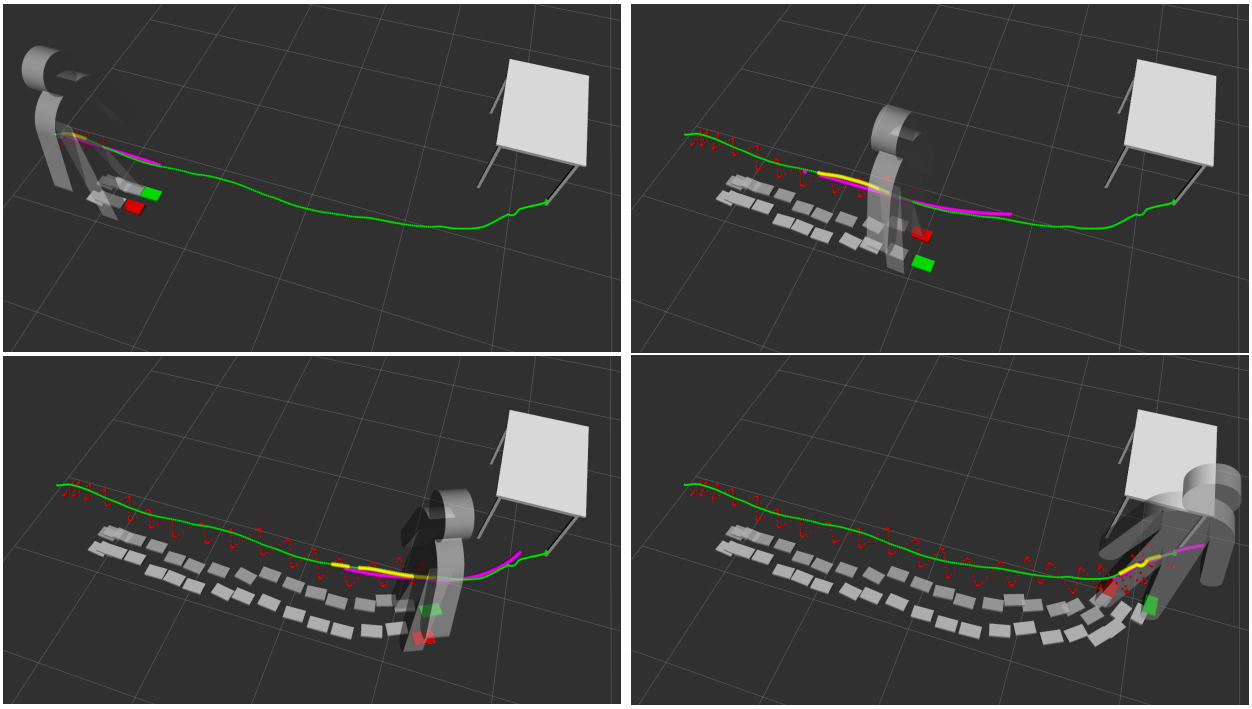

Figure 3.8: The robot CoM (in *red*) and footsteps (past steps in *grey*, current support foot in *red* and future support foot in *green*) are generated from the current optimal solution given by the prediction process (in *purple*) which takes the recent past trajectory of the human (in *yellow*) as an input. Here, the prediction parameters are $N_0 = 50$ and $N_{OC} = 100$.

this process, namely the whole-body controller (the green box in Fig.1.2) and the simulation on the TALOS robot on Gazebo are presented.

3.5 Integration of the whole framework in simulation

The final step to use the trajectory tracking based WPG coupled with the prediction process on the robot is to send the generated CoM and feet trajectories to a whole-body controller developed by Noëlie Ramuzat, another PhD student from the Gepetto team.

3.5.1 Whole-body controller

The whole-body controller computes a stable command from the reference trajectories and the current state of the robot. In this study, the controller used in simulation is a Weighted Quadratic Program (WQP), which solves the inverse dynamics of a robot in rigid contact with the environment [135]. It has been successfully tested on the humanoid robot TALOS in simulations in Ramuzat et al. [136, 137]. The controller takes as inputs the reference trajectories of the WPG and implements task functions with them, such as an acceleration-based tracking law. The controller optimizes a cost function using these tasks, prioritized with weights, while respecting constraints such as the robot dynamics and foot contacts. The interest of this controller is that it implements an Angular Momentum (AM) regularization task, which allows to control the angular momentum part generated by the contact transition[138]. In Ramuzat et al. [136, 137] three controllers are compared. In this work, the torque controller is used. It

is based on the Task Space Inverse Dynamic (TSID) library [139].

3.5.2 Simulation

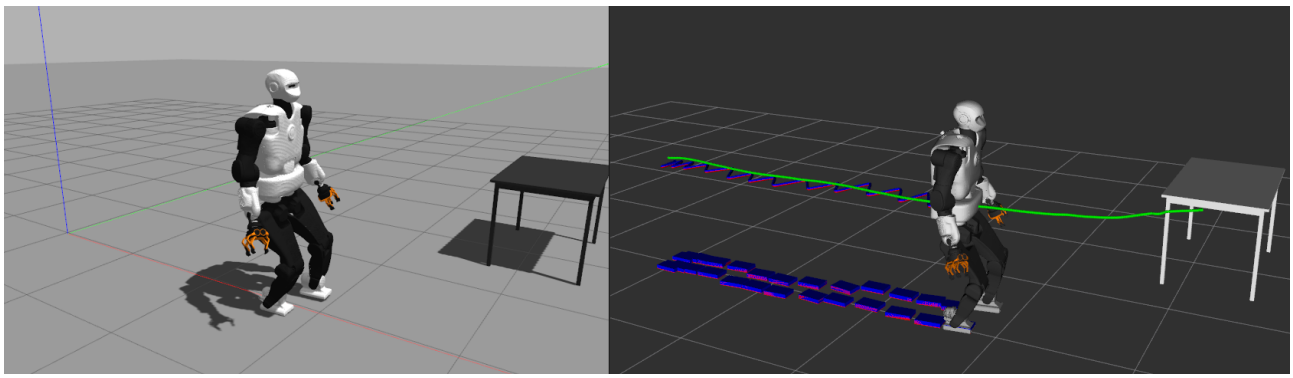

Figure 3.9: Simulation on Gazebo (*left*) of the robot executing the predicted trajectory with $N_0 = 50$ and $N_{OC} = 100$. The CoM, footsteps (desired in *red*, real in *blue*) and human trajectories (in *green*) are also displayed in RViz (*right*) for comparison.

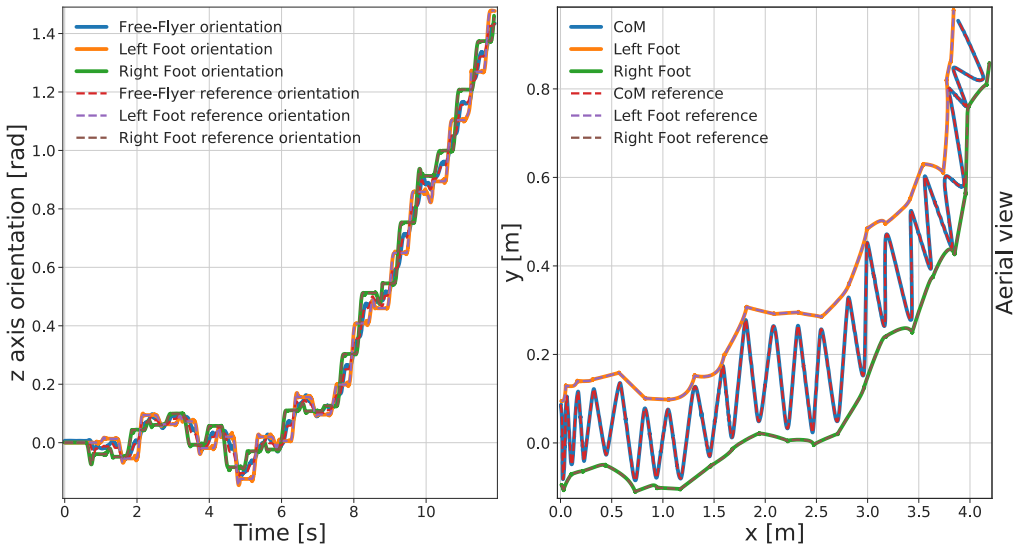

Figure 3.10: Tracking of the CoM and foot trajectories in the Gazebo simulation.

The simulation has been realized using Gazebo on a standard laptop (Intel CPU i7-8850H @ 2.6 GHz). Gazebo is an open-source 3D simulator. This simulator embeds a physics engine which simulates rigid body dynamics and collisions. Thus, in the described simulations, the whole body of the TALOS robot is simulated along with its software framework.

The reference trajectories generated using the WPG are registered in files which are read by the whole-body controller during the simulation. The controller computes the desired torque for all the joints of the robot at 1kHz and sends this command to the simulated robot in Gazebo. The simulation results of the same trajectory presented in Fig.3.8 is shown in Fig.3.9. The CoM and foot references are well followed by the controller, allowing the robot to successfully

perform the motion. Their tracking is presented in Fig.3.10. Compared to Ramuzat et al. [136, 137], gains tuning were needed to make the controller successfully perform the trajectory wide side steps (the CoM proportional gains were raised to 800 and the AM ones decreased to 2.5). The whole prediction process and some simulations are shown in the video available at `https://youtu.be/hu-cuUYl-58`.

3.6 Discussion

3.6.1 Human walking trajectory model

The presented OC model used to predict the human trajectory depends a lot on the chosen human trajectory model. In this work, the chosen model is the one described in Sec.1.4. This model has been optimized in Sec.1.4.3 to generate smooth trajectories of the human CoM. That is to say that it does not take into account the oscillations of the CoM due to the steps. Thus, a human locomotion model which would take into account these oscillations may be considered in case of the prediction model needs to be more precise. Moreover, the chosen human trajectory model has been shown to well fit the average human behaviour while its performance could be poorer when applied to individual subjects. However, when testing the prediction model over trajectories of numerous subjects, it seems to achieve its goals whoever the subject is. The results of 4 predictions for 4 different subjects going from the same starting pose $(x_0, y_0, \theta_0) = (-1.5, 4, \frac{\pi}{2})$ to the same goal pose $(x_f, y_f, \theta_f) = (0, 0, \frac{\pi}{2})$ are presented on Fig.3.11. This demonstrates that the coupling of the prediction process and the WPG provides consistent results which do not depend on the human partner with whom the robot interacts.

3.6.2 Impact of the distance between the subject and the robot

The precision of the human tracking performed by the WPG relies on the chosen scenario and on the potential chosen distance to the human. The greater d_{behind} is, the cleaner the footsteps are because the part of the predicted trajectory used by the WPG is mostly in the measured part. On the opposite, the greater d_{ahead} is, the messier the footsteps are because all those generated footsteps are based on a prediction which can vary a lot according to the measurements as shown in Fig.3.12.

3.6.3 Feasibility of the SQP for high velocity

When the robot is required to walk at a velocity higher than 0.25m.s^{-1} following a trajectory with a non-zero curvature, the SQP turns out to be infeasible and the robot cannot walk with its human partner anymore. This may be solved by relaxing the constraint on the foot rotation or adapting the foot constraint bounds for a TALOS robot as, in this work, we used the ones computed for HRP-2 in Naveau et al. [115]. We could also use another solver like the ones implemented in the Crocoddyl library [70]. The improvement of the WPG to achieve a higher maximum velocity in non-zero curvature trajectories will be the focus of future works.

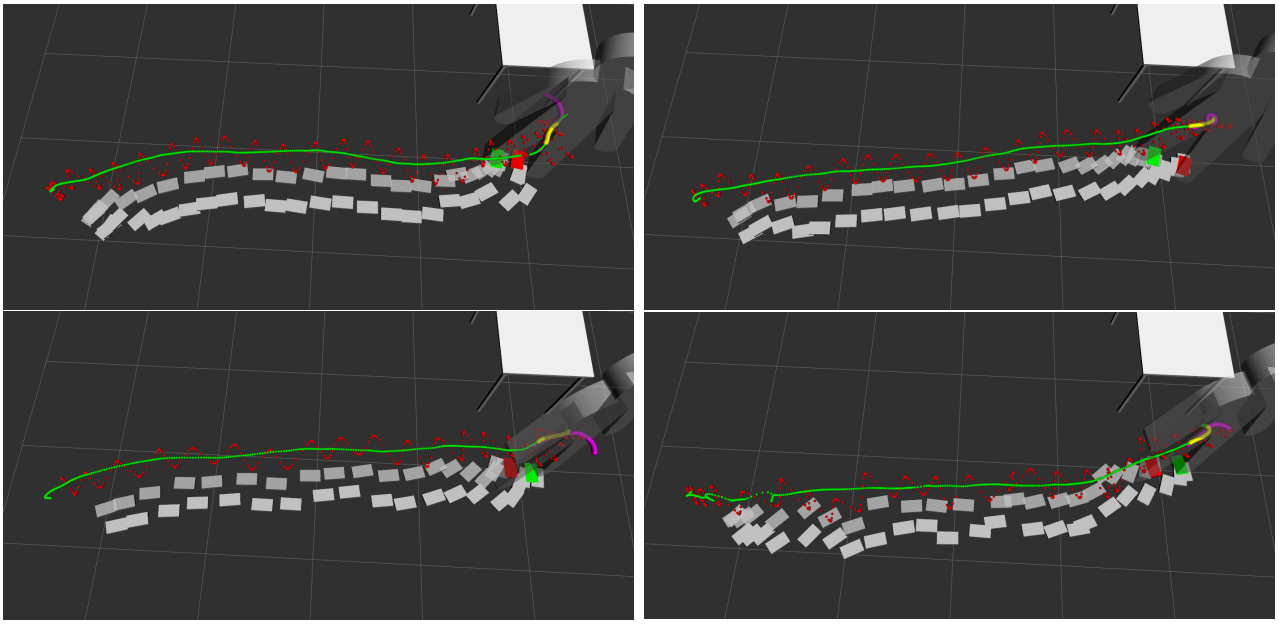

Figure 3.11: Result of the coupling of the prediction model and the WPG for 4 different human subjects. The CoM trajectory of the human is in *green*, the CoM trajectory of the robot is in *red* and the performed footsteps of the robot are in *grey*.

3.6.4 Toward a real human-robot co-navigation task

The transition from the simulation to the real experiment is very challenging.

First of all, an online version of the WPG needs to be built. The version that was presented in this chapter was coded in Python. The computation time of each iteration of the NMPC was about 0.03 s. This is too slow to be directly embedded into the robot. Implementing this NMPC using another programming language, like Cython or C++, may improve this computation time.

Moreover, even if the torque-based walking has been successfully realized on the robot, the TALOS robot cannot reach a human walking pace (more than $1\,\mathrm{m.s^{-1}}$). In this work, with zero curvature trajectories, the controller architecture can reach $0.6\,\mathrm{m.s^{-1}}$ in simulation as Ramuzat et al. [136, 137] shows. However, the robot hardware does not allow to reach higher velocities due to the flexibility of the hip. Developments are under way to reach a sufficient speed to achieve a human-humanoid robot interaction.

Finally, supposing we perform the co-navigation task with a robot able to move as fast as a human, the human CoM will be measured in real-time using a MoCap. Indeed, the horizontal CoM position can be approximated by the middle of two markers placed on the postero-superior iliac spine [62] and the orientation of the pelvis can be computed using a vector constructed with two markers placed on the antero-superior iliac spine. The same method was used to measure the human trajectories to test our prediction process (see Sec.1.2). Thus, the measurement noise will be the same in the case of a real-time experiment. This is why we can assume that our prediction model is not sensitive to the noise we can encounter during the real-time measurement of the human CoM. Moreover, unpublished works, performed at LAAS-CNRS, already demonstrated the ability of the robot to interact, in real-time, with objects localized with our MoCap (Qualisys). This work is presented in Sec.5.2.1.

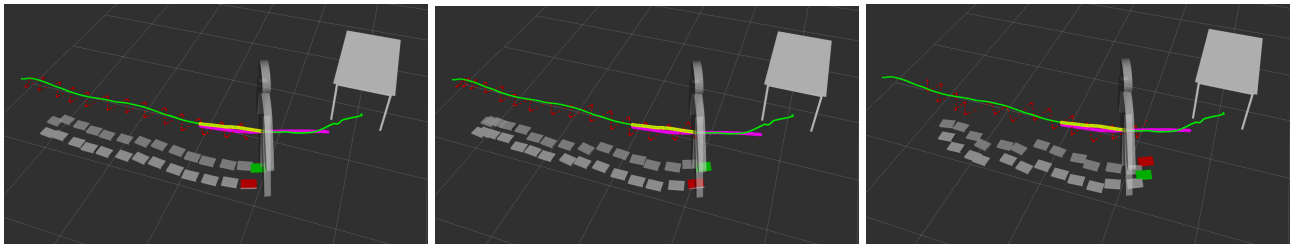

(a) Scenario 1 ($d_{behind} = 0.2\,\text{m}$). (b) Scenario 2. (c) Scenario 3 ($d_{ahead} = 0.2\,\text{m}$).

Figure 3.12: Comparison between the different scenarios. The robot CoM (in *red*) and footsteps (past steps in *grey*, current support foot in *red* and future support foot in *green*) are generated from the current optimal solution given by the prediction process (in *purple*) which takes the recent past trajectory of the human (in *yellow*) as an input.

3.7 Conclusion

In this chapter, we first sent velocity commands, derived from a clothoid-based and an OC model presented in Sec.1.3, to a real TALOS humanoid robot. During those experiments, the WPG provided by *PAL Robotics* was used. Those experiments demonstrated that computing a velocity command based on a human-like locomotion model is not a good solution to make the robot walk in a human-like way. To achieve this purpose, an accurate human locomotion model needs to be directly embedded in the robot WPG. In the wake of that conclusion, we developed a WPG based on the NMPC introduced by Naveau et al. [115]. This new WPG allows to generate CoM and feet trajectories along a given trajectory. Moreover, a constraint on the capture point was added in order to avoid the internal instability of the problem formulation. Once coupled with the prediction process described in Chapter 2, this WPG can generate the footsteps that follow the predicted trajectory. Then, the generated data are sent to a torque whole-body controller which computes a stable command achievable by the humanoid robot. This was successfully tested in simulations with a TALOS humanoid robot. Thus, with this coupling, a robot can proactively follow a human, simultaneously perform the same trajectory or even outpace him. We achieve here a proactive co-navigation task in simulation. As a reminder, the successful framework developed in this chapter is summarized in Fig.3.1.

Let us denote that we target a co-navigation task in this chapter although the topic of this thesis is about a co-manipulation task. Regarding our choice of approach, we chose, in a first time, to target a co-navigation task because we will need a similar scheme to make the robot navigate its way to the table for setting up the co-manipulation task. Indeed, before assisting a human partner to carry a table, the robot will need to walk to the available side of the table. However, the next step, namely the co-manipulation task, will be quite different from a co-navigation task as the human and the robot will be coupled through a table which will add haptic interactions. Nevertheless, we plan to use a similar real-time model using OC. Even if this method is far more complex to set up and more costly in a time computation way than a model parameters estimation, it will allow us more versatility. Indeed, optimization problems allow quite easily, by adding new terms to the cost function, to incrementally add obstacles or new constraints. Thus, in the following part, we, first, study human-human collaborations to handle a table and, then, apply the developed approach to build a prediction model of the table's motions in order to perform a proactive human-robot co-manipulation task.

Part II

Final Problem

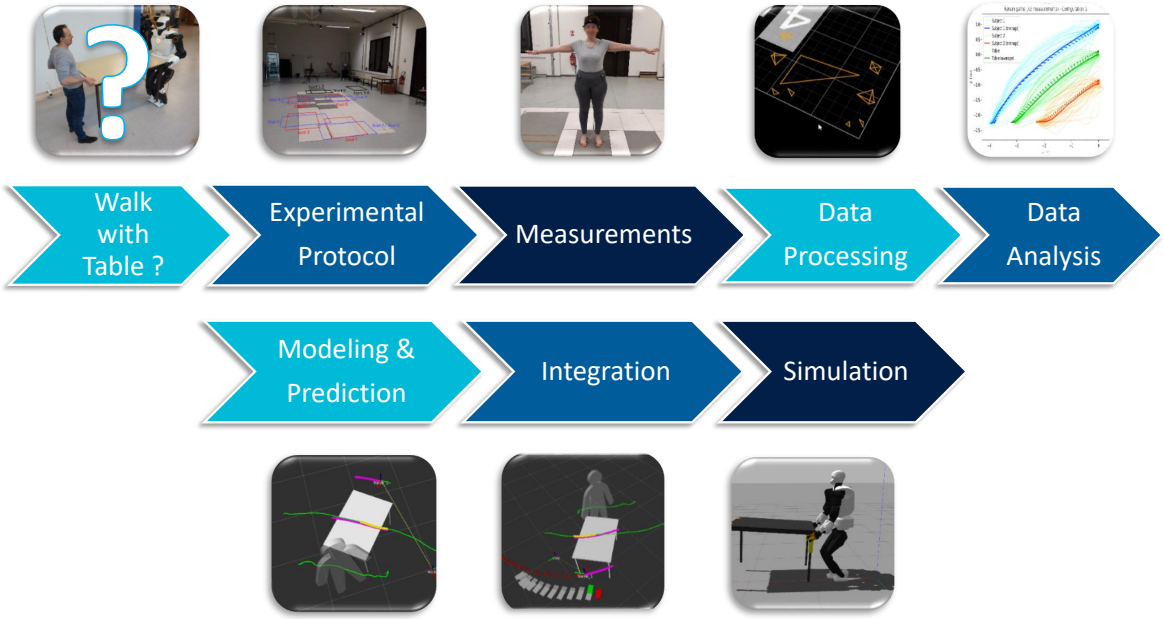

The second part of this thesis focuses on the main goal of this thesis, namely the achievement of a proactive human-robot interaction to move a table. The method developed in the previous part to embed a human locomotion model in a robot's footsteps planner is aimed to be used to solve this final problem.

This part is divided into two chapters. In Chapter 4, a study of the trajectories of subjects during collaborative carriages is proposed. Then, in Chapter 5, the problems of the localization and of the gait generation of the robot to perform a table handling task with a human partner are handled.

Chapter 4

Pair Locomotion During a Table Handling Task

Contents

4.1 Introduction

4.1.1 Motivations

It is a great challenge to generate safe physical collaboration tasks between a robot and a human, particularly with biped robots which are inherently unstable. To efficiently perform such collaborations, a good modeling of human behaviour is necessary as it may turn the robot into a proactive partner which anticipates the human's motions. However, providing to the robot an accurate model of its human partner is still regarded as a great challenge in HRIs [15]. Thus, studying and modeling human motion is relevant in the HRI context. As a reminder, this study is part of the ANR-CoBot project which aims at achieving a table handling task in collaboration between a humanoid robot and a human. Thus, this chapter focuses on the study of the behaviour of two humans carrying a table from one position to another with the objective of modeling their dynamics. The reliability of simulating their spontaneous trajectories in the aim of collaborating with a robot is also explored. Based on the anterior works on the modeling of the spontaneous locomotion of single walking humans presented in Chapter 1, the algorithm was adapted to simulate the trajectories of pairs of subjects carrying a table.

4.1.2 Related Works

In biomechanics, collaborative carriage has already been studied from different angles.

On the one hand, some works focused on the walking gait of two individuals performing a collaborative task. For example, Fumery et al. [140] studied the gait pattern of two subjects walking side by side while carrying a load. In this paper, the authors demonstrated that the CoM of each subject during a collaborative handling task follows the same pendulum-like behaviour as the one of a single subject walking without any load. In another work [141], they also showed that the more a pair of subjects practiced a carriage task, the more efficiently they performed it. Similarly, Lanini et al. [121] studied the adjustment of the gait of two individuals interacting with one another. In contrast to the experiment proposed by Fumery et al. [140, 141], the authors instructed the two subjects to walk one in front of the other carrying a load. They concluded that, in most of the experiments, the subjects synchronized their walking gait during the carriage and that quadrupedal gait patterns, like pace, trot or diagonal sequence, emerged from the coupling of the two humans' gaits. A gait synchronization phenomenon was also observed by Sylos-Labini et al. [142]. In these experiments, the subjects, unable to see or hear each other, unintentionally synchronized their steps while they walked side-by-side with hand contact.

On the other hand, some works aimed studying the behaviour of the subjects during a collaborative task. Indeed, the forces shared through the haptic feedback can influence the subjects' behaviour during the task. For example,in the context of collaborative target acquisition tasks, it was demonstrated that each member of the pair "specialized" in one specific role during the motion [143, 144]. This result was obtained by looking at the recorded forces and motions. The leader handled the early part of the motion when the follower managed the latter part of the motion [145, 146, 147]. This is why during human-human haptic interaction experiments the two partners are commonly assigned a "leader" and a "follower" role [122, 148]. Thus, when two partners interact through an object, they exchange haptic signals as internal force patterns which influence their behaviour during the collaboration. This is called haptic communication. Moreover, in Lanini et al. [122], the focus was on basic human intention detection (start/stop

and walk forward/backward) during a collaborative carriage. The authors recorded handling experiments where a deaf and blind subject, the follower, was connected to its partner, the leader, only through haptic feedback. Then, using this human-human interaction, a multiclass classifier was successfully trained to detect human intentions during load transportation. This demonstrated that haptic communication allowed humans to infer their partner 's intentions, which eases the conduct of the collaborative task.

However, to the best of our knowledge, none of the studies about collaborative carriage focused on the spontaneous walking paths taken by the subjects. They have neither been analyzed nor modeled yet.

On the contrary, as presented in Sec.1.1.2.1, human walking paths out of collaborative tasks have already been studied in multiple works. As a reminder, human-like CoM trajectories can be generated using a non-holonomic system when a human is walking a straight line [31]. However, when he has to take sideways steps, a holonomic model is needed to better fit human behaviour as it allows more degrees of freedom in the locomotion [1, 26, 38]. In **Maroger** et al. [1], a holonomic model based on an OC problem was designed to generate human-like trajectories between a given starting and goal positions. It was optimized using a bi-level IOC scheme, first introduced in Mombaur et al. [38], to well fit average human CoM trajectories during locomotion. Using a similar OC model which takes as an input the recent past trajectory of a single walking human, it is even possible to accurately predict his future trajectory without knowing his goal position [4]. This kind of model does not exist, as far as we know, for humans walking during collaborative tasks.

4.1.3 Contributions

Thus, the main goals of this work are three-fold. First, there was a need to create a database of spontaneous human walking trajectories during carriage tasks. In this work, the tackled tasks are various table handling tasks. Those tasks were performed by pairs which were asked to act naturally. Experiments were carried out to create such a database: 20 pairs performed a total of 1080 trajectories carrying a table all over the experimental room. They are detailed in the following section. Then, the recorded subject's CoM trajectories are analyzed for a better understanding of human behaviour during table handling tasks. This analysis investigates the emergence of a potential strategy which would be shared by all the pairs. In this chapter, the word "strategy" names all the choices made by a pair when handling the table, such as the path they choose to move the table to a given position or how they choose to place the table on a given position. Moreover, we say that a "shared" strategy emerges from all the experiments if most of the pairs make similar choices leading to similar behaviours. Then, the possibility to reconstruct the subjects' trajectories from the table trajectories is addressed. Finally, an OC based model was built to simultaneously generate the CoM trajectories of both subjects during table handling tasks. This model was designed using the same method as the human locomotion model described in Chapter 1. Thus, the model, introduced in this chapter, was optimized to fit the average measured trajectories. The purposes of this approach are two-fold. First, this model aimed to be accurate and representative of most humans in order to, in future works, target a proactive HRI to carry a table. Then, it aimed to investigate the hypothesis that we could use the same method to simulate single walking humans and walking humans during a carriage task.

This work is currently under review by Scientific Reports [6] and published in **Maroger** et al. [7]. Moreover, the implementation of all the presented models uses open-source softwares with the aim to ease reproducibility. The data base of human CoM trajectories and the code of the models are available on: `https://github.com/imaroger/pair_during_collaborative_carriage/tree/main`.

4.2 Experiments

4.2.1 Participants

Forty volunteers (15 females and 25 males) took part in these experiments with a mean ($\pm$ standard deviation) age of 26.7 ± 5.9 years, weight of 71.7 ± 14.6 kg and height of 1.76 ± 0.09 m. They were all healthy subjects with no known pathological disorder likely to alter their gait. In order to preserve their natural behaviour, the participants were not briefed on the goals and expected results of this study. They were just informed about the experiments procedure and gave their written informed consent before taking part in this study. These experiments were conducted at the CREPS laboratory in Toulouse (France) in accordance with the declaration of Helsinki and with the approval of the University of Toulouse ethical committee.

The participants took part in the experiments as pairs. Once a subject assigned to a pair, the subject performed all the experiments with the same partner. Moreover, the twenty pairs were randomly formed without taking into account the physical features (weight and height), the ages or the genders of the subjects.

4.2.2 Experimental protocol

The pairs were asked to carry a table to 9 different goal positions and then return it to its starting position. Those positions are represented in Fig.4.1a and their arrangement in the experiment room is shown in Fig.4.1b. The goal positions were chosen in order to record table handling experiments including various destinations within a range of 2.7 m to 5.4 m from the starting position and with different orientations. On Fig.4.1a, let us denote that there is no orthogonal orientation associated with Goal 9 as it would be equivalent to Goal 2. Furthermore, the table was the same for all the experiments. It measured $1.22 \times 0.8 \times 0.77$ m and weighed 20.7 kg. To limit non-haptic interactions between the subjects, they were asked not to talk to one another during the table transport.

During all the experiments, the subjects were instructed to walk at a self-selected casual pace. The experiment started with each member of the pair walking toward a table placed on a starting position. In every pair, one subject was appointed as *Subject 1* and the other as *Subject 2*. According to the label they were given, the participant was instructed to always grab the table on the same side. The starting positions of the two members of the pair according to their label are shown in Fig.4.1a. There were no given instructions on whether the subjects had to face the table or to stand their backs to the table nor on how the subjects should grab the table. Then, the pair grabbed and carried the table toward a goal position. In what follows, this path was named *forward path*. The goal positions were indicated on the floor with 4 pieces of adhesive tape, one for each table leg. The only instruction given to the participants

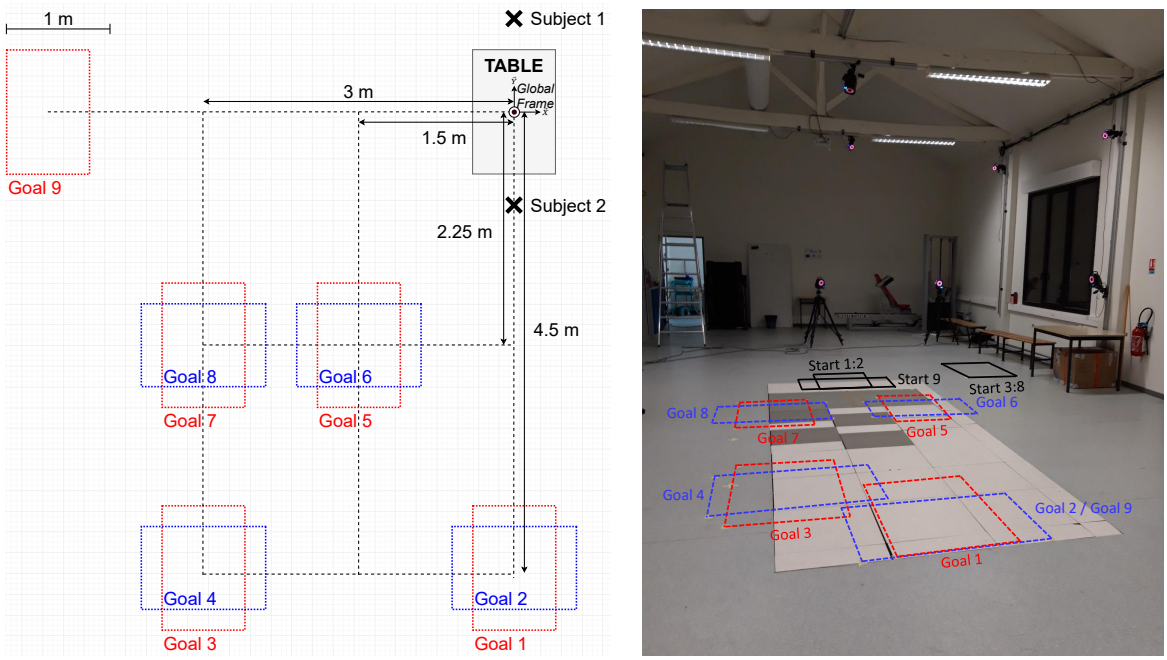

(a) Representation of the 9 different goal positions.

(b) Experiment room. The goal positions correspond to the ones represented in Fig.4.1a

Figure 4.1: Experimental setup

was that all the table legs must match with the markers on the floor. There was no instruction on the orientation of the table at the end of the handling. So, for each goal position, there were two possible configurations for the table. The configuration was characterized by the orientation of the table on the given goal position. An example is illustrated in Fig.4.2. Once the table has reached the goal position, the subjects laid the table on the floor and released it. Then, the pair grabbed the table again and carried it back to the starting position. This path was named *return path*. Once the table has reached the starting position, the subjects laid the table on the floor and released it. The trial was over.

The 9 table handling experiments were performed 3 times by each pair following 3 different scenarios:

- Scenario 1: Only Subject 1 knows the goal position.
- Scenario 2: Only Subject 2 knows the goal position.
- Scenario 3: Both subjects know the goal position.

In the following, the subject which knows the goal position is called the *leader* while the other one is called the *follower*, in accordance with the literature. In the third scenario, both subjects are called *leaders*. Thus, in this manuscript, *leader* refers to the knowledge of the target rather than the rule of one subject over the other one. Within a scenario, the goal positions were randomly given to the leader in order to avoid the follower from anticipating where the pair had to bring the table. For the same reason, the participants were instructed not to communicate during the table handling.

However, the 3 scenarios were not carried out randomly, they were performed one after the other. Moreover, when the pair returned the table to its starting position, both subjects

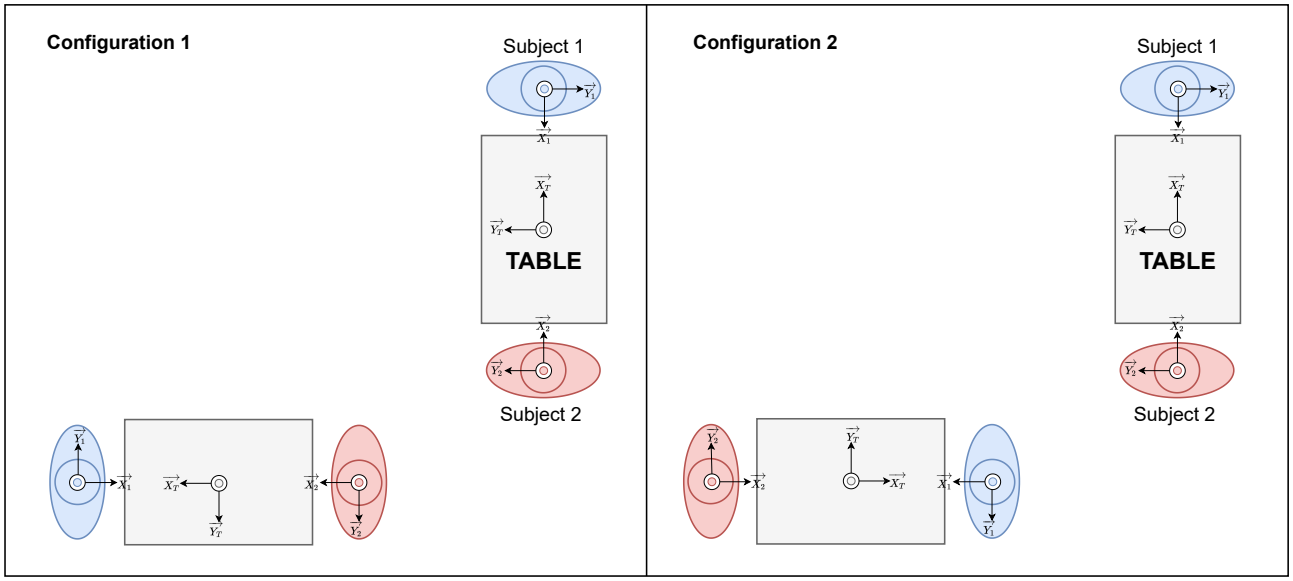

Figure 4.2: Two achievable configurations when handling the table to the goal positions 2, 4, 6 or 8. Each configuration is characterized by the orientation of the table on the given goal position.

knew where they had to carry the table. This is why, in those cases, the scenario was always the third one, whatever the scenario dictated to go to the goal position was. Thus, each pair performed a total of 54 trajectories (9 goals $\times$ 2 paths $\times$ 3 scenarios). In the end, 1080 trials were performed by the 20 pairs involved in this experiment. This results in 3240 measured trajectories of subjects and of the table.

4.2.3 Data collection

3D kinematic data of the subjects and of the table were recorded using a motion capture system (15 infrared VICON cameras sampled at 200 Hz). Each subject wore 14 passive markers. 4 markers were placed on the pelvis, 2 on the postero-superior iliac spines and 2 on the antero-superior iliac spines . 6 other markers were put on the feet of the subjects in order to record their footsteps and the last 4 markers were put on the head (see Fig.1.4 in Sec.1.2.3). Regarding the table, its CoM positions and orientations were recorded using 3 passive markers placed on 3 of the 4 corners of the table. The experiment room is shown in Fig.4.1b.

4.2.4 Data processing

The kinematic data were filtered using a 4th order, zero phase-shift, low-pass Butterworth with a 10 Hz cutoff frequency. Then, the recorded data from all the experiments were sequenced in three sections: walk to the table, table handling during the forward path and table handling during the return path. This sequencing was based on the height of the table. The onset and offset of each motion were determined as when the height of the table exceeded and returned below 5 mm from the floor, respectively. Finally, the kinematic data of interest, which are, in this manuscript, the CoM positions and orientations of the 2 subjects and of the table, were computed for every extracted sequence. The horizontal position (x, y) of the CoM of the subjects and the orientation θ of their pelvis, with respect to the global frame were computed using the 4 markers placed on the pelvis of the subjects according to a previously

published methodology [62]. For each experiment, those datasets are called *the measured trajectories* and denoted X_1, X_2 and X_T for Subject 1, Subject 2 and the table respectively. In what follows, the measured trajectories for the j^{th} pair ($j \in [\![1, 20]\!]$) during the k^{th} scenario ($k \in [\![1, 3]\!]$) is denoted $X_j^{mes,k} = \begin{pmatrix} X_{j,1}^{mes,k} & ... & X_{j,N}^{mes,k} \end{pmatrix}$ with $X \in \{X_1, X_2, X_T\}$, with N the number of measurements in this trajectory and $X_{j,i}^{mes,k} = (x_{j,i}^{mes,k}, y_{j,i}^{mes,k}, \theta_{j,i}^{mes,k})$, $\forall i \in [\![1, N]\!]$.

The CoM trajectories were analyzed after normalizing the time from 0 to 100 % on 500 points. Thus, in this work $N = 500$. Using the normalized trajectories, the *average trajectories* (arithmetic mean) were computed for the 2 subjects and the table for every goal position with the 2 different configurations and for every scenario. They are denoted $\bar{X}^{mes,k} = \begin{pmatrix} \bar{X}_1^{mes,k} & ... & \bar{X}_N^{mes,k} \end{pmatrix}$ with $\bar{X}_i^{mes,k} = \frac{1}{20} \sum_{j=1}^{20} X_{j,i}^{mes,k}$, $\forall i \in [\![1, N]\!]$.

4.3 Data analysis

4.3.1 Tackled questions

One of the main goals of this data analysis is to study the strategies implemented by the pairs to move the table. In this context, the analysis focused on the trajectories and the configurations chosen by the pairs for all the experiments. First, we wanted to figure out if the choices made by one pair to handle the table depend on the given scenario or on the direction of the motion (forward or return path). Then, this study focused on the optimality of the strategy chosen by the pairs. The final aim of this analysis was to determine whether or not a shared strategy emerges from all the experiments, i.e. whether or not the majority of the pair makes similar choices while carrying a table. For such analysis, we chose to compare the average trajectories with the variety of the measured trajectories. Indeed, we made the assumption that, if the average trajectories are representative of all the performed trajectories, it can be stated that all the pairs have a non-distinguishable behaviour and that a shared optimal strategy globally emerged spontaneously, as already observed for individuals in Sec.1.5. Thus, this data analysis tackled four main topics and aimed to answer the following questions:

- **Differences between scenarios**: Is there a scenario where the pair moves the table faster than in the others? (Q1.1) Does a pair choose a similar path to carry the table to the same goal position during different scenarios? (Q1.2) Does the path taken by a pair when there is two leaders closer to the path chosen when Subject 1 was the leader or when Subject 2 was the leader? (Q1.3)
- **Differences between the forward and the return paths**: Are the forward paths similar to their respective return paths? Are the trajectories during a carriage task asymmetrical like those of a single walking human [38]? (Q2.1) Is one path performed faster than the other? (Q2.2)
- **Optimality of the chosen configuration**: Does a subject tend to choose the configuration that allows him to travel the minimal distance? That allows their partner to travel the minimal distance? Or that allows the pair as a whole to travel the minimal distance? (Q3)
- **Variability of the trajectories**: Is there a great variability between pairs? (Q4.1) or even within a pair? (Q4.3) Are the average trajectories representative of all the pairs for all the trajectories? (Q4.2) Does the distance to the goal increase the variability of the

performed trajectories? (Q4.4)

To answer those questions, some parameters needed to be introduced:

- Travel time was defined as the elapsed time between the moment the table took off the floor and the moment it lied on the floor again.
- Traveled distance was defined as the euclidean distance between the starting position $(x_{i,s}, y_{i,s})$ and the goal position $(x_{i,f}, y_{i,f})$ of Subject 1 $(i = 1)$ or Subject 2 $(i = 2)$ or the table $(i = T)$:

$$D_i = \sqrt{(x_{i,f} - x_{i,s})^2 + (y_{i,f} - y_{i,s})^2} \tag{4.1}$$

  One can denote that this distance is not the exact distance traveled by the subjects as they never chose the straight path. The traveled distance of the table D_T is named *global distance* in what follows.
- Distance between curves: To determine if a chosen path was "similar" to another, a metric needed to be defined. This metric needed to assess if the geometric trajectories were close to one another and if the orientations of the subjects were alike. This is why using the metric introduced in Sec.1.3.4.1 was suitable. Given 2 trajectories X_1 and X_2, the following *linear* and *angular distances* , respectively d_{xy} and d_θ, were computed as follows:

$$\begin{cases} d_{xy}(X_1, X_2) = \frac{1}{N} \sum_{i=1}^{N} \sqrt{(x_{1,i} - x_{2,i})^2 + (y_{1,i} - y_{2,i})^2} \\ d_\theta(X_1, X_2) = \frac{1}{N} \sum_{i=1}^{N} |\theta_{1,i} - \theta_{2,i}| \end{cases} \tag{4.2}$$

  With those definitions, the smaller the distances are, the closer the compared trajectories are. The linear and angular distances between the paths taken by the same pair during different scenarios, between the forward and return paths and also between the average and the measured trajectories were computed.
- Symmetry between the forward and the return path: In this manuscript, the smaller the linear and angular distances between the forward path and its respective reversed return path were, the more symmetrical a forward path and a return path might be considered.
- Optimal configuration: The chosen configuration was identified by measuring the orientation of the table on its goal position. The criterion used to tell if the chosen configuration was optimal with respect to another was based on the traveled distance by each of the subjects and by the whole pair. Thus, the chosen configuration was qualified as optimal for Subject 1, Subject 2 or the pair if it respectively minimized the distance traveled by Subject 1 (D_1), by Subject 2 (D_2) or the sum of the distance traveled by the two subjects $(D_1 + D_2)$. Let us denote that, for Goal 2 (see Fig.4.1a), both subjects walked the same distance regardless of the configuration they chose. In that specific case, the two configurations were regarded as optimal.

4.3.2 Statistical analysis

All the statistical tests described below were performed using the Python Scipy library[72].

To compare the scenarios, the forward and return paths or the pairs, distances between curves, as defined in Sec.4.3.1, were computed. As the data was not normal according to a Shapiro-Wilk test, only non-parametric tests were used. First, Kruskal-Wallis tests were used to assess the differences between:

- The travel time performed during the different scenarios.
- The linear and angular distances between the forward and return paths for the subjects and for the table.
- The linear and angular distances between the average trajectories and the measured forward and return paths during Scenario 3.
- The linear distances between the average trajectories and the measured trajectories for all the pairs.
- The linear distances between the different return paths that a pair performed to go back from the same goal.

Then, Mann-Whitney U rank tests were performed for a side-by-side comparison of the data. The significance of all those tests was set at $p < 0.05$.

Furthermore, Fisher's Exact Tests were used to determine if the chosen trajectories during Scenario 3 and the linear distances between the different return paths that a pair performed to go back from the same goal depended on the subject. The same test was also used to check that the choices of configuration between the different scenarios were not random.

Moreover, some of those distances are represented in the form of box and whisker plots in what follows. Those plots show the median, the lower and upper quartile values (Q_{low} and Q_{up}) and extend from the maximum to the minimum within $[Q_{low} - 1.5(Q_{up} - Q_{low}), Q_{up} + 1.5(Q_{up} - Q_{low})]$. The other printed values are considered as outliers.

4.4 Data reconstruction

This section addresses the following question: Can the trajectories performed by the subjects be inferred from the trajectory of the load they carry? In other words, we want to figure out if the knowledge of the table trajectory allows to accurately determine the CoM trajectory of both subjects carrying it. This work was published in **Maroger** et al. [7].

To answer the previous question, the average coordinates and orientations of both subjects for all the experiments in the table coordinate system were computed. They are denoted $(\bar{x}_{i(S_1/T)}, \bar{y}_{i(S_1/T)}, \bar{\theta}_{i(S_1/T)})_{\forall i \in [\![1,N]\!]}$ and $(\bar{x}_{i(S_2/T)}, \bar{y}_{i(S_2/T)}, \bar{\theta}_{i(S_2/T)})_{\forall i \in [\![1,N]\!]}$.

Then, using those average coordinates, the trajectories of both subjects were reconstructed for the measured table trajectories as follows:

$$\forall i \in [\![1, N]\!],\ k \in \{1, 2\},\ \begin{cases} x^{rec}_{S_k,i} = x^{mes}_{T,i} + \bar{x}_{i(S_k/T)} \times \cos\left(\theta^{mes}_{T,i}\right) - \bar{y}_{i(S_k/T)} \times \sin\left(\theta^{mes}_{T,i}\right) \\ y^{rec}_{S_k,i} = y^{mes}_{T,i} + \bar{x}_{i(S_k/T)} \times \sin\left(\theta^{mes}_{T,i}\right) + \bar{y}_{i(S_k/T)} \times \cos\left(\theta^{mes}_{T,i}\right) \\ \theta^{rec}_{S_k,i} = \theta^{mes}_{T,i} + \bar{\theta}_{i(S_k/T)} \end{cases} \tag{4.3}$$

This was done arbitrarily only for Scenario 3 and this method was applied to the forward paths and their respective return paths.

Finally, in order to assess the accuracy of the reconstruction, the linear and angular distances between the reconstructed trajectories and the respected measured trajectories were computed.

4.5 Modeling

Another purpose of this chapter is to model the walking trajectories of two humans carrying a table. Accurately modelling the subjects' behaviour is a first step toward the prediction of their motion during a table handling task. To achieve this goal, an OC model optimized through an IOC scheme to fit the average measured trajectories was introduced. As a reminder, the choice to model average trajectories instead of individual ones came from the hypothesis that the same method could be used to accurately simulate single walking humans and walking humans carrying a table. In this section, the focus is on the modeling of the subjects' average trajectories during Scenario 3 only. We did not optimize the model for the other scenarios. We chose to only focus on Scenario 3 because both forward and return paths were performed in this scenario and, thus, it multiplied the number of trajectories to fit for the inverse optimization.

4.5.1 Optimal control model

The OC model introduced in Sec.1.4 was adapted to simultaneously generate the CoM trajectories of the two subjects. Originally, this model was designed to generate the trajectories of one human walking alone without constraints. Here, the model was modified in order to simulate the trajectories of two humans coupled through a table handling task. This new model is named *coupled OC model*. Thus, the dynamics of the system is not the dynamics of one holonomic system anymore (see Eq.1.3), but the dynamics of two holonomic systems:

$$\begin{cases} \dot{x_1} = \cos\theta_1 \times v_{1,forw} - \sin\theta_1 \times v_{1,orth} \\ \dot{y_1} = \sin\theta_1 \times v_{1,forw} + \cos\theta_1 \times v_{1,orth} \\ \dot{\theta_1} = \omega_1 \\ \dot{v}_{1,forw} = u_{1,1} \\ \dot{v}_{1,orth} = u_{1,2} \\ \dot{\omega_1} = u_{1,3} \end{cases} \quad \begin{cases} \dot{x_2} = \cos\theta_2 \times v_{2,forw} - \sin\theta_2 \times v_{2,orth} \\ \dot{y_2} = \sin\theta_2 \times v_{2,forw} + \cos\theta_2 \times v_{2,orth} \\ \dot{\theta_2} = \omega_2 \\ \dot{v}_{2,forw} = u_{2,1} \\ \dot{v}_{2,orth} = u_{2,2} \\ \dot{\omega_2} = u_{2,3} \end{cases} \tag{4.4}$$

(x_i, y_i) is the generated position of the CoM in the horizontal plane of the subject i with $i \in \{1, 2\}$. θ_i is the generated orientation of its pelvis in the global frame. $v_{i,forw}$ and $v_{i,orth}$ are the tangent and orthogonal velocities with respect to the orientation of its pelvis and ω_i is its angular velocity. All those variables are represented in Fig.4.3. The state of the coupled OC model is $X = (X_1, X_2)^T = ((x_1, y_1, \theta_1), (x_2, y_2, \theta_2))^T$ and the control is $U = (u_{1,1}, u_{1,2}, u_{1,3}, u_{2,1}, u_{2,2}, u_{2,3})^T$. So, this new model counts twice as many variables as the OC model presented in Sec.1.4. The problem is of the following form and was solved using a DDP solver [69] from the Crocoddyl library [70]:

$$\min_{X(.),U(.),T} \int_0^T \phi_r(X(t), U(t))\, \mathrm{d}t + \phi_t(X(T)) \tag{4.5}$$

with ϕ_r and ϕ_t the running and terminal cost functions. T is the time needed to go from the starting position to the goal position. This problem was solved under the following constraints:

$$\begin{cases} \dot{X}(t) = f(X(t), U(t)) & \text{Dynamical constraint (Eq.4.4)} \\ X(0) = X_s & \text{Initial constraint} \end{cases} \tag{4.6}$$

with $X_s = (x_{1,s}, y_{1,s}, \theta_{1,s}, 0, 0, 0, x_{2,s}, y_{2,s}, \theta_{2,s}, 0, 0, 0)^T$ the starting state as the initial velocities are always null.

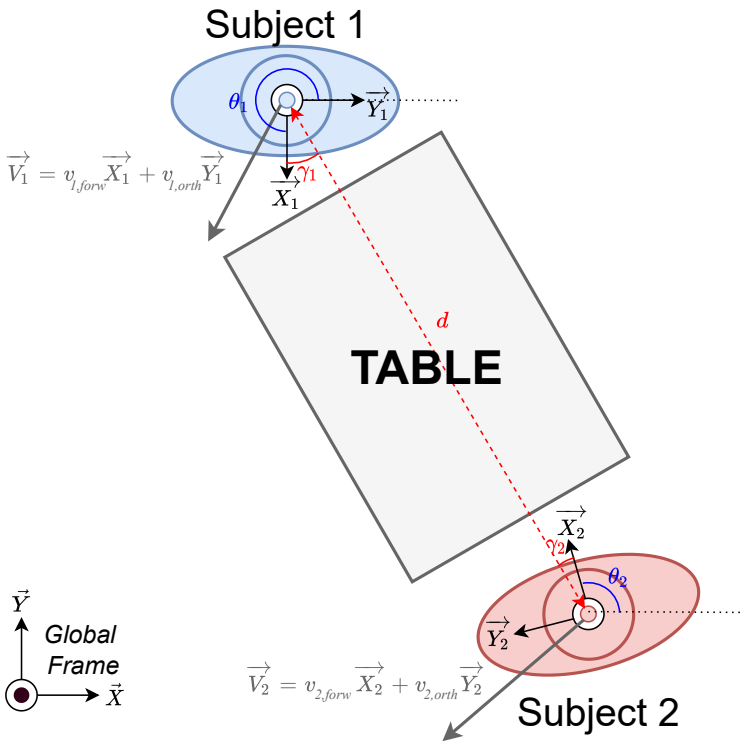

Figure 4.3: Coordinate systems and orientations in the coupled OC problem to solve.

The cost functions are as follows:

$$\begin{cases} \phi_r(X(t),U(t)) = \alpha_0 + \alpha_1 u_{1,1}^2(t) + \alpha_2 u_{1,2}^2(t) + \alpha_3 u_{1,3}^2(t) + \alpha_4 u_{2,1}^2(t) + \alpha_5 u_{2,2}^2(t) + \alpha_6 u_{2,3}^2(t) \\ \qquad +\alpha_7\psi_1(X(t),X_f)^2 + \alpha_8\psi_2(X(t),X_f)^2 + \alpha_9\chi(X(t)) + \alpha_{10}(\xi_1(X(t)) + \xi_2(X(t))) \\ \phi_t(X(T),U(T)) = \beta_0((x_{1,f} - x_1(T))^2 + (y_{1,f} - y_1(T))^2 + (x_{2,f} - x_2(T))^2 + (y_{2,f} - y_2(T))^2) \\ \qquad +\beta_1((\theta_{1,f} - \theta_1(T))^2 + (\theta_{2,f} - \theta_2(T))^2) + \beta_2(v_{1,forw}(T)^2 + v_{1,orth}(T)^2 + v_{2,forw}(T)^2 \\ \qquad +v_{2,orth}(T)^2) + \beta_3(\omega_1(T)^2 + \omega_2(T)^2) \end{cases} \tag{4.7}$$

In this equation, $\psi_i(X(t),X_f) = \arctan\frac{y_{i,f}-y_i(t)}{x_{i,f}-x_i(t)} - \theta_i(t)$ with $i \in \{1,2\}$ and $X_f = (x_{1,f}, y_{1,f}, \theta_{1,f}, x_{2,f}, y_{2,f}, \theta_{2,f})$ the final state. Then, χ and ξ_i are exponential barrier functions. This means that they enforce some physical constraints of the system in the cost function. Indeed, the χ function imposes that the subjects are separated with a distance between 1.6 m and 2.1 m due to the table length and the ξ_i function imposes that the difference between the orientation of the vector from the subject i to the subject j and the orientation of the subject i does not exceed $\frac{\pi}{3}$ rad. In other words, those constraints respectively mean that both subjects hold one side of the table and that the subjects almost face each other. The coupling of the two subjects is implemented through these exponential barriers. Mathematically, they can be written as follows:

$$\chi(X(t)) = \begin{cases} 0 \text{ if } 1.6 < d = \sqrt{(x_1(t) - x_2(t))^2 + (y_1(t) - y_2(t))^2} < 2.1 \\ \exp\left(\min\left(|d - 2.1|, |d - 1.6|\right)\right) - 1 \text{ otherwise} \end{cases}$$

$$\xi_i(X(t)) = \begin{cases} 0 \text{ if } \gamma_i = |\arctan\frac{y_j - y_i}{x_j - x_i} - \theta_i| < \frac{\pi}{3} \\ \exp\left(\gamma_i - \frac{\pi}{3}\right) - 1 \text{ otherwise} \end{cases}$$

with $j \in \{1,2\}$ and $j \neq i$. d and γ_i are shown in Fig.4.3. Moreover, $\alpha = (\alpha_0, \alpha_1, \alpha_2, \alpha_3, \alpha_4, \alpha_5, \alpha_6, \alpha_7, \alpha_8, \alpha_9, \alpha_{10})$ are the weights of the running cost and $\beta = (\beta_0, \beta_1, \beta_2, \beta_3)$ the weights of the terminal cost. Both α and β were first determined with the IOC scheme described below.

In what follows, the trajectories generated with this coupled OC model for Subject 1 and Subject 2 are respectively denoted X_1^{gen} and X_2^{gen}.

4.5.2 Inverse Optimal Control

To allow this model to fit well the average human measurements, it was needed to optimize the cost function weights α and β with an IOC scheme as in Sec.1.4.3. This scheme was first introduced in Mombaur et al.[46] The purpose of this method was to find the weights of the cost function, described in Eq.4.7, which allowed the OC model to generate trajectories that best fit the mean measured trajectories. This bi-level method finds the optimal weights of the OC problem, solving another optimization problem defined as follows:

$$\min_{\alpha,\beta} \frac{1}{N_{traj}} \sum_{n=1}^{N_{traj}} d_{xy_{1,n}}(\bar{X}_{1,n}^{mes,3}, X_{1,n}^{gen}(\alpha,\beta)) + d_{xy_{2,n}}(\bar{X}_{2,n}^{mes,3}, X_{2,n}^{gen}(\alpha,\beta)) + \frac{1}{2}(d_{\theta_{1,n}}(\bar{X}_{1,n}^{mes,3}, X_{1,n}^{gen}(\alpha,\beta)) + d_{\theta_{2,n}}(\bar{X}_{2,n}^{mes,3}, X_{2,n}^{gen}(\alpha,\beta))) \quad (4.8)$$

with N_{traj} the number of measured trajectories that the model tries to fit. Here $N_{traj} = 31$ as the IOC scheme was performed using all the average forward paths and average return paths measured during Scenario 3. Let us denote that there were more than 9 paths for each direction (13 forward paths and the 18 return paths) because the table was not always placed in the same configuration for every trial. Furthermore, we hypothesized that for the return paths Subject 1 became Subject 2 and reversely. Indeed, broadly speaking, during the experiments, Subject 1 faced the goal position while Subject 2 faced the starting position (see Fig.4.1a). So, when performing the forward path, Subject 1 faced the position where the table had to be placed and, conversely, when performing the return path, Subject 2 faced this position. Thus, we made the assumption that the behaviour of the subjects was switched between the forward and the return paths. Otherwise, let us denote that the cost function in Eq.4.8 was a weighted sum in order to make the linear and the angular distance of the same magnitude.

The IOC problem was solved with a derivative free method called the Powell method [74] provided by the Scipy library [72].

Once the optimal weights were found, the linear and angular distances between the generated and the measured trajectories were computed in order to assess the ability of the OC model to fit the average measured data.

4.6 Results

4.6.1 Data Analysis

First of all, examples of average trajectories for the forward and return paths toward two different goals for Scenario 3 are represented in Fig.4.4a and Fig.4.4b.

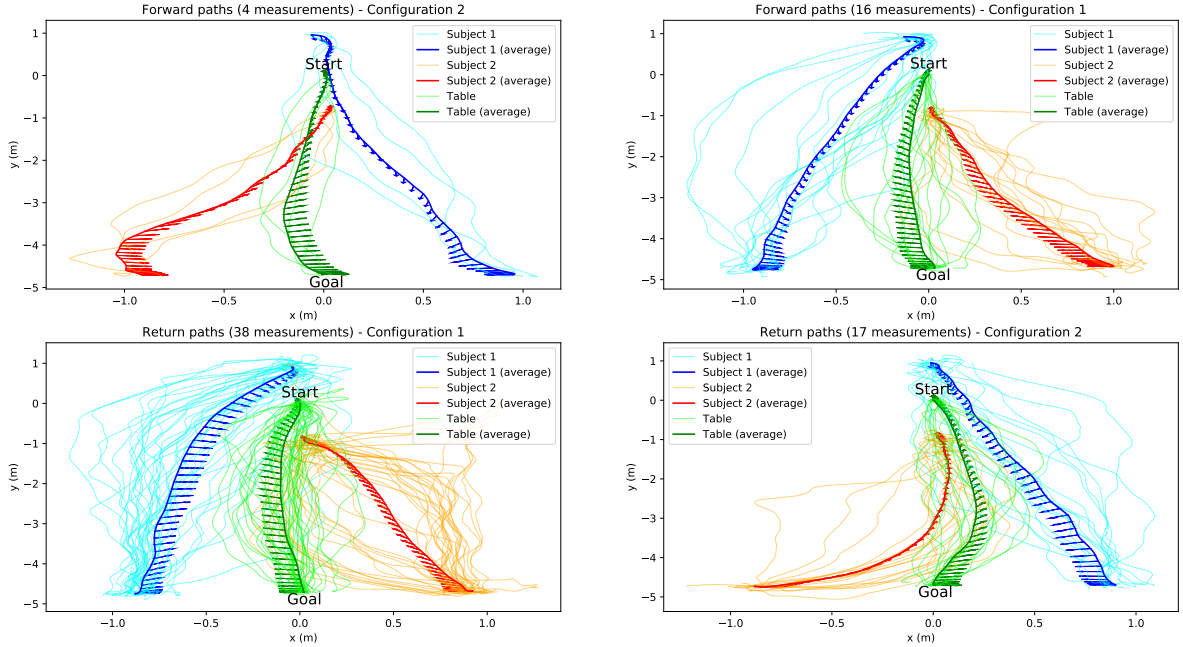

(a) Trajectories toward Goal 2.

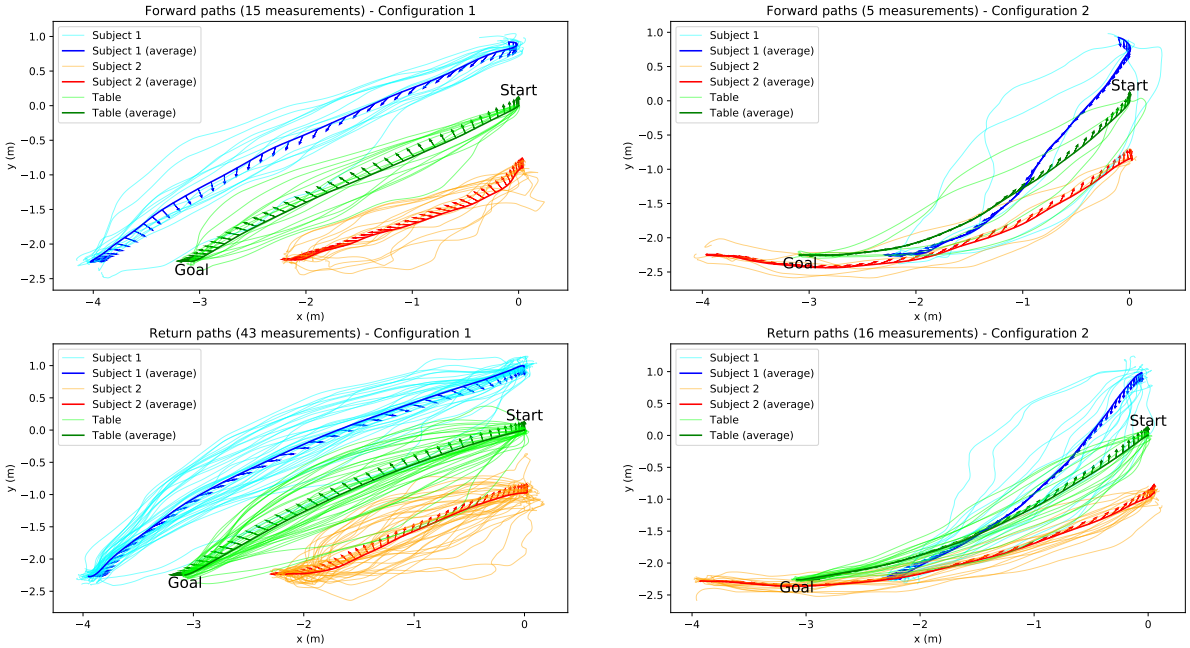

(b) Trajectories toward Goal 6.

Figure 4.4: Trajectories performed by each pair and average trajectories during Scenario 3 for two different goals. The trajectories performed for these two goals are typical of the observed straight (Goal 2) and oblique (Goal 6) motions. The arrows represent the average orientation of the pelvis of Subject 1 (in *blue*) and Subject 2 (in *red*) and of the table (in *green*) during locomotion.

4.6.1.1 Differences between scenarios

(Q1.1) The travel time of all the forward and return paths are represented in Fig.4.5. There is a significant difference between the scenarios where only one subject knows the goal position and the scenario where both partners know it (Kruskal-Wallis test, $p < 0.001$). Indeed, the pairs performed the carriage task faster when each member of the pair knows the

goal, namely in the third scenario . The travel time in the first and second scenarios are not similar (Mann-Whitney test, $p < 0.05$). The experiments with Subject 2 as a leader were performed slightly faster than the ones with Subject 1 as a leader, with an average travel time of 8.9 ± 1.8 s versus 9.6 ± 2.2 s.

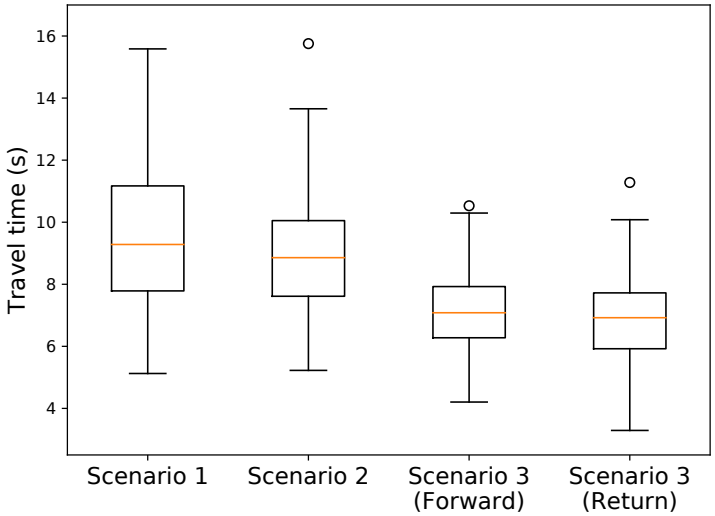

Figure 4.5: Boxplot of the travel times according to the different scenarios. For Scenario 3, the boxplots for the forward and return paths were split in order to determine if the pairs move faster or slower during the forward path or the return path.

(Q1.2) Then, to study the impact of the different leaderships on the table configuration, the chosen configurations were analyzed for each scenario. The choice of configuration is represented in Fig.4.6. This plot shows that, for the major part of the experiments (about 70%), when placing the table on a same goal position, the pairs chose the same configuration. When it was not the case, the choice did not seem to depend on the scenario. Thus, the chosen configuration did not rely on the leader. Moreover, the analysis of the chosen configurations for each pair supports this result. Indeed, while 10% of the pairs always placed the table in the same configuration for the 3 scenarios, the others often changed the configuration for the carriage to the same goal during different scenarios. Moreover, for every goal position, only one pair never placed the table in one same configuration for the 3 scenarios.

(Q1.3) For a better understanding of the differences of the subjects' behaviour according to every scenario, we computed the linear distance between the trajectories taken during the different scenarios for all the pairs. Naturally, only the trajectories leading to the same final configuration of the table were compared. Thus, for every pair and every forward path to the 9 different goal positions, the linear distances between the trajectories performed in the different scenarios by Subject 1, Subject 2 and the table were computed and are represented in Fig.4.7. These results demonstrated that all the scenarios were equally distant from each other. In other words, similar differences are observed between the paths performed during the different scenarios. However, when focusing on Scenario 3, we can highlight that the paths of Subject 1 were significantly closer to the one spontaneously chosen in Scenario 1, whereas the paths of Subject 2 were closer to the path spontaneously chosen in Scenario 2 (Fisher test, $p < 0.05$). The paths of the table in Scenario 3 presented similar closeness to Scenarios 1 and 2 (Fig.4.8). To conclude, when both partners knew the goal, they tended to follow the path

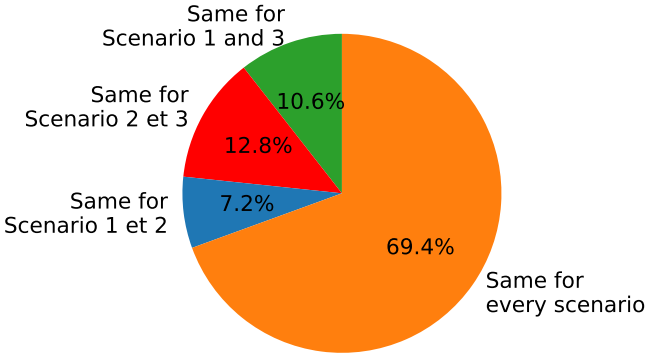

Figure 4.6: At the end of each forward path, every pair laid the table in the configuration they chose. This pie chart shows the percentage of experiments where the pairs put the table in the same configuration during Scenario 1 and 3 but not during 2 (*green*), where they put it in the same configuration during Scenario 2 and 3 but not during 1 (*red*), where they put it in the same configuration during Scenario 1 and 2 but not during 3 (*blue*) and where they always put it in the same configuration during the three scenarios (*orange*).

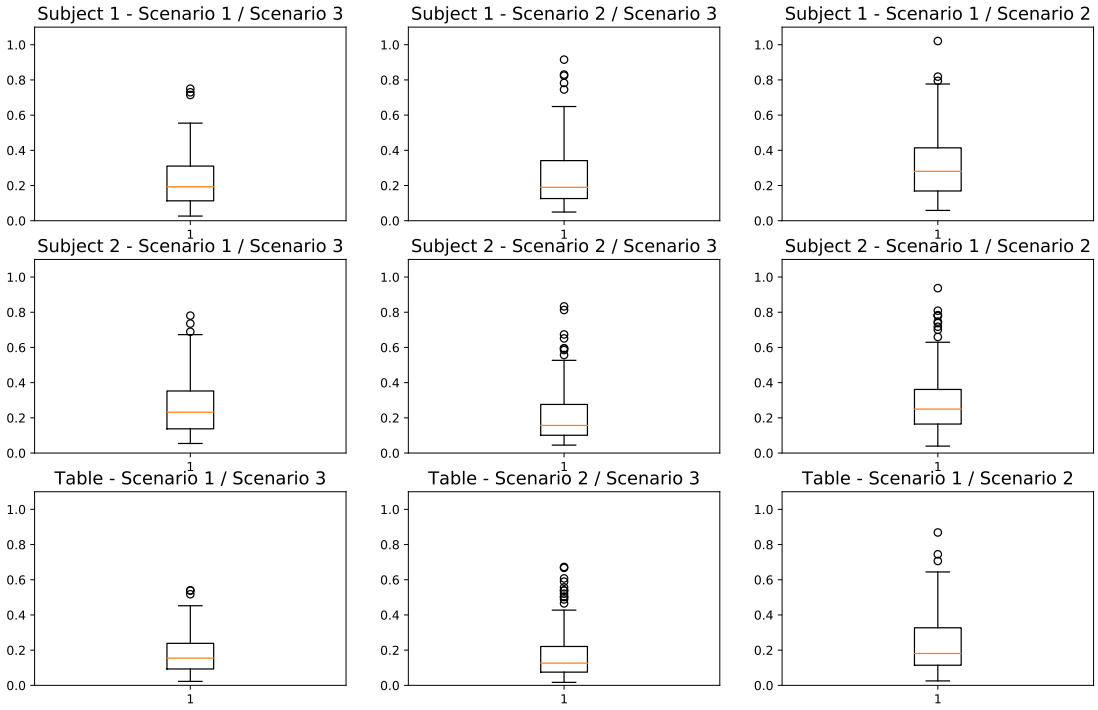

Figure 4.7: Boxplots of the linear distances (m) between the trajectories performed during Scenario 1 and 3 (on the *left*), Scenario 2 and 3 (in the *middle*) and Scenario 1 and 2 (on the *right*) for Subject 1, Subject 2 and the table.

they spontaneously chose when they were alone to know the goal. Thus, the position of the subjects with respect to the table seems to bias the chosen trajectories when both partners are leaders. In spite of the significance of the observed differences, this strategy was true only for 60% of the trials and thus cannot be generalized. Indeed, for some pairs, during Scenario 3, the subjects were closer to the paths they took when they were not the leaders. Obviously, this result alleviated the previous conclusion.

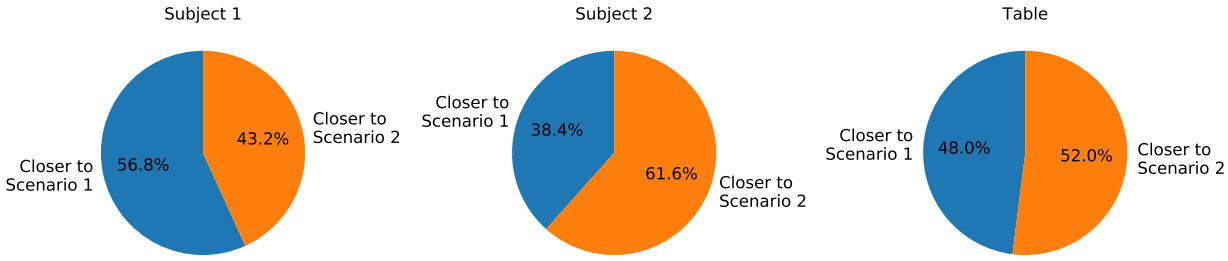

Figure 4.8: Closeness of the trajectory performed in Scenario 3 with the two others according to the linear distance for Subject 1, Subject 2 and the table.

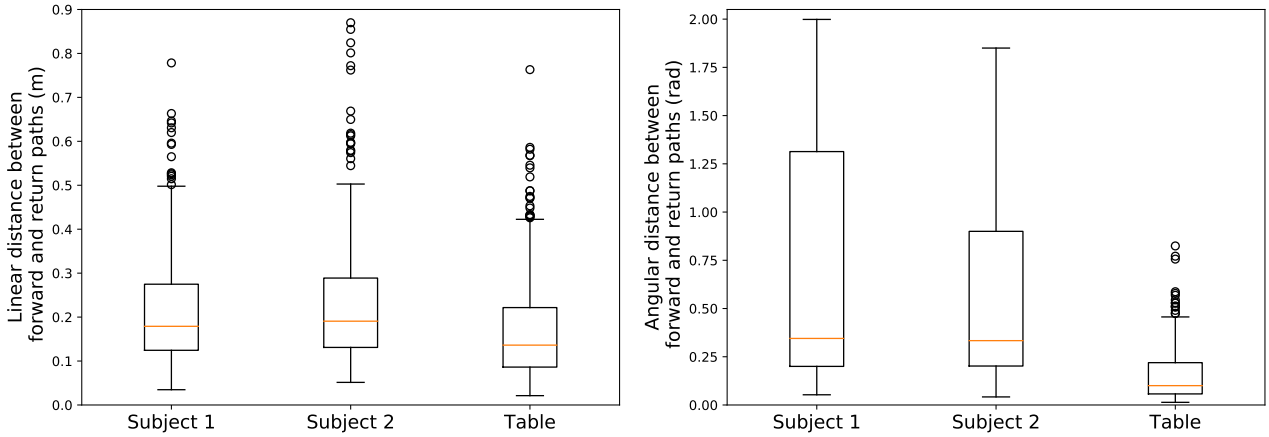

Figure 4.9: Boxplots of the linear (on the *left*) and angular (on the *right*) distances between forward and return paths for Subject 1, Subject 2 and the table trajectories for all pairs.

4.6.1.2 Differences between the forward and the return paths.

(Q2.1) The boxplots of the linear and angular distance between the forward and their respective return paths for Subject 1, Subject 2 and the table are represented in Fig.4.9. The linear distances exhibited means of 0.21 ± 0.12 m, 0.23 ± 0.15 m and 0.17 ± 0.12 m for Subject 1, Subject 2 and the table trajectories. While the means of the angular distances respectively amounted to 0.69 ± 0.59 rad, 0.56 ± 0.47 rad and 0.15 ± 0.13 rad. The data suggested that most of the forward and return paths performed by Subject 1 and Subject 2 were asymmetrical while the paths taken by the table might be close to being symmetrical in most cases. The linear and angular distances for Subject 1 and 2 are significantly different from the one for the table (Mann-Whitney test, $p < 0.001$).

(Q2.2) Otherwise, the travel time during the forward paths during Scenario 3 and all the return paths were similar (Mann-Whitney test, $p > 0.1$) as represented in Fig.4.5. So, when both partners knew where the goal position was, they performed the carriage task as swiftly during the forward path as during the return path.

4.6.1.3 Optimality of the chosen configuration.

(Q3) For every forward path, the traveled distance of the two subjects was computed and labelled as optimal or not optimal for each subject and for the whole pair. The results of this study are shown in Fig.4.10. First, the choice of configurations for the different scenarios

cannot be considered random (Fisher test, $p > 0.05$ for Subject 1, Subject 2 and the pair). Then, similar results were acquired in every scenario. Indeed, in every scenario, Subject 1 mostly walked the shortest possible distance while Subject 2 took the longest path in almost half of the experiment, even more when the subject was the leader. This means that the position of the subject with respect to the table position affected more the path they took than being or not the leader of the pair. Moreover, it can be denoted that the pair chose the optimal configuration for the whole pair in most cases. To conclude, the pair seemed to mostly choose the optimal path for the whole pair at the expense of the very same subject. Their collective strategy favored the group rather than the individuals.

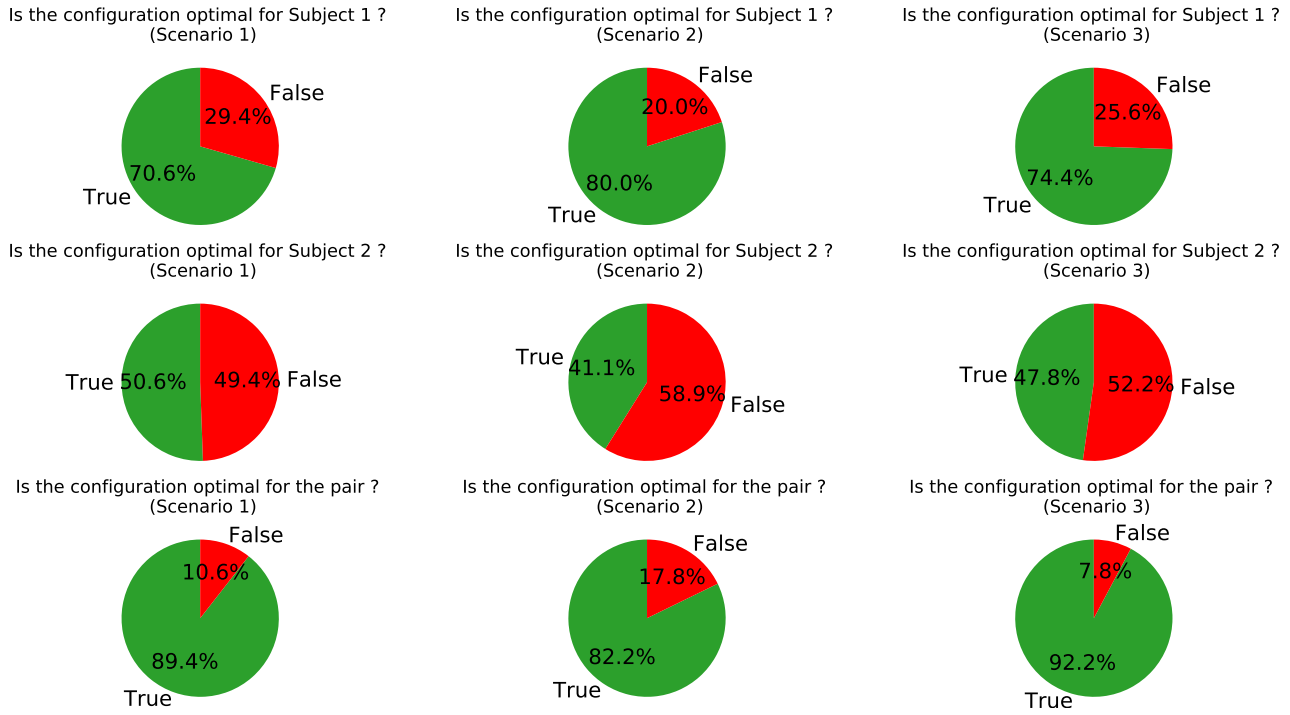

Figure 4.10: When the table configuration minimizes the traveled distance of Subject 1, Subject 2 and the pair, it is called optimal. These pie charts show the percentage of experiments where the pair put the table in an optimal configuration for Subject 1 (at the *top*), for Subject 2 (in the *middle*) and for the pair (at the *bottom*) according to the different scenarios.

4.6.1.4 Variability of the trajectories.

(Q4.1) First of all, the pair trajectories represented in Fig.4.4a and Fig.4.4b seem to show a great range of behaviours. The mean of the linear distances between the average trajectory and the measurements for Subject 1, Subject 2 and the table respectively amounted to 0.20 ± 0.14 m, 0.20 ± 0.14 m and 0.15 ± 0.12 m, while the mean angular distances were equal to 0.20 ± 0.16 rad, 0.21 ± 0.15 rad and 0.11 ± 0.10 rad. Moreover, the maximum linear distances for Subject 1, Subject 2 and the table respectively were 1.28 m, 1.27 m and 1.32 m and the maximum angular distances are 1.12 rad, 0.99 rad and 0.71 rad. The boxplots of those distances according to the different scenarios are represented in Fig.4.11. Furthermore, the boxplots in Scenario 3 for the forward and the return path looked alike. This is corroborated by a statistical test which revealed no significant differences between the linear distances

(Kruskal-Wallis test, $p > 0.1$ for Subject 1, Subject 2 and the table).

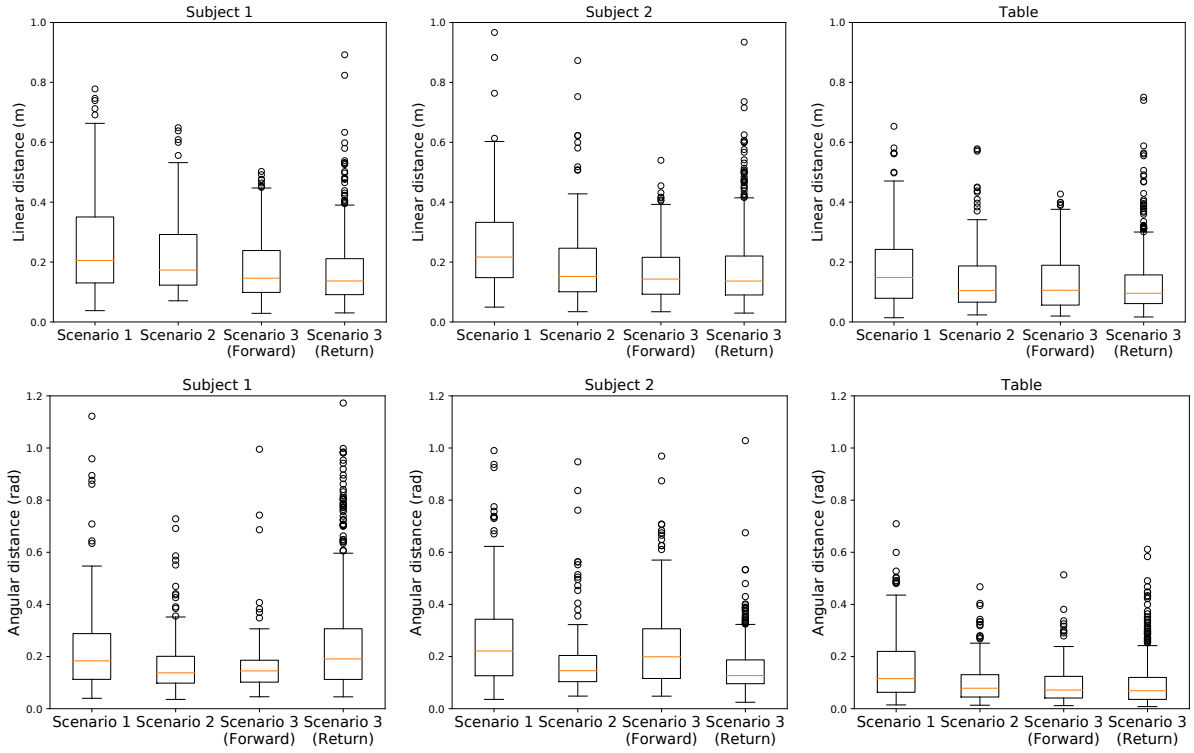

Figure 4.11: Boxplots of the linear (at the *top*) and angular (at the *bottom*) distances between the average trajectories and the measured trajectory for all goal positions according to the different scenarios.

(Q4.2) Then, we computed the linear distance between the average and the measured trajectories according to the pairs. Most of the pairs exhibited a boxplot similar to the one shown in Fig.4.11 while others present significant differences with greater medians and quartile values (Kruskal-Wallis test, $p < 0.001$ for Subject 1, Subject 2 and the table). Thus, the pairs demonstrated various behaviours.

(Q4.3) It is important to notice that a great variability also existed among the trajectories performed by the same pair. Indeed, the same return path was measured 3 times for each goal position and for each pair and we performed a Kruskal-Wallis test to assess their differences. The pie chart represented in Fig.4.12 shows the p-value computed during those Kruskal-Wallis tests. They show that around 42%, 52% and 38% of the return paths of respectively Subject 1, Subject 2 and the table have a p-value lower than 0.05. This means that around half of the returns from the same goal position performed by the same pair were significantly different. Moreover, it is interesting to denote that those percentages did not depend on whether we look at the trajectories performed by Subject 1, Subject 2 or the table (Fisher test, $p > 0.1$). So, when a pair demonstrated such variability in its own behaviour, it is not surprising that the variability between pairs was even greater.

(Q4.4) Finally, the linear distances between the average and the measured trajectories is plotted with respect to the global distance to be covered in Fig.4.13. Another information is held in this plot: the markers are of different colors whether the table orientation is the same or not at the beginning and at the end of the motion. For example, the orientation

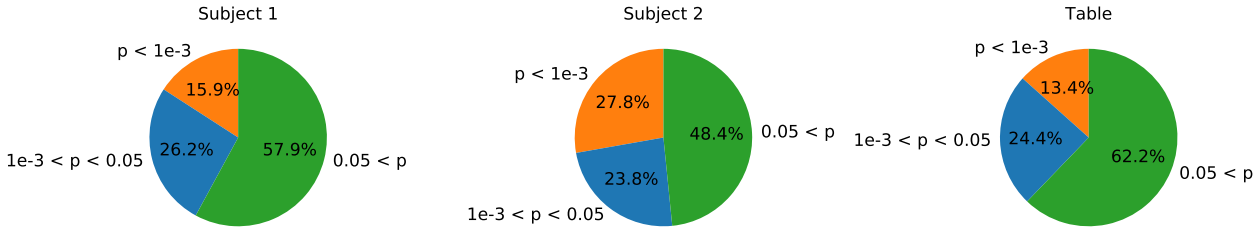

Figure 4.12: The pairs returned the table 3 times in the same conditions from each goal position. Thus, we can compute the linear distances between these 3 returns for every pair and every goal. Kruskal-Wallis tests were performed to assess if these distance are significantly different. These pie charts show the results of these statistical tests.

of the table changed for all the experiments performed with the goal position represented in blue on Fig.4.1a. This plot shows that the mean linear distance between the average and the measured trajectories increased when the global distance increased and when the table was moved along both $\vec{x}$ and $\vec{y}$ axis. Indeed, when the global distance was equal to 4.5 and 4.7 m, the goal positions were Goal 1,2 or 9, which only matched motion along one axis. In those cases, the increase according to the global distance did not emerge. Moreover, at a constant global distance, the linear distance was a little bit higher on average when the table changed of orientation between the start and the end of the motion. However, there was not enough data to state that those results are always true.

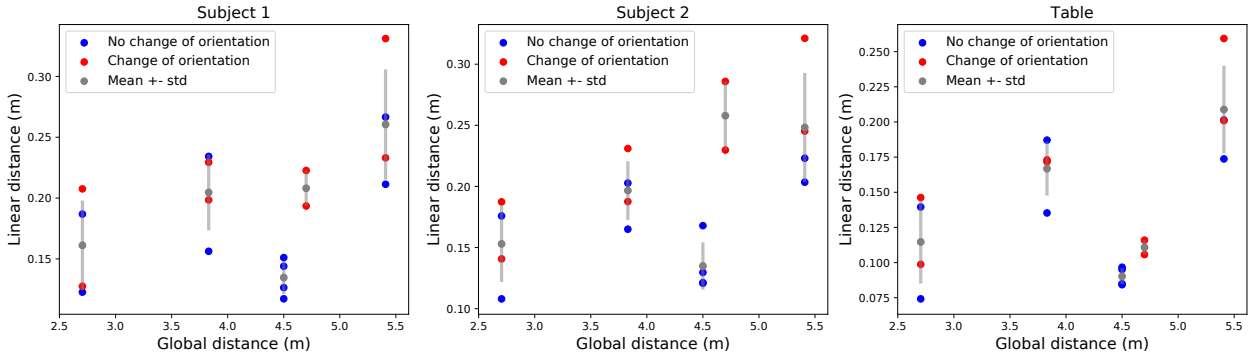

Figure 4.13: Mean linear distances between the average trajectories and the measured trajectories according to the global distance . In *blue* are plotted the distances for the trajectories which require a change of the table's orientation (Goal 2, 4, 6, 8) while the others are plotted in *red*. Let us denote, that there is an even number of points of each color for every global distances because there are two achievable configurations per goals.

4.6.2 Accuracy of the reconstruction

First of all, the average evolution of the coordinates and orientations of both subjects in the table coordinate system are represented in Fig.4.14. Those plots show that when the subjects leave the starting position or get close to the goal position, they simultaneously move away from the table along the $\vec{X_T}$ and $\vec{Y_T}$ axes. Moreover, it is interesting to denote that the orientation of the subjects is switched between the forward and the return paths. Otherwise,

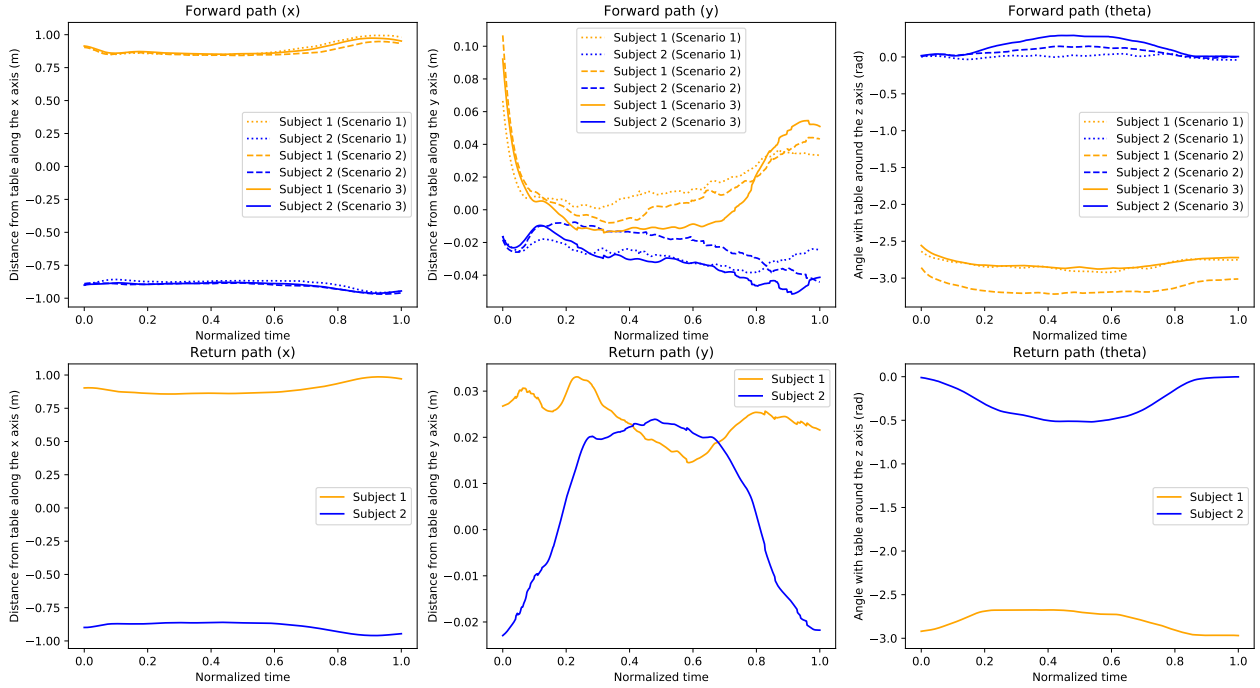

Figure 4.14: Average coordinates and orientations of the subjects expressed in the table coordinate system for all experiments.

no relevant difference can be observed between the different scenarios.

Then, examples of reconstructed trajectories are represented in Fig.4.15 for one forward measured path and its respective return path. Moreover, the average linear and angular distances between all the measured and reconstructed trajectories are presented in Tab.4.1. Thus, inferring the trajectories of the subjects using the average positioning of the subjects with respect to the table gives accurate results for the CoM position. The results for the orientation of the pelvis are, however, less relevant, especially for Subject 1. This could be explained by the average standard deviation, which is far bigger on the θ orientation (0.75 rad) than on the x and y coordinates (respectively 0.07 and 0.06 m).

	Subject 1	Subject 2
$\bar{d}_{xy}$ (m)	0.082 ± 0.051	0.084 ± 0.051
$\bar{d}_{\theta}$ (rad)	0.58 ± 0.26	0.27 ± 0.15

Table 4.1: Average linear and angular distances between the reconstructed trajectories for both subjects and their respective measured trajectories

4.6.3 Model Assessment

4.6.3.1 IOC results

Once the coupled OC problem introduced, the weights of the cost functions introduced in Eq.4.7 were optimized using the IOC problem defined in Eq.4.8. Thus, the optimal weights

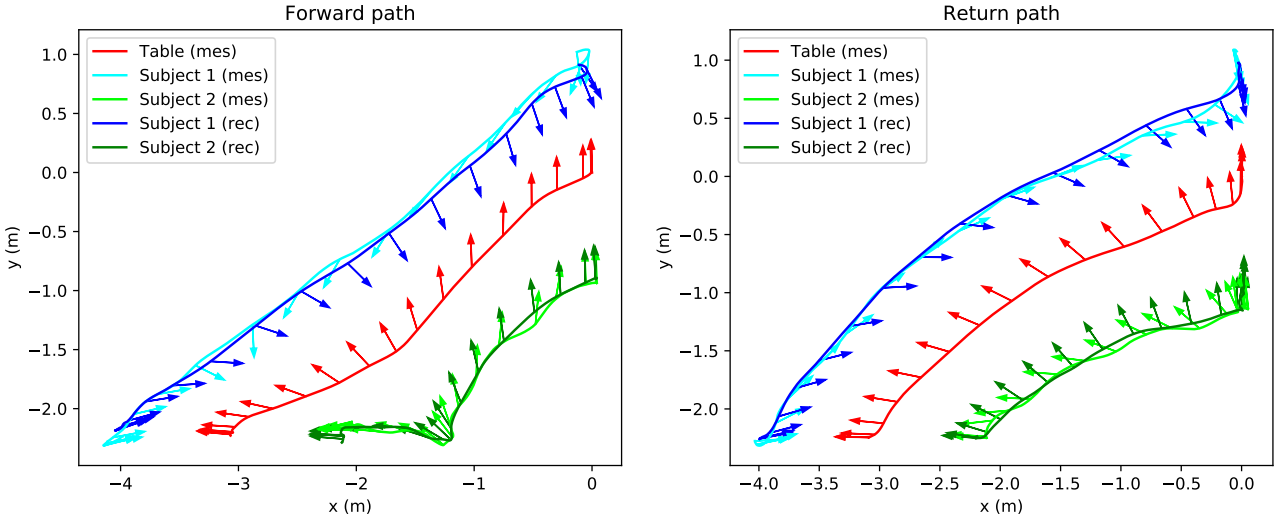

Figure 4.15: Example of reconstructed trajectories for one given pair for Goal 6.

which allowed the generated trajectories to best fit the average trajectories for Scenario 3 are:

$$\begin{cases} (\alpha_0, \alpha_1, \alpha_2, \alpha_3, \alpha_4, \alpha_5, \alpha_6, \alpha_7, \alpha_8, \alpha_9, \alpha_{10}) \approx (3.85, 2.29, 10.37, 0.10, 2.7, 8.99, 3.00, \\ \qquad\qquad\qquad\qquad\qquad\qquad\qquad\qquad 10.42, 1.81 \times 10^{-6}, 0.50, 0.03) \\ (\beta_0, \beta_1, \beta_2, \beta_3) \approx (19.77, 30.24, 8.77, 9.15) \end{cases} \tag{4.9}$$

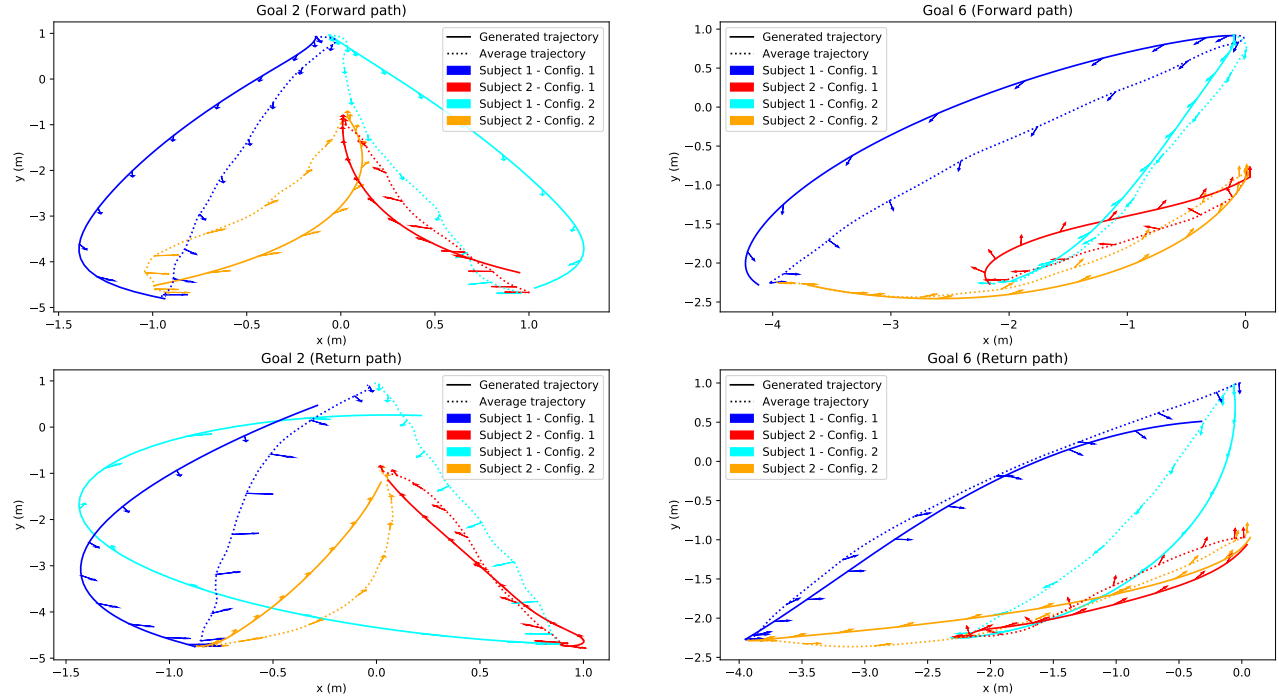

Figure 4.16: Average (*dotted line*) and generated trajectories (*full line*) for both subjects, with both configurations when measured. The arrows represent the orientation of the pelvis of the subjects during locomotion.

4.6.3.2 Comparison of the generated and the measured trajectories

Trajectories between the same starting and goal positions as the average trajectories were generated using the OC model with the computed optimal weights. Two examples are shown in Fig.4.16.

Then, the linear and angular distances between the generated and the average trajectories were computed. For all the forward paths and for both subjects, the average distances were $\bar{d}_{xy} = 0.26 \pm 0.11\,\text{m}$ and $\bar{d}_{\theta} = 0.51 \pm 0.6\,\text{rad}$. For all the return paths, they were $\bar{d}_{xy} = 0.44 \pm 0.36\,\text{m}$ and $\bar{d}_{\theta} = 0.93 \pm 1.17\,\text{rad}$. The boxplots showing the distances per subject and per direction are represented in Fig.4.17. Those linear and angular distances showed significant differences (Kruskal-Wallis test, $p < 0.05$) with the linear and angular distance between the average and the measured trajectories during Scenario 3 for both subjects. Thus, the gap between the model and the reality was greater than the variability of the measurements. Moreover, as the final constraint was weak, the model could generate trajectories which did not exactly reach the goal position. It is the case for 3 different trajectories plotted in Fig.4.16. Thus, we computed the euclidean distances between the goal position and the final position of each generated trajectory. The distances on average were 0.19 m and 0.59 rad for the forward paths and 0.26 m and 1.24 rad for the return paths.

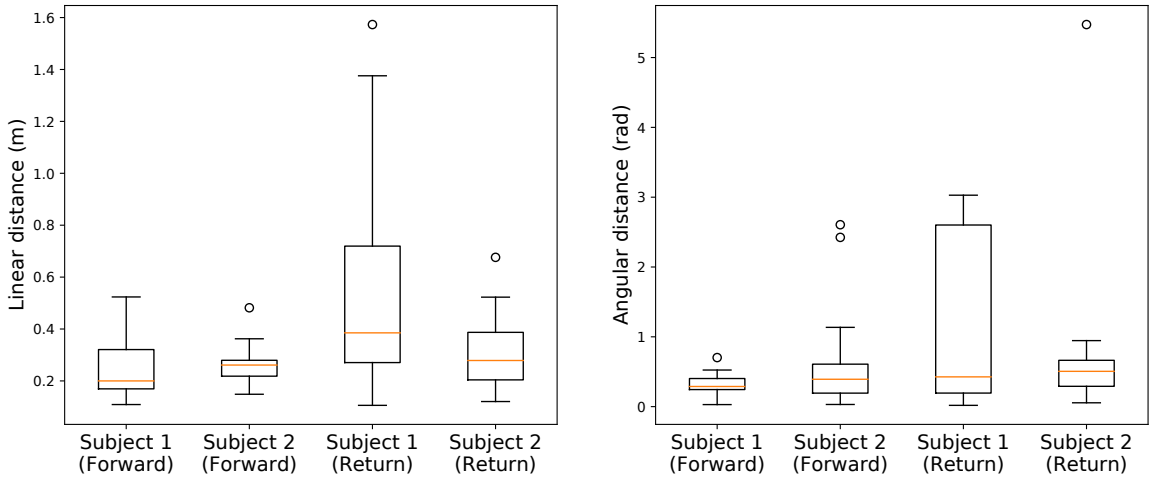

Figure 4.17: Boxplot of the linear (on the *left*) and angular (on the *right*) distances between the generated and the average measured trajectories for every goal positions according to both subjects and to the direction of the motion.

4.7 Discussion

4.7.1 Does a shared strategy emerge from the study of walking paths during collaborative carriages?

First of all, let us focus on the main question the data analysis aimed to answer: Is there a shared strategy implemented by the pairs to move a table around? The first conclusion drawn from the data analysis was that, during Scenario 3, 60% of the subjects chose a trajectory

closer to the one they performed when they were the only one to know the goal position. However, this result could not be generalized to all the pairs. Thus, leadership was not the only determinant of the strategy implemented by a pair. Indeed, other results showed that the choices of configuration (i.e. the final orientation of the table for a given goal position) made when both partners were leaders were not systematically the same as the one made when Subject 1 was leader or when Subject 2 was leader. This leads to the conclusion that, broadly speaking, the strategy chosen by a pair did not depend on who knew where the table should be placed. The leadership only impacted the travel time. If both partners knew the goal position, the task was sped up.

Then, it can be stated that the subjects did not choose the same trajectories when they carried a table from one start to one goal compared to when they carried it backwards. Thus, the pairs' strategy changed according to who walked forwards and who walked backwards. Moreover, it is interesting to denote that even if the subjects were allowed to grasp the table while standing theirs back to it, they always chose to face the table. Thus, for the forward paths, Subject 1 always moved forwards while Subject 2 moved backwards and reversely for the return paths.

Another conclusion resulting from the data analysis was that the pairs chose the optimal configuration for the whole pair in more than 80% of the experiments, even if it was, most of the time, at the expense of the same member of the pair. Besides, it is still interesting to denote that the privileged subject was Subject 1, the one who walked forwards for the forward paths. This may be due to the fact that this subject was on average further from the goal position (see Fig.4.1a) and so the optimal strategy involved reducing its traveled distance. This means that a shared strategy aiming to reduce the traveled distance of the whole pair globally emerged from the experiments. However, it still means that, in around 20% of the experiments, pairs did not follow this strategy. The experimental conditions did not allow to understand the reason why some pairs acted in a sub-optimal manner for their whole group while most did. So this strategy was implemented by the majority of the pairs, but it was not universal.

Finally, the comparison between the average trajectories and the measured trajectory shows that a great range of behaviour exists. As the various trajectories shown in Fig.4.4a and Fig.4.4b could indicate, when walking with a table, the pairs took very different trajectories, which made the average trajectory barely representative. Even when looking at one pair, significant differences can be noted between trajectories performed from the same start to the same end. All those results suggested that a shared optimal strategy which would be implemented by every pair to carry a table around did not seem to exist. However, it is important to outline that there was one same choice that every subject made: each member of the pair chose to face the table instead of standing its back to it. Apart from this choice, all the choices made by the pairs did not seem to follow a shared strategy. As the trajectories of single walking humans already presented a great variability (see Sec.1.4.4), it is not surprising that with two coupled humans the observed variability was even bigger. Indeed, the linear distances between the trajectories measured as part of this study and their respective averages were about two times higher than the distances between the trajectories of single walking humans and their average (0.11 ± 0.06 m for the linear distance and 0.48 ± 0.18 rad for the angular distance computed in Sec.1.4.4). Thus, we can conclude that the variability of human

trajectories increased when two humans were interacting with each other. This is consistent with the results of some studies about collaborative work which demonstrated that individuals were less efficient when performing a task as a group than when performing alone [149, 150]. Moreover, it is interesting to denote that the variability of the table trajectories was lower than the variability of the subjects' trajectories.

Thus, in this context, we can state that no universal strategies have emerged for carrying a table. Indeed, even if some shared strategies emerged from the experiments, none was implemented by every pair. Moreover, the large trajectory profiles and the different configurations observed tended to demonstrate that there was not one optimal path followed by every pair. In other words, if such optimal trajectories existed, the subjects were not able to find and follow them. Pairs did not demonstrate an optimal behaviour for the structure of the cost function tested with our IOC scheme. Let us denote, that the result may be different if the experiments were performed by trained participants such as professional movers who know their partner well.

4.7.2 Limitations of the modelling approach

This great variability may explain the hardship of getting accurate results when modeling the CoM trajectories of two humans walking with a table. In Sec.1.4.3, an IOC scheme was used to build an OC model which accurately fits average CoM trajectories of single walking humans. In this chapter, we applied the exact same method to investigate if an identical approach could provide similar results and build a coupled OC model to simultaneously simulate two humans handling a table. The generated trajectories could be considered as consistent as they are, most of the time, included in the corridors of observed trajectories. However, this model could not succeed in generating accurate human-like CoM trajectories. Indeed, we hypothesized that the model can be considered as accurate if the mean distances between the generated and the average measured trajectories are of the same order of magnitude as the mean distances between the individual and the average measured trajectories. According to this assumption, even if the results for the forward path along the $\vec{x}$ and $\vec{y}$ axis were suitable, the results for orientations and the return paths were not accurate enough. Thus, the starting hypothesis stating that we could model pairs of humans carrying a table with the same method used to model single walking humans turned out to be wrong. Indeed, the method, which worked well to model (Chapter 1) and even predict (Chapter 2) a single human behaviour, did not succeed in building an accurate model for two humans walking with a table. It was not totally unexpected as two humans carrying a table were not two independent holonomic systems coupled through a table. Their interactions may not just be haptic interactions, but some other non-verbal interactions may play a role during the carriage task. For example, they may induce sudden changes in the implemented strategy resulting in unusual behaviours. As it could be expected, those potential interactions were not taken into account in the OC model. Moreover, the inaccurate results may also be due to the great range of behaviour observed during the experiments. The different average trajectories may reflect inconsistent behaviours which resulted in an impossible fitting of the average trajectories with on single set of weights. However, when trying to fit the individual measured trajectories performed by one pair instead of the average trajectories, this problem remained as one pair also displayed a too great range of behaviours, as Fig.4.12 shows. Moreover, as better results were obtained for the forward path, the hypothesis made for the return paths may be wrong: the subjects' roles may not be switched between the forward and the return paths. One solution may be to compute

time-varying weights in order to identify changes in the subjects' behaviour. Changing the dynamics of the system to model both subjects as a mass spring system might also be better than coupling the subjects with weak constraints put in the cost function. Indeed, low weights were assigned to the exponential barriers implemented in this manuscript. This means that the constraints they represented were not always observed. Another solution might be to remove outlier trajectories before computing the average trajectory. This might provide a model which fits the trajectories of pairs which have the most homogeneous behaviour. Thus, the main conclusion of this inaccurate modeling was that two interacting individuals cannot be modeled using the same optimization criteria that were used to model a single individual. The haptic interactions seemed to induce a change in the subjects' behaviour which made them fundamentally different from one single walking subject and, thus, less predictable. To conclude, during the recorded interaction, the collaborating subjects set aside their individual behaviour to achieve a less predictable collective behaviour. As the model was unable to generate accurate trajectories for at least one scenario, we chose not to present the results regarding Scenario 1 and 2 as we can already state that this approach was not relevant to model pairs during collaborative carriage tasks. In the same way, we chose not to test the addition of other terms in the cost function, such as the direction of the gaze. Indeed, we believe that the observed variability may prevent finding an accurate universal OC model, whatever the terms in the cost function are.

In the next chapter, the focus will be on modeling only the trajectory of the table using the same method as in Sec.1.4. This must be more successful than trying to model human trajectories that are too varied. Indeed, the data analysis showed a lesser variability regarding the table trajectories. Thus, the solution to accurately model the behaviour of a human during a table handling task may be to model the table behaviour first and then to infer the carriers' behaviour. Then, a prediction model may be developed based on this trajectory model as it was done in Sec.2.2 to predict in real-time single walking human trajectories.

However, it is important to denote that other approaches, which do not assume the existence of an optimal trajectory, could have been considered to analyze the performed experiments. For example, the uncontrolled manifold analysis [151], or other dynamical approaches [152], could have also been applied here, perhaps, using the position of the table or its orientation as the performance variable. Another solution to model the subjects' trajectories could be to reconstruct them from the table trajectory. Indeed, in Sec.4.6.2, we showed that the position of the CoM of the subjects can be accurately reconstructed from the position of the CoM of the table they carry. This demonstrates that there is a low variability in the behaviours exhibited by the subjects with respect to the table. However, the orientations of the subjects cannot be inferred with as much precision because the orientations of the subjects with respect to the table present a greater standard deviation. Moreover, this method requires the full table trajectory as an input to determine the subjects' trajectories. This makes it irrelevant for real-time prediction.

4.7.3 Discussion about the experimental protocol

A few remarks needed to be made on the experiments. A total of 3240 CoM trajectories were performed as part of this study. However, due to marker loss, 1.7% of the data was

unprocessed. For every subject, 100% of the forward paths and 96.7% return paths were collected. Moreover, as mentioned in Sec.4.2.3, markers were put on the feet and on the heads of the subjects. Thus, the database created from the performed experiments includes data that has not been analyzed yet. So, future works could study the remaining data that might provide new insights on the results, especially regarding the step length, the analysis of the equilibrium or the orientation of the gaze during the carriage task.

Then, it is important to denote that we chose not to take into account the physical features of the individuals to make up the pairs in order to gather recordings of carriage tasks representative of two random people who would like to move a furniture together. Moreover, a T-test confirmed that the weights and heights of the group gathering all the subjects appointed as "*Subject 1*" and of the group gathering all the subjects appointed as "*Subject 2*" are not significantly different (T-test, $p > 0.05$). Furthermore, here is some data which shows that the impact of this choice seems to be minor. In Fig.4.18, we represent the average linear distances between the average and the measured trajectories during Scenario 3 for both members of each pair with respect to the differences in weight and height between both members. This plot, along with the Pearson Correlation coefficient computations, shows that there is no correlation between the linear distances and the difference in weight (-0.09 for Subject 1 and 0.18 for Subject 2) or height (-0.27 for Subject 1 and -0.10 for Subject 2) in the pairs. Thus, this short analysis tends to point out that it is not a problem not to take into account the physical features of individuals inside the pairs.

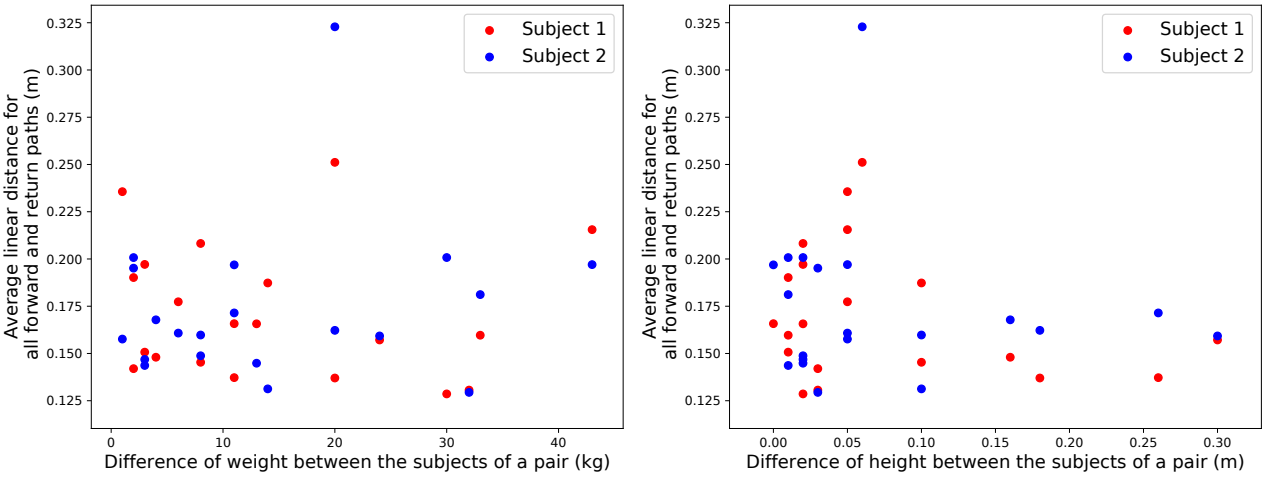

Figure 4.18: Average linear distances between the average and measured trajectories with respect to the difference of weight in the pair (on the *left*) and with respect to the difference of height in the pair (on the *right*) for Scenario 3.

Furthermore, the experimental protocol could be improved. Indeed, as pairs always performed Scenario 1 before Scenario 2, some results cannot be easily interpreted. For example, the experiments during Scenario 2 were performed a little faster than the ones during Scenario 1. It is hard to say if this slight difference may be due to the change of leadership or just to the fact that the scenarios were performed one after the other. In other words, it remains unclear if a learning process emerged between the scenarios. However, if an order effect was present, e.g., partners might know each other better in the last scenarios, it

	Scenario	Subject 1	Subject 2	Table
d_{xy} (m)	1	0.25 ± 0.16	0.26 ± 0.15	0.18 ± 0.13
d_{xy} (m)	2	0.22 ± 0.15	0.20 ± 0.16	0.15 ± 0.14
d_{xy} (m)	3	0.18 ± 0.11	0.17 ± 0.09	0.13 ± 0.10
d_{θ} (rad)	1	0.23 ± 0.18	0.27 ± 0.19	0.16 ± 0.14
d_{θ} (rad)	2	0.17 ± 0.12	0.18 ± 0.13	0.10 ± 0.08
d_{θ} (rad)	3	0.16 ± 0.11	0.24 ± 0.17	0.09 ± 0.08

Table 4.2: Average linear and angular distances ($\pm$ standard deviation) according to the scenario.

cannot be set apart. However, we believe that the impact of the non-randomization between the scenarios on the results was minor. Indeed, two observations make us believe that no clear learning process occurred between the different trials. First, standard deviations of the linear and angular distances between the average and the measured trajectories computed for the 3 scenarios (see Tab.4.2) are not significantly different (Kruskal-Wallis test, $p \approx 0.06$ for the linear distances and $p \approx 0.11$ for the angular distances). This means that the variability observed during the different scenarios seems consistent. If a learning process was at stake, the variability should decrease between the scenarios. Then, we observed pairs which chose to put the table in a different configuration between the different scenarios (see Fig.4.6). This observation makes us believe that the subjects do not remember how they carried the table to the same goal in the previous scenario. Thus, we believe that the non-randomization is a clear limitation of our experimental protocol and should be avoided when reproducing these experiments, but it may have only a minor impact on the results of this study.

Another improvement could be added to the experimental protocol. In these experiments, the subjects were asked to stay silent in order to avoid non-haptic collaborations. However, even if verbal communication was forbidden, no action was taken to avoid non-verbal communication like gazes. To remove this bias in future experiments, subjects should not see each other's eyes, they should wear masks or be separated by a board placed in the middle of the table.

4.8 Conclusion

To conclude, this chapter provided a study of the trajectories performed during table handling tasks. As part of this work, 20 pairs of subjects performed 54 forward and return paths between various starting and goal positions according to different scenarios. The experimental protocol was described in Sec.4.2. Thus, more than 3000 CoM trajectories of the subjects and of the table were recorded and analysed in Sec.4.6. This analysis demonstrated the great variability in the choices made by the pairs to move a table around. No shared strategy, that all pairs would implement, emerged from those experiments. The only choice made by every subject was to face the table during the task instead of turning their backs to it. Regarding the chosen trajectories or configurations, a great range of behaviours was observed. Because of this variability, simultaneously generating the CoM trajectories of the two members of a pair carrying a table was much more complex than generating the CoM trajectories of a single walking human, like it was done in Chapter 1. Thus, even if the simulated paths are, most of the time, included in the corridors of observed trajectories, the OC model introduced and

optimized with an IOC scheme in this chapter did not succeed in accurately simulating the pairs locomotion.

Thus, as the behaviour of the subjects during a collaborative carriage is too variable, it is difficult to provide to the robot a locomotion model to make it able to adapt to such erratic behaviour. However, it may be possible to model the table's trajectories instead of the subject's ones. Indeed, the data analysis showed a lesser variability regarding the table trajectories. It would seem that the subject optimized the table trajectory at the expense of their own. Thus, modeling and predicting the table's trajectories may be the solution to make the robot able to proactively interact with a human to carry a table. The achievement of such a task is the focus of the following chapter. Thus, in this chapter, the focus will be on the real-time localization of the table and on the modeling and the prediction of the table's trajectories, using the same method as in Chapter 1 and Chapter 2, in the context of a proactive human-robot collaborative carriage.

Chapter 5

Table Handling Task

Contents

5.1 Introduction

5.1.1 Motivations

This chapter deals with the final goal of the ANR-CoBot project, namely the HRI to collaboratively carry a table. The first requirement to perform such interaction is to be able to accurately place the robot in front of the table. Indeed, without this first step, the robot would not be able to lift and even less carry the table with a human partner. Then, the robot needs to lift the table. Finally, the robot has to walk while handling the table without losing its balance. Thus, the whole-body controller needs to be robust enough to compensate for the perturbations induced by the carried table. Moreover, the WPG has to generate in real-time the positions and the orientations of the robot CoM and footsteps in accordance with where the human partner wants to bring the table. Thus, to achieve such interaction, multiple matters need to be dealt with: localization, walk generation and whole-body control. The goal of this chapter is to present how those problems can be handled, separately and together, to perform a human-robot table handling task.

5.1.2 Related Works

In the context of the growing number of robots in the industrial world or even in people's daily lives, HRI is a booming field of study [15, 118, 153]. However, achieving a successful and useful HRIs is far from easy, especially when dealing with humanoid robots. Indeed, these robots are complex to control and might be harmful to a human partner due to their heavy weight and wide range of motions. Moreover, due to the redundancy of the musculoskeletal system of humans, there is a great variability in the range of motions between individuals and the robot should be able to adapt to every human partner. Thus, making a humanoid robot interact with a human partner requires a safe and robust controller along with an effective and adaptive planner.

5.1.2.1 Study of human collaboration to improve human-robot interactions

Even if there is a significant variability inherent in human movements [154], humans have the ability to quickly adapt their behaviour when collaborating with others. They can even predict their partners' intentions using visual, verbal and haptic signals. To move towards efficient HRIs, the robots have to be as reactive as human beings. This is why numerous works study human collaboration in order to improve HRIs. For example, [155] studied a beam transportation task. They measured the postures of the subjects and the forces and torques applied on the beam while being carried by two subjects. From those measurements, they proposed a control scheme for physical interactions for a HRP-2 robot. [122] also performed human-human experiments to carry a beam. Using a multiclass classification problem, they developed an algorithm which detected human's intentions while walking with a beam and embedded it in a COMAN robot controller to make it more proactive during beam transportation with a human partner. Furthermore, the goal of some studies in the HRI field is to enable robots to actively assist a human during collaborative tasks. One solution, proposed by [119], was to reconstruct a pre-recorded human motion and replicate it on the robot. This work resulted in a simulation of a collaborative pick-and-place experiment where a HRP-4 robot assisted its partner in a human-like manner. This demonstrated the ability to mimic human motions on

a humanoid robot. However, this method demanded an initial recording of a human motion, which prevented real-time applications.

Conversely, it is interesting to denote that HRIs can also be used to study human motions. An interaction with a 7 DoFs robot arm can, for example, help to characterize and model the human arm impedance using the measured force profiles [156].

5.1.2.2 Physical human-robot interactions

Physical Human-Robot Interactions (pHRIs) refer to the HRIs where a direct contact or a contact through an object occurs between the robot and its human partner. Two main strategies exist to deal with pHRIs according to Jarrassé et al. [118].

The first classic approach is to use impedance control [157, 158, 159, 160]. For example, using impedance control, Mujica et al. [161] studied the influence of a load's knowledge (weight and inertia) on a human-robot co-manipulation task. In this work, the authors demonstrated that when the object's properties are included and compensated by the controller, less efforts are needed to start and stop the motion. However, this approach usually considers the human partner as a perturbation. Doing that, the robot is the leader of the motion instead of assisting the human to do the motion. Impedance control can also be used copy [162] or learn [163] human control. For example, in Gribovskaya et al. [163], the authors made a robot "learn" a task during a pHRI. In this work, a HRP-2 robot collaborated with a human partner to lift a beam only through haptic feedback. Those demonstrations were recorded and used by a learning model based on GMM in order to make the robot as reactive as a human being when performing this task. Making a robot learn motion through demonstrations can also be useful for the control of exoskeletons [164, 165] by reducing human efforts or by amplifying human power or for rehabilitation robots [166].

The other method focuses on the prediction of human intentions to adapt the robot's behaviour to its partner's motions [167]. For example, Bussy et al. [102] performed a transportation task where a HRP-2 robot guessed its partner's intentions using motion primitives (stop, walk, side, turn). In this work, the prediction of the human's intentions was based on the velocity of the human partner. However, other criteria, such as the velocity transmission of a robot arms [168], the measurements of the contact forces with a robotic skin [169] or the human past trajectory [4], could be used to predict the human's motions as part of HRIs.

5.1.2.3 Safety

Another key topic in the HRI field is about guaranteeing the safety of the human partner [170]. Indeed, when a robot works with humans around it, undesired, or even voluntary, contacts may occur. Thus, during HRIs, it is necessary to perform safe motions with the robot in order not to endanger people's health. To reduce the risk of dangerous contacts, collision avoidance systems can be set up. Those systems are based on visual feedback. For example, to detect obstacles or the human partner, depth images were generated in Flacco et al. [171]. Another way to reduce the danger induced by collisions is to detect the collision and to make the robot appropriately react to them [172]. This can be achieved through a robust and adaptive controller. For example, Navarro et al. [173] proposed a two-layer damping controller with built-in safety measures to safely operate robots during pHRIs. Moreover, apart from ensuring the safety of a potential partner, detecting collisions can also protect the robot's hardware.

5.1.3 Contributions

This chapter presents the implementation of different requirements needed to perform a proactive human-robot collaboration to carry a table.

First of all, in Sec.5.2, two approaches to localize the robot and the table are presented and assessed. The first one is based on a MoCap while the other one is based on a LiDAR which was embedded on the robot by Thibaud Lasguignes, another PhD student in the Gepetto team. The main contribution of this section is the demonstration of the ability of both localization systems to localize the robot with respect to its surrounding environment. However, for now, only the MoCap can be used to accurately place the robot in front of the table because it not only allows to localize the robot, but it, also, allows to know where the table stands in the room.

The experimental work about the MoCap-based localization is unpublished, it was not submitted to any conference or journal. Nevertheless, a video of this work is available on: `https://youtu.be/GSx3bYOrFAI`.

The work assessing the LiDAR-based localization was published in Lasguignes et al. [9]. A video of this work is available on: `https://www.youtube.com/watch?v=0t1bBjDTqMA`.

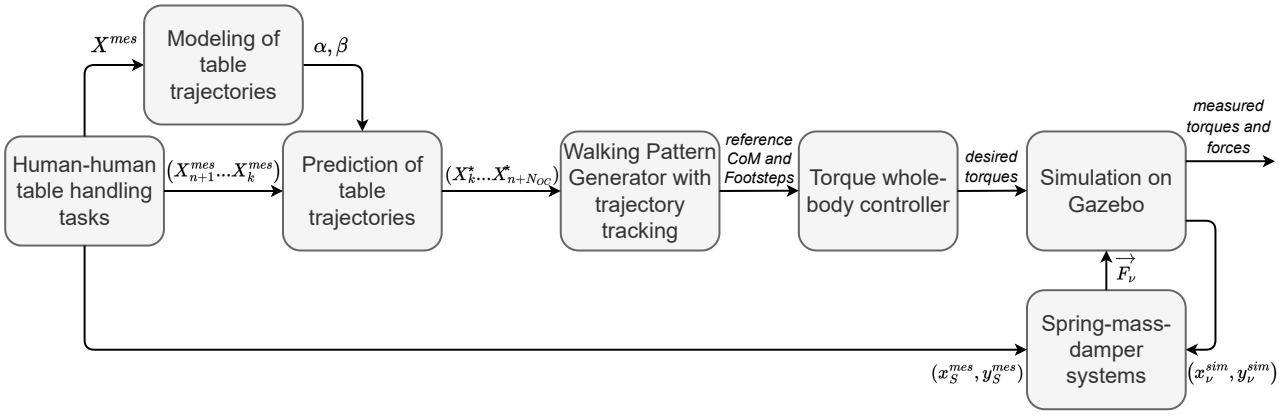

Figure 5.1: Description of the whole framework presented in Sec.5.3. The notations introduced in this chart are defined throughout Sec.5.3.

Then, in Sec.5.3, the focus is on the achievement of the proactive human-robot table handling task in simulation. To achieve this goal, we implemented the framework presented in Fig.5.1. The main contributions of this section are threefold. First, it provides a short analysis of the experimental trajectories performed by a table handled by two subjects. We already showed, in Chapter 4, that the trajectories performed by the subjects are too different to be simulated with the same method used to simulate single walking humans in Chapter 1. Thus, the work presented in this section focuses on the analysis of the table trajectories in order to investigate the variability of those trajectories and the possibility to model the table behaviour

instead of the subjects' behaviour. Then, we demonstrate that the same method can be applied to model and predict the CoM table trajectories during carriage tasks as to model and predict in real-time the CoM trajectories of single walking humans like in Chapter 2. Once the prediction model is built, it is embedded in the WPG of the TALOS humanoid robot as in Chapter 3. Finally, this work proposes a simulation of a table carried by a robot on one side and a simulated human on the other side. This simulation is aimed at being as realistic as possible. Thus, in simulation, a TALOS humanoid robot is able to actively carry a 20.7 kg table without losing its balance or performing sharp motions which could endanger its simulated partner.

This work is currently under review for IEEE Humanoids 2022 [8]. However, a video of this work is already available on: `https://www.youtube.com/watch?v=PbUySwCP9s8`. Moreover, the code is open-source and available on: `https://github.com/imaroger/table_trajectories_during_collaborative_carriage/tree/main`

5.2 Localization of the robot

To perform a collaboration between a real TALOS humanoid robot and a human to handle a table, we need to make sure that the robot knows where the table is with respect to its free-flyer. Two methods of localization were investigated as part of this work. First, a MoCap was used to track a robot and a table to demonstrate the ability of the robot to interact in real-time with objects localized using a MoCap. Then, the same MoCap was taken as the ground truth to assess a LiDAR-based localization system.

5.2.1 Walking experiments using a motion capture system

This section focuses on experiments performed with a real TALOS humanoid robot as part of my Master internship. These experiments aim to demonstrate that the robot is able to walk toward and follow a table localized using a MoCap.

5.2.1.1 Experimental setup

The experiment room is equipped with a MoCap including 20 infrared Qualisys Miqus M3 cameras sampling at up to 650 Hz with a 3×10^{-4} m accuracy on the viewed area. The experiment room is shown in Fig.5.2.

Figure 5.2: Experiment room (the Qualisys cameras are circled in yellow).

For these experiments, 5 passive reflective markers were placed on a table and 8 markers were put on the torso of the TALOS robot. These markers allow to measure the position and orientation of both objects in real-time. The data is streamed on a ROS[103] topic `/tf`. Thus, the robot and the table localization can be visualized on RViz software as Fig.5.3 shows.

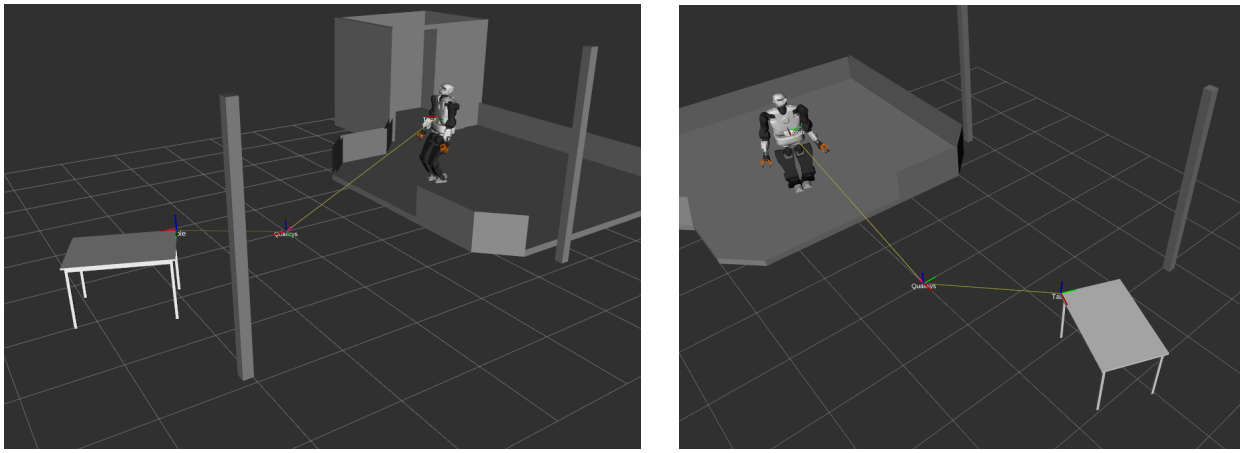

Figure 5.3: Visualization of the TALOS robot and of the table on RViz

5.2.1.2 Walk generation

During the experiments, the robot had to walk toward
a target placed at 0.9 m from the closest side of the table. The walking algorithm used to generate the motion is the one provided by *PAL-Robotics*. It was used to send a velocity command to the robot on the topic `/walking_controller/cmd_vel` at a 2 Hz frequency. The velocity command was merely computed as the euclidean distance between the table and the robot along the $\vec{x}$ and $\vec{y}$ axis in the coordinate frame linked to the robot and the angle between the robot and the table orientation around the $\vec{z}$ axis. Thresholds of $0.1\,\mathrm{m.s^{-1}}$ for the linear velocities and $0.12\,\mathrm{rad.s^{-1}}$ for the angular velocity were applied on the command in order to not reach the robot limits. Moreover, the command was designed so that the robot stops walking when it is at short enough distances and angle from its target, respectively 0.08 m and 0.07 rad. This stopping distance was implemented to prevent the robot from trampling on its target instead of stopping on it. This allows a swift stop once on the spot.

5.2.1.3 Experiments

The robot successfully walked toward the table during 5 experiments in a row. The time-lapse of one experiment is represented in Fig.5.4. The starting position and orientation of the robot and of the table was changed between every experiment in order to demonstrate the robustness of the localization. During some experiments, when the robot had reached its target, the table was moved. Each time, the robot successfully followed it and walked toward the moving table. One of these situations is shown in Fig.5.5.

5.2.2 Assessment of a LiDAR-based localization system

During this thesis, a new head was designed for the TALOS robot. This head, represented in Fig.5.6, embeds an Ouster OS1-64 LiDAR, an Intel RealSense T265 tracking camera and an Intel RealSense D435i RGB-D camera. The flash LiDAR system allows to get 3D clouds at 10 Hz. Coupled with the Intel RealSense T265, which provides visual-inertial odometry, it is possible to localize the robot and use this information to generate foot steps in real-time to reach specific points. This localization system is based on an Iterative Closest Point (ICP) algorithm developed by Pomerleau et al. [174] and implemented by Thibaud Lasguignes on the TALOS

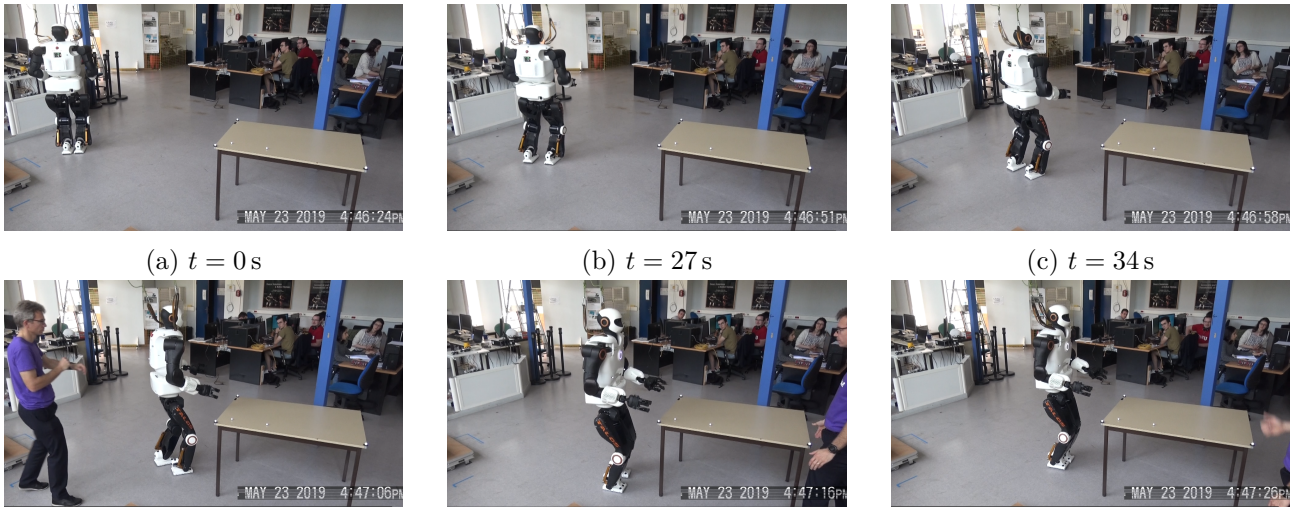

(a) $t = 0\,\mathrm{s}$ (b) $t = 27\,\mathrm{s}$ (c) $t = 34\,\mathrm{s}$

(d) $t = 42\,\mathrm{s}$ (e) $t = 52\,\mathrm{s}$ (f) $t = 62\,\mathrm{s}$

Figure 5.4: Walk to the table

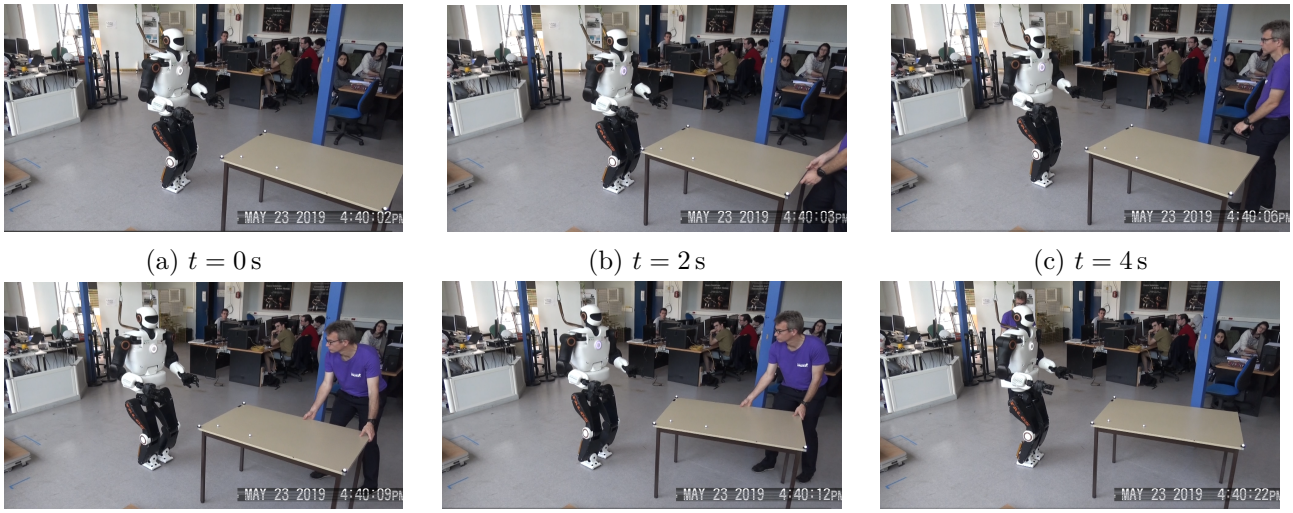

(a) $t = 0\,\mathrm{s}$ (b) $t = 2\,\mathrm{s}$ (c) $t = 4\,\mathrm{s}$

(d) $t = 7\,\mathrm{s}$ (e) $t = 10\,\mathrm{s}$ (f) $t = 20\,\mathrm{s}$

Figure 5.5: Tracking of the table (*Translation of the table toward the robot at* $t = 2\,\mathrm{s}$ *and rotation of the table at* $t = 10\,\mathrm{s}$)

robot [9]. Regarding this new localization system on the TALOS robot, my contributions were to achieve walking experiments to collect localization data with both the MoCap and the LiDAR-based localization system and to compare the recorded data to assess the accuracy and the performance of the LiDAR-based localization. In this study, the MoCap measurements are hypothesized to be the ground truth data. This work was published in Lasguignes et al. [9].

5.2.2.1 Experimental setup

The MoCap used in those experiments is the same as the one described in Sec.5.2.1.1. This motion capture system was used to record the positions and orientations of the robot's head. We placed 5 passive reflective markers on its torso and 1 on the top of its head.

For the LiDAR-based localization systems, only the Ouster OS1-64 LiDAR and the Intel

RealSense T265 were used. The LiDAR has a range between 0.8 m to 120 m, an horizontal field-of-view of 360° and a vertical field-of-view of 33.2° using its 64 laser beams. For the experiment, the LiDAR was set to take 1024 horizontal samples per scan and to return point clouds at 10 Hz. The Intel RealSense T265 is a tracking camera embedding two Fish-Eye cameras, an IMU and a Vision Processing Unit (VPU). This camera runs a Simultaneous Localisation And Mapping (SLAM) algorithm on the VPU with an output frequency of 200 Hz.

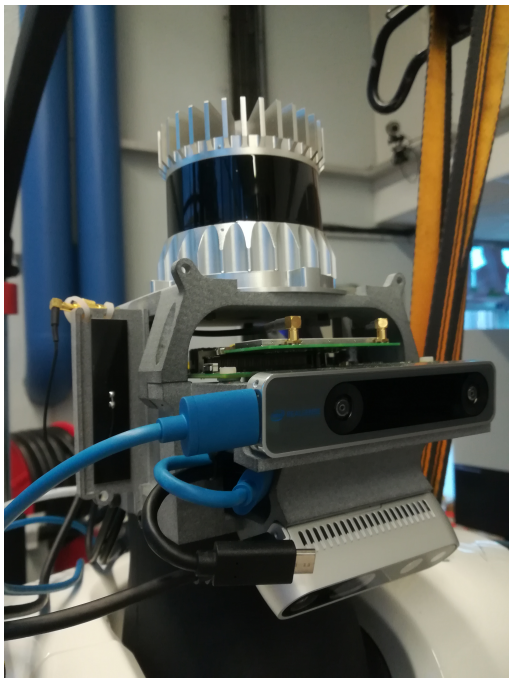

Figure 5.6: New TALOS head with sensors.

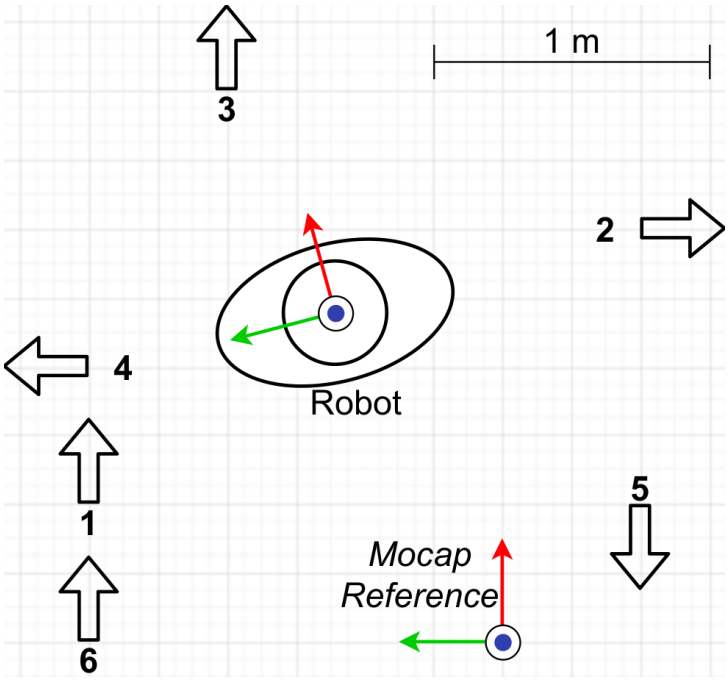

Figure 5.7: Goal positions in the experimental room

5.2.2.2 Experimental protocol

The performed experiment consists of a series of targets the robot has to successively reach. Thus, six goal positions were defined in the experimental room. Those positions are represented in Fig.5.7. They have been chosen in such a way that the robot ranges the whole MoCap viewed area and faces diverse orientation changes. The position of the robot at the beginning of the experiment is not defined in advance, it could be anywhere in the viewed area. Note that, if the robot starts from the origin of the MoCap reference frame, it will have to travel around 10.6 m to perform the whole experiment.

To reach the goal positions, the robot walks using the walking algorithm described in Sec.5.2.1.2. The only difference is that the target of the robot is no longer a table but a given goal position. Once the robot stops on a target, the robot is programmed to stay still during 8 s before moving on to its next target.

During the experiments, a dataset was recorded on a *rosbag* including the measurements made by the MoCap, the velocity commands sent to the robot, the LiDAR data, the tracking camera images and estimations and the LiDAR-based localization results.

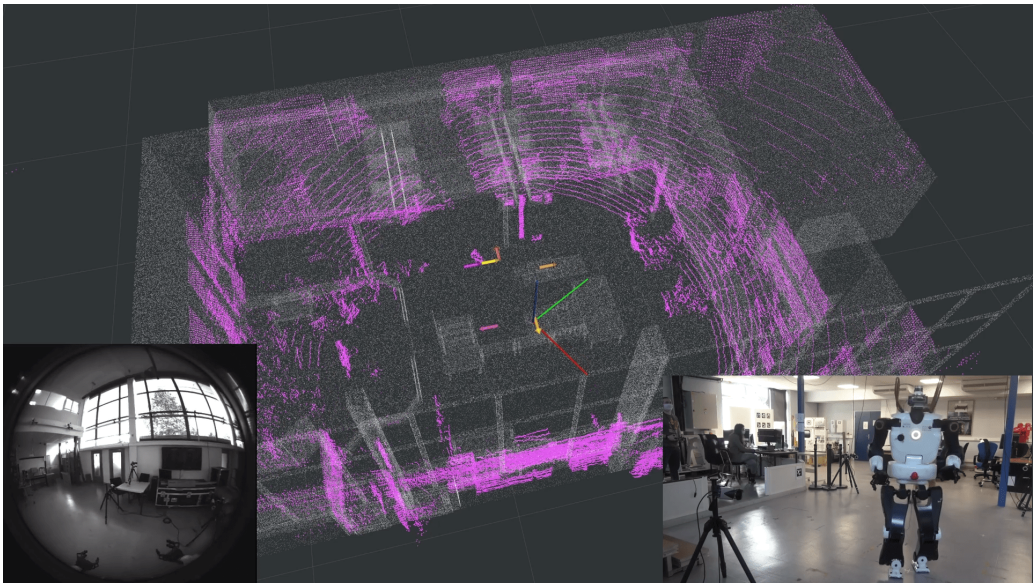

Figure 5.8: Frame extracted from the video of the first experiment. The video shows the ICP data (prior map in *grey*, read point cloud aligned in *pink*, axis: estimated pose) and the targeted poses (arrows) in the middle, the image from a sensor of the Intel RealSense T265 on the left and the video of the experimental room and the robot on the right.

This experiment was successfully performed 3 times with a TALOS robot. Due to technical problems and hardware issues on the robot's legs and ankles, further experiments resulted in failures and the fall of the robot, preventing us from gathering more data. Among those successful experiments, the first one was performed with the map built from the architectural 3D model whereas the second and the third ones were performed using the map built using a scanning device. More details about the map building are available in Lasguignes et al. [9]. A screenshot from the video of the first experiment is shown in Fig.5.8.

5.2.2.3 Data analysis

Comparison between the motion capture system and the LiDAR-based localization system.

During the experiments on the robot, two data sets were collected simultaneously: one with the positions and orientations of the robot head recorded by the MoCap and another recorded by the LiDAR localization system. As both localization systems do not have the same sampling frequencies, the raw datasets cannot be compared directly. Indeed, the MoCap dataset includes around 40 times the amount of data of the ICP one as Fig.5.9 shows. This is why both data sets were interpolated in order to have the same length.

First of all, for the three datasets, a delay between the ICP system and the MoCap can be measured by shifting the two datasets to minimize the difference between the (x, y, z) positions and the θ orientation measured by the two localization systems. This delay scores between 0.51 s and 0.62 s depending on the experiment and is mainly due to the computation time of the ICP. In the following, this delay has been removed from the ICP set.

Figure 5.9: Visualization of the recorded data on Rviz (in *red* the MoCap set and in *green* the ICP set)

	On $\vec{x}$ (mm)	On $\vec{y}$ (mm)	On $\vec{z}$ (mm)	Around $\vec{z}$ (rad)
Exp. 1	18.7 ± 17.2	24.9 ± 19.3	9.2 ± 7.2	0.025 ± 0.019
Exp. 2	14.8 ± 17.3	19.9 ± 17.8	5.4 ± 4.4	0.023 ± 0.027
Exp. 3	13.8 ± 15.9	18.9 ± 15.7	5.6 ± 4.8	0.024 ± 0.027

Table 5.1: Computed errors between the MoCap and the ICP data sets for all the experiments

Then, the differences between the two datasets on the position and on the orientation can be computed. These differences will now be referred to as offsets. The evolution of these offsets over the whole experiment is shown in Fig.5.10. These offsets are of two kinds:

- Structural offsets due to a difference between the coordinate frames of both localization systems. We make the assumption that these offsets are constant, as it seems to be the case in Fig.5.10 and can easily be computed as the mean of the differences between the datasets over the experiment duration. Thus, these offsets score 0.19 m, 0.058 m, 0.097 m respectively along the x, y and z axis and 1.12×10^{-4} rad around the z axis for the first experiment. These offsets are lower for the second and the third experiment (respectively 0.045 m, 0.021 m, 0.058 m and 0.048 rad) because the coordinate systems were reset after the first experiment. In the following, these structural offsets are considered equal to zero as they have been removed from the ICP dataset as the MoCap was taken as the ground truth. The results after removing these offsets are represented in Fig.5.11.
- Errors due to real differences in the results between the two localization systems. They can be computed as the mean of the differences between the two datasets after removing the structural offset. These errors are presented in Tab.5.1.

During the 3 experiments, the robot started from 3 different positions with diverse orientations. As the results shown in Tab.5.1 are similar regardless of the experiment, we can conclude that the LiDAR-based localization system does not depend on the starting pose. Moreover, the robot traveled different distances according to the experiments, respectively 8.93 m, 11.05 m and 10.69 m. As Fig.5.11 shows, the error does not seem to increase with the traveled distance, at least for distances around 10 m .

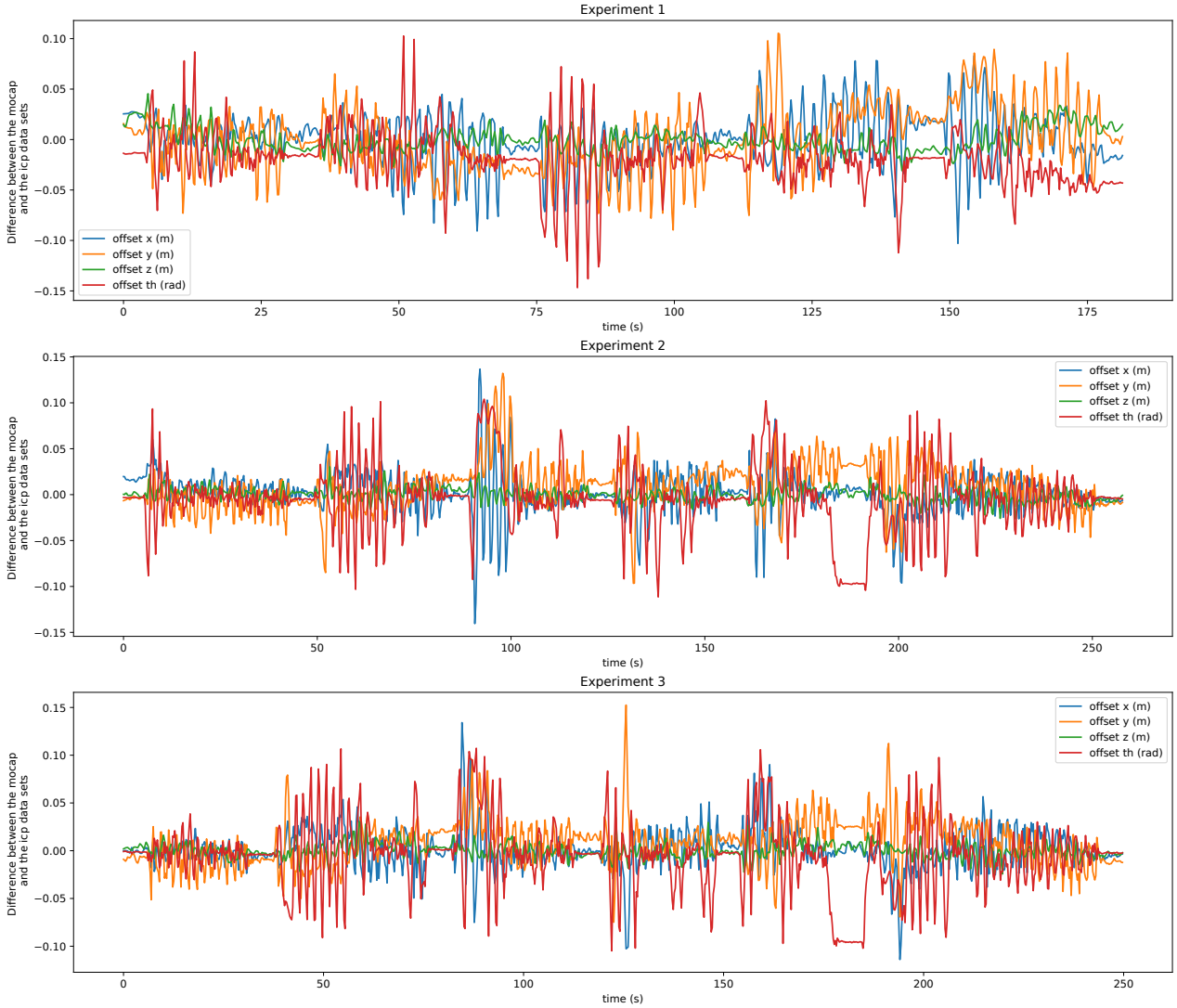

Figure 5.10: Errors between the 2 datasets during the 3 experiments (x in *blue*, y in *orange*, z in *green* and θ in *red*)

Accuracy of the goal positions

The goal positions can easily be identified on the datasets as they match with the points with zero velocity. To assess the accuracy of the LiDAR-based localization system on achieving the goal positions, the difference between the measured position and the desired goal position can be computed. The absolute average error on the goal positions ($\pm$ standard deviation) is 0.025 ± 0.016 m on the x axis, 0.039 ± 0.042 m on the y axis and 0.028 ± 0.012 rad around the z axis. All these errors are lower than the tolerance admitted on stops stated in Sec.5.2.1.2 which means that the accuracy of the LiDAR localization system is satisfactory for the targeted application. Moreover, with such accuracy, more complex localization tasks could be considered. In future work, the LiDAR-based localization system will be used to place the robot in front of an object to perform a task requiring accuracy, such as drilling or crossing debris.

Effect of the map on the LiDAR-based localization system

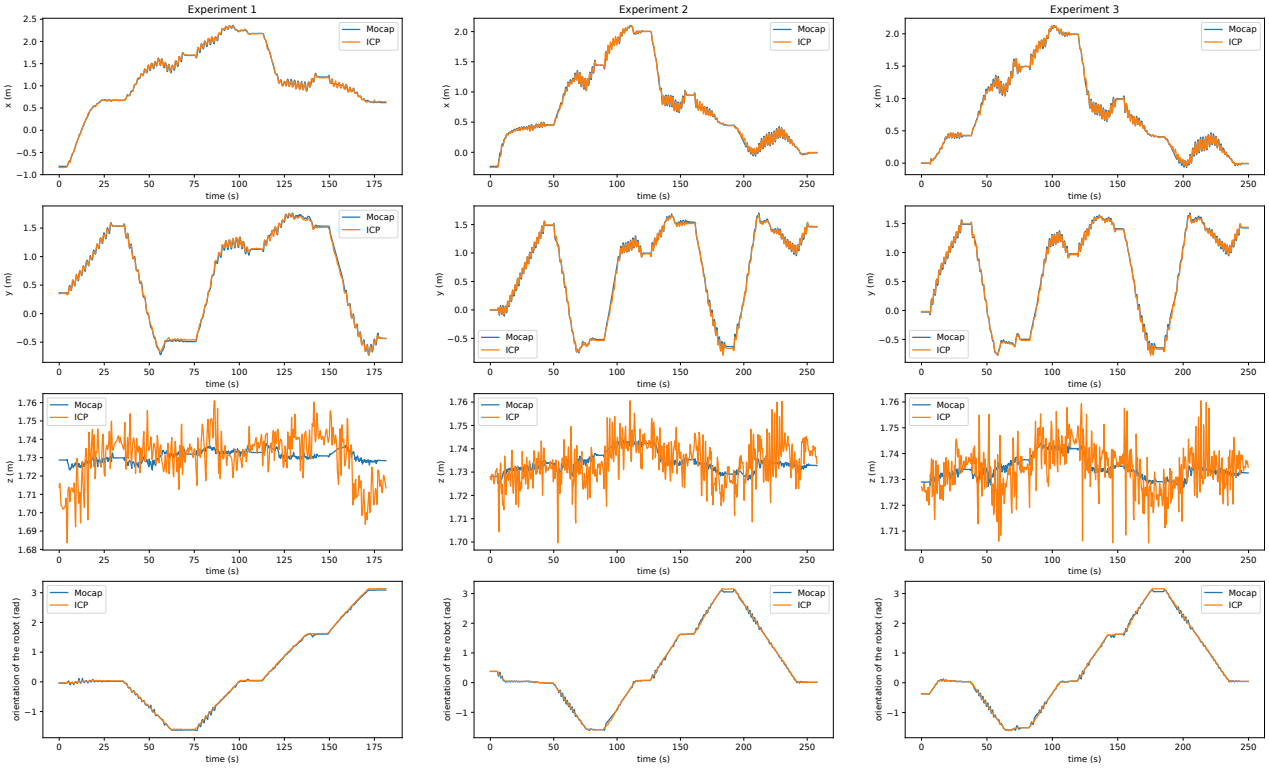

Figure 5.11: Position (x on the first row, y on the second row, z on the third row) and orientation (θ on the last row) of the robot measured by the MoCap (in *blue*) and by the ICP localization system with the removed delays and structural offsets (in *orange*) during the 3 experiments

As Tab.5.1 shows, there is no significant difference (less than the standard deviations) in the errors between the first experiment and the second and the third experiments, whereas the LiDAR-based localization system was performed with different maps. This means that, even if the map built from the architectural 3D model is a priori less accurate than the map built using a scanning device, the LiDAR localization system has an accurate behaviour in both cases.

5.2.3 Conclusion

First of all, the work presented in this section demonstrates the ability of the robot to interact in real-time with objects localized with our MoCap (Qualisys). Then, a LiDAR-based localization system was tested. This system exhibits an average error of 0.016 m, 0.021 m and 0.0067 m along the x, y and z axis and of 0.024 rad around the z axis with respect to the MoCap taken as the ground truth. Those results show that the LiDAR-based localization is accurate enough to target more challenging localization tasks such as precisely placing the robot in front of a table to interact with it.

However, for now, the LiDAR-based localization system is not able to detect an object, like a table, or a human being. Thus, in the context of the targeted HRI, only the MoCap can be used as we at least need to know the robot and the table poses in real-time. Thus, this section brings a solution to the localization problem during the human-robot table handling task. The following section tackles the gait generation problem in the context of the same task.

5.3 Simulation of a human-robot table handling task

5.3.1 Modeling and Prediction of the Table Trajectories

In Chapter 4, we showed that the trajectories of subjects carrying a table are too various to be accurately modeled with an OC model optimized through an IOC scheme. This is why, in this section, the focus will not be on the human partner trajectory but on the table trajectory. The goal of this section is to investigate the possibility to use the same approach to model and predict the table trajectory as the one designed through Chapter 1 and 2.

5.3.1.1 Experiments

Data collection and processing

As a reminder, experiments where pairs of subjects carry a table toward different goal positions (see Fig.5.12) are described in Sec.4.2. During those experiments, the table trajectories were recorded alongside the subject's trajectories. In what follows, we only considered the trajectories performed during Scenario 3. We chose to focus on Scenario 3 because both forward and return paths were performed in this scenario. Nevertheless, the method proposed below would be identical for the other scenarios.

Indeed, three markers were placed on 3 of the 4 corners of the table to reconstruct a local frame. Then, the 3D positions of those markers were recorded using a MoCap (15 infrared VICON cameras sampled at 200 Hz). The collected data was filtered using a 4th order, zero phase-shift, low-pass Butterworth with a 10 Hz cutoff frequency. The CoM trajectories of the table, i.e. the CoM horizontal positions (x, y) and the orientations θ of the table with respect to the global frame over each trial, were computed using a previously published method [62]. Let us outline that the table orientation is the orientation of its local frame with respect to the global frame represented in Fig.5.12. In what follows, a measured table trajectory performed by the j^{th} pair ($j \in [\![1, 20]\!]$) is denoted $X_j^{mes} = \begin{pmatrix} X_{j,1}^{mes} & \dots & X_{j,N}^{mes} \end{pmatrix}$ with N the number of measurements in this trajectory and $\forall i \in [\![1, N]\!]$, $X_{j,i}^{mes} = (x_{j,i}^{mes}, y_{j,i}^{mes}, \theta_{j,i}^{mes})$. All the measured trajectories were normalized from 0 to 100 % in order to have the same length $N = 500$. For each forward and return paths to and from the same goal position, the average table trajectories $\bar{X}^{mes}$ were computed as follows: $\forall i \in [\![1, N]\!], \bar{X}_i^{mes} = \frac{1}{20} \sum_{j=1}^{20} X_{j,i}^{mes}$.

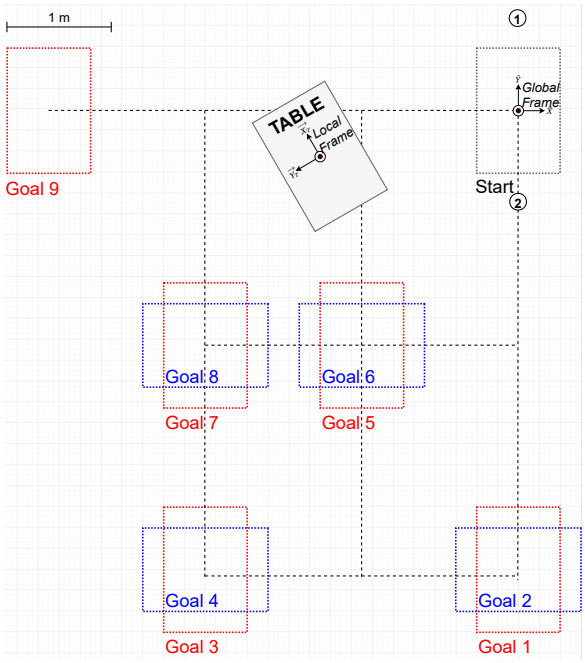

Figure 5.12: Starting positions for both subjects (1 and 2 respectively for Subject 1 and Subject 2) and for the table and the 9 different goal positions for the table. The global and local frame are also represented in this figure.

Data analysis

This analysis aims to assess the variability of the table trajectories during various table handling tasks. To this end, we used a metric first introduced in Sec.1.3.4.1 to compare 2 trajectories X_1 and X_2:

$$\begin{cases} d_{xy}(X_1, X_2) = \frac{1}{N}\sum_{i=1}^{N}\sqrt{(x_{1,i} - x_{2,i})^2 + (y_{1,i} - y_{2,i})^2} \\ d_{\theta}(X_1, X_2) = \frac{1}{N}\sum_{i=1}^{N}|\theta_{1,i} - \theta_{2,i}| \end{cases} \tag{5.1}$$

d_{xy} and d_{θ} are respectively named *linear* and *angular distances*. First, the distances between the forward and the return paths were computed for all the pairs. Then, the distances between the average and all the measured forward and return paths were also computed to assess the variability of the measurements with respect to the average trajectories.

Results

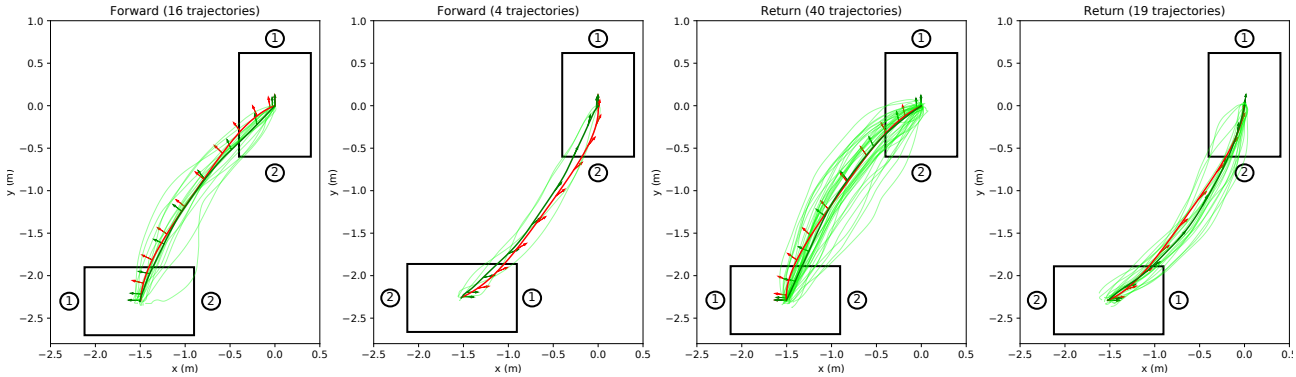

Figure 5.13: Comparison between table trajectories (average in *bold green* and measurements in *lime green*) and generated trajectories (in *red*) for one goal position (Goal 8 on Fig.5.12). The arrows represent the orientation of the table during locomotion and the number 1 and 2 the position of both subjects at the beginning and at the end of the motion.

The first conclusion that can be drawn from the previously described experiments is that the table must be considered as a holonomic system. As a reminder, a holonomic system can take oblique or sideways motion in contrast with non-holonomic systems which always move forward. The table orientation was not always tangent to its trajectory as it is shown in Fig.5.13. For example, when carried toward Goal 9, the table orientation was orthogonal to its trajectory.

Then, the mean linear and angular distances between the forward and the return paths were respectively 0.17 ± 0.11 m and 0.16 ± 0.14 rad. Both paths would be perfectly symmetrical if those distances were equal to zero. Here it was not the case. However, those means were lower than those observed for non-straight human trajectories [26]. Thus, we can state that the table trajectories were not perfectly symmetrical but they were closer to symmetry than single walking human trajectories.

Furthermore, the linear and angular distances between the individual measurements and their respective average trajectories are represented in Fig.5.14. In this boxplot, distances for forward and return paths are set apart to check if the results are similar for both directions. A Mann-Whitney U test confirmed this similarity with a p-value greater than 0.05 for both

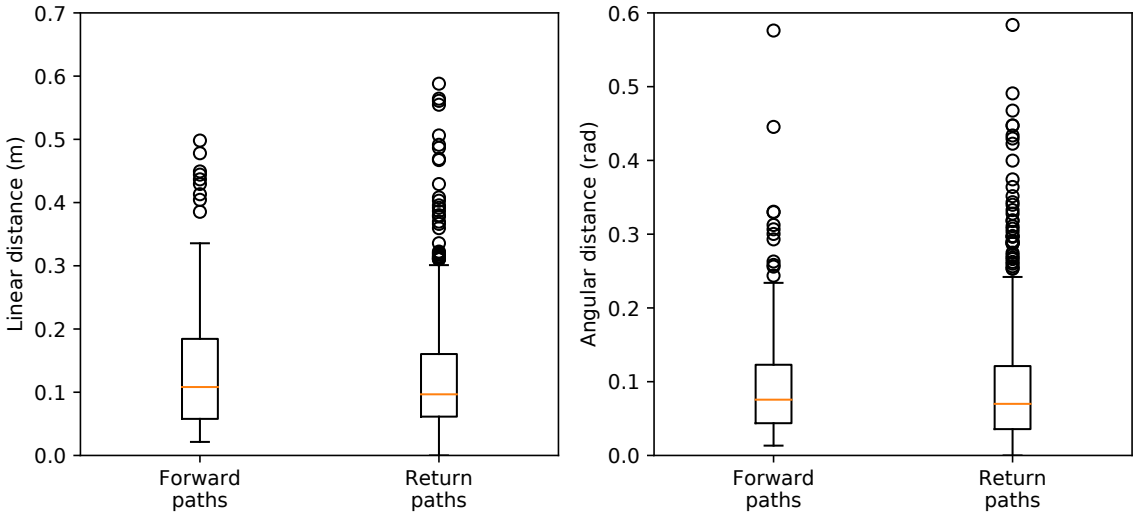

Figure 5.14: Linear and angular distances between the individual table trajectories and the average trajectories for every goal.

distances. The mean linear and angular distances were respectively 0.13 ± 0.10 m and 0.10 ± 0.12 rad. Moreover, a Kruskal test showed that there was no significant difference between the linear distances for every pair ($p > 0.05$), it was not the case for the angular distances though ($p < 0.01$). This means that the average trajectories were at least representative of all the performed carriages in terms of positions. Thus, in contrast with the subjects' trajectories which showed a high variability, as demonstrated in Chapter 4, the table trajectories were more reproducible. As a conclusion, the carriage tasks performed by the different pairs resulted in similar trajectories for the table even if the subjects tended to perform various trajectories themselves. In accordance with this result, in the next section, the focus is on modeling and predicting the table trajectories to allow the robot to act proactively during a collaborative table handling task.

5.3.1.2 Modeling

The goal of this section is to provide an accurate model of table trajectories between whatever starting and goal positions. Such a model already exists to generate the CoM trajectories of single walking humans. It was adapted from Mombaur et al. [38] and introduced in Sec.1.4. As a reminder, this model is based on the solving of an OC problem (Eq.1.10) using a DDP algorithm [69] from the open-source Crocoddyl library [70]. This OC problem can generate trajectories of full holonomic systems which follow the dynamics described in Eq.1.3. As a human is a holonomic system, this model was suitable to model human CoM trajectories. Moreover, in Sec.1.4.3, the cost functions' weights $\alpha = (\alpha_0, \alpha_1, \alpha_2, \alpha_3, \alpha_4)$ and $\beta = (\beta_0, \beta_1, \beta_2, \beta_3)$ were optimized using a bi-level IOC scheme.

As this approach gave accurate results for single walking humans and as a table carried by two humans is also a holonomic system, the choice was made to apply the same method to model the table trajectories. In what follows, the optimal trajectories generated with this OC model are denoted $X^{gen} = \begin{pmatrix} X_1^{gen} & \dots & X_N^{gen} \end{pmatrix}$. We assumed that the generated trajectories have the same length as the measurements. It was not necessarily the case, but, when it was not, the generated trajectory was interpolated to count N points.

IOC results

The IOC scheme, detailed in Sec.1.4.3, was used to optimize the cost functions weights in order to minimize the linear and angular distances between the average table trajectories and the trajectories generated by the OC problem described in Eq.1.10. The weights which allow the best fitting of average and generated trajectories are the following:

$$\begin{cases} \alpha \approx (3.01 \times 10^{-3}, 6.03, 5.99, 8.63 \times 10^{-2}, 1.00 \times 10^{-7}) \\ \beta \approx (9.98, 7.99, 14.99, 0.42) \end{cases} \tag{5.2}$$

One can denote that the weight α_4, which weights the asymmetry of the back and forth trajectory, is close to 0. This confirms the conclusion made in the previous section. Thus, the table trajectories are more symmetrical than the humans' ones for which $\alpha_4 = 10$ (Eq.1.17). Then, using these new sets of weights in the OC cost functions, the table trajectories between the experimental starting position and all the goal positions were generated for the forward and the return paths.

Comparison with measurements

All the measured, average and generated trajectories to go and return from one given goal are represented in Fig.5.13. On this figure, the generated trajectories are quite accurate. To confirm this guess, $d_{xy}(X^{mes}, X^{gen})$ and $d_\theta(X^{mes}, X^{gen})$ were computed for every forward and return paths. The linear and angular distances respectively amounted to 0.12±0.12 m and 0.36± 0.61 rad. All the results are represented in Fig.5.15. As for the measured data, no significant difference existed between the results for the forward and the return paths (Mann-Whitney U test, $p > 0.05$). Thus, the distances were of the same magnitude as the ones computed between the average and the measured trajectories. Moreover, a Kruskal test demonstrated that the linear distances between the average and measured trajectories were non-distinguishable from the linear distances between the average and the generated trajectories ($p > 0.05$). However, that was not the case for angular distances. Thus, on one hand, we can conclude that the presented OC model provides accurate trajectories in terms of x and y coordinates. On the other hand, the generated orientations might not always be accurate. Thus, we built an OC model which accurately simulates the average paths of the table given whatever starting and goal positions. However, during a human-robot table handling task, the robot may not know the goal position or may have to adapt to an atypical behaviour. Thus, the next section focuses on the prediction of where the table is going according to the table's current and recent past positions.

5.3.1.3 Prediction process

Prediction model

In Sec.2.2, a prediction process was designed to predict the future CoM trajectory of a walking subject from its recent past trajectory of size N_0. We assumed that the trajectory is recorded in real-time at a rate of $\frac{1}{T_{OC}}$. This process is based on the solving of a similar OC problem to the one used to generate the trajectories of single walking humans in Sec.1.4. In the previous section, we demonstrated that the same model, with different weights (Eq.5.2), succeeded in generating the trajectories of a table handled by two subjects. Thus, the same

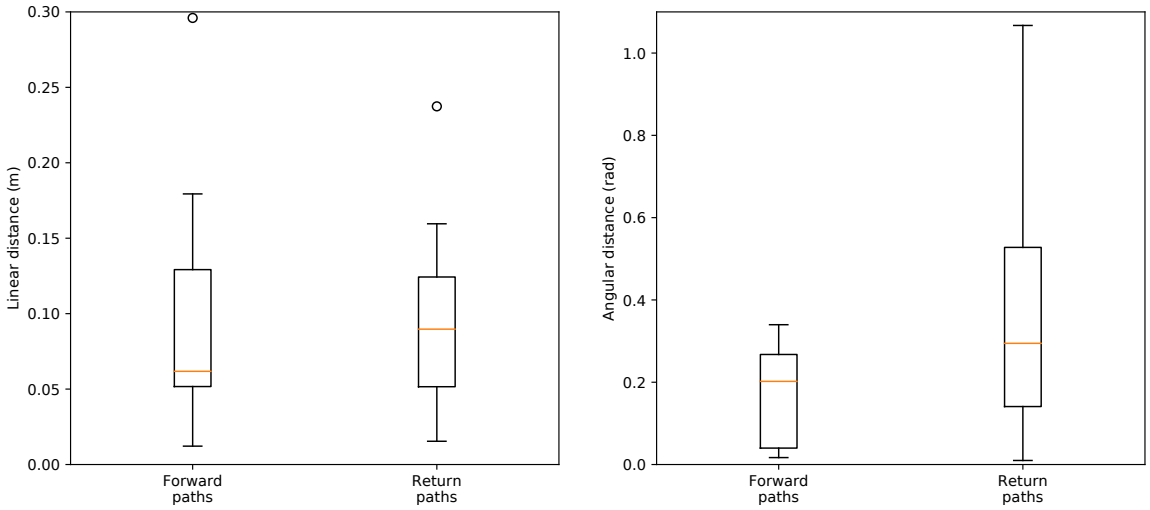

Figure 5.15: Linear and angular distances between the individual table trajectories and the average trajectories for every goal.

OC problem can be used to predict the table trajectories with identical running and terminal cost functions.

At each time $t = kT_{OC}$ ($k = n + N_0$), this OC problem fits the recent past trajectory $\begin{pmatrix} X^m_{n+1} & \dots & X^m_k \end{pmatrix}^T$ and generates a trajectory of size $N_{OC} > N_0$, denoted $\tilde{X}^*_{n+1} = \begin{pmatrix} X^*_{n+1} & \dots & X^*_k & \dots & X^*_{n+N_{OC}} \end{pmatrix}^T$. In this solution, the *predicted trajectory* is $\begin{pmatrix} X^*_k & \dots & X^*_{n+N_{OC}} \end{pmatrix}^T$.

An example of the trajectory generated by this OC prediction problem is shown in Fig.5.16. More details about this prediction process are available in Sec.2.2.

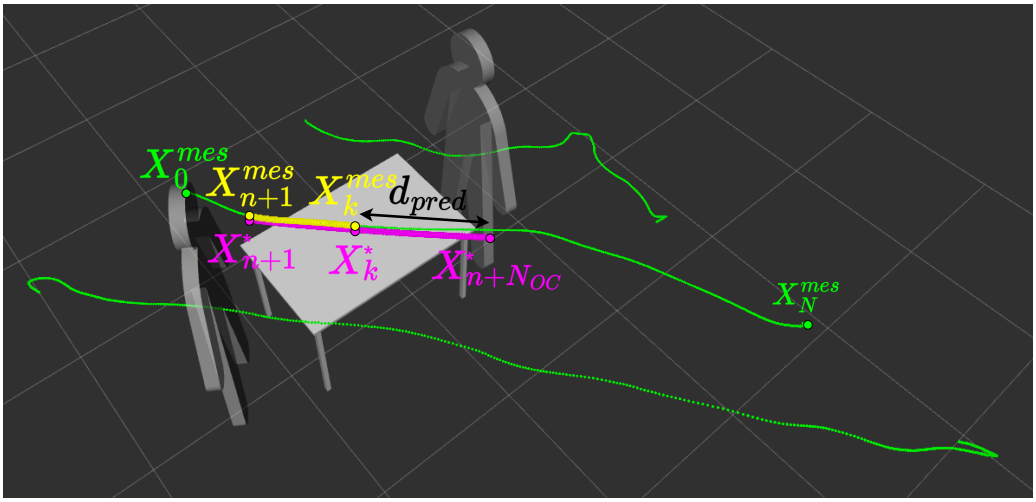

Figure 5.16: Predicted trajectory at time $t = kT_{OC}$ with $N_0 = 50$ and $N_{OC} = 100$ for one given trial. The measured trajectories of both subjects and of the table are in *green*, the recent past trajectory of the table is in *yellow* and the solution provided by the prediction process is in *purple*.

Assessment

N_0	N_{OC}	d_{xy} (m)	d_θ (rad)	d_{pred} (m)
25	100	0.08 ± 0.07	0.08 ± 0.09	0.74 ± 0.32
50	100	0.04 ± 0.02	0.04 ± 0.02	0.45 ± 0.11
50	200	0.07 ± 0.07	0.07 ± 0.06	0.76 ± 0.37

Table 5.2: Average distances for various N_0 and N_{OC}.

Then, the accuracy of the predicted trajectory of the table was assessed with the same metrics used in Sec.2.3. At each time, for each measured table trajectory, the predicted trajectory was computed along with the linear and angular distances between this prediction and the real performed trajectory. Moreover, the predicted distance d_{pred}, which is defined as the Euclidean distance between the first and the last point of the prediction, was also computed. This distance is represented in Fig.5.16. The averages of these distances for all the measurements are presented in Tab.5.2 for multiple values of N_0 and N_{OC}. This table shows better results than the one obtained for single walking humans (see Sec.2.3). Even if the predicted distances are lower, the linear and, especially, the angular distances demonstrate better accuracy. Moreover, it is interesting to denote that those linear and angular distances are low enough to expect an accurate and reactive prediction of where the human wants to carry the table during the targeted collaborative table handling task.

5.3.2 Walking with table

5.3.2.1 Coupling of the prediction process and the robot WPG

The same WPG as the one introduced in Sec.3.3 is used in this section. As a reminder, this WPG generates the CoM and the feet trajectories of a humanoid robot along a given trajectory by solving a NMPC problem. When the trajectory given as an input to the WPG is the real-time solution of the prediction process, the WPG is said to be coupled with the prediction process. In this work, the input given to the WPG is the table's predicted trajectory translated so that the robot is placed on the free side of the table. Moreover, this trajectory is interpolated in order to be traveled at the measured table velocity. More details about this interpolation are given in Sec.3.4. Two examples of CoM and footsteps generated by this WPG are shown in Fig.5.17.

5.3.2.2 Whole-body controller of the robot

Once the CoM and the footsteps trajectories are computed, they have to be executed on the robot through a whole-body controller. In this section, we used the torque controller as in Sec.3.5, namely the one introduced in Ramuzat et al. [136, 137]. It is a weighted quadratic program based on the TSID library [139]. This controller computed stable torque commands for all the joints of the robot from the reference trajectories generated by the WPG and the current state of the robot. These commands were sent to the simulated robot at 1 kHz. To achieve this rate, the trajectories computed by the WPG had to be interpolated using polynomial functions.

This controller was used not only to make the robot walk but also to make the robot lift the table. Indeed, in addition to the tasks ensuring the tracking of the reference trajectories, the contacts on the floor and the robot's balance, a posture task was added to make the robot fetch and grab the table. At first, this task made the robot lower it CoM and align its gripper with

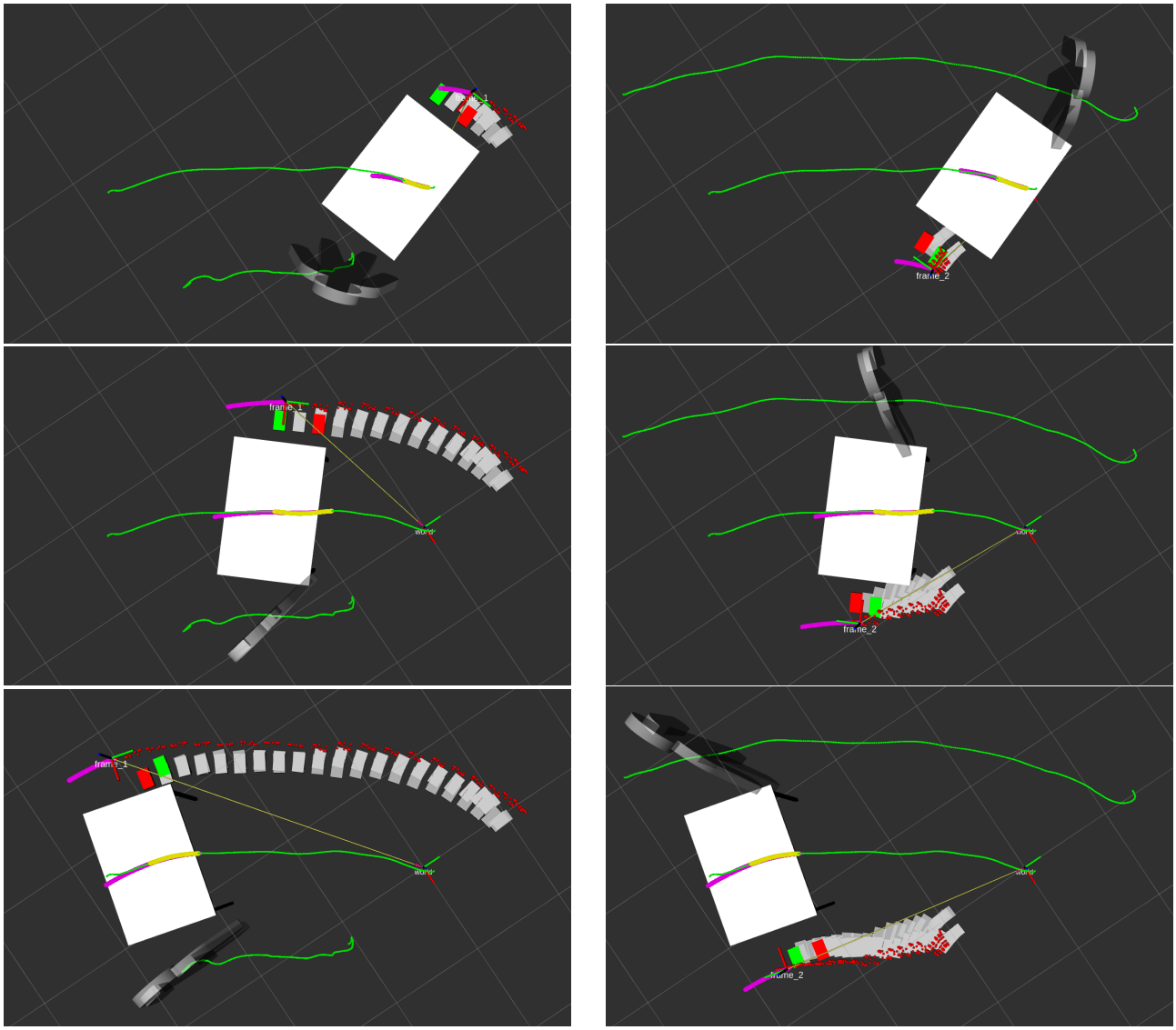

Figure 5.17: The robot CoM (in *red*) and footsteps (past steps in *grey*, current support foot in *red* and future support foot in *green*) are generated from the predicted table trajectory (in *purple*) with $N_0 = 50$ and $N_{OC} = 100$. On the left, the robot substitutes Subject 1 while, on the right, it substitutes Subject 2.

the table legs in front of it. Then, this task was updated to make the robot close its gripper and return to its initial CoM height. Thus, this posture task forced the robot's hands to stay closed while walking. The different steps of the table lifting by the TALOS robot in simulation on Gazebo are represented in Fig.5.18.

5.3.2.3 Simulation of the collaborative table handling task

The last step of the work presented in this section is to test the whole framework described in the previous sections in simulations. They are aimed at being as realistic as possible. For example, in the simulations, the 3D model of the table had the same characteristics (length, width, height and weight) as the real one carried by the subjects in the experiments presented in Sec.4.2.

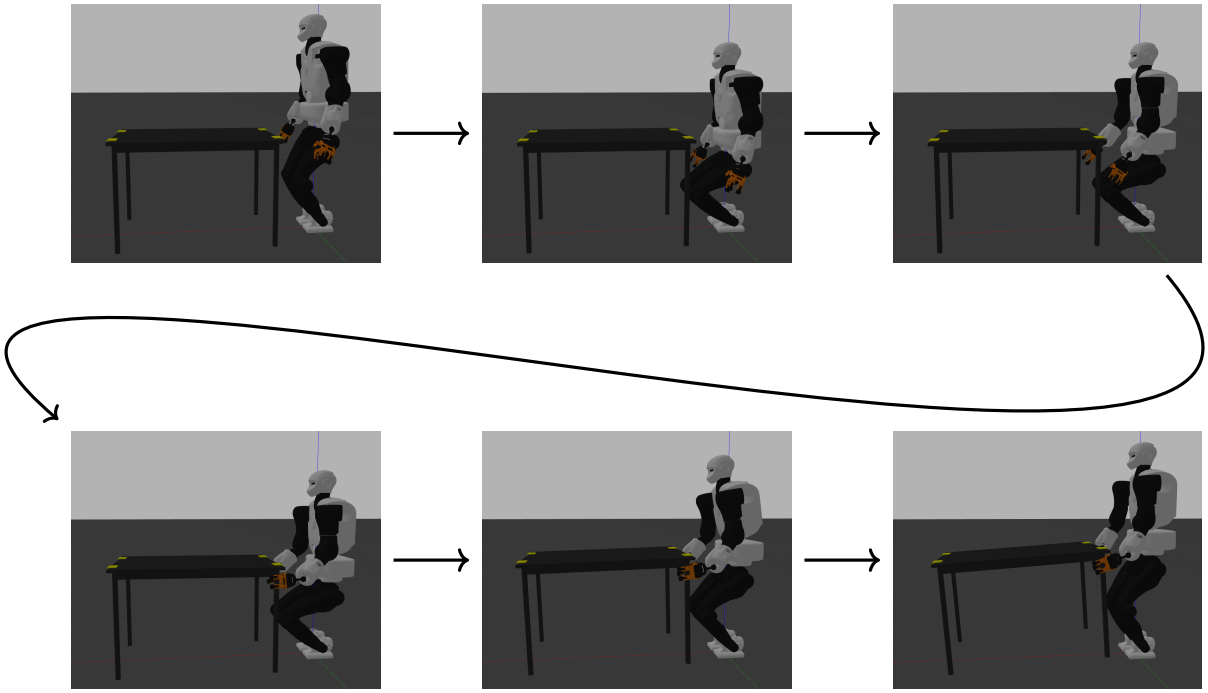

Figure 5.18: Grab and lift the table in simulation on Gazebo.

The simulations realized in this section were run on Gazebo on a standard laptop (Intel(R) Core(TM) i5-8400H CPU @ 2.50GHz). The challenges of these simulations were twofold. First, the impact of the human on the table needed to be simulated to create a haptic interaction with the robot through the table. Then, the whole body controller needed to keep the robot's balance despite the perturbations induced by the table.

Simulation of the human partner

To achieve the simulation of a human-robot collaborative carriage, the robot behaviour was not the only one which needed to be simulated in Gazebo. Indeed, the impact of the human on the carried load also needed to be simulated. As no force sensor was used during the experiments described in Sec.4.2, only the recorded CoM trajectories of the subjects could be used to mimic the haptic feedback produced by the subject during a table handling task. In Lanini et al. [121], the authors studied a collaborative carriage where two subjects carried a stretcher-like object. The motions of the subjects were recorded also as the force data on each handle. Then, a comparison between the data and the solutions of paired Spring Loaded Inverted Pendulums (SLIPs) demonstrated that this SLIPs model can reproduce human walking behaviour during a collaborative carriage. Based on this conclusion, in the simulation presented in this section, the human partner was simulated using spring-mass-damper systems as represented in Fig.5.19. Using the ROS [103] service `/gazebo/apply_body_wrench`, forces were applied on the yellow spots in Fig.5.20 and Fig.5.19 to simulate the human right and left hands on the table. They are denoted $\overrightarrow{F_\nu} = F_{\nu,x}\overrightarrow{X} + F_{\nu,y}\overrightarrow{Y} + F_{\nu,z}\overrightarrow{Z}$ with $\nu \in \{RH, LH\}$ and they are defined as follows:

$$\begin{cases} F_{\nu,x} = -K(x_\nu^{sim} - x_S^m) - \mu v_{\nu,x}^{sim} \\ F_{\nu,y} = -K(y_\nu^{sim} - y_S^m) - \mu v_{\nu,y}^{sim} \\ F_{\nu,z} = -K_z(z_\nu^{sim} - z^{ref}) - \mu_z v^{ref} \end{cases} \tag{5.3}$$

$(x_\nu^{sim}, y_\nu^{sim}, z_\nu^{sim})$ are the 3D positions in the global frame of the yellow spots measured by

Gazebo and streamed on the topic `/gazebo/link_states`, (x_S^m, y_S^m) is the measured horizontal position in the global frame of the subject and $z^{ref} = 0.9$ m is the reference height where we want the table to be. The stiffness and damping coefficients were heuristically found: $K = 1$, $\mu = 4$, $K_z = 300$ and $\mu_z = 50$.

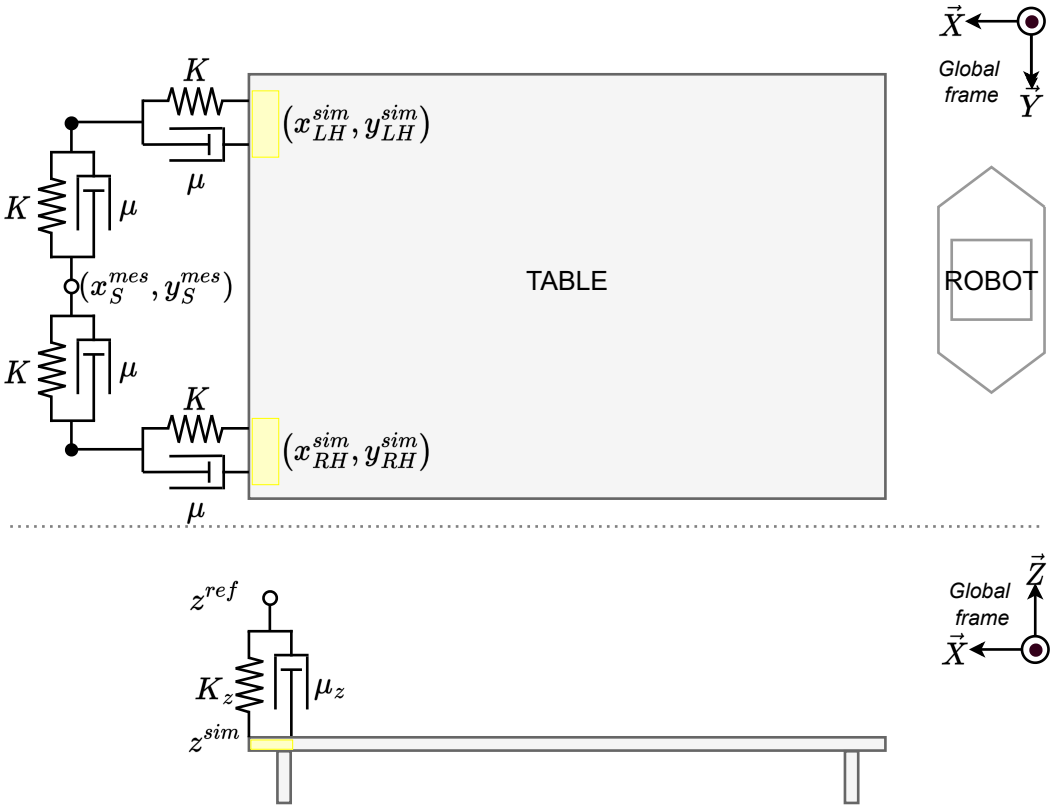

Figure 5.19: Simulation of the human partner with a spring-mass-damper system to hold the table on Gazebo.

Results

Simulations for various measured table trajectories were successfully achieved. A video showing one simulation is available on: `https://peertube.laas.fr/videos/watch/a2382b7e-4a7f-454b-8dcc-6c93b27a8a50`. Those different simulations succeeded whoever (Subject 1 or Subject 2) the robot substituted. This result is interesting as it demonstrates that the robot can carry the table with its simulated partner, walking forward and walking backward. Moreover, the robot's balance was not disturbed by the table. Indeed, the forces measured by the 6-axis force sensors in both ankles showed similar profiles, as it is shown in Fig.5.21 whether the robot walks with or without the table. This means that the controller properly compensated for the perturbations induced by the table.

5.3.3 Discussion

5.3.3.1 Table trajectories versus human trajectories

Interesting conclusions can be drawn from the table trajectories and from the assessment of the prediction model. The table trajectories presented a lesser variability compared to the

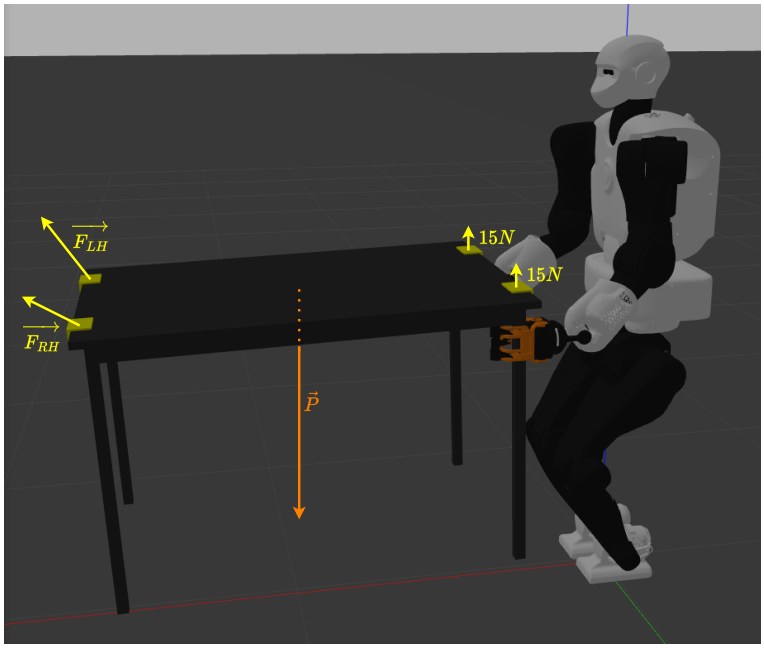

Figure 5.20: Simulation on Gazebo where a TALOS humanoid robot holds a 20.7 kg table. $\vec{P}$ is the weight of the table. $\vec{F_{RH}}$ and $\vec{F_{LH}}$ are the forces applied on the left yellow spots to simulate the forces applied on the table by the hands of the human partner.

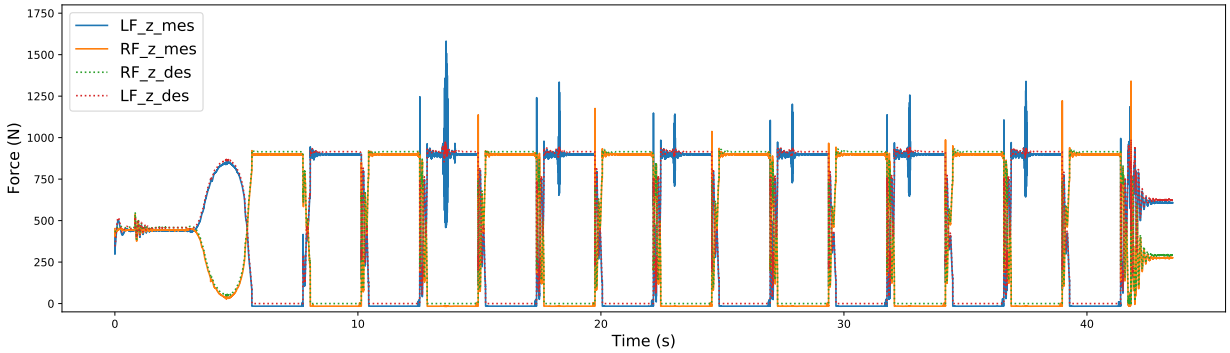

(a) Walk without table: Setting gains ($\approx$ 2 s), Walking (4 $\rightarrow$ 42 s).

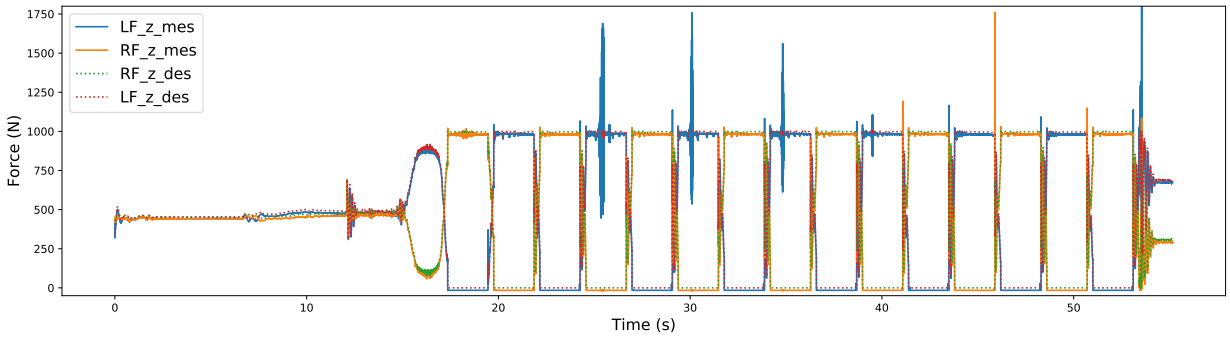

(b) Walk with table: Lifting table (0 $\rightarrow$ 12 s), Setting gains ($\approx$ 12 s), Walking (16 $\rightarrow$ 55 s).

Figure 5.21: Forces along the $\vec{z}$ axis desired and measured during the simulation by the 6-axis force sensors placed on the right (RF) and left (LF) ankles.

subjects' trajectories. This resulted in the building of an OC model which accurately fitted the average measurements. Moreover, the prediction of table trajectories were closer to the measurements than the prediction of single walking human trajectories (see Sec.2.3). Two phenomena could explain those results. First, as the table was heavy (20.7 kg) and cumbersome ($1.22 \times 0.8 \times 0.77$ m), the subjects may want to reduce the amplitude of the table motions. By doing so, they may optimize the table trajectory rather than their own. This may explain why the IOC succeeded here, while the same scheme failed to find optimal cost function weights to model the subjects' trajectories (see Sec.4.6.3). Then, the table trajectories were smoother than human trajectories as they were not subject to the CoM oscillations induced by footsteps which can be observed when studying human trajectories. Thus, as the OC problems modeling and predicting trajectories did not take into account these oscillations, they may work better on table trajectories rather than on human trajectories.

5.3.3.2 Realism of the forces applied on the table in the simulation

First of all, the simulation of the human with spring-mass-damper systems depended on the values of the stiffness and damping coefficients. As already stated, those coefficients were heuristically found. They were chosen because they resulted in consistent behaviour of the table when two simulated humans carried the table. In this study, we checked that the trajectory performed by the table with spring-mass-systems linked to the measured positions of the subjects on both sides of the table was similar to the respective measured one. However, as we did not have measured forces data during the recorded table handling tasks, it is unclear if the forces applied on the table to simulate the human partner were of the same magnitude as the ones a real human would apply. Ongoing works are investigating this issue.

Finally, let us denote that in Fig.5.20, two forces of 15 N each are represented on the yellow spots on the side of the table held by the robot. Those forces, applied on the table using the ROS service `/gazebo/apply_body_wrench`, were not realistic. Indeed, if it was not a simulation, no one else than the robot could apply forces on this side of the table. However, in the simulation, if those forces were not applied, the robot was not able to lift the table. It was probably due to the torque control, which was too soft. Indeed, former experiments performed during my Master internship, in position control, already showed that the robot was strong enough to lift and hold this 20.7 kg table with a human partner. However, the fact that the robot was position-controlled made the robot stiffer. In future works, the stiffness in the robot arms could be increased by adding an impedance task at the hand level. This may ensure a stiffer behaviour along the vertical axis. This task will be implemented later. For now, we assume that those 15 N forces are a good approximation of this task. Moreover, it is important to denote that the robot still carried between 60 and 80 N, as it is plotted in Fig.5.22. This force was measured using the 6-axis force sensors in the robot's hands. This demonstrated the ability of the robot to carry quite a heavy table with a human partner.

5.3.3.3 Walking patterns achieved on the simulated robot

In this work, the footsteps performed in simulation were more challenging than the ones tested in Ramuzat et al. [136, 137] and in Sec.3.5. Indeed, some tested trajectories included large sideways or backward steps and significant rotations of the feet. Those kinds of motions have not been tested with the used torque controller before. To achieve those motions, the time of the double support phase had to be increased from 0.2 s to 0.3 s. Thus, in all the simulations presented in this section, the sampling period time of the NMPC was 0.3 s, the size of the

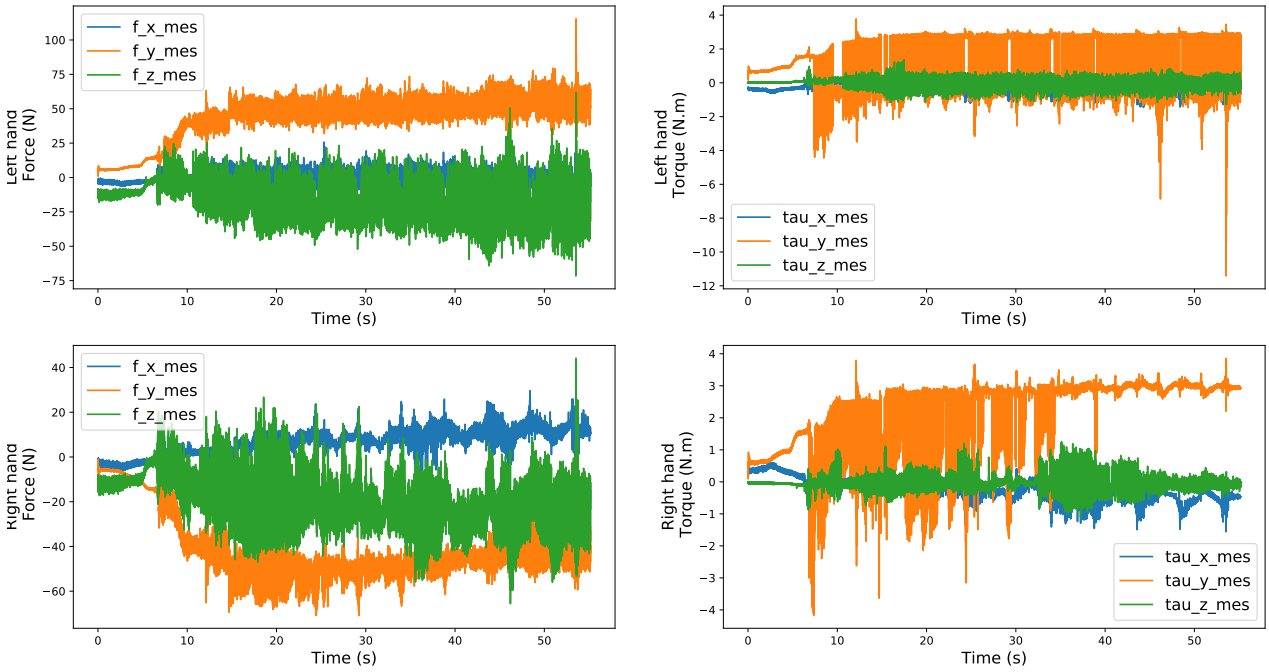

Figure 5.22: Forces and torques measured during the simulation by the 6-axis force sensors placed on the right and left hands.

preview horizon was 16 and the duration of one step was 2.4 s. With those parameters, footsteps up to 0.4 m were generated.

Moreover, in Sec.3.6, we pointed out that the NMPC became unfeasible if the trajectory to track had a non-zero curvature and had to be quickly traveled. This problem was avoided, in this work, by changing the weights in the cost function of the NMPC. In particular, the weight ensuring that the ZMP is under the ankle was increased. This resulted in no more unfeasibility problems. However, when the velocity to travel the trajectory was higher than $0.2\,\mathrm{m.s^{-1}}$, the predicted trajectory was not well tracked. Thus, we simulated the robot following the predicted table trajectories for a table moving at a maximum velocity of $0.2\,\mathrm{m.s^{-1}}$.

5.3.4 Conclusion

In this section, a framework allowing a proactive human-robot collaborative carriage is presented (see Fig.5.1). This framework includes a prediction model of table trajectories during various carriage tasks. This model was designed using data measured during human-human table handling tasks as part of this study. It is based on a similar OC model to the one designed to predict single walking human trajectories in Chapter 2, except that the cost function weights were optimized to fit the measured table trajectories. The assessment of this new model demonstrated that it accurately predicted the future table trajectory from its recent past trajectory. Thus, this prediction was coupled with the TALOS robot WPG in order to embed the table behaviour into the robot CoM and footsteps planner. Then, a torque whole-body controller was used to send a torque command to the robot joints in order to follow the CoM and feet trajectories generated by the WPG. Once the robot controlled on Gazebo, the force applied on the table by the human partner was simulated using spring-mass-damper systems. Finally, this whole framework was successfully tested in simulation on Gazebo.

5.4 Toward a real-time experiment on the real robot

In this chapter we solved two issues that needed to be dealt with to perform a real-time human-robot collaboration to handle a table. First, we demonstrated that a MoCap is an efficient solution to localize the robot and the table to perform such an interaction. Moreover, if we want not to depend on the MoCap, which requests a complex set-up, a LiDAR-based localization system can also be used to localize the robot. This solution is smarter as the localization system is embedded directly into the robot, which results in a completely autonomous robot. However, it is not mature enough to detect the table yet. Second, we developed a whole framework enabling the real-time generation of the robot CoM and footstep trajectories according to the table's predicted trajectory. This framework was implemented and successfully tested in simulation.

Nevertheless, a few challenges remain to face in order to perform a real proactive human-robot collaborative carriage. For example, the duration of one iteration of the NMPC was around 0.03 s. Nevertheless, to be embedded in real-time on the real robot, the duration of one iteration should be around 0.005 s. Currently, the NMPC is implemented in Python. An implementation in Cython was tested to speed up the NMPC. However, the duration only decreased by 40%. In current work, the WPG is being coded in C++ to decrease the computation time. Once this work is done, an online version of the WPG will be plugged into the whole-body controller and tested on the real robot.

Moreover, the simulations achieved in this chapter demonstrated that, using a prediction of the table trajectory, a humanoid robot can follow this trajectory. By doing so, it can be active during the carriage anticipating where its partner wants to set the table. However, two flaws might prevent real proactive interaction. First, in this chapter, the predicted trajectory was computed from the recent past trajectory of a table carried by two subjects. If one of the subjects is replaced by the robot, the table may not take the same trajectory. In this situation, we expect that the initial motion given by the human to the table will be enough for the prediction process to start predicting a trajectory to give to the robot. Once the robot is walking, it should give to the table a motion that looks like the motion a human would have given. Nevertheless, as we cannot perform a real experiment yet, we cannot check if the prediction model will behave as expected. Furthermore, as previously stated, the robot cannot walk faster than $0.2\,\mathrm{m.s^{-1}}$. During the experiments, the pairs made the table move at average velocities between 0.35 and $0.8\,\mathrm{m.s^{-1}}$. Thus, with the current WPG, a humanoid robot cannot actively assist a human partner as it cannot walk as fast as its partner. Thus, to target a proactive carriage task, the embedding of the table prediction into a robot planner will be more relevant on a faster robot like a wheeled robot, for example.

Conclusion

Contents

Summary

The study of human motions is essential for a better understanding of human behaviour during various tasks. This knowledge is not only interesting in life science but can also be useful in robotic science. Indeed, to efficiently assist a human partner during a human-robot collaboration, the robot needs to be as reactive as a human would be. This can only be achieved by embedding a model of human behaviour into the robot control scheme. This is the idea that guided this whole thesis.

In the frame of the ANR-CoBot project, the main goals of this thesis were to study human behaviour during collaborative carriage and to use the acquired knowledge to perform an efficient human-humanoid robot collaboration to carry a table. At first, in Part I, the focus was on a reduced problem, namely the study of human locomotion. We wanted to develop a method to model human CoM trajectories in a simpler case than a table handling task. Then, in Part II, the final problem of the thesis was tackled. Human and table trajectories during collaborative carriages were measured and analyzed. Finally, the previously developed framework was adapted to work in the case of table handling tasks.

In Chapter 1, an OC model to accurately generate human-like CoM trajectories was proposed. This model was adapted from the one introduced by Mombaur et al. [38]. It was optimized using a bi-level IOC scheme to fit human trajectories measured during various walking tasks. Those trajectories were recorded during experiments conducted as part of this study. Despite the variability observed in the measured trajectories, the optimization of the OC weights resulted in an accurate model of the average human behaviour.

Even if this model generated human-like trajectories between one given starting position and one given goal position, it is of no use when the goal position is unknown. This is the case, for example, when someone wants to know the trajectory of a human who is currently walking. This is the problem addressed in Chapter 2. In this chapter, a prediction model of the CoM trajectories of a walking human was developed. This OC model, using the weights optimized in the previous chapter, predicted a human future trajectory based on its recent past measured trajectory. This model was tested over all the previously measured trajectories. It was demonstrated that its real-time performances were good enough to accurately predict a walking human trajectory during a human-robot co-navigation task for example.

Thus, to follow through on this preliminary study about human locomotion, we decided to target a co-navigation task as a first step before targeting a co-manipulation task. We wanted to build a framework which enables a TALOS humanoid robot to perform the same trajectory as a currently walking human in real-time or even in advance. To achieve this goal, in Chapter 3, we wanted to embed a human locomotion model into a TALOS humanoid robot's WPG. At first, the WPG developed by *PAL Robotics* was used to follow trajectories generated with previously existing human trajectory models. Then, a WPG was developed, based on the one introduced by Naveau et al. [115]. This new WPG was designed to generate the robot CoM and feet trajectories along a trajectory given as an input. Once coupled with the previously presented prediction model, the robot was able to track a human in real-time, it can even precede him. This framework was successfully tested in simulation on Gazebo using the torque whole-body controller introduced in Ramuzat et al. [136].

Once this preliminary work was finished, we wanted to use the same approach (measurements $\Rightarrow$ model $\Rightarrow$ prediction $\Rightarrow$ embedding in the robot WPG $\Rightarrow$ simulation) to achieve a

human-robot table handling task where the robot would be proactive. To this end, 20 pairs of subjects carried a table to various goal positions and their CoM trajectories and the table trajectories were recorded. The experimental protocol and the data analysis were presented in Chapter 4. This analysis showed that a great range of behaviours were recorded. All the pairs did not implement the same strategy to move a table. This resulted in the inability of the method used to model single walking human trajectories to build an accurate OC model of neither the average trajectories of both subjects nor the individual ones.

Nevertheless, the table trajectories presented less variability than the subjects' ones. Thus, we concluded that the previously described method may be efficient to model the table trajectories instead of the subjects' ones. Moreover, we assumed that if we could predict the table trajectory during a collaborative carriage, we could make the robot actively assist a human partner to carry a table toward an unknown goal. Following this assumption, the final goal of the thesis, namely a proactive human-robot collaboration to carry a table, is targeted in Chapter 5. First of all, we demonstrated through experiments on the real robot that we can accurately localize the robot in real-time using a MoCap or an ICP-based localization system implemented by Lasguignes et al. [9]. However, to also be able to localize the table or the human partner, only the MoCap is mature enough. Then, using the same approach used to model and predict single walking human trajectories, a prediction model of the CoM table trajectories was introduced. It was successfully coupled to the robot WPG and tested in simulation on Gazebo. In this simulation, the robot actively carried a table with a simulated human partner. However, work remains to be done to perform an experiment on the real TALOS robot.

Perspectives

Some ideas can be proposed to improve the work conducted in this thesis on both the biomechanical and the robotic sides. In this section, the focus is, first, on the potential improvements, in terms of knowledge of human behaviour, which could be done to better predict human intentions in the context of a table handling task. Then, the problems posed by the current robot's hardware and software are tackled in order to propose potential solutions to perform, in the future, a human-robot collaboration like the one targeted in this thesis.

Perspectives in human locomotion modelling

During the experiments described in Sec.1.2 and in Sec.4.2, some data was collected but not analyzed. Indeed, although we chose to only focus on the CoM trajectories in this work, we also recorded the feet and the head positions and orientations of the subjects. It would be interesting to broaden the CoM trajectory model using the extra collected data.

In the case of single walking humans, using footsteps information, we could design a locomotion model which takes into account the oscillations of the CoM due to the footsteps. This may improve the performance of the model.

In the case of table handling tasks, using footsteps or head information could help us detect the changes in the subject's behaviour. For example, a sudden change in a subject's pace or in the orientation of a subject's head could suggest a change in the strategy of the pair to move the table. These kinds of hints could report that a different set of weights should be used to model the rest of the motion. Thus, it would be interesting to see if clusters of behaviours which would be described by the same set of weights could be identified using all the available collected data. Moreover, it would be interesting to measure the forces applied on the table by

the subjects during collaborative carriages, using 3D force sensors. It could help to classify the pairs according to their measured behaviour.

Perspectives in human locomotion prediction

The measurements of the orientation of the head of the subject could also be used to improve the prediction model. Indeed, the subject's gaze orientation may be a good hint to predict the subject's goal position. Studying how the gaze orientation changes during human locomotion may be a promising way for improving the developed prediction model.

Furthermore, the human locomotion prediction model, introduced in Chapter 2, is designed to predict the CoM trajectories of single walking humans. Indeed, the weights of the model cost functions were computed based on a database of trajectories performed by subjects walking alone, without any perturbation. Thus, this prediction model may not perform well to predict the trajectories of individuals in crowded environments. However, it would be interesting to investigate if small additions could make it more suitable for this kind of situation. The formulation of this problem as an optimization problem makes it very flexible. For example, a term keeping humans away from others in the crowd could be added to the cost function. Investigating the improvements that can be made to this prediction model to take part in a challenge like TrajNet++ (`https://www.aicrowd.com/challenges/trajnet-a-trajectory-forecasting-challenge`) would be very interesting and challenging. It would be a very nice application of this work.

Another interesting idea would be to test how the prediction model works in the case of "discontinuous" human trajectories. However, in the set of 400 trajectories we measured as part of the study presented in Chapter 1, we did not observe stops during gait. During those experiments, we asked the subjects to walk at a natural pace between a starting and a goal positions with given orientations in an environment free of obstacles. This is probably why all the measured trajectories were quite smooth. It would be interesting to extend this work by measuring trajectories with obstacles or perturbations during gait in order to be able to assess our prediction model on "discontinuous" trajectories.

Moreover, from my point of view, it would be more relevant to use this prediction model to target interactions between humans and wheeled robots rather than humanoid robots to keep up. Indeed, during co-navigation or co-manipulation tasks, humans walk far too fast for humanoid robots. Thus, this prediction model would be useful during HRIs only if the robot can match the human speed. For example, we could imagine, for the table handling task, a wheeled robot, like a strong TIAGo (*PAL Robotics*), proactively assisting its human partner to carry the table.

Perspectives in robot walk generation

First of all, it would be interesting to check if the WPG with trajectory tracking really makes the robot more reactive than the WPG with velocity tracking. Instead of using the predicted table trajectory, we could use the current velocity of the table. The assumption is that using the prediction must generate more reactive and more stable footsteps when the table follows a trajectory with sharp changes of orientation or of direction. Indeed, we supposed that the

prediction model may be able to predict those changes while a constant velocity order is not adapted to react to changes. However, this is only a hypothesis, it still remains to be checked.

Moreover, due to the lack of time, many ideas to improve the TALOS robot WPG remain untested. First, to generate a stable and faster gait with the WPG for trajectory tracking, a few solutions could be implemented. We could try to tune the weights of the cost function. For now, two sets exist. The first one, used in Chapter 3, resulted in faster walks but also in unfeasible QP problems. The second one, used in Chapter 5, always resulted in feasible QP problems but also in a less accurate tracking of the trajectory. Maybe another set of weights may result in a better behaviour of the WPG. Another solution may be to reduce the safety margins or not to track the trajectory with the CoM of the robot but with the point which is between the two feet of the robot. This may result in a steadier walk generation.

Another important improvement remains to be made on this WPG to be able to use it on the robot. Currently, only an offline version of the WPG exists. In this thesis, the trajectories performed in simulation on the robot are pre-computed, they are not generated online. Indeed, in its current Python version, the WPG for trajectory tracking is too slow. Moreover, it is not plugged directly into the controller. Currently, a C++ version is being implemented to decrease the computation time. Once this version is finished, an entity will need to be implemented to plug the WPG into the robot control framework.

Perspectives in human-robot collaboration

Even if we did not have the time to perform a collaboration between a real TALOS robot and a human partner for now, it is still one goal of this thesis. To achieve an experiment on the real robot, we will have to use another controller than the one used for the simulations presented in this thesis. Indeed, as presented in Ramuzat et al. [137], the torque controller used in this thesis was tested without success on the real robot because of the too great hip flexibility of the TALOS 1 robot. It should not be a big deal to change of controller as the framework developed in this thesis (prediction + WPG for trajectory tracking) did not depend on the used controller.

Moreover, the goal of this thesis was to achieve a table handling task with the TALOS 1 robot available at LAAS. However, as it is the first TALOS humanoid robot ever built, the choice of this robot to perform the targeted HRI should be discussed. Indeed, this robot is fragile and shows a great flexibility at the hip and ankles level. This makes every walking experiment with this robot quite challenging. Moreover, knowing that even a $20\,\mathrm{cm.s^{-1}}$ walk is challenging, we cannot expect the robot to achieve a walking speed close to the human one. Thus, even if the recently developed controller compensates most of the TALOS 1's weaknesses, it would be better to perform the experiment on the real robot with another TALOS robot or, even, with another faster humanoid robot as long as it is strong enough to carry a $\sim 20\,\mathrm{kg}$ table.

Furthermore, two ideas may be interesting to implement to make the developed framework for HRI more adaptive and more robust. First, an obstacle avoidance constraint could be added at the WPG level to make sure that the planned footsteps do not collide with the table's legs. Then, it would be interesting to implement a contact task with TSID to make the robot grab and keep the contact with the table. This kind of task would be much more adaptative than

a simple position task as it is implemented for now. As the robot has 6-axis force sensors in its wrist, implementing such a task is possible. Moreover, based on the measurements of the forces at the hand level, a trigger criterion could be added to start the walk generation only when the human partner moves. Thus, the robot may rely on haptic data, besides the MoCap data, to adapt its behaviour according to its partner's starts and stops.

Bibliography

[1] **I. Maroger**, O. Stasse, and B. Watier. "Inverse Optimal Control to Model Human Trajectories during Locomotion". In: *Computer Methods in Biomechanics and Biomedical Engineering*. Taylor & Francis, 2021, pp. 1–13 (cit. on pp. 8, 19, 30, 82).

[2] **I. Maroger**, O. Stasse, and B. Watier. "Walking Human Trajectory Models and Their Application to Humanoid Robot Locomotion". In: *IEEE/RSJ Int. Conf. on Intelligent Robots and Systems (IROS)*. IEEE. 2020, pp. 3465–3472 (cit. on pp. 8, 19, 22, 55, 56).

[3] **I. Maroger**, O. Stasse, and B. Watier. "Comparison of Human Experimental Trajectories and Simulations during Gait". In: *45ème congrès de la Société de Biomécanique*. 2020 (cit. on pp. 8, 19, 22).

[4] **I. Maroger**, N. Ramuzat, O. Stasse, and B. Watier. "Human Trajectory Prediction Model and Its Coupling With a Walking Pattern Generator of a Humanoid Robot". In: *IEEE/RAS Robotics and Automation Letters (RA-L)*. Vol. 6. 4. IEEE. 2021, pp. 6361–6369 (cit. on pp. 8, 43, 46, 55, 58, 66, 82, 112).

[5] **I. Maroger**, O. Stasse, and B. Watier. "Description and Assessment of a Human Trajectory Prediction Model during Gait". In: *46ème congrès de la Société de Biomécanique*. 2021 (cit. on pp. 8, 43, 46).

[6] **I. Maroger**, M. Silva, H. Pillet, N. Turpin, O. Stasse, and B. Watier. "Walking Paths during Collaborative Carriages do not Follow the Simple Rules Observed in the Locomotion of Single Walking Subjects". In: *Scientific Reports*. Vol. 12. 15585. 2022 (cit. on pp. 8, 83).

[7] **I. Maroger**, M. Silva, O. Stasse, and B. Watier. "Can the trajectories performed by the subjects be inferred from the trajectory of the load they carry?" In: *47ème congrès de la Société de Biomécanique*. 2022 (cit. on pp. 8, 83, 88).

[8] **I. Maroger**, O. Stasse, and B. Watier. "From the Study of Table Trajectories during Collaborative Carriages toward Proactive Human-Robot Table Handling Tasks". In: *IEEE/RAS Int. Conf. on Humanoid Robotics (Humanoids)*. 2022 (cit. on pp. 8, 114).

[9] T. Lasguignes, **I. Maroger**, M. Fallon, M. Ramezani, L. Marchionni, O. Stasse, et al. "ICP Localization and Walking Experiments on a TALOS Humanoid Robot". In: *Int. Conf. on Advanced Robotics (ICAR)*. IEEE. 2021, pp. 800–805 (cit. on pp. 8, 113, 116, 118, 137).

[10] O. Stasse, T. Flayols, R. Budhiraja, K. Giraud-Esclasse, J. Carpentier, J. Mirabel, et al. "TALOS: A new humanoid research platform targeted for industrial applications". In: *IEEE/RAS Int. Conf. on Humanoid Robotics (Humanoids)*. ieee. 2017, pp. 689–695 (cit. on pp. 2, 3).

[11] Boston Dynamics. *ATLAS™*. 2022. URL: `https://www.bostondynamics.com/atlas` (cit. on p. 2).

[12] Agility Robotics. *Meet Digit*. 2022. URL: https://agilityrobotics.com/robots (cit. on p. 2).

[13] J. Englsberger, A. Werner, C. Ott, B. Henze, M. Roa, G. Garofalo, et al. "Overview of the torque-controlled humanoid robot TORO". In: *IEEE/RAS Int. Conf. on Humanoid Robotics (Humanoids)*. 2014, pp. 916–923 (cit. on p. 3).

[14] P. Lasota, T. Fong, and J. Shah. "A survey of methods for safe human-robot interaction". In: *Foundations and Trends® in Robotics*. Vol. 5. 4. 2017, pp. 261–349 (cit. on p. 3).

[15] T. Sheridan. "Human–Robot Interaction: Status and Challenges". In: *Human Factors*. Vol. 58. 4. 2016, pp. 525–532 (cit. on pp. 4, 15, 55, 81, 111).

[16] J. Kim and J. Bertram. "Compliant walking appears metabolically advantageous at extreme step lengths." In: *Gait & posture*. Vol. 64. 2018, pp. 84–89 (cit. on p. 15).

[17] G. Bovi, M. Rabuffetti, P. Mazzoleni, and M. Ferrarin. "A multiple-task gait analysis approach: kinematic, kinetic and EMG reference data for healthy young and adult subjects". In: *Gait & Posture*. Vol. 33. 1. 2011, pp. 6–13 (cit. on p. 15).

[18] P. Basili, M. Saglam, T. Kruse, M. Huber, A. Kirsch, and S. Glasauer. "Strategies of locomotor collision avoidance." In: *Gait & posture*. Vol. 37 3. 2013, pp. 385–90 (cit. on p. 15).

[19] M. Heijnen, B. C. Muir, and S. Rietdyk. "Factors leading to obstacle contact during adaptive locomotion". In: *Experimental Brain Research*. Vol. 223. 2012, pp. 219–231 (cit. on p. 15).

[20] G. C. Nandi, V. B. Semwal, M. Raj, and A. Jindal. "Modeling bipedal locomotion trajectories using hybrid automata". In: *2016 IEEE Region 10 Conference (TENCON)*. 2016, pp. 1013–1018 (cit. on p. 15).

[21] V. B. Semwal, C. Kumar, P. K. Mishra, and G. C. Nandi. "Design of Vector Field for Different Subphases of Gait and Regeneration of Gait Pattern". In: *IEEE Transactions on Automation Science and Engineering*. Vol. 15. 1. 2018, pp. 104–110 (cit. on p. 15).

[22] S. Paris, J. Pettré, and S. Donikian. "Pedestrian reactive navigation for crowd simulation: a predictive approach". In: *Computer Graphics Forum*. Vol. 26. 3. 2007, pp. 665–674 (cit. on p. 15).

[23] J. Pettré, J. Ondřej, A.-H. Olivier, A. Cretual, and S. Donikian. "Experiment-Based Modeling, Simulation and Validation of Interactions between Virtual Walkers". In: *Proceedings of the 2009 ACM SIGGRAPH/Eurographics Symposium on Computer Animation*. 2009, pp. 189–198 (cit. on p. 15).

[24] A. Koilias, M. G. Nelson, C.-N. Anagnostopoulos, and C. Mousas. "Immersive walking in a virtual crowd: The effects of the density, speed, and direction of a virtual crowd on human movement behavior". In: *Computer Animation and Virtual Worlds*. Vol. 31. 6. 2020, e1928 (cit. on p. 15).

[25] Y. Zhu, D. Ren, M. Fan, D. Qian, X. Li, and H. Xia. "Robust Trajectory Forecasting for Multiple Intelligent Agents in Dynamic Scene". In: *arXiv preprint*. Vol. arXiv:2005.13133. 2020 (cit. on p. 15).

[26] M. Sreenivasa, K. Mombaur, and J.-P. Laumond. "Walking Paths to and from a Goal Differ: On the Role of Bearing Angle in the Formation of Human Locomotion Paths". In: *PLOS ONE*. Vol. 10. 4. Public Library of Science, Apr. 2015, pp. 1–16 (cit. on pp. 15, 82, 123).

[27] H. Hicheur, Q.-C. Pham, G. Arechavaleta, J.-P. Laumond, and A. Berthoz. "The formation of trajectories during goal-oriented locomotion in humans. I. A stereotyped behaviour". In: *European Journal of Neuroscience*. Vol. 26. 8. 2007, pp. 2376–2390 (cit. on p. 15).

[28] M. Sreenivasa, I. Frissen, J. L. Souman, and M. O. Ernst. "Walking along curved paths of different angles: the relationship between head and trunk turning". In: *Experimental Brain Research*. Vol. 191. 2008, pp. 313–320 (cit. on p. 15).

[29] M. Boukheddimi, R. Budhiraja, P. Souères, and B. Watier. "Anthropomorphic Gait Generation using Differential Dynamic Programming with a Reduced Number of Cost Criteria". In: *IEEE/RAS/EMBS Int. Conf. on Biomedical Robotics and Biomechatronics (BioRob)*. 2020, pp. 1036–1042 (cit. on p. 15).

[30] K. Yin, K. Loken, and M. Van de Panne. "Simbicon: Simple biped locomotion control". In: *ACM Transactions on Graphics (TOG)*. Vol. 26. 3. 2007, p. 105 (cit. on p. 15).

[31] G. Arechavaleta, J.-P. Laumond, H. Hicheur, and A. Berthoz. "The nonholonomic nature of human locomotion: a modeling study". In: *IEEE/RAS/EMBS Int. Conf. on Biomedical Robotics and Biomechatronics (BioRob)*. IEEE. 2006, pp. 158–163 (cit. on pp. 15, 22, 82).

[32] G. Arechavaleta, J.-P. Laumond, H. Hicheur, and A. Berthoz. "On the nonholonomic nature of human locomotion". In: *Autonomous Robots*. Vol. 25. 2008, pp. 25–35 (cit. on pp. 15, 22, 26, 37).

[33] A. Papadopoulos, L. Bascetta, and G. Ferretti. "Generation of human walking paths". In: *IEEE/RSJ Int. Conf. on Intelligent Robots and Systems (IROS)*. Nov. 2013 (cit. on p. 15).

[34] M. Elbanhawi, M. Simic, and R. Jazar. "Continuous Path Smoothing for Car-Like Robots Using B-Spline Curves". In: *Journal of Intelligent & Robotic Systems*. Vol. 80. Jan. 2015 (cit. on p. 16).

[35] P. Soueres and J. -. Laumond. "Shortest paths synthesis for a car-like robot". In: *IEEE Transactions on Automatic Control*. Vol. 41. 5. 1996, pp. 672–688 (cit. on p. 16).

[36] J.-P. Laumond. "Robot MotionPlanning and Control". In: *Lectures Notes in Control and Information Sciences 229*. Springer. 1998 (cit. on pp. 16, 22).

[37] M. Raković, S. Savić, J. Santos-Victor, M. Nikolić, and B. Borovac. "Human-Inspired Online Path Planning and Biped Walking Realization in Unknown Environment". In: *Frontiers in Neurorobotics*. Vol. 13. 2019, p. 36 (cit. on p. 16).

[38] K. Mombaur, A. Truong, and J.-P. Laumond. "From human to humanoid locomotion—an inverse optimal control approach". In: *Autonomous Robots*. 2010, pp. 369–383 (cit. on pp. 16, 18, 23–26, 29–31, 37–39, 82, 86, 124, 136).

[39] R. E. Kalman. "When Is a Linear Control System Optimal?" In: *Journal of Basic Engineering*. Vol. 86. 1. Mar. 1964, pp. 51–60 (cit. on p. 16).

[40] G. Fadini, T. Flayols, A. Del Prete, N. Mansard, and P. Souères. "Computational design of energy-efficient legged robots: Optimizing for size and actuators". In: *IEEE/RAS Int. Conf. on Robotics and Automation (ICRA)*. 2021, pp. 9898–9904 (cit. on pp. 16, 17).

[41] N. Sylla, V. Bonnet, G. Venture, N. Armande, and P. Fraisse. "Human arm optimal motion analysis in industrial screwing task". In: *IEEE/RAS/EMBS Int. Conf. on Biomedical Robotics and Biomechatronics (BioRob)*. 2014, pp. 964–969 (cit. on pp. 16, 17).

[42] N. Ab Azar, A. Shahmansoorian, and M. Davoudi. "From inverse optimal control to inverse reinforcement learning: A historical review". In: *Annual Reviews in Control*. Vol. 50. 2020, pp. 119–138 (cit. on p. 16).

[43] A. M. Panchea, N. Ramdani, V. Bonnet, and P. Fraisse. "Human Arm Motion Analysis Based on the Inverse Optimization Approach". In: *IEEE/RAS/EMBS Int. Conf. on Biomedical Robotics and Biomechatronics (BioRob)*. 2018, pp. 1005–1010 (cit. on pp. 16, 17).

[44] O.S. Oguz, Z. Zhou, S. Glasauer, and D. Wollherr. "An Inverse Optimal Control Approach to Explain Human Arm Reaching Control Based on Multiple Internal Models". In: *Scientific Reports*. Vol. 8. 1. 2018, p. 5583 (cit. on p. 16).

[45] K. Mombaur and M. Sreenivasa. "Inverse Optimal Control as a Tool to Understand Human Yoyo Playing". In: *AIP Conference Proceedings*. Vol. 1281. 1. 2010, pp. 394–397 (cit. on pp. 16, 17).

[46] K. Mombaur, J.-P. Laumond, and A. Truong. "An Inverse Optimal Control Approach to Human Motion Modeling". In: *Springer Tracts in Advanced Robotics*. Vol. 70. Springer. 2009, pp. 451–468 (cit. on pp. 16, 17, 31, 91).

[47] D. Clever, R. Malin Schemschat, M. L. Felis, and K. Mombaur. "Inverse optimal control based identification of optimality criteria in whole-body human walking on level ground". In: *IEEE/RAS/EMBS Int. Conf. on Biomedical Robotics and Biomechatronics (BioRob)*. 2016, pp. 1192–1199 (cit. on p. 16).

[48] D. Clever and K. Mombaur. "An Inverse Optimal Control Approach for the Transfer of Human Walking Motions in Constrained Environment to Humanoid Robots". In: *Robotics: Science and systems*. 2016 (cit. on p. 17).

[49] V. Q. Nguyen, R. T. Johnson, F. C. Sup, and B. R. Umberger. "Bilevel Optimization for Cost Function Determination in Dynamic Simulation of Human Gait". In: *IEEE Transactions on Neural Systems and Rehabilitation Engineering*. Vol. 27. 7. 2019, pp. 1426–1435 (cit. on p. 17).

[50] Anne-Sophie Puydupin-Jamin, Miles Johnson, and Timothy Bretl. "A convex approach to inverse optimal control and its application to modeling human locomotion". In: *IEEE/RAS Int. Conf. on Robotics and Automation (ICRA)*. 2012, pp. 531–536 (cit. on p. 17).

[51] J. F.-S. Lin, V. Bonnet, A. M. Panchea, N. Ramdani, G. Venture, and D. Kulić. "Human motion segmentation using cost weights recovered from inverse optimal control". In: *IEEE/RAS Int. Conf. on Humanoid Robotics (Humanoids)*. 2016, pp. 1107–1113 (cit. on p. 17).

[52] P. Englert, N. A. Vien, and M. Toussaint. "Inverse KKT: Learning cost functions of manipulation tasks from demonstrations". In: *SAGE journals*. Vol. 36. 13. 2017, pp. 1474–1488 (cit. on p. 17).

[53] K. Westermann, J. F.-S. Lin, and D. Kulić. "Inverse optimal control with time-varying objectives: application to human jumping movement analysis". In: *Scientific Reports*. Vol. 10. 1. 2020, p. 11174 (cit. on p. 17).

[54] F.C. Chittaro, F. Jean, and P. Mason. "On Inverse Optimal Control Problems of Human Locomotion: Stability and Robustness of the Minimizers." In: *Journal of Mathematical Sciences*. Vol. 195. 2013, pp. 269–287 (cit. on p. 17).

[55] M. Johnson, N. Aghasadeghi, and T. Bretl. "Inverse optimal control for deterministic continuous-time nonlinear systems". In: *52nd IEEE Conference on Decision and Control*. 2013, pp. 2906–2913 (cit. on p. 17).

[56] E. Pauwels, D. Henrion, and J.-B. Lasserre. "Inverse optimal control with polynomial optimization". In: *53rd IEEE Conference on Decision and Control*. 2014, pp. 5581–5586 (cit. on p. 17).

[57] Y. Engel, S. Mannor, and R. Meir. "Reinforcement learning with Gaussian processes". In: *ICML: Proceedings of the 22nd International Conference on Machine Learning*. 2005, pp. 201–208 (cit. on p. 17).

[58] B. D. Ziebart, A. Maas, J. A. Bagnell, and A. K. Dey. "Maximum Entropy Inverse Reinforcement Learning". In: *Proceedings AAAI*. 2008, pp. 1433–1438 (cit. on p. 18).

[59] Tae Bum Park and Sergey Levine. "Inverse Optimal Control for Humanoid Locomotion". In: 2013 (cit. on p. 18).

[60] J. Mainprice, R. Hayne, and D. Berenson. "Goal Set Inverse Optimal Control and Iterative Replanning for Predicting Human Reaching Motions in Shared Workspaces". In: *IEEE Transactions on Robotics (T-RO)*. Vol. 32. 4. 2016, pp. 897–908 (cit. on p. 18).

[61] S. Levine, Z. Popovic, and V. Koltun. "Nonlinear Inverse Reinforcement Learning with Gaussian Processes". In: *Advances in Neural Information Processing Systems (NIPS)*. Vol. 24. Curran Associates, Inc., 2011 (cit. on p. 18).

[62] M. Saini, D. C. Kerrigan, M. A. Thirunarayan, and M. Duff-Raffaele. "The Vertical Displacement of the Center of Mass During Walking: A Comparison of Four Measurement Methods". In: *Journal of Biomechanical Engineering*. Vol. 120. 1. 1998, pp. 133–139 (cit. on pp. 20, 72, 86, 122).

[63] G. Maldonado, P. Soueres, and B. Watier. "Whole-body musculo-skeletal model V1". [Technical Report] Rapport LAAS n° 18233, hal-01841355. 2018 (cit. on p. 20).

[64] S. Fleury, P. Soueres, J. -. Laumond, and R. Chatila. "Primitives for smoothing mobile robot trajectories". In: *IEEE Transactions on Robotics and Automation*. Vol. 11. 3. June 1995, pp. 441–448 (cit. on p. 22).

[65] Y. Kanayama and N. Miyake. "Trajectory generation for mobile robot". In: *Robotics Research: The Third International Symposium*. Cambridge, Mass., 1986, pp. 333–340 (cit. on p. 22).

[66] M. Brezak and I. Petrovic. "Path Smoothing Using Clothoids for Differential Drive Mobile Robots". In: *IFAC Proceedings Volumes*. Elsevier, 2011, pp. 1133–1138 (cit. on p. 22).

[67] G. Arechavaleta, J. Laumond, H. Hicheur, and A. Berthoz. "An Optimality Principle Governing Human Walking". In: *IEEE Transactions on Robotics (T-RO)*. Vol. 24. 1. Feb. 2008, pp. 5–14 (cit. on p. 22).

[68] E. Bertolazzi and M. Frego. "G1 fitting with clothoids". In: *Mathematical Methods in the Applied Sciences*. Vol. 38. Mar. 2014 (cit. on p. 23).

[69] Y. Tassa, N. Mansard, and E. Todorov. "Control-limited differential dynamic programming". In: *IEEE/RAS Int. Conf. on Robotics and Automation (ICRA)*. 2014 (cit. on pp. 25, 89, 124).

[70] C. Mastalli, R. Budhiraja, W. Merkt, G. Saurel, B. Hammoud, M. Naveau, et al. "Crocoddyl: An Efficient and Versatile Framework for Multi-Contact Optimal Control". In: *IEEE/RAS Int. Conf. on Robotics and Automation (ICRA)*. 2020 (cit. on pp. 25, 45, 71, 89, 124).

[71] H.G.Bock and K.J.Plitt. "A Multiple Shooting Algorithm for Direct Solution of Optimal Control Problems". In: *IFAC Proceedings Volumes*. Elsevier, 1984, pp. 1603–1608 (cit. on p. 25).

[72] P. Virtanen, R. Gommers, T. Oliphant, M. Haberland, T. Reddy, David Cournapeau, et al. "SciPy 1.0: Fundamental Algorithms for Scientific Computing in Python". In: *Nature Methods*. Vol. 17. 2020, pp. 261–272 (cit. on pp. 30, 32, 87, 91).

[73] A. R. Conn, K. Scheinberg, and L. N. Vicente. "Introduction to Derivative-Free Optimization". In: *Society for Industrial and Applied Mathematics*. 2009 (cit. on p. 32).

[74] M. J. D. Powell. "An efficient method for finding the minimum of a function of several variables without calculating derivatives". In: *The Computer Journal*. Vol. 7. 2. 1964, pp. 155–162 (cit. on pp. 32, 91).

[75] P Viviani and T Flash. "Minimum-jerk, two-thirds power law, and isochrony: converging approaches to movement planning". In: *Journal of experimental psychology. Human perception and performance*. Vol. 21. 1. Feb. 1995, pp. 32–53 (cit. on pp. 38, 61).

[76] T. Flash and N. Hogan. "The coordination of arm movements: an experimentally confirmed mathematical model". In: *The Journal of Neuroscience*. 1985 (cit. on p. 38).

[77] A. Biess, D. Liebermann, and T. Flash. "A Computational Model for Redundant Human Three-Dimensional Pointing Movements: Integration of Independent Spatial and Temporal Motor Plans Simplifies Movement Dynamics". In: *The Journal of Neuroscience*. Vol. 27. 2007, pp. 13045–13064 (cit. on p. 38).

[78] J. Krüger, T.K. Lien, and A. Verl. "Cooperation of human and machines in assembly lines". In: *CIRP Annals*. Vol. 58. 2. 2009, pp. 628–646 (cit. on p. 42).

[79] H. Liu and L. Wang. "Gesture recognition for human-robot collaboration: A review". In: *International Journal of Industrial Ergonomics*. Vol. 68. 2018, pp. 355–367 (cit. on p. 42).

[80] J. Mainprice and D. Berenson. "Human-robot collaborative manipulation planning using early prediction of human motion". In: *IEEE/RSJ Int. Conf. on Intelligent Robots and Systems (IROS)*. 2013, pp. 299–306 (cit. on p. 42).

[81] "Human motion prediction for human-robot collaboration". In: *Journal of Manufacturing Systems*. Vol. 44. Special Issue on Latest advancements in manufacturing systems at NAMRC 45. 2017, pp. 287–294 (cit. on p. 42).

[82] M. S. Ryoo. "Human activity prediction: Early recognition of ongoing activities from streaming videos". In: *2011 International Conference on Computer Vision*. 2011, pp. 1036–1043 (cit. on p. 42).

[83] H. S. Koppula and A. Saxena. "Anticipating Human Activities Using Object Affordances for Reactive Robotic Response". In: *IEEE Transactions on Pattern Analysis and Machine Intelligence*. Vol. 38. 1. 2016, pp. 14–29 (cit. on p. 42).

[84] L. Bruckschen, K. Bungert, N. Dengler, and M. Bennewitz. "Human-Aware Robot Navigation by Long-Term Movement Prediction". In: *IEEE/RSJ Int. Conf. on Intelligent Robots and Systems (IROS)*. 2020, pp. 11032–11037 (cit. on p. 42).

[85] L. Bruckschen, K. Bungert, N. Dengler, and M. Bennewitz. "Predicting human navigation goals based on Bayesian inference and activity regions". In: *Robotics and Autonomous Systems*. Vol. 134. 2020, p. 103664 (cit. on p. 42).

[86] G. Ferrer, A. G. Zulueta, F. H. Cotarelo, and A. Sanfeliu. "Robot social-aware navigation framework to accompany people walking side-by-side". In: *Autonomous Robots*. Vol. 41. 4. 2017, pp. 775–793 (cit. on p. 42).

[87] A. Bayoumi and M. Bennewitz. "Learning optimal navigation actions for foresighted robot behavior during assistance tasks". In: *IEEE/RAS Int. Conf. on Robotics and Automation (ICRA)*. 2016, pp. 207–212 (cit. on p. 42).

[88] M. Tee Kit Tsun, B. T. Lau, and H. Siswoyo Jo. "An Improved Indoor Robot Human-Following Navigation Model Using Depth Camera, Active IR Marker and Proximity Sensors Fusion". In: *Robotics*. Vol. 7. 1. 2018 (cit. on p. 42).

[89] A. Rudenko, L. Palmieri, M. Herman, K. M. Kitani, D. M. Gavrila, and K. O. Arras. "Human motion trajectory prediction: a survey". In: *SAGE journals*. Vol. 39. 8. 2020, pp. 895–935 (cit. on p. 42).

[90] J. F. Kooij, N. Schneider, F. Flohr, and D. M. Gavrila. "Context-Based Pedestrian Path Prediction". In: *Computer Vision - ECCV 2014*. Vol. 8694. Springer International Publishing, 2014 (cit. on p. 42).

[91] J. F. Kooij, F. Flohr, E. A. Pool, and D. M. Gavrila. "Context-Based Path Prediction for Targets with Switching Dynamics". In: *International Journal of Computer Vision*. Vol. 127. 3. Springer, 2019, pp. 239–262 (cit. on p. 42).

[92] A. Alahi, K. Goel, V. Ramanathan, A. Robicquet, L. Fei-Fei, and S. Savarese. "Social LSTM: Human Trajectory Prediction in Crowded Spaces". In: *2016 IEEE Conference on Computer Vision and Pattern Recognition (CVPR)*. 2016, pp. 961–971 (cit. on p. 43).

[93] B. Ivanovic and M. Pavone. "The Trajectron: Probabilistic Multi-Agent Trajectory Modeling With Dynamic Spatiotemporal Graphs". In: *2019 IEEE/CVF International Conference on Computer Vision (ICCV)*. 2019, pp. 2375–2384 (cit. on p. 43).

[94] H. Wallach, H. Larochelle, A. Beygelzimer, F. d'Alche-Buc, E. Fox, and R. Garnett. "Social-BiGAT: multimodal trajectory forecasting using Bicycle-GAN and graph attention networks". In: *Advances in Neural Information Processing Systems (NIPS)*. Vol. 32. 2019, pp. 137–146 (cit. on p. 43).

[95] D. Helbing and P. Molnár. "Social force model for pedestrian dynamics". In: *Physical review E*. Vol. 51. 5. 1995, p. 4282 (cit. on p. 43).

[96] K. Yamaguchi, A. C. Berg, L. E. Ortiz, and T. L. Berg. "Who are you with and where are you going?" In: *CVPR 2011*. 2011, pp. 1345–1352 (cit. on p. 43).

[97] J. Elfring, R. van de Molengraft, and M. Steinbuch. "Learning intentions for improved human motion prediction". In: *Int. Conf. on Advanced Robotics (ICAR)*. 2013, pp. 1–7 (cit. on p. 43).

[98] Henrik Kretzschmar, Markus Kuderer, and Wolfram Burgard. "Learning to predict trajectories of cooperatively navigating agents". In: *IEEE/RAS Int. Conf. on Robotics and Automation (ICRA)*. 2014, pp. 4015–4020 (cit. on p. 43).

[99] F. Giuliari, I. Hasan, M. Cristani, and F. Galasso. "Transformer Networks for Trajectory Forecasting". In: *2020 25th International Conference on Pattern Recognition (ICPR)*. IEEE Computer Society, 2021, pp. 10335–10342 (cit. on p. 43).

[100] C. Schöller, V. Aravantinos, F. Lay, and A. Knoll. "What the Constant Velocity Model Can Teach Us About Pedestrian Motion Prediction". In: *IEEE/RAS Robotics and Automation Letters (RA-L)*. Vol. 5. 2. 2020, pp. 1696–1703 (cit. on pp. 43, 49).

[101] B. Chen, D. Li, and Y. He. "Simultaneous Prediction of Pedestrian Trajectory and Actions based on Context Information Iterative Reasoning". In: *IEEE/RSJ Int. Conf. on Intelligent Robots and Systems (IROS)*. 2021, pp. 1007–1014 (cit. on p. 43).

[102] A. Bussy, P. Gergondet, A. Kheddar, F. Keith, and A. Crosnier. "Proactive behavior of a humanoid robot in a haptic transportation task with a human partner". In: *IEEE International Conference on Robot and Human Interactive Communication (RO-MAN)*. 2012, pp. 962–967 (cit. on pp. 43, 54, 112).

[103] Stanford Artificial Intelligence Laboratory et al. *Robotic Operating System*. Version ROS Melodic Morenia. 2018. URL: `https://www.ros.org` (cit. on pp. 46, 68, 114, 129).

[104] K. Kosuge, H. Yoshida, and T. Fukuda. "Dynamic control for robot-human collaboration". In: *Proceedings of 2nd IEEE International Workshop on Robot and Human Communication*. 1993, pp. 398–401 (cit. on p. 53).

[105] A. Herdt, N. Perrin, and P. Wieber. "Walking without thinking about it". In: *IEEE/RSJ Int. Conf. on Intelligent Robots and Systems (IROS)*. 2010, pp. 190–195 (cit. on p. 53).

[106] M. Vukobratović and J. Stepanenko. "On the stability of anthropomorphic systems". In: *Mathematical Biosciences*. Vol. 15. 1. 1972, pp. 1–37 (cit. on p. 53).

[107] S. Kajita, F. Kanehiro, K. Kaneko, K. Fujiwara, K. Harada, K. Yokoi, et al. "Biped walking pattern generation by using preview control of zero-moment point". In: *IEEE/RAS Int. Conf. on Robotics and Automation (ICRA)*. Vol. 2. 2003, 1620–1626 vol.2 (cit. on pp. 53, 59).

[108] P. Wieber. "Trajectory Free Linear Model Predictive Control for Stable Walking in the Presence of Strong Perturbations". In: *IEEE/RAS Int. Conf. on Humanoid Robotics (Humanoids)*. 2006, pp. 137–142 (cit. on p. 53).

[109] D.Q. Mayne, J.B. Rawlings, C.V. Rao, and P.O.M. Scokaert. "Constrained model predictive control: Stability and optimality". In: *Automatica*. Vol. 36. 6. 2000, pp. 789–814 (cit. on p. 53).

[110] S. Faraji, S. Pouya, C. G. Atkeson, and A. J. Ijspeert. "Versatile and robust 3D walking with a simulated humanoid robot (Atlas): A model predictive control approach". In: *IEEE/RAS Int. Conf. on Robotics and Automation (ICRA)*. 2014, pp. 1943–1950 (cit. on p. 53).

[111] R. J. Griffin and A. Leonessa. "Model predictive control for dynamic footstep adjustment using the divergent component of motion". In: *IEEE/RAS Int. Conf. on Robotics and Automation (ICRA)*. 2016, pp. 1763–1768 (cit. on p. 53).

[112] S. Feng, X. Xinjilefu, C. G. Atkeson, and J. Kim. "Robust dynamic walking using online foot step optimization". In: *IEEE/RSJ Int. Conf. on Intelligent Robots and Systems (IROS)*. 2016, pp. 5373–5378 (cit. on p. 53).

[113] N. Scianca, D. De Simone, L. Lanari, and G. Oriolo. "MPC for Humanoid Gait Generation: Stability and Feasibility". In: *IEEE Transactions on Robotics (T-RO)*. Vol. 36. 4. 2020, pp. 1171–1188 (cit. on pp. 53, 65).

[114] D. De Simone, N. Scianca, P. Ferrari, L. Lanari, and G. Oriolo. "MPC-based humanoid pursuit-evasion in the presence of obstacles". In: *IEEE/RSJ Int. Conf. on Intelligent Robots and Systems (IROS)*. 2017, pp. 5245–5250 (cit. on pp. 53, 54).

[115] M. Naveau, M. Kudruss, O. Stasse, C. Kirches, K. Mombaur, and P. Souères. "A Reactive Walking Pattern Generator Based on Nonlinear Model Predictive Control". In: *IEEE/RAS Robotics and Automation Letters (RA-L)*. Vol. 2. 1. 2017, pp. 10–17 (cit. on pp. 54, 58, 61–64, 71, 73, 136).

[116] S. Caron and A. Kheddar. "Dynamic walking over rough terrains by nonlinear predictive control of the floating-base inverted pendulum". In: *IEEE/RSJ Int. Conf. on Intelligent Robots and Systems (IROS)*. 2017, pp. 5017–5024 (cit. on p. 54).

[117] Néstor Bohórquez and Pierre-Brice Wieber. "Adaptive step rotation in biped walking". In: *IEEE/RSJ Int. Conf. on Intelligent Robots and Systems (IROS)*. 2018, pp. 720–725 (cit. on p. 54).

[118] N. Jarrassé, V. Sanguineti, and E. Burdet. "Slaves no longer: review on role assignment for human–robot joint motor action". In: *Adaptive Behavior, SAGE Publications*. Vol. 22. 1. 2013, pp. 70–82 (cit. on pp. 54, 111, 112).

[119] K. Otani, K. Bouyarmane, and S. Ivaldi. "Generating Assistive Humanoid Motions for Co-Manipulation Tasks with a Multi-Robot Quadratic Program Controller". In: *IEEE/RAS Int. Conf. on Robotics and Automation (ICRA)*. 2018, pp. 3107–3113 (cit. on pp. 54, 111).

[120] S.P. Teja and R. Alami. "HATEB-2: Reactive Planning and Decision making in Human-Robot Co-navigation". In: *IEEE International Conference on Robot and Human Interactive Communication (RO-MAN)*. 2020, pp. 179–186 (cit. on p. 54).

[121] J. Lanini, A. Duburcq, H. Razavi, C.G. Le Goff, and A. Ijspeert. "Interactive locomotion: Investigation and modeling of physically-paired humans while walking". In: *PLOS ONE*. Vol. 12. 2017, pp. 1–25 (cit. on pp. 54, 81, 129).

[122] J. Lanini, H. Razavi, J. Urain, and A. Ijspeert. "Human Intention Detection as a Multiclass Classification Problem: Application in Physical Human–Robot Interaction While Walking". In: *IEEE/RAS Robotics and Automation Letters (RA-L)*. Vol. 3. 4. 2018, pp. 4171–4178 (cit. on pp. 54, 81, 111).

[123] D. Aarno and D. Kragic. "Motion intention recognition in robot assisted applications". In: *Robotics and Autonomous Systems*. Vol. 56. 8. 2008, pp. 692–705 (cit. on p. 55).

[124] R. Kelley, M. Nicolescu, A. Tavakkoli, M. Nicolescu, C. King, and G. Bebis. "Understanding human intentions via Hidden Markov Models in autonomous mobile robots". In: *ACM/IEEE International Conference on Human-Robot Interaction (HRI)*. 2008, pp. 367–374 (cit. on p. 55).

[125] Q. Li, Z. Zhang, Y. You, Y. Mu, and C. Feng. "Data Driven Models for Human Motion Prediction in Human-Robot Collaboration". In: *IEEE Access*. Vol. 8. 2020, pp. 227690–227702 (cit. on p. 55).

[126] M. Awais and D. Henrich. "Human-robot collaboration by intention recognition using probabilistic state machines". In: *19th International Workshop on Robotics in Alpe-Adria-Danube Region (RAAD 2010)*. 2010, pp. 75–80 (cit. on p. 55).

[127] A. Herdt, H. Diedam, P.-B. Wieber, D. Dimitrov, K. Mombaur, and M. Diehl. "Online Walking Motion Generation with Automatic Footstep Placement". In: *Advanced Robotics*. Vol. 24. 5-6. Taylor & Francis, 2010, pp. 719–737 (cit. on p. 59).

[128] A.L. Hof, M.G.J. Gazendam, and W.E. Sinke. "The condition for dynamic stability". In: *Journal of Biomechanics*. Vol. 38. 1. 2005, pp. 1–8 (cit. on p. 60).

[129] J. Pratt, J. Carff, S. Drakunov, and A. Goswami. "Capture Point: A Step toward Humanoid Push Recovery". In: *IEEE/RAS Int. Conf. on Humanoid Robotics (Humanoids)*. 2006, pp. 200–207 (cit. on p. 60).

[130] H.J. Ferreau, C. Kirches, A. Potschka, H.G. Bock, and M. Diehl. "qpOASES: A parametric active-set algorithm for quadratic programming". In: *Mathematical Programming Computation*. Vol. 6. 2014, pp. 327–363 (cit. on p. 63).

[131] J. Englsberger, C. Ott, M. A. Roa, A. Albu-Schäffer, and G. Hirzinger. "Bipedal walking control based on Capture Point dynamics". In: *IEEE/RSJ Int. Conf. on Intelligent Robots and Systems (IROS)*. 2011, pp. 4420–4427 (cit. on p. 64).

[132] P.-B. Wieber, R. Tedrake, and S. Kuindersma. "Modeling and control of legged robots". In: *Springer Handbook of Robotics*. 2016, pp. 1203–1234 (cit. on p. 64).

[133] T. Koolen, T. De Boer, J. Rebula, A. Goswami, and J. Pratt. "Capturability-based analysis and control of legged locomotion, Part 1: Theory and application to three simple gait models". In: *The International Journal of Robotics Research*. Vol. 31. July 2012, pp. 1094–1113 (cit. on p. 65).

[134] M. Ciocca, P.-B. Wieber, and T. Fraichard. "Strong recursive feasibility in model predictive control of biped walking". In: *IEEE/RAS Int. Conf. on Humanoid Robotics (Humanoids)*. Nov. 2017, pp. 730–735 (cit. on p. 65).

[135] A. Herzog, N. Rotella, S. Mason, F. Grimminger, S. Schaal, and L. Righetti. "Momentum Control with Hierarchical Inverse Dynamics on a Torque-Controlled Humanoid". In: *Autonomous Robots*. 40. 2014, pp. 473–491 (cit. on p. 69).

[136] N. Ramuzat, G. Buondonno, S. Boria, and O. Stasse. "Comparison of Position and Torque Whole-Body Control Schemes on the Humanoid Robot TALOS". In: *Int. Conf. on Advanced Robotics (ICAR)*. 2021, pp. 785–792 (cit. on pp. 69, 71, 72, 127, 132, 136).

[137] N. Ramuzat, O. Stasse, and S. Boria. "Benchmarking Whole-Body Controllers on the TALOS Humanoid Robot". In: *Frontiers in Robotics and AI*. Vol. 9. 2022 (cit. on pp. 69, 71, 72, 127, 132, 139).

[138] S. Kajita, F. Kanehiro, K. Kaneko, K. Fujiwara, K. Harada, K. Yokoi, et al. "Resolved momentum control: humanoid motion planning based on the linear and angular momentum". In: *IEEE/RSJ Int. Conf. on Intelligent Robots and Systems (IROS)*. Vol. 2. 2003, pp. 1644–1650 (cit. on p. 69).

[139] A. Del Prete, N. Mansard, O. E. Ramos, O. Stasse, and F. Nori. "Implementing Torque Control with High-Ratio Gear Boxes and Without Joint-Torque Sensors". In: *International Journal of Humanoid Robotics*. Vol. 13. 1. 2016, p. 1550044 (cit. on pp. 70, 127).

[140] G. Fumery, H. Mérienne, V. Fourcassié, and P. Moretto. "Locomotor pattern and mechanical exchanges during collective load transport". In: *Human Movement Science*. Vol. 66. 2019, pp. 327–334. DOI: https://doi.org/10.1016/j.humov.2019.05.012 (cit. on p. 81).

[141] G. Fumery, L. Claverie, V. Fourcassié, and P. Moretto. "Walking pattern efficiency during collective load transport". In: *Gait and Posture*. Vol. 64. 2018, pp. 244–247 (cit. on p. 81).

[142] F. Sylos-Labini, A. d'Avella, F. Lacquaniti, and Y. Ivanenko. "Human-Human Interaction Forces and Interlimb Coordination During Side-by-Side Walking With Hand Contact". In: *Frontiers in Physiology*. Vol. 9. 2018 (cit. on p. 81).

[143] K. B. Reed, M. Peshkin, M. J. Hartmann, M. Grabowecky, J. Patton, and P. M. Vishton. "Haptically Linked Dyads: Are Two Motor-Control Systems Better Than One?" In: *Psychological Science*. Vol. 17. 5. 2006, pp. 365–366 (cit. on p. 81).

[144] K. B. Reed and M. A. Peshkin. "Physical Collaboration of Human-Human and Human-Robot Teams". In: *IEEE Transactions on Haptics*. Vol. 1. 2. 2008, pp. 108–120 (cit. on p. 81).

[145] K. B. Reed, M. Peshkin, M. J. Hartmann, J. Patton, P. M. Vishton, and M. Grabowecky. "Haptic cooperation between people, and between people and machines". In: *IEEE/RSJ Int. Conf. on Intelligent Robots and Systems (IROS)*. 2006, pp. 2109–2114 (cit. on p. 81).

[146] R. Groten, D. Feth, H. Goshy, A. Peer, D. A. Kenny, and M. Buss. "Experimental analysis of dominance in haptic collaboration". In: *IEEE International Conference on Robot and Human Interactive Communication (RO-MAN)*. 2009, pp. 723–729 (cit. on p. 81).

[147] P. Evrard and A. Kheddar. "Homotopy switching model for dyad haptic interaction in physical collaborative tasks". In: *World Haptics 2009 - Third Joint EuroHaptics conference and Symposium on Haptic Interfaces for Virtual Environment and Teleoperator Systems*. 2009, pp. 45–50 (cit. on p. 81).

[148] A. Sawers, T. Bhattacharjee, J. L. McKay, M. E. Hackney, C. C. Kemp, and L. H. Ting. "Small forces that differ with prior motor experience can communicate movement goals during human-human physical interaction". In: *Journal of NeuroEngineering and Rehabilitation*. Vol. 14. 2017, p. 8 (cit. on p. 81).

[149] A. G. Ingham, G. Levinger, J. Graves, and V. Peckham. "The Ringelmann effect: Studies of group size and group performance". In: *Journal of Experimental Social Psychology*. Vol. 10. 4. 1974, pp. 371–384 (cit. on p. 103).

[150] J. W. Hart, D. J. Bridgett, and S. J Karau. "Coworker ability and effort as determinants of individual effort on a collective task". In: *Group Dynamics: Theory, Research, and Practice*. Vol. 5. 3. 2001, pp. 181–190 (cit. on p. 103).

[151] V. Romero, R. Kallen, M. A. Riley, and M. J. Richardson. "Can discrete joint action be synergistic? Studying the stabilization of interpersonal hand coordination." In: *Journal of Experimental Psychology: Human Perception and Performance*. Vol. 41. 5. 2015, pp. 1223–1235 (cit. on p. 104).

[152] A. W. Kiefer, K. Rio, S. Bonneaud, A. Walton, and W. H. Warren. "Quantifying and Modeling Coordination and Coherence in Pedestrian Groups". In: *Frontiers in psychology*. Vol. 8. 2017, p. 949 (cit. on p. 104).

[153] A. Ajoudani, A. M. Zanchettin, S. Ivaldi, A. Albu-Schäffer, K. Kosuge, and O. Khatib. "Progress and prospects of the human–robot collaboration". In: *Autonomous Robots*. Vol. 42. 5. 2018, pp. 957–975 (cit. on p. 111).

[154] N. Stergiou and L.M. Decker. "Human movement variability, nonlinear dynamics, and pathology: is there a connection?" In: *Human Movement Science*. Vol. 30. 5. 2011, pp. 869–88 (cit. on p. 111).

[155] A. Bussy, A. Kheddar, A. Crosnier, and F. Keith. "Human-humanoid haptic joint object transportation case study". In: *IEEE/RSJ Int. Conf. on Intelligent Robots and Systems (IROS)*. 2012, pp. 3633–3638 (cit. on p. 111).

[156] P. Artemiadis, P. Katsiaris, M. Liarokapis, and K. Kyriakopoulos. "Human arm impedance: Characterization and modeling in 3D space". In: *IEEE/RSJ Int. Conf. on Intelligent Robots and Systems (IROS)*. 2010, pp. 3103–3108 (cit. on p. 112).

[157] M. Sharifi, S. Behzadipour, and G. Vossoughi. "Nonlinear model reference adaptive impedance control for human–robot interactions". In: *Control Engineering Practice*. Vol. 32. 2014, pp. 9–27 (cit. on p. 112).

[158] D. J. Agravante, A. Cherubini, A. Bussy, P. Gergondet, and A. Kheddar. "Collaborative human-humanoid carrying using vision and haptic sensing". In: *IEEE/RAS Int. Conf. on Robotics and Automation (ICRA)*. 2014, pp. 607–612 (cit. on p. 112).

[159] SY. Lo, CA. Cheng, and Huang HP. "Journal of Intelligent & Robotic Systems". In: *Virtual Impedance Control for Safe Human-Robot Interaction*. Vol. 82. 1. 2016, pp. 3–19 (cit. on p. 112).

[160] Luka Peternel, Nikos Tsagarakis, and Arash Ajoudani. "Towards multi-modal intention interfaces for human-robot co-manipulation". In: *IEEE/RSJ Int. Conf. on Intelligent Robots and Systems (IROS)*. 2016, pp. 2663–2669 (cit. on p. 112).

[161] M. Mujica, M. Benoussaad, and J.-Y. Fourquet. "Evaluation of Human-Robot Object Co-manipulation Under Robot Impedance Control". In: *IEEE/RAS Int. Conf. on Robotics and Automation (ICRA)*. 2020, pp. 9143–9149 (cit. on p. 112).

[162] A. Dutta and O. Obinata. "Impedance control of a robotic gripper for cooperation with humans". In: *Control Engineering Practice*. Vol. 10. 4. 2002, pp. 379–389 (cit. on p. 112).

[163] E. Gribovskaya, A. Kheddar, and A. Billard. "Motion learning and adaptive impedance for robot control during physical interaction with humans". In: *IEEE/RAS Int. Conf. on Robotics and Automation (ICRA)*. 2011, pp. 4326–4332 (cit. on p. 112).

[164] H.-D. Lee, B.-K. Lee, W.-S. Kim, J.-S. Han, K.-S. Shin, and C.-S. Han. "Human–robot cooperation control based on a dynamic model of an upper limb exoskeleton for human power amplification". In: *Mechatronics*. Vol. 24. 2. 2014, pp. 168–176 (cit. on p. 112).

[165] J. Xia, D. Huang, Y. Li, and N. Qin. "Iterative learning of human partner's desired trajectory for proactive human–robot collaboration". In: *International Journal of Intelligent Robotics and Applications*. Vol. 4. 2. 2020, pp. 229–242 (cit. on p. 112).

[166] C. Lauretti, F. Cordella, E. Guglielmelli, and L. Zollo. "Learning by Demonstration for Planning Activities of Daily Living in Rehabilitation and Assistive Robotics". In: *IEEE/RAS Robotics and Automation Letters (RA-L)*. Vol. 2. 3. 2017, pp. 1375–1382 (cit. on p. 112).

[167] A. Fishman, C. Paxton, W. Yang, D. Fox, B. Boots, and N. Ratliff. "Collaborative Interaction Models for Optimized Human-Robot Teamwork". In: *IEEE/RSJ Int. Conf. on Intelligent Robots and Systems (IROS)*. 2020, pp. 11221–11228 (cit. on p. 112).

[168] P. Mohammadi, E. M. Hoffman, L. Muratore, N. G. Tsagarakis, and J. J. Steil. "Reactive Walking Based on Upper-Body Manipulability: An application to Intention Detection and Reaction". In: *IEEE/RAS Int. Conf. on Robotics and Automation (ICRA)*. 2019, pp. 4991–4997 (cit. on p. 112).

[169] T. Kobayashi, E. Dean-Leon, J. R. Guadarrama-Olvera, F. Bergner, and G. Cheng. "Multi-Contacts Force-Reactive Walking Control during Physical Human-Humanoid Interaction". In: *IEEE/RAS Int. Conf. on Humanoid Robotics (Humanoids)*. 2019, pp. 33–39 (cit. on p. 112).

[170] A. De Santis, B. Siciliano, A. De Luca, and A. Bicchi. "An atlas of physical human–robot interaction". In: *Mechanism and Machine Theory*. Vol. 43. 3. 2008, pp. 253–270 (cit. on p. 112).

[171] F. Flacco, T. Kröger, A. De Luca, and O. Khatib. "A depth space approach to human-robot collision avoidance". In: *IEEE/RAS Int. Conf. on Robotics and Automation (ICRA)*. 2012, pp. 338–345 (cit. on p. 112).

[172] S. Haddadin, A. Albu-Schaffer, A. De Luca, and G. Hirzinger. "Collision Detection and Reaction: A Contribution to Safe Physical Human-Robot Interaction". In: *IEEE/RSJ Int. Conf. on Intelligent Robots and Systems (IROS)*. 2008, pp. 3356–3363 (cit. on p. 112).

[173] B. Navarro, A. Fonte, P. Fraisse, G. Poisson, and A. Cherubini. "In Pursuit of Safety: An Open-Source Library for Physical Human-Robot Interaction". In: *IEEE Robotics & Automation Magazine*. Vol. 25. 2. 2018, pp. 39–50 (cit. on p. 112).

[174] F. Pomerleau, F. Colas, R. Siegwart, and S. Magnenat. "Comparing ICP variants on real-world data sets". In: *Autonomous Robots*. Vol. 34. 3. 2013, pp. 133–148 (cit. on p. 115).

Glossary

AM Angular Momentum.

ANOVA ANalysis Of VAriance.

ANR Agence Nationale de la Recherche.

BoW Bag-of-Words.

CoBot CollaBorative roBot.

CoM Center of Mass.

CoP Center of Pressure.

CP Capture Point.

CRCA Centre de Recherches sur la Cognition Animale.

CREPS Centre de Ressources d'Expertise et de Performance Sportive.

CRF Conditional Random Field.

CVM Constant Velocity Model.

DBN Dynamic Bayesian Network.

DCM Divergent Component of Motion.

DDP Differential Dynamic Programming.

DoF Degree of Freedom.

GMM Gaussians Mixture Model.

HMM Hidden Markov Model.

HRI Human-Robot Interaction.

ICP Iterative Closest Point.

IOC Inverse Optimal Control.

IRISSE Laboratoire Ingénierie, Recherche, Intervention, Sport, Santé, Environnement.

IRL Inverse Reinforcement Learning.

KKT Karush-Kuhn-Tucker.

LAAS-CNRS Laboratoire d'Analyse et d'Architecture des Systèmes.

LIPM Linear Inverted Pendulum Model.

LSTM Long Short-Term Memory.

McMC Markov chain Monte Carlo.

MDP Markov Decision Process.

MoCap Motion Capture system.

MPC Model Predictive Control.

NMPC Non-linear Model Predictive Control.

OC Optimal Control.

pHRI physical Human-Robot Interaction.

QP Quadratic Problem.

RMSE Root Mean Square Error.

ROS Robot Operating System.

SLAM Simultaneous Localisation And Mapping.

SLIPs Spring Loaded Inverted Pendulums.

SQP Sequential Quadratic Problem.

TSID Task Space Inverse Dynamic.

VPU Vision Processing Unit.

WPG Walking Pattern Generator.

WQP Weighted Quadratic Program.

ZMP Zero Moment Point.

Résumé

Ma thèse est financée par l'Agence Nationale de la Recherche (ANR) à travers le projet intitulé ANR-CoBot. Ce projet pluri-disciplinaire a pour but d'étudier les interactions entre 2 individus lors d'un transport de charges collaboratif et de réaliser une collaboration homme-robot pour transporter une charge. Dans le cadre de ce projet, ma thèse s'intéresse spécifiquement à la réalisation d'un transport de table en collaboration entre un humain et un robot de type TALOS produit par l'entreprise *PAL Robotics*.

Lorsqu'on s'intéresse à une telle interaction homme-robot, les deux principaux enjeux à relever sont les suivants : comprendre le comportement de l'humain, d'une part, et contrôler le robot pour qu'il puisse adapter ses actions à celles de son partenaire humain d'autre part. Le premier enjeu est d'ordre biomécanique, tandis que le second est d'ordre robotique. Ma thèse allie donc ces deux disciplines. En biomécanique, mon travail s'est focalisé sur l'étude des trajectoires de Centre de Masse (CdM) d'individus marchant seuls sans contraintes puis marchant en transportant une table en binôme. Le but de cette étude est de modéliser ces trajectoires de marche avec un problème de contrôle optimal afin de pouvoir prédire où va un individu à partir de sa trajectoire passée. Cette information est nécessaire pour réaliser une interaction homme-robot fluide où le robot arrive à anticiper le comportement de son partenaire lors du transport, comme le ferait un être humain. En robotique, cinq aspects sont à maîtriser afin de réaliser un transport de charge :

- La localisation: le robot doit pouvoir "voir" la table et son partenaire pour pouvoir interagir avec eux.
- La génération de la marche : le robot doit pouvoir marcher jusqu'à l'endroit où l'humain veut amener la table, endroit qui est a priori inconnu au robot.
- Le contrôle corps-complet : le robot doit pouvoir soulever la table et marcher en la tenant.
- La stabilisation : le robot doit pouvoir réaliser tous ces mouvements sans perdre l'équilibre.
- La sécurité : le robot ne doit pas mettre en danger l'intégrité physique de son partenaire humain.

Parmi ces différents aspects, ma thèse se focalise sur la génération de la marche tandis que les autres points font l'objet de travail d'autres gens au sein de l'équipe Gepetto du LAAS-CNRS. Lors d'une interaction homme-robot, la génération des trajectoires du CdM du robot et de ses pieds doit être rapide et doit prend en compte les mouvements de l'humain en temps réel. Ainsi, ma principale contribution au générateur de marche du robot, lors de ma thèse, a été de le coupler au modèle de prédiction des trajectoires humaines.

Abstract

To improve human-robot collaborations, more and more researches focus on the study of human behaviour. It is in this context of growing relationships between robotics and biomechanics that the CollaBorative roBot (CoBot) project has emerged. Funded by the French Agence Nationale de la Recherche (ANR), this project (ANR-CoBot) targets a human-humanoid robot collaboration in the context of a load-carriage task. During this collaboration, the robot is aimed to safely and proactively assist its human partner to handle a load. The idea of the ANR-CoBot project is, first, to understand the mechanisms at stake during a human-human collaboration and, then, to model and simulate them to finally implement them on a humanoid robot TALOS from *PAL Robotics* to perform the same task with a human partner.

As part of this project, this thesis deals with the transition from the modelling of the human behaviour to the integration of this model in a humanoid robot. The final goal of this thesis is to perform a proactive human-robot interaction to carry a table. From a biomechanics point of view, this thesis aims to better understand human locomotion in order to enable the robot to anticipate its partner's behaviour. To achieve this goal, experiments were performed to measure Center of Mass (CoM) human trajectories, first during simple locomotion and then during carriage task. Then, models based on optimal control problems were designed to generate human-like trajectories or even predict them. This prediction may improve the human-robot interactions making the robot acting proactively. Then, from a robotics point of view, to achieve a collaborative carriage task, five matters need to be handled:

- Localization: the robot needs to locate the table and its human partner in order to interact with them.
- Walk generation: the robot needs to walk toward the table at the beginning of the experiment and also needs to walk with the table towards an unknown location chosen by its human partner.
- Whole-body control: the robot needs to lift the table and handle it while walking.
- Balance: the robot should not fall during the experiment.
- Safety: the robot should not harm its human partner.

Among those matters, this thesis mainly focuses on the walk generation. The other topics are handled by other members of the Gepetto team in LAAS-CNRS. One major contribution of this thesis is to embed the prediction trajectory model into the robot walking pattern generator. This aims to improve the human-robot interaction for two main reasons. First, it may allow the robot to be more reactive by anticipating its partner motions and, then, it may make the interaction less disturbing and more natural for the human as the robot may act in a human-like manner.